A study into the effect of ground movement on the deformation of typical local structures consisting of load-bearing HCB walls and reinforced concrete in-situ slabs

STEWART AQUILINA

Dissertation submitted to the Faculty for the Built Environment, University of Malta in part fulfilment of the requirement for the attainment of the degree of Master of Engineering (Structural Engineering)

June 2025

To my family.

"Power comes in response to a need, not a desire. You have to create that need."

Toriyama, A. (Goku) in Dragon Ball Z

FACULTY~~/INSTITUTE/CENTRE/SCHOOL~~ for the Built Environment

DECLARATIONS BY POSTGRADUATE STUDENTS

(a) Authenticity of Dissertation

I hereby declare that I am the legitimate author of this Dissertation and that it is my original work.

No portion of this work has been submitted in support of an application for another degree or qualification of this or any other university or institution of higher education.

I hold the University of Malta harmless against any third party claims with regard to copyright violation, breach of confidentiality, defamation and any other third party right infringement.

(b) Research Code of Practice and Ethics Review Procedures

I declare that I have abided by the University's Research Ethics Review Procedures. Research Ethics & Data Protection form code BEN-2025-00079.

As a Master's student, as per Regulation 77 of the General Regulations for University Postgraduate Awards 2021, I accept that should my dissertation be awarded a Grade A, it will be made publicly available on the University of Malta Institutional Repository.

Acknowledgments

I wish to express my deepest gratitude to my tutor, Dr. Adrian Mifsud B.E.&A.(Hons), M.Sc.(Lond), Ph.D.(Melit.), D.I.C., Perit, for his unwavering support throughout this study. His insightful guidance and thoughtful advice were instrumental in enriching my understanding of the subject.

I extend my heartfelt thanks to all the other tutors who generously shared their expertise and provided valuable insights on various aspects of this research.

Furthermore, I sincerely appreciate the ongoing support and guidance provided by the Dlubal support team throughout the course of this dissertation.

Finally, I am deeply thankful to my loved ones for their unwavering support, patience, and encouragement. Their steadfast presence and motivation played a crucial role in helping me bring this research to completion.

Abstract

The 20th century saw rapid growth in the construction industry, especially in recent years, with traditional homes and vacant plots being replaced by apartment blocks. This urban densification has introduced various challenges, particularly the impact of construction on adjacent buildings. Ground movement, notably settlement, can lead to structural deformation, internal stress, strain, and ultimately cracking, which may compromise stability. Weak regulatory enforcement, limited awareness, and profit-driven practices have resulted in severe damage or even collapse of neighbouring structures during nearby construction and excavation.

Public awareness about serviceability issues, such as the development of cracks, has grown, driven not only by safety considerations, but also by insurance requirements covering issues like subsidence. Property owners are increasingly vigilant, often escalating concerns into legal disputes, prompting insurance companies to demand stability assessments before issuing coverage.

This dissertation aims to investigate the effects of ground settlement on masonry load-bearing structures using numerical modelling in RFEM 6. The focus is on understanding structural behaviour through analysis of deformations, stresses, and strain concentrations. The local masonry construction model was initially calibrated against a full-scale 2D masonry wall. It was then applied to a smaller-scale 3D room structure to further validate its performance. Finally, the calibrated model was used to simulate the deformations observed at Ta' Kenuna Tower in Nadur, Gozo, enabling a direct comparison between the model's predictions and the actual deformations. The study culminates in the modelling of an apartment block, reflecting Malta's construction trends and contributing to safer design practices.

The results clearly demonstrate that numerical modelling is a powerful and effective tool for simulating the deformations and stresses experienced by masonry structures subjected to settlement. In some cases, the damage observed in real-life structures was closely reflected in the model's predicted deformations, highlighting the reliability of this approach. In conclusion, numerical modelling offers a cost-effective and insightful method for analysing the impact of ground settlement on masonry load-bearing structures.

Table of Contents

List of Figures

List of Tables

1. Introduction

1.1. Insight into the study

During the 20th century—and especially in recent years—the construction industry in Malta has seen substantial growth. Traditionally, families lived in two-storey terraced houses or villas, but over time, these properties were inherited and redeveloped into apartment blocks ranging from three to six storeys. Often, adjacent properties were combined to increase the number of units, generating higher income and contributing to increasingly dense urban environments. This shift has significantly transformed residential building types across the islands. Despite some environmental and social drawbacks, apartment living remains highly popular due to strong demand and economic advantages, with no signs of slowing down. However, this intensified development has also brought negative consequences, including inconvenience and structural damage to neighbouring buildings.

The ever-increasing number of floors allowed in such construction implies higher loads, which increases the risk of settlement within the structure and its underlying terrain, potentially compromising its overall stability. Consequently, the structure can experience deformation, accompanied by the development of internal stresses, which can lead to strain concentration and hence the formation of cracks within the structure.

Due to a lack of regulatory enforcement, limited awareness, complacency toward good construction practices, and economic greed, the industry has witnessed cases where construction on neighbouring plots resulted in severe damage—even the collapse—of adjacent buildings.

As a result, assessing the impact of construction projects on nearby structures has become increasingly important, particularly in relation to the development of structural cracks. This growing concern is understandable, as residents now expect neighbouring construction activities to be carried out safely, knowing that such works could compromise the stability of their own properties. In fact, the appearance of even minor cracks often causes immediate alarm, with many fearing the possibility of structural failure.

In Malta, the recent rise in structural collapses has raised public concern about building safety. Property owners are increasingly questioning the condition of their residences, often escalating matters into legal disputes. Consequently, insurers may take a more cautious stance, at times requiring structural appraisals for buildings in areas exposed to excavation or construction activities.

1.2. Aim of study

This dissertation aims to examine the impact of ground movement, particularly settlement, on typical masonry load-bearing structures prevalent in the Maltese Islands. The study employs numerical modelling, calibrated against real full-scale case studies, to achieve this objective.

Although this is a broad subject, the primary focus will be on understanding the structural behaviour of these masonry systems under induced foundation settlement. Both two-dimensional and three-dimensional models have been utilised for this purpose, as the structural response can vary significantly depending on the dimensionality of the structure.

1.3. Objectives

The effect of foundation settlement is deformation of the structure to varying degrees. In addition, it is essential to examine the development of stress and strain within the structural fabric, through which critical zones of the structure can be identified. In real life, this often results in cracks within the brittle masonry, but this is difficult to observe in a numerical model, unless a discrete element approach is adopted. While crack propagation cannot be directly observed due to software limitations, the analysis of strain can provide insight into the likely locations of crack formation.

In the case of two-dimensional structures, it is often possible to reasonably predict structural behaviour. However, three-dimensional structures present greater complexity, making it more challenging to visualise and anticipate their response to settlement.

1.4. Method of Analysis

The method of analysis employed in this dissertation is numerical modelling using RFEM 6[1]. The study begins with the modelling of simple structural elements, with results compared against hand calculations to ensure a thorough understanding of the software and to validate its accuracy before progressing to more complex structures.

In addition to basic models, real-life structures are also analysed, including a wall model previously studied in Mifsud J. (2012) and, subsequently the full-scale case of the Ta' Kenuna Tower in Nadur, Gozo. The results from the models representing these real structures are compared to the actual damage observed, allowing for calibration of the models and verification of the software's reliability.

Following this calibration process, and once the results are deemed consistent and dependable, a more complex structure—an apartment block—is analysed. This type of structure, although hypothetical for the purposes of this research, was selected due to the significant increase in apartment block construction across the Maltese Islands in recent years, making it highly relevant to the local context.

[1] DLUBAL RFEM6 is a structural analysis and design software used by engineers to model, analyse, and design structures in 2D and 3D. It supports materials like steel, concrete, and masonry, and allows for the simulation of forces, deformations, and load combinations.

2. Introduction to Fundamental Concepts

2.1. Brief Overview

This section introduces the fundamental concepts that are relevant to this study. This is necessary to enable an understanding of the context and of the complexity of each situation. The Chapter is divided into two parts: the first introduces settlement and its various forms, while the second examines building deformation, focusing on methods to classify, describe, and quantify structural changes. This chapter provides insight into how settlement leads to damage, the classification and forms of such damage, and methods to assess its extent. It also explores the impact of this damage on the structural integrity of masonry buildings.

2.2. Settlement in Buildings

2.2.1. Settlement & Subsidence

Settlement refers to the displacement experienced by a structure as a result of changes in the underlying ground material. It is generally caused by issues related to both the ground and the structure, such as the imposed load exceeding the bearing capacity of the soil, soil consolidation due to excess pore pressure dissipation, uneven loading, poorly designed foundations, inadequately compacted fill material, and the gradual compression of soil layers over time (creep).

Settlement can be categorised in distinct patterns, of varying degrees of consequence to the affected building. These include uniform settlement, tipping settlement, and differential settlement, illustrated in Figure 2:1. Uniform settlement generally causes the fewest and least severe cracks, as the structure undergoes vertical translation with minimal distortion (Dickinson P.R. & Thornton N., 2006). In contrast, differential settlement results in the greatest number and most critical cracks, as different parts of the same structure settle to varying degrees.

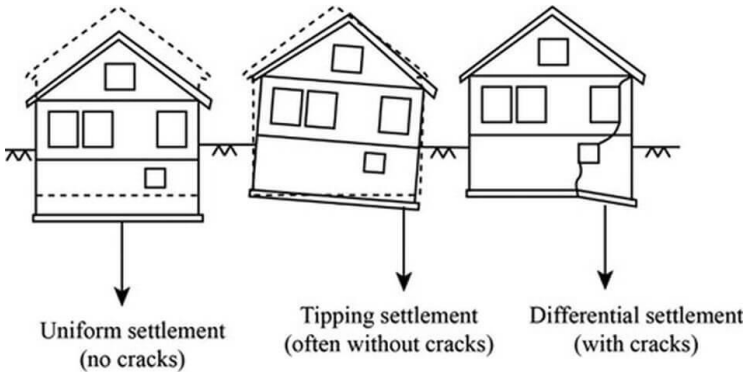

Figure 2:1 - Three main types of settlement

Settlement can also be triggered by external factors such as the removal of supporting materials beneath the ground (e.g., groundwater extraction or tunnelling), natural processes like the dissolution of soluble rocks leading to sinkholes, and tectonic activity, as shown in Figure 2:2. As a result, subsidence may occur suddenly or gradually, depending on the extent of the disturbance to the ground and the nature of the ground itself. These factors typically have a more significant impact on the surrounding environment, as they affect a larger area. Settlement caused by these factors is also known as subsidence (Dickinson P.R. & Thornton N., 2006).

The effect of such inconsistent changes can also lead to differential settlement of the supports, resulting in structural deformation—such as upward concavity in the case of ground heave and downward concavity in the case of subsidence. Structural tilting may also occur, accompanied by the formation of severe crack patterns.

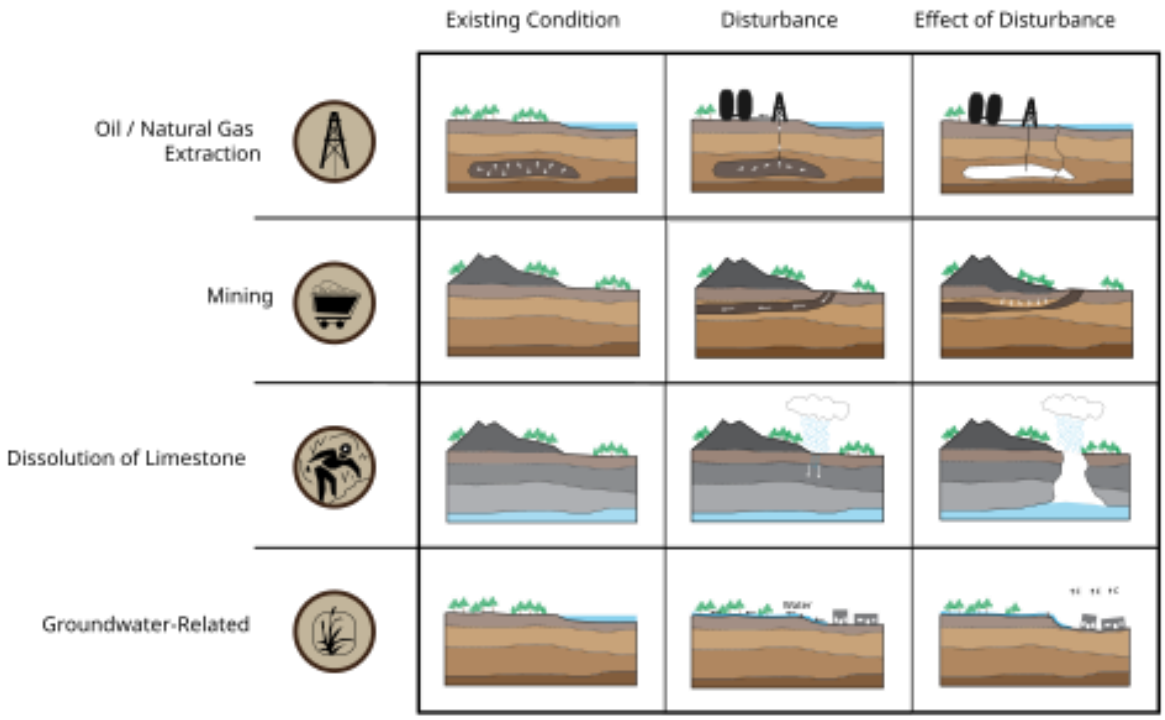

Figure 2:2 - Different factors leading to subsidence (Dickinson P.R. & Thornton N., 2006)

Differential settlement can take various forms, with the resulting crack patterns largely reflecting the specific type of settlement experienced by the structure. This occurs because the structural deformation depends on which support undergoes settlement. For example, if the ends of a structure remain stationary while an intermediate support settles, the building may assume one of two main deformation profiles - a sagging or a hogging profile.

2.2.2. Sagging Profile

This displacement profile is characterized by an upward concavity in the structure due to differential settlement, resulting in crack patterns that are wider at the base and narrower toward the top of the building (Dickinson P.R. & Thornton N., 2006), as shown in Figure 2:3.

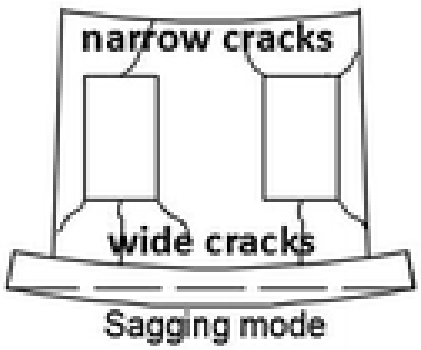

Figure 2:3 - Structure undergoing sagging

2.2.3. Hogging Profile

This displacement profile can be described as a downward concavity in the structure, caused by differential ground heave. The resulting crack pattern is essentially the opposite of that observed in a sagging displacement mode, with cracks wider at the top and narrowing toward the lower levels of the building (Dickinson P.R. & Thornton N., 2006) , as shown in Figure 2:4.

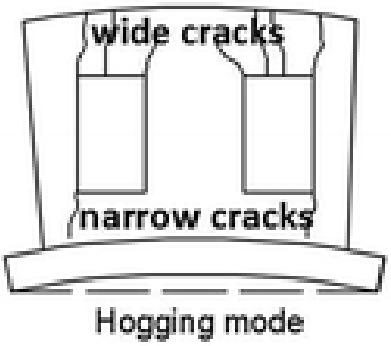

Figure 2:4 - Structure undergoing hogging

2.3. Deformation in Buildings

2.3.1. Classification of Damage

Damage classification bridges the effects of settlement with the severity and type of structural and non-structural damage. By identifying damage patterns, it highlights the nature of settlement—whether uniform or differential—and informs assessment and repair strategies. While extensive research has been conducted on predicting settlement, less attention has been given to classifying damage and understanding its impact on building performance. Despite significant resources allocated to studying soil behaviour and forecasting settlement, the resulting damage to structures remains less explored.

Progress in this area has been relatively limited due to several complex and interrelated factors (Institution of Structural Engineers, 1989). One major challenge lies in the subjective nature of assessing building damage, which is often influenced by individual interpretation. Moreover, serviceability is influenced not only by structural performance but also by the perceptions and responses of building users. Another difficulty arises from the diversity of structures—variations in architectural design, structural systems, and detailing make it challenging to establish universal guidelines for allowable movements. Additionally, the actual performance of structural elements and ground materials may deviate from initial design assumptions due to inaccuracies in predictive models, unforeseen site conditions, or factors beyond the designer's control. Adding to these issues is the fact that structural movements can arise not only from ground settlement or excessive loading but also from factors such as creep, shrinkage, and temperature fluctuations. This is particularly problematic given the limited availability of quantitative data on these secondary effects.

An important consideration often overlooked by engineers is that some degree of cracking is inevitable in structures designed to be economical (Skempton A.W. & MacDonald D.H., 1970). Preventing the formation of these cracks would increase the cost by more than 10% of the total structure cost. This value varies depending on the type of structure (Little M.E.R., 1969). The principle that some cracking

is unavoidable in cost-effective structural design remains relevant today, as modern codes still focus on crack control rather than total prevention. While materials, construction methods, and design expectations have evolved significantly, the trade-off between minimizing cracks and increasing costs continues to apply. However, specific figures from older studies, such as the 10% cost increase, may no longer reflect current building practices or typologies.

Guidelines that help indicate the extent of building damage have been proposed to reduce subjectivity and prevent potential misconceptions (Dickinson P.R. & Thornton N., 2006). Previous research has proposed a damage severity classification system that considers both crack width and ease of repair as equally significant factors in determining the appropriate category. This classification comprises five levels, ranging from 0 (negligible severity) to 5 (very severe), each accompanied by a typical damage description, as shown in Table 2:1. The severity of damage can be classified into three main categories: aesthetic damage, serviceability damage, and structural damage (Burland J. B. & Wroth C. P., 1974).

Category of damage	Normal degree of severity	Description of typical damage (Ease of repair is underlined)
0	Negligible	Hairline cracks less than about 0.1mm
1	Very Slight	Fine cracks which are easily treated during normal decoration. Damage generally restricted to internal wall finishes. Close inspection may reveal some cracks in external brickwork or masonry. Typical crack widths up to approximately 1mm.
2	Slight	Cracks easily filled. Re-decoration probably required. Recurrent cracks can be masked by suitable linings. Cracks may be visible externally and some repointing may be required to ensure weathertightness. Doors and windows may stick slightly. Typical crack widths up to approximately 5mm.
3	Moderate	The cracks require some opening up and can be patched by a mason. Repointing of external brickwork and possibly a small amount of brickwork to be replaced. Doors and windows sticking. Service pipes may fracture. Weathertightness often impaired. Typical crack widths are approximately 5mm to 15mm or several closely spaced cracks > 3mm.
4	Severe	Extensive repair work involving breaking-out and replacing sections of walls, especially over doors and windows. Windows and door frames distorted, floor sloping noticeably[1]. Walls leaning[1] or bulging noticeably, some loss of bearing in beams. Service pipes disrupted. Typical crack widths are 15 to 25mm but also depends on the number of cracks.
5	Very Severe	This requires a major repair job involving partial or complete rebuilding. Beams lose bearing, walls lean badly and require shoring. Windows broken with distortion. Danger of instability. Typical crack widths are greater than 25mm but depends on the number of cracks.

Table 2:1 - Classification of visible damage to walls

This damage classification is predominantly applicable to brickwork, blockwork, and stone-masonry constructions (Burland J.B., 1995). Furthermore, the ease of repair for blockwork and masonry provides a useful guideline for assigning the appropriate damage category. The boundary between Category 2 and Category 3 is particularly fine and sensitive, as there is uncertainty regarding whether the damage is aesthetic or impacts serviceability (Burland J.B., 1995). Serviceability-related damage may result from various movements, such as expansion or shrinkage cracks, moisture or thermal movements, and chemical action. However, it can also be linked to ground movement.

Aesthetic damage in Category 2 typically results in very narrow cracks that can be easily repaired. However, cracks approaching the upper limit of Category 2 may indicate a more serious underlying issue, such as support movement. As a result, distinguishing between Category 2 and Category 3 damage can be challenging. In contrast, damage exceeding Category 3 is typically easier to identify, as it is frequently linked to ground movement. Annex H attempts to define the boundary between these two categories by establishing a limiting value for relative rotation, ensuring that the structure remains within the serviceability limit state. This approach provides a more practical method for identifying the threshold, as well as the likely causes and severity of the structural damage.

Table 2:1 should be used as an indicator of the extent of damage rather than a precise measurement of damage. It is important to note that this table classifies only the visible damage to walls. Additionally, it is crucial to consider how visible damage affects the functionality of the structure. As previously mentioned, the acceptability of damage may vary between structures, as some may be more sensitive to ground movement, affecting their functionality (Thorburn S. & Hutchinson J.F., 1985), as shown in Table 2:2.

crack width mm	degree of damage: dwelling	commercial or public	industrial	effect on structure and building use
≯0.1	insignificant	insignificant	insignificant	none
0.1 to 0.3	very slight	very slight	insignificant	none
0.3 to 1	slight	slight	very slight	aesthetic only.
1 to 2	slight to moderate	slight to moderate	very slight	accelerated weathering to external features
2 to 5	moderate	moderate	slight	serviceability of the building will be affected, and towards the upper bound, stability may also be at risk
5 to 15	moderate to severe	moderate to severe	moderate	
15 to 25	severe to very severe	moderate to severe	moderate to severe	
>25	very severe to dangerous	severe to dangerous	severe to dangerous	increasing risk of structure becoming dangerous

Table 2:2 - Serviceability limits according to building's function

Although these classifications of visible damage provide a useful guideline and serve as an indication for classifying damage, it is important to note that damage assessment should not rely solely on crack widths. This is because a wall experiencing tensile strain may exhibit deformation in the form of one wide crack, which would be considered severe, or multiple narrower cracks, which would be classified as moderate (Boone S.J., 2001). Therefore, the damage classification should serve as an indication of deformation, rather than a direct measure of it. A proper assessment should take into account the structural elements carrying the vertical and horizontal loads, the overall stability of the structure, the nature of the cracking, and whether ground movement is expected to continue (Institution of Structural Engineers, 1989).

Damage can vary widely in severity, from minor cosmetic flaws to serious structural problems. In masonry, the extent and pattern of cracking offer a valuable basis for classifying settlement-related damage. Such damage compromises the durability and serviceability of the structure, potentially causing misalignments, moisture ingress, corrosion of embedded materials, and, if left unaddressed, more severe structural failures. This underscores the importance of early detection, accurate classification, and timely repair to preserve structural integrity over time.

2.3.2. The Concept of Limiting Tensile Strain

Building on Section 2.3.1 focusing on damage classification, this section introduces the concept of limiting tensile strain. Understanding these strain limits is essential for connecting observed damage patterns to the material behaviour that causes them, providing a more precise basis for assessing structural performance and safety under settlement.

The tensile strength limit is also referred to as the critical tensile strength. Once this limit is surpassed, cracks begin to form, compromising the structural integrity of the building. The serviceability aspect is addressed by using the term "limiting tensile strain" (ε_{lim}) to indicate the threshold at which cracks exceed the serviceability limit, allowing for the calculation of the deflection ratio value (Δ/L) (Burland J. B. & Wroth C. P., 1974) (Skempton A.W. & MacDonald D.H., 1970).

In previous research papers, several attempts have been made to provide limiting relative settlements, considering the geometry of the load-bearing walls and the failure profile (sagging or hogging). It is evident that the failure profile and geometry of the wall will influence the distribution and degree of strains. Table 2:3 indicates that load-bearing walls experiencing hogging are more prone to deformations than those subjected to sagging (Burland J. B. & Wroth C. P., 1974), (Institution of Structural Engineers, 1989).

	Meyerhof (1969)	Polshin & Tokar (1957)	Burland & Wroth (1975)
Sagging	1/2500	If L/H < 3, deflection ratio ranges from 1/3500 to 1/2500 If L/H < 5, deflection ratio ranges from 1/2000 to 1/1500	If L/H = 1, deflection ratio is 1/2500 If L/H = 5, deflection ratio is 1/1250
Hogging	-	-	If L/H = 1, deflection ratio is 1/5000 If L/H = 5, deflection ratio is 1/2500

Table 2:3 - Allowable deflection ratio (Δ/L) limits for unreinforced load-bearing walls at the onset of cracking

Even though Table 2:3 provides a useful general guide, it is unsatisfactory for several reasons. The criteria are empirical and based on observations, without providing insights into the causes of damage. Additionally, this criterion is only applicable to conventional materials and structures. Furthermore, the criteria do not encourage designers to consider the details of the structures and finishes, thereby overlooking important aspects of serviceability (Institution of Structural Engineers, 1989).

Burland J. B. and Wroth C. P. (1974) tested the concept of limiting tensile strain by modelling a building as a simple, weightless, equivalent elastic rectangular beam with length L and height H. The deflected shape of the beam is assumed to be known. The mode of deformation does not influence the value of tensile strain; however, it does affect the distribution of strains, as the way in which a building deforms will clearly indicate where tensile strains will arise. Sagging and hogging profiles may lead to either bending deformation, shear deformation, or a combination of both. The primary challenge lies in establishing the deflection criteria for initial cracking once the limiting tensile strain is reached within the beam.

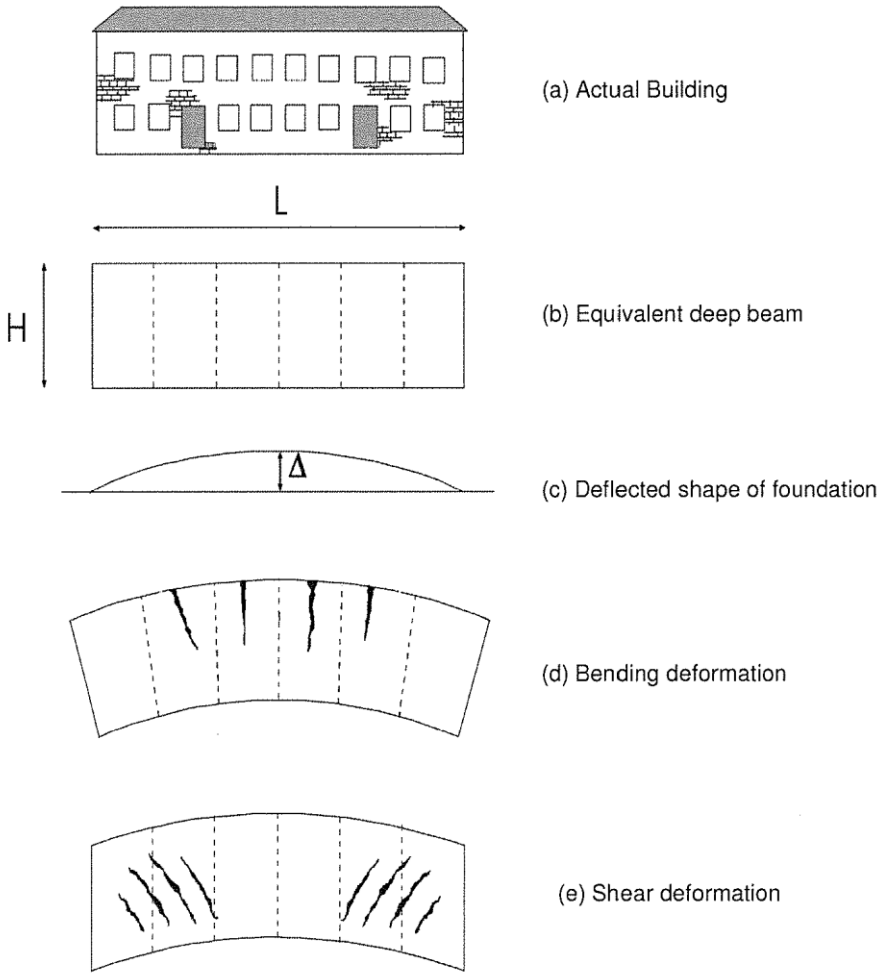

Figure 2:5 - Equivalent Elastic Rectangular Beam

Figure 2:5 clearly shows that the limiting deflection for initial cracking of a simple beam depends on its geometry (length and height) as well as the beam's relative stiffness in shear and bending (Institution of Structural Engineers, 1989).

Bending deformation is characterized by the free rotation of both ends of the beam as well as the supports, resulting in straight cracks at the tensile end that narrow down towards the compression end. On the other hand, shear deformation is characterized by fixed ends of the beam (meaning that the ends are prohibited from rotating), resulting in diagonal cracks oriented according to the bending deformation profile (whether it is sagging or hogging).

Burland J. B. & Wroth C. P. (1974) describe the deformation using the deflection ratio and note that the maximum tensile strain is significantly more influenced by the deflection ratio (Δ/L) than by the exact loading distribution. In fact, they relate the deflection ratio to the radius of curvature (the shape taken by the building during hogging/sagging). It is important to mention that a wall with an L/H ratio greater than 1.5 tends to experience more bending deformation than shear deformation. In simpler terms, a wall with such an L/H ratio behaves as a shallow beam.

Burland J. B. & Wroth C. P. (1974) concluded that hogging deformation is generally more severe than sagging deformation because the neutral axis during bending in hogging tends to be located at the bottom of the beam or wall. In fact, once cracking begins at the top of the wall during hogging deformation, nothing prevents it from spreading downward (Institution of Structural Engineers, 1989).

By combining equations for the bending of deep beams with the critical strain (εc), a relationship was established between the onset of cracking and the beam's geometry (length and height) (Boone S.J., 2001).

Boscardin M.D. & Cording E.G. (1989) also emphasized the significance of horizontal strain (ε_h) in damage initiation. This general state of strain damage criterion is based on the idea that buildings tend to deflect due to a combination of parameters such as relative rotation (β) and lateral strain. Boscardin M.D. & Cording E.G. (1989) established a relationship between relative rotation and lateral strain, which in turn determines the maximum principal tensile strain (ε_p). This relationship is demonstrated by a graph plotting lateral strain vs. angular distortion, as shown in Figure 2:6. An array of such points plotted on this graph represents a constant value of principal strain (ε_p), depicted by boundaries that represent the damage criteria. The damage criterion they developed was initially derived from the strain response of a simple deep beam. Alterations have been made to this damage criterion, resulting in a more generalized form that is based on the state of strain at a point, as shown in Figure 2:7.

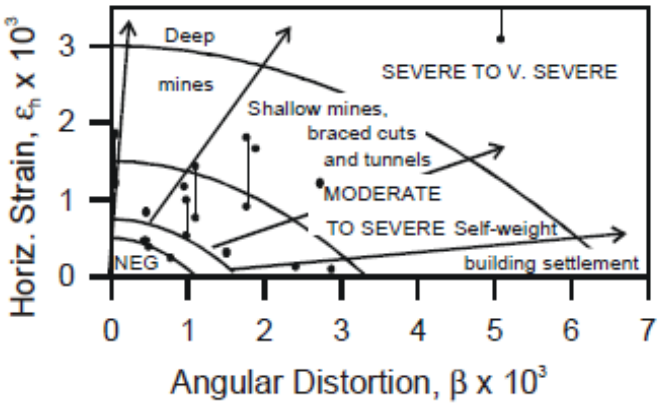

Figure 2:6 - Relationship between angular distortion, horizontal strain, and damage category (Boscardin and Cording, 1989)

In Figure 2:6, angular distortion is defined as the maximum change in slope along the beam or wall, combined with horizontal strains.

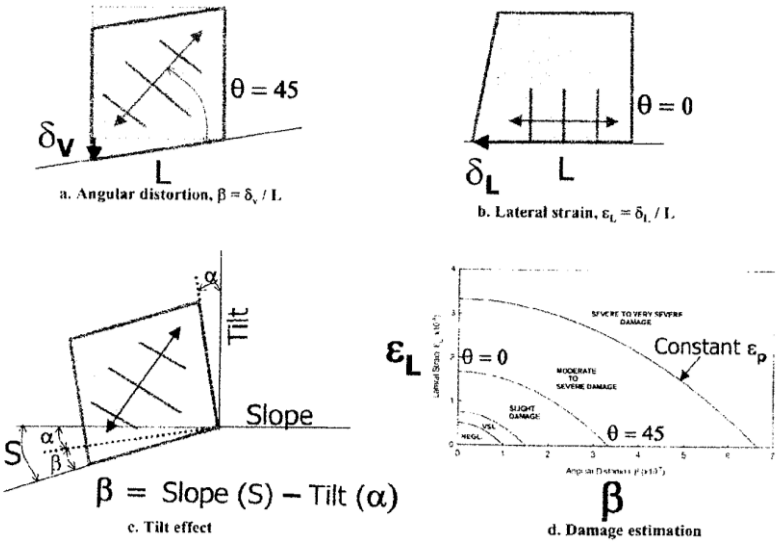

Figure 2:7 - The state of strain/average strain between two points of a building (Son and Cording, 2005)

Timoshenko S. (1947) derived an expression for the central deflection of a centrally loaded beam with unit thickness in both shear and bending. These expressions establish the limiting values of the deflection ratio (Δ/L) for cracking in simple beams by relating the maximum bending strain ($\varepsilon_{b,max}$) and the maximum shear strain ($\varepsilon_{d,max}$). In addition, the resultant limiting tensile strains can be assessed by considering the inclusion of horizontal strain (ε_h).

$$\triangle = \frac{P}{48}\frac{L^3}{EI}\left[1 + \frac{18}{L^2}\cdot\frac{I}{H}\cdot\frac{E}{G}\right]$$

Where E = Young's Modulus, G = Shear Modulus, and I = Moment of Inertia

Equations can be expressed in terms of (Δ/L):

Bending deformation (maximum extreme fibre strain)

$$\frac{\triangle}{L} = \varepsilon_{b(max)}\cdot\frac{L}{12y}\left[1 + \frac{18}{L^2}\cdot\frac{I}{H}\cdot\frac{E}{G}\right]$$

Incorporating horizontal strain (ε_h) yields the resultant extreme fibre strain.

$$\varepsilon_{br} = \varepsilon_{b\,max} + \varepsilon_h$$

Shear deformation (maximum diagonal strain)

$$\frac{\triangle}{L} = \varepsilon_{d(max)}\left[1 + \frac{L^2}{18}\cdot\frac{H}{I}\cdot\frac{G}{E}\right]$$

Introducing horizontal strain (ε_h) will give the resultant diagonal tensile strain.

$$\varepsilon_{dr} = \varepsilon_h\left(\frac{1-\nu}{2}\right) + \sqrt{\varepsilon_h^2\left(\frac{1+\nu}{2}\right)^2 + \varepsilon_{d\,max}^2}$$

When horizontal strain is ignored by setting $\varepsilon_{lim} = \varepsilon_{max}$, the smaller value between the bending and shear deformation equations provides the limiting deflection ratio (Δ/L). This limiting value helps determine the primary deformation mode of the elastic deep beam. Additionally, these equations depend on the beam's geometry (L/H), the modulus ratio (E/G), and the position of the neutral axis. However, as previously discussed, Son M. & Cording E. (2005) generalized this approach by making the strain state independent of L/H, G/H, and the neutral axis position. Instead, it now depends on the average strain between two points in the structure (as shown in Figure 2:7), confirming that relative rotation or angular distortion depends on the relationship between these adjacent points.

In other studies, Burland J.B. (1995) linked lateral strains to the earlier work of Boscardin M.D. & Cording E.G. (1989), adopting different critical strain values and comparing them with the damage categories, as shown in Figure 2:8.

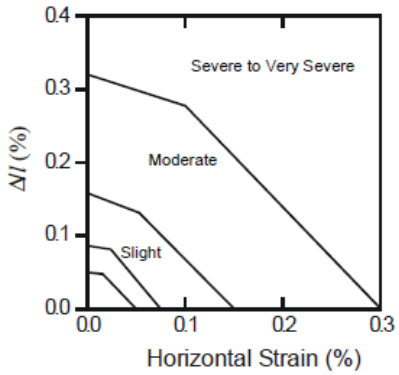

Figure 2:8 - Damage category vs. deflection ratio and tensile strain in hogging (l/H = 1) (Burland, 1997)

In addition, Boscardin M.D. & Cording E.G. (1989) provided a table with the limiting tensile strain values corresponding to all five damage categories, as shown in Table 2:4. This represents an improvement in the classification of damage, as it incorporates not only the visual aspects—such as crack widths and ease of repair—but also the tensile strains developed within the structure that lead to cracking.

Category of damage	Normal degree of severity	Limiting tensile strain (ε_{lim}) (%)
0	Negligible	0 - 0.05
1	Very slight	0.05 - 0.075
2	Slight	0.075 - 0.15
3	Moderate	0.15 - 0.3
4	Severe to very severe	> 0.3

Table 2:4 - Limiting tensile strain for all five categories of damage

Geddes J.D. (1991) contradicted Boscardin M.D. & Cording E.G. (1989) by suggesting that lateral strains in the ground may not necessarily result in horizontal strains in the foundation. As a result, Geddes J.D. (1991) concluded that Boscardin M.D. & Cording E.G. (1989) have overestimated horizontal strain.

Boone S.J. (2001) investigated structural damage by examining the total width of cracks resulting from tensile strain. Boone S.J. (2001) compared the concept of horizontal strain with other indicators such as deflection ratio (Δ/L) and angular distortion (β), using the methods proposed by Burland J.B. (1995) and Boscardin M.D. & Cording E.G. (1989). The study found that both approaches could potentially overestimate or underestimate damage. This is primarily because the methods do not account for different structural systems. Additionally, when cracks are smaller than 7.5 mm, the damage level is typically based only on the largest crack, which introduces a high degree of subjectivity.

Boone S.J. (2001) suggested a strain superimposition method that examines how ground movement affects walls by considering how the walls deform, as shown in Figure 2:9. The main advantages of the strain superposition method are that it does not rely solely on graphical charts depicting modes of deformation; instead, it accounts for differences in building geometry and all modes of deformation. Crack widths are directly calculated, allowing for comparison with damage classification, and the approach enables the evaluation of building distortions using fundamental geometric and engineering principles.

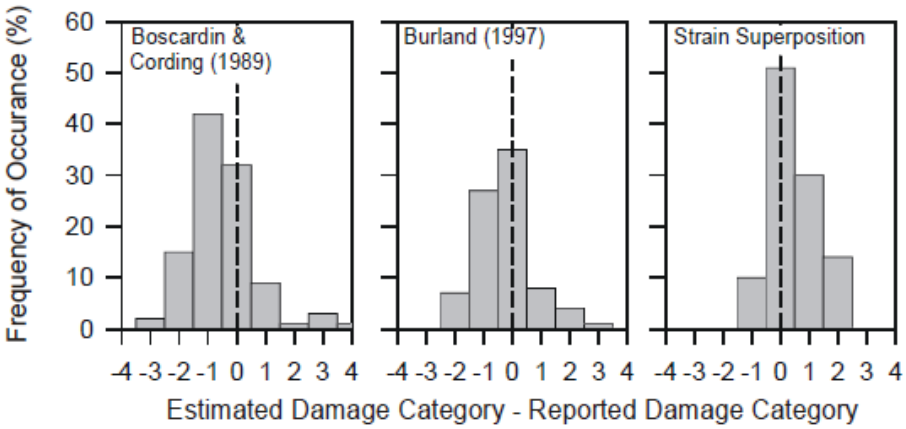

Figure 2:9 - Comparison of the damage category estimation methods

Finno R.J. (2005) added that floors and roofs help hold a building together by making the walls stiffer, as the slabs provide sufficient restraint. Thus, the whole building works as one unit. Son M. & Cording E. (2005) examined how a building's shear stiffness affects ground movement. The more stories a building has, the stiffer it becomes. A stiffer building is more likely to tilt (ω) than to experience angular distortion (β) when the ground shifts. However, as cracks form in the building, the walls become less stiff, making the building more likely to follow the shape of the ground as it settles.

2.3.3. Limit states for Deformation & Foundation Movement (Eurocode 7)

Building on Section 2.3.2, this section examines deformation limit states as outlined in Eurocode 7 Annex H. These limit states provide a practical framework for assessing how strain-induced damage translates into overall structural movement, offering criteria to evaluate performance and serviceability under settlement conditions.

Annex H of Eurocode 7, provides three diagrams featuring three spans supported by four supports, illustrating the displacements, relative rotations, and angles experienced by the structure when the foundations are displaced. This structural behaviour is influenced by several parameters, which are discussed in this section (Skempton A.W. & MacDonald D.H., 1970), (Polshin D.E. & Tokar R.A., 1957), (Institution of Structural Engineers, 1989) and (Burland J. B. & Wroth C. P., 1974). These include;

Rotation/slope (θ) can be described as the change in the gradient of a line connecting two supports due to differential settlement (δ_s) between those points (e.g., AB in Figure 2:10). Differential settlement (δ_s) occurs when the supports of a structure experience different displacement (s).

Angular strain (α) (Figure 2:10) can be described as the difference in gradient between two adjacent spans. As a result, angular strain occurs only in the internal spans. Rotation (θ), angular strain (α), and the length of the spans between the supports (e.g., AB and BC) are all correlated.

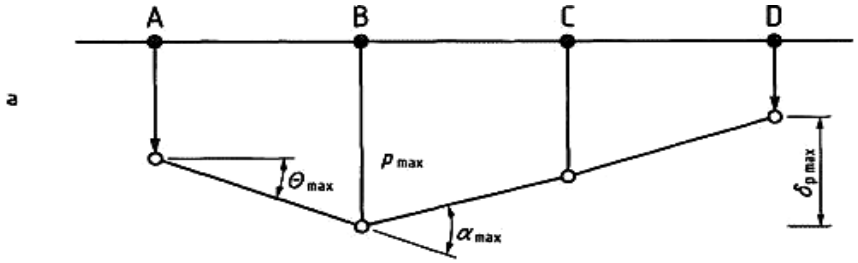

Figure 2:10 - Rotation & Angular Strain (EN1997-1, 2004)

Relative displacement (Δ) (Figure 2:11) can be defined as the displacement of a point relative to a line connecting two reference points on either side. This line typically represents the structure's tilt allowing the calculation of the deflection ratio (Δ/L). The maximum deflection ratio (Δ_{max}) is often used in this context. The curvature of the subsiding structure is related to the deflection ratio.

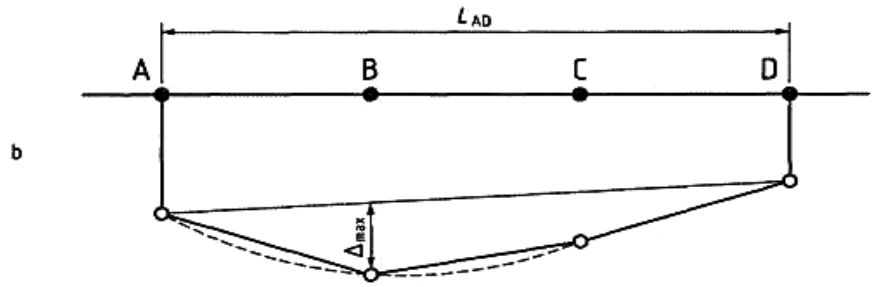

Figure 2:11 - Relative displacement (EN1997-1, 2004)

Tilt (ω) (Figure 2:12) is represented by the angle to the vertical and can be described as the rigid body rotation of the structure induced by the differential settlement of the two farthest end supports (e.g., A and D). It can also be used to describe the tilt of a specific part of the structure (e.g., the tilt of span ABC).

Relative rotation/angular distortion (β) (Figure 2:12) can be described as the rotation (θ) of the line joining two points relative to the tilt (ω). Section 2.3.4 provides further details on this aspect.

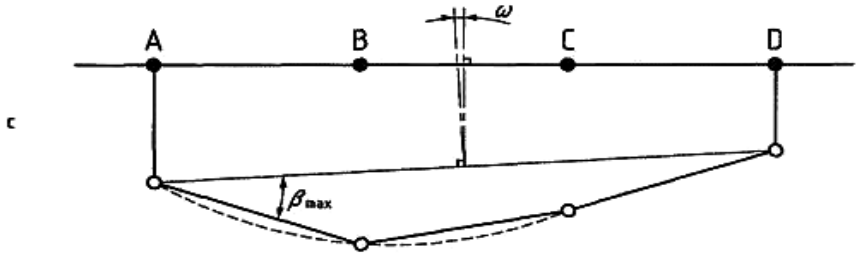

Figure 2:12 - Tilt & Relative rotation (EN1997-1, 2004)

2.3.4. The Relative Rotation Framework (Eurocode 7)

Building on Section 2.3.3, this section introduces the relative rotation framework, which refines the criteria discussed earlier to more accurately characterize the damage a structure sustains from settlement. This framework serves as a practical tool for assessing structural response, deformation, and their impact on the building's integrity.

The relative rotation (β), as defined in Annex H of Eurocode 7, represents a limiting parameter for structural movement. It describes the relationship between rotation (θ) and tilt (ω) experienced by a structure, as shown in Figure 2:13. In his study, Mifsud J. (2012) adopts the same setup outlined in Annex H of Eurocode 7 - comprising three spans supported by four supports—to illustrate how various types of settlement manifest in terms of the parameters specified within the annex. Therefore, this section will use the above-mentioned parameters to explain the structural behaviour based on the type of settlement experienced by the structure.

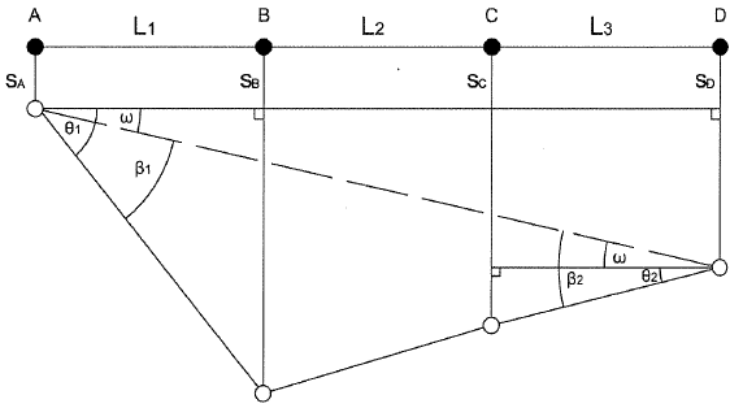

Figure 2:13 - Relationship between relative rotation, tilt and rotation

2.3.4.1 Uniform Settlement

The structure does not rotate or tilt when all of its supports settle by the same amount; hence, there is no differential settlement (δ_s), as shown in Figure 2:14. As a result, the relative rotation (β) is zero, and the limit suggested by the code is not exceeded. However, even in the absence of visible fractures in the structure, the integrity of service connections between the structure and adjacent infrastructure may still be compromised.

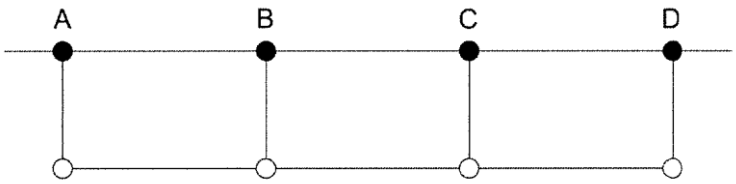

Figure 2:14 - Uniform Settlement

2.3.4.2 Tipping Settlement

Pure tilt is another structural response resulting from differential settlement, where the supports—and therefore the spans—rotate and settle, producing a slope of uniform gradient, as shown in Figure 2:15. In this case, the rotation (θ) of the supports is equal to the tilt (ω) of the structure and thus also equal to the relative rotation (β), such that $\beta = \theta = \omega$. Since no angular strain (α) is generated between the spans, finishes are far less likely to experience fractures. Although the induced rotation may not cause internal movement between different parts of the structure, it may still be uncomfortable or disorienting for occupants. It is important to note that there is a limit to the permissible slope, as excessive tilt can ultimately lead to structural collapse.

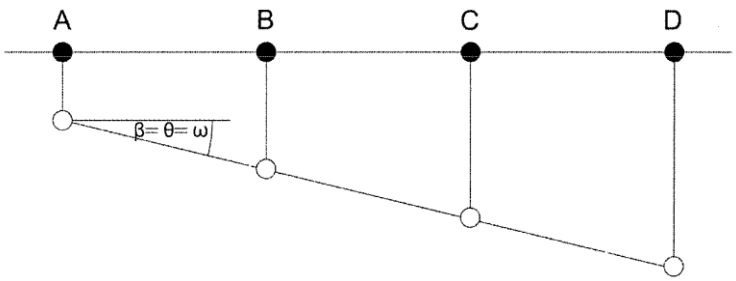

Figure 2:15 - Tipping Settlement

2.3.4.3 Differential Settlement

If only the middle supports were to displace (for instance, B and C in Figure 2:16), the structure would not experience tilting. In this case, the rotation (θ) of the spans is equal to the relative rotation (β), and therefore β = θ. Nonetheless, angular strain (α) is still expected due to the rotation between adjacent spans, and structural elements above the supports are likely to rotate relative to one another, resulting in distortions within the structure and its finishes.

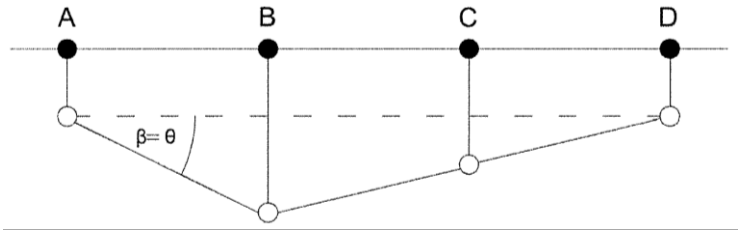

Figure 2:16 - Differential Settlement

Several other combinations of tilt and rotation of the spans and supports can result in a variety of settlement profiles. The deformation experienced by the structure will depend on the specific combination of the aforementioned parameters.

2.3.5. Serviceability Limit State (Eurocode 7)

Building on Section 2.3.4, this section focuses on the serviceability limit state, applying deformation concepts to establish practical limits that ensure a structure remains functional and safe throughout its service life under settlement conditions. A key reference is Annex H of Eurocode 7, which offers detailed guidance on structural deformation and foundation movement. This section discusses the serviceability and ultimate limit state ratios provided by Annex H for various structural systems affected by settlement.

The maximum acceptable relative rotations vary depending on the structural system; however, they typically range from 1/2000 to 1/300 (EN1997-1, 2004), which helps prevent a structure from reaching its serviceability limit state. For many structures, a maximum relative rotation of 1/500 is commonly deemed acceptable (EN1997-1, 2004). On the other hand, relative rotations approaching 1/150 are likely to result in the Ultimate Limit State (EN1997-1, 2004). It is important to note that the above ratios apply specifically to sagging profiles. For hogging profiles, these values should be halved.

Annex H also presents an alternative method for assessing relative rotation, using the ratio of span length to settlement rather than angular measurements. This approach simplifies the definition of limit states and is often easier to interpret. Additionally, Annex H states that these ratios are primarily intended for open-framed structures, infilled frames, load-bearing walls, or continuous brick walls. This brings into question their applicability to local construction methods that utilize blockwork.

In his dissertation, Mifsud J. (2012) investigated the serviceability limit state of local unreinforced blockwork construction through full-scale experiments on a masonry wall subjected to support movement. The study concluded that the maximum allowable relative rotations specified in Eurocode 7 Annex H are conservative, and that factors such as construction techniques and building systems may influence their suitability and applicability.

2.4. Conclusion

The relationship between ground movement and building behaviour is fundamental to understanding settlement and deformation. How a building responds to subsidence and differential settlement depends not only on its structural characteristics but also on the interaction between the soil and the structure. This soil-structure interaction plays a critical role in distributing stresses and determining the extent of deformation and damage. Frameworks such as damage classification, limiting tensile strain, relative rotation, and serviceability limit states are essential for evaluating structural performance. By integrating these concepts with an understanding of soil-structure interaction, engineers can enhance design and assessment practices, mitigate ground-induced deformations and ensuring the long-term safety and serviceability of buildings.

This chapter examines structural behaviour during settlement from a technical and theoretical perspective. Chapter 3 will take a more practical and technical approach, exploring the behaviour and failure mechanisms of unreinforced masonry construction.

3. An Introduction to Unreinforced Masonry Construction

3.1. Brief Overview

Building on Chapter 2, which explored structural behaviour from a specific perspective, this chapter offers essential context on local masonry construction from both practical and technical angles. It begins by examining the composition of local unreinforced masonry, emphasizing the impact of materials, construction methods, and practices on settlement behaviour. The discussion then shifts to a technical analysis of masonry performance under various loading conditions, highlighting common failure mechanisms.

3.2. Composition of unreinforced masonry

3.2.1. Introduction

Understanding the composition of unreinforced masonry is essential for assessing its structural behaviour and performance. This chapter examines the key components of unreinforced masonry walls—namely the masonry units, mortar, construction techniques, and potential construction errors. Each element contributes to the overall strength, durability, and deformation characteristics of the masonry wall. By analysing the interaction between these materials, along with common local practices and variations, this chapter provides a foundational understanding for evaluating the performance of unreinforced masonry, particularly in relation to settlement.

3.2.2. Block work

Locally, the blocks are made from natural globigerina limestone or concrete, whilst the mortar mixture is dependent on the type of block that is used. In this dissertation, the main focus will be on masonry walls constructed from concrete hollow blocks. Concrete hollow blocks come in various types and sizes. Locally, their widths range from 2.5" to 9", with special sizes also available. However, the length (approximately 460mm) and height (around 225mm) remain consistent, as these blocks are often used alongside local limestone masonry. The 9-inch blocks are classified into two types: 'Dobblu,' commonly used for external walls, and 'Singlu,' typically used for internal partitions, as illustrated in Figure 3:1.

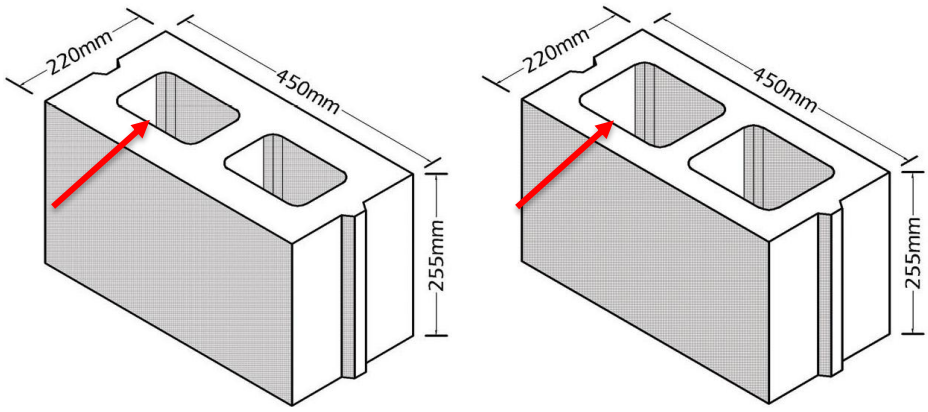

Figure 3:1 - Comparison between 9" 'Dobblu' & 9" 'Singlu' Wall

In masonry construction, blocks are bonded together to form a cohesive structure, distributing vertical and lateral loads across the wall to increase stiffness and resistance to deformation. This is achieved by displacing the vertical joints across successive courses, thus eliminating continuous vertical joints that would otherwise seriously compromise the integrity of the wall as a whole.

Masonry wall construction utilizes various assembly techniques, each tailored to meet specific structural and functional needs. The stretcher pattern, commonly used for half-brick walls or cavity walls, relies on metal ties to secure layers. For greater strength, the English pattern alternates courses of headers and stretchers, creating a robust connection without metal ties. Similarly, the Flemish pattern alternates headers and stretchers within each course, offering enhanced shear resistance and increased stiffness. While English and Flemish patterns are not commonly used locally, they are discussed here for comparative analysis of structural performance. All of the above-mentioned patterns are illustrated in Figure 3:2.

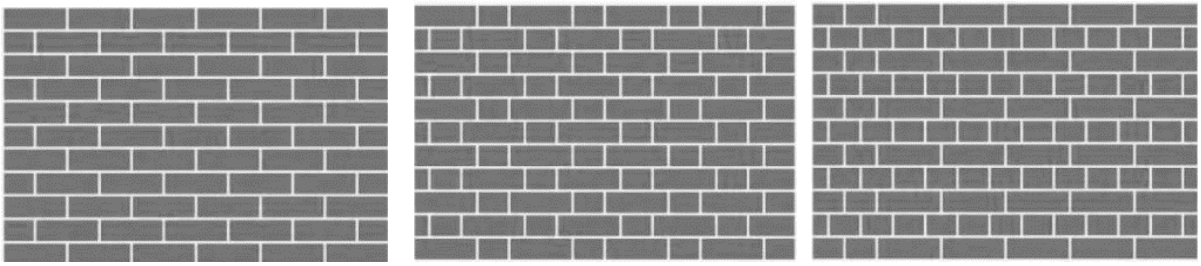

Figure 3:2 - Comparison between Stretcher, Flemish & English patterns of laying

Locally, masonry construction typically employs concrete blockwork arranged in a pattern similar to the Stretcher pattern. Typical concrete blocks often feature tongue-and-groove joints, which improve alignment (Figure 3:3). The use of the stretcher pattern with local blockwork offers a significant advantage: the greater thickness of local blocks, compared to bricks commonly used in foreign countries, provides enhanced shear resistance comparable to that achieved with English or Flemish patterns.

However, despite this thickness advantage, blockwork may exhibit reduced stiffness due to the smaller contact area between units and specific characteristics of local construction practices. Even so, the use of well-laid and level mortar beds helps mitigate movement-related issues. In contrast, walls constructed using English or Flemish patterns are generally thicker, offering superior shear resistance and structural stiffness.

Figure 3:3 - Tongue-and-groove joint at the edges of the block

3.2.3. Mortar

Mortar in masonry construction bonds the units, reduces stress concentrations, and ensures proper load distribution. The mortar is typically designed to be slightly weaker than the masonry blocks, allowing stress redistribution and ensuring that any cracking occurs within the mortar joints rather than the blocks themselves. As the bond between the block and mortar represents the weakest link in masonry, this design strategy helps manage damage, simplifies repairs, and improves the overall durability and flexibility of the structure. The interaction between mortar and block keeps them interlocked, preventing unnecessary failures. Therefore, for optimal structural performance, the mortar must be effective, compatible with the blocks, and durable.

Mortar is generally made from lime and/or cement, aggregate, and water. Lime-based mortars are more flexible and less prone to cracking due to minor structural movements, while cement-based mortars provide greater strength. Locally, lime—commonly known as ‘tajn helu’—is often used for delicate stonework, such as arches. Mortars typically consist of fine limestone sand, cement, and water, creating a soft bed for concrete blocks. Variations may include additives like plasticizers to enhance specific performance characteristics.

Several factors can affect the performance of mortar and, consequently, the overall strength of masonry. Wetting masonry units before laying helps retain mortar moisture and removes loose particles, thereby improving bonding. According to Lynch (1994), other factors influencing wall strength include incomplete filling of bed joints—which can reduce strength by up to 33%—excessively thick joints that may decrease strength by up to 30%, and improper handling during laying. Mifsud J. (2003) also emphasizes that poorly filled vertical joints negatively impact both the lateral and vertical strength of the wall. Additionally, walls should be constructed level and true to line. Wherever possible, newly built walls should be protected from natural elements to preserve their integrity.

Lynch (1994) asserts that both jointing and pointing enhance the quality and durability of masonry. Jointing involves forming the mortar joint by applying mortar to the face of a hollow concrete block, typically using shell bedding. Pointing, in contrast, refers to the finishing of the joint. Once mortar is applied to one block, the subsequent block is placed on top, causing excess mortar to be squeezed out of the joint. This excess mortar is then scraped against the block to create a flush joint as illustrated in Figure 3:4, and the scraped mortar is used to fill any voids within the joint, ensuring even mortar coverage. In the local construction industry, pointing is commonly referred to as "tberfil."

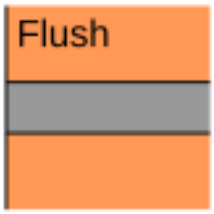

Figure 3:4 - Flush joint finish for the mortar layer

3.2.4. Wall Finishes

Local concrete blockwork is often finished to enhance aesthetics, as the exposed blocks are generally considered visually unappealing. A range of finishing systems can be applied to walls constructed from hollow concrete blocks to improve both appearance and performance. Several common wall finishes are discussed below.

Cladding systems are typically supported at discrete points along the wall, offering increased stiffness but requiring the use of movement joints to prevent cracking, especially in cases of structural subsidence, as shown in Figure 3:5. In contrast, facing materials such as stone or tiles demand continuous support. Unlike traditional plastering or rendering, both cladding and facing systems significantly stiffen the wall. If this added stiffness is not properly accounted for, it can result in excessive deformation and cracking in the backing material—regardless of any corbelling features of the blockwork. A combination of cladding or facing systems with conventional finishes can be applied to both interior and exterior walls. To reduce the risk of cracking and maintain wall serviceability under differential movement, the integration of movement joints between cladding panels is essential.

Figure 3:5 - Cladding systems supported by the masonry wall

Apart from cladding and facing systems, other common wall finishes in Malta include rendering and plastering. These finishes are particularly noteworthy as they provide essential context for understanding serviceability defects in unreinforced masonry walls subjected to settlement.

For external applications, the term rendering is more appropriate than plastering, to avoid confusion with gypsum-based interior finishes. Locally, cement-based renders are the most commonly used exterior wall treatments. These are typically composed of Portland cement as the binder, sand as the filler, and lime as a plasticizer. Such renders also serve as a base for additional surface finishes. The final texture of the render depends on the chosen materials, the tools used, and the skill of the applicator. Popular external finishes include ‘graffiato’ and other coarse-textured renders made from a mix of rough sand, cement, and water, as shown in Figure 3:6. Modern rendering methods may also incorporate fiberglass mesh and flexible additives to improve tensile strength and overall durability.

Figure 3:6 - Rendering of external masonry walls

As previously noted, gypsum plaster is used for internal applications. It is favoured for its smooth finish, ease of use, and quick setting time, as shown in Figure 3:7. Composed primarily of gypsum mixed with water, it forms a workable paste that is spread over internal hollow concrete block walls to create a level surface suitable for painting or decorative finishes. A major advantage of gypsum plaster is its ease of repair—damaged areas can be scraped, patched, and blended seamlessly, making it a highly practical solution for interior walls.

Figure 3:7 - Plastering of internal masonry walls

3.2.5. Construction Process & Errors

When examining local masonry construction, it is important to outline the construction process and highlight common human errors, as these provide essential context and can significantly influence the structural performance of the masonry. Identifying such issues is also critical when selecting an appropriate constitutive model to ensure that the resulting analysis is both valid and reliable.

Construction Process

Before laying mortar, blocks are wetted to improve bonding. Mortar is applied in small amounts along the edges of the course below (face shell bedding), but vertical joints are often left unfilled, which weakens the wall. Long mortar beds are avoided to prevent premature drying and poor bonding. A string line is used for alignment, and blocks are positioned with a hammer and spirit level. Excess mortar is scraped off, sometimes creating voids that are later filled. Blocks of different lengths may be used to adjust the wall's dimensions.

Construction Errors - Issues related to mortar

One of the most common problems in local masonry construction is the use of substandard mortar mixes. These mixes are often inconsistent, with incorrect proportions of constituent materials—most notably, a significant underuse of cement. In many cases, the amount of cement is so low that it is nearly absent, likely due to attempts to make the mix easier to work with by increasing the sand or water content. While this may improve short-term workability, it severely compromises the long-term strength and durability of the wall.

Mortar placement is also frequently inadequate. For bed joints, full bedding is rarely achieved; instead, face shell bedding—where mortar is only applied along the edges of the block—is commonly used, as shown in Figure 3:8. In some cases, even this is poorly executed. Similarly, head joints are often left unfilled, with blocks placed directly against one another without vertical mortar joints, as illustrated in Figure 3:9.

Post-construction, other issues include uneven or excessively thick mortar layers and poorly finished joints, both of which negatively affect the structural performance of the masonry, as shown in Figure 3:9.

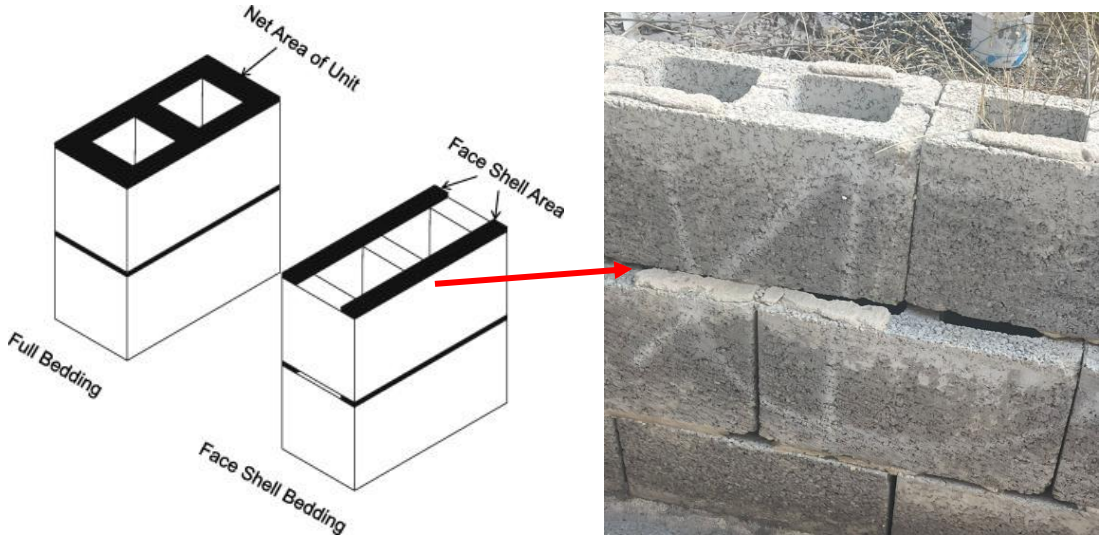

Figure 3:8 - Full bedding & face shell bedding of mortar on the face of the block

Figure 3:9 - Unfilled head joints, uneven mortar coverage & poor jointing finish

After the wall is built, inadequate curing is another critical issue. Without sufficient curing time, mortar does not develop its intended strength, leading to weak bonding, increased cracking from rapid moisture loss, and greater porosity. This increases the risk of water infiltration, efflorescence, and reduced durability. Proper curing is essential to ensure the structural integrity and longevity of the wall.

Construction Errors - Issues related to blocks

On many construction sites, the blocks used are inconsistent in size and shape, which leads to misalignment between courses. This inconsistency can result in the vertical alignment of joints across successive courses, effectively creating weak vertical columns in the wall. Such patterns disrupt the intended load path and compromise the wall's structural capacity, as shown in Figure 3:10.

Additionally, the use of irregular blocks leads to slanted courses and poor overall alignment and levelling, further undermining the strength and visual quality of the masonry structure, as shown in Figure 3:10.

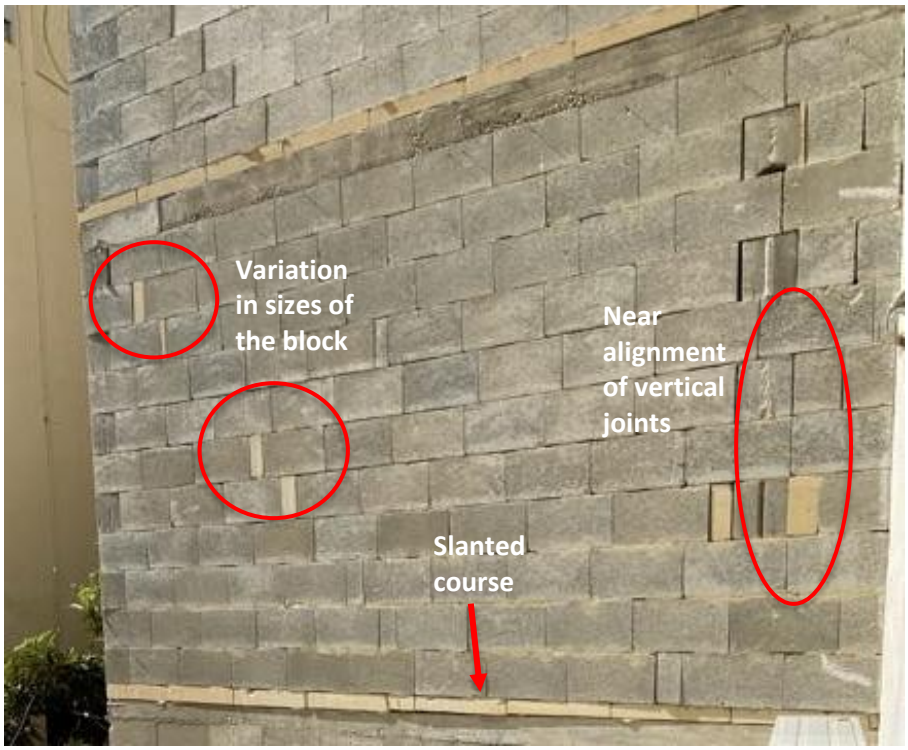

Figure 3:10 - Variation in sizes of the block, slanted courses & near alignment of vertical joints

3.3. Behaviour of Unreinforced Masonry

Building on Section 3.2, this section shifts from a practical overview of masonry construction to a technical analysis of unreinforced masonry behaviour under various loads and load combinations.

Masonry is a composite, anisotropic, and heterogeneous material composed of individual blocks bonded by mortar. These blocks, typically classified as quasi-brittle materials, often exhibit softening—a gradual reduction in mechanical resistance with increasing deformation (D'Altri et al, 2020). Quasi-brittle materials are characterized by two key aspects of their fracture behaviour: (1) failure occurs through fracture rather than plastic yielding, and (2) the fracture process involves a surrounding zone where cracks or damage propagate (Bazant, Z. P., Xi, Y., & Reid, S. G., 1991). The brittleness of these materials leads to the progressive growth of internal cracks, resulting in micro-cracks that diminish overall strength.

Materials such as mortar and clay bricks inherently contain micro-cracks even before loading. In mortar, these micro-cracks typically result from shrinkage during curing and the presence of

aggregates, while in bricks, they arise from shrinkage during the manufacturing process. Locally used concrete blocks also exhibit micro-cracks, often caused by the dry concrete mix employed to minimize the water-to-cement ratio, which frequently leads to small voids within the concrete matrix. Under loading, these micro-cracks initially remain stable but begin to grow as the applied load increases. At peak load, crack growth becomes unstable, resulting in the formation of macro-cracks, which necessitate a reduction in load to prevent uncontrolled propagation.

In deformation-controlled tests, this leads to softening, where cracking localizes in a small region while the surrounding material unloads. This behaviour is well-documented for tensile failure Hordijk (1991), is also observed as cohesion degradation in shear failure (as described by Coulomb friction models), and applies to compressive failure, where it depends on boundary conditions and specimen size (Vonk, 1992) & (Mier, 1984). Data from Vonk (1992) shows that uniaxial compression behaviour is influenced by both local and continuum-scale fracturing processes.

Figure 3:11 illustrates stress–strain diagrams for quasi-brittle materials under uniaxial tension and compression. In general, the compressive strength of masonry is significantly higher than its tensile strength. It is assumed that the inelastic behaviour under both tension and compression is represented by the integrals of the stress–strain curves, defined as tensile fracture energy G_f and compressive fracture energy G_C (Lourenco P. B., 1996). These values are treated as material properties. This unified, energy-based approach is appropriate, as both types of failure stem from the same fundamental mechanism: progressive micro-crack growth.

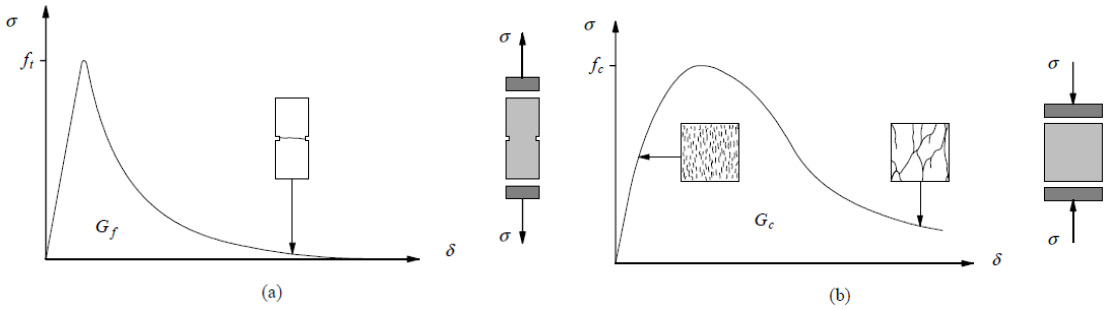

Figure 3:11 - Stress-strain diagrams for quasi-brittle materials under uniaxial tension and compression

Masonry also exhibits a distinct failure mechanism under shear loading, known as Mode II, where slippage occurs at the unit–mortar interface. This shear behaviour is characterised by the Mode II fracture energy, G_{IIf}, which is derived from the integral of the shear stress–strain curve in the absence of normal confining pressure. Shear failure is a critical aspect of masonry behaviour and must be considered in micro-modelling. However, in continuum models—where unit and mortar geometries are not explicitly defined—shear failure is represented indirectly through tension and compression failure within the principal stress space.

It is also important to consider the effect of mortar on the overall behaviour of masonry construction. Research has shown that the mechanical performance of masonry varies depending on whether the masonry units are softer or stiffer than the mortar, as illustrated in Figure 3:12. This was studied by Hilsdorf (1969), who analysed the behaviour of soft bricks and observed that, under compression, the mortar deforms more than the units due to its lower stiffness and the Poisson effect. This deformation causes horizontal compression in the units, as the mortar in the head joints expands laterally.

Additionally, McNary, W. S., & Abrams, D. P. (1985) investigated assemblies composed of stiff bricks and soft mortar. In their uniaxial compression tests, the mortar exhibited greater lateral expansion

than the units due to its Poisson's ratio. However, the lateral expansion of the mortar was constrained by the surrounding units, due to chemical and mechanical bonding at the interface. This interaction induced an internal stress state at the unit–mortar interface, characterised by shear stresses. The resulting stress distribution included triaxial compression within the mortar and both lateral tension and uniaxial compression within the units. As this stress developed, it often led to failure, typically manifesting as vertical splitting cracks.

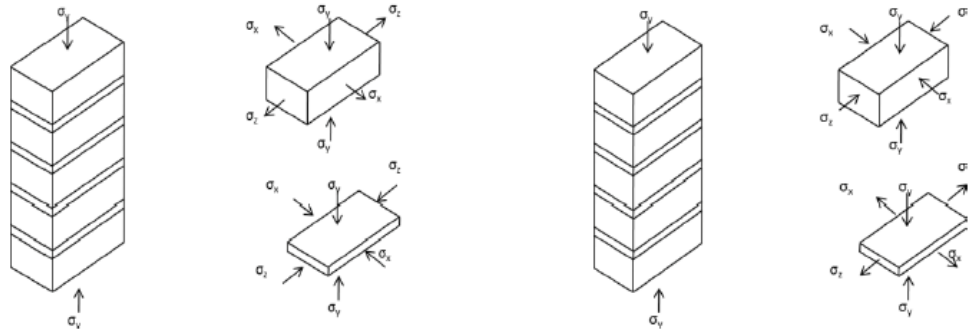

Figure 3:12 - The stress distribution and directions vary depending on whether the mortar or the units are stiffer. In the figure on the left, the units are stiffer, while in the figure on the right, the mortar is stiffer.

Dhanasekar, M., Page, A., & Kleeman, P. (1985) studied the failure modes of brick masonry under various stress conditions, including uniaxial (compression and tension at different angles) and biaxial (compression–compression and compression–tension) stresses. Their findings, illustrated in Figure 3:13, indicate that the extent of the failure surfaces is primarily influenced by the strength properties of the masonry units. In contrast, under tensile or shear conditions, the mortar properties play a more significant role. When tensile splitting or sliding failure occurs, the bonding characteristics of the mortar largely determine the nature and location of the failure surface.

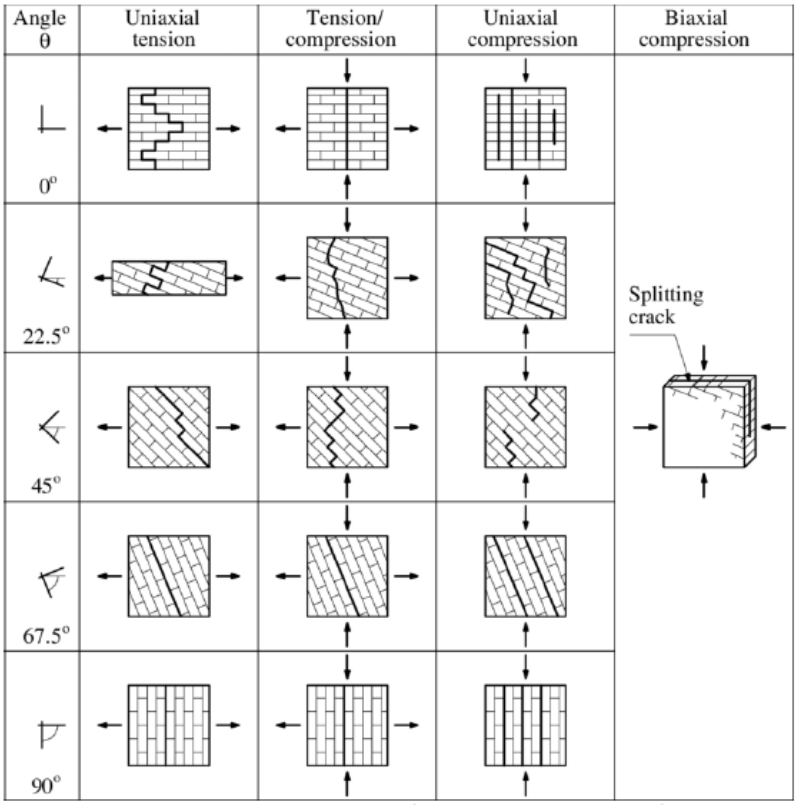

Figure 3:13 - Different failure modes of masonry

3.3.1. Arch Effect Formation & Behaviour

In between two supports, a continuous masonry wall must develop corbelling action, where the lateral displacement of stacked units combines with frictional interaction between them to generate an arching effect. This arching effect relies on compressive stresses, allowing the masonry structure to accommodate greater movement at the supports.

When the masonry wall is supported by a beam (in concrete, steel or timber), studies show that composite action also develops between the wall's corbelled units (Mifsud J. , 2003), (Schembri, 1989). Frictional resistance between the masonry and the beam causes this underlying support element to work like a tie, creating in the process the typical structural arrangement of a tied-arch or deep beam. The wall acts as a compression arch, transferring vertical and horizontal shear stresses to the supports, while the base acts as a tension tie to stabilize the arch, as shown in Figure 3:14. This behaviour therefore challenges the traditional elastic beam models, which do not accurately represent masonry walls

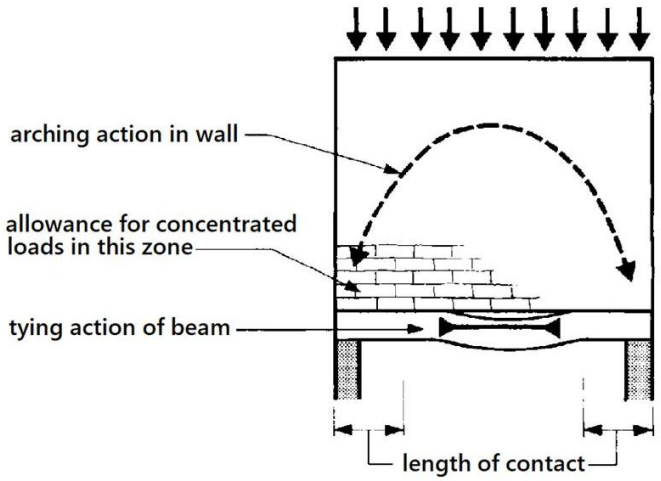

Figure 3:14 - Composite arching action of a wall

Mifsud J. (2003) observed that the lower courses of a wall exhibit no composite action (line loading), but further up, corbelling action on both sides induces an arching effect. This effect depends on the triangulation formed by the thrust lines, support contact length, and the aspect ratio of masonry blocks.

Adding more loads does not alter the corbelling pattern but affects the stresses at contact points. The degree of arching relates to the stiffness ratio between the wall and the beam. As noted by Schembri (1989), a stiffer beam experiences a greater bending moment because it transmits a larger proportion of the load. Smith, S. & Riddington (1977) demonstrated that relative stiffness also influences the contact length and stress distribution, with stiffer beams increasing contact area, thereby reducing stress at the beam-wall interface.

For arching to occur, sufficient horizontal resistance at the wall ends is required to counteract horizontal forces. Rosenhaupt (1962) found that horizontal shear stresses at the beam-wall interface enable composite action. Burhouse (1969) suggested maintaining an H/L ratio greater than 0.3 to prevent slipping and enhance horizontal shear transfer. Hardy, S.J. & Al-Salka, M.A. (1995) emphasised considering the wall-beam interface's coefficient of friction.

In fact, this concept becomes clearer when examining the beam-wall interface: the degree of slippage is entirely governed by the friction between the beam and the wall. This friction provides horizontal restraint, which plays a crucial role in the formation of an arch within the wall. Essentially, the friction at the interface acts as a horizontal reaction force, counteracting the arch's natural tendency to spread at its supports.

This interaction results from the beam working in compression, transmitting inclined compressive forces at its ends. When resolved into components using vector analysis, these inclined forces can be broken down into horizontal and vertical components—the horizontal component being resisted by friction, thereby stabilising the arch formation, as shown in Figure 3:15.

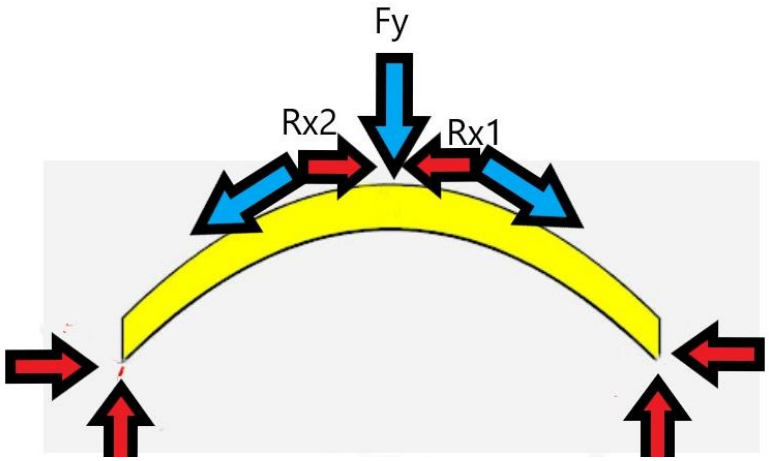

Figure 3:15 - Forces transmitted by the arch (blue) and the corresponding counteracting forces providing stability (red)

A similar principle can be directly observed in traditional Maltese construction, where arches are often built within masonry walls, to form openings. In these cases, the abutments provide the necessary horizontal support to maintain the arch's shape and stability, as shown in Figure 3:16. It is important to note, however, that this comparison is used purely to illustrate the role of lateral restraint. The behaviour of a constructed arch—governed by its thrust line—differs from that of an arch formed within a masonry wall, as shown in Figure 3:17.

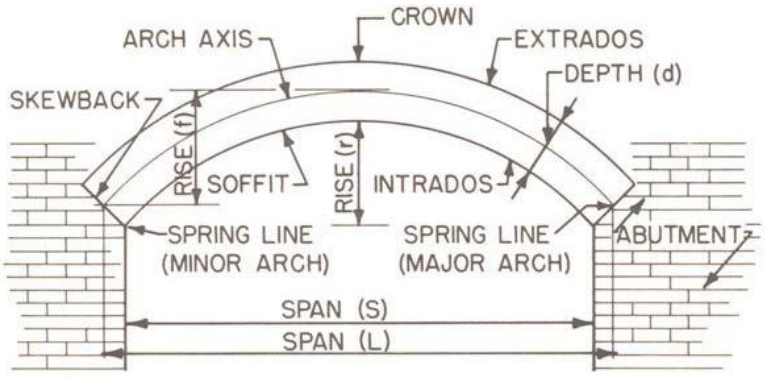

Figure 3:16 - The use of abutments to provide the horizontal support

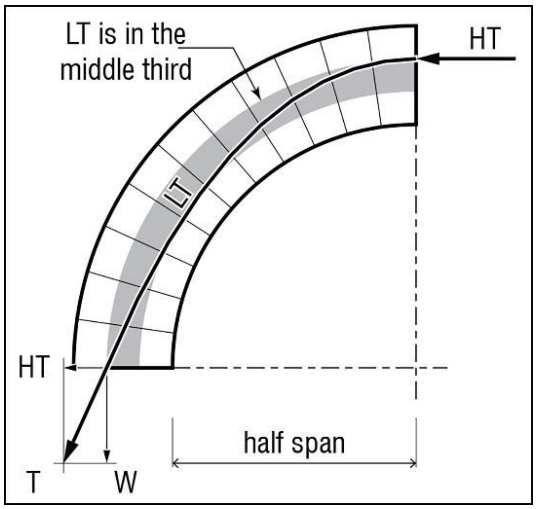

Figure 3:17 - Thrust line determining the stability of an arch

To fully understand the scenario illustrated in the Figure 3:14, it is essential to examine how the arch formed within the masonry wall responds to increasing loads. As the load increases, the horizontal thrust exerted by the arch also increases. At a certain point, this horizontal force may exceed the resisting abutment force or frictional force between the masonry voussoirs and their support. When this happens, the arch begins to spread at its ends and therefore experiences lowering of its upper section, or crown. If this process continues, plastic hinges will form within the arch, eventually leading to instability and collapse, as shown in Figure 3:18.

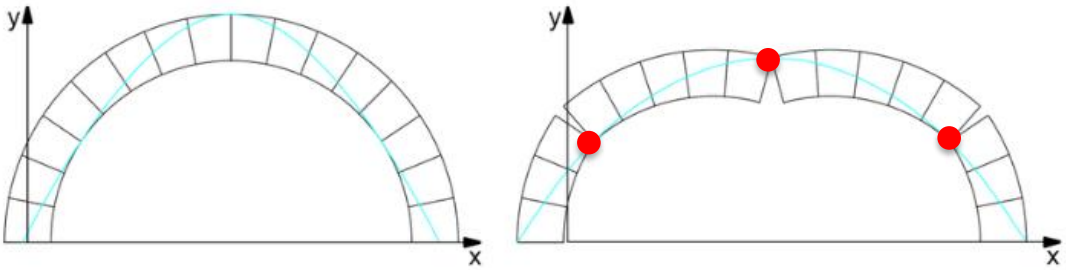

Figure 3:18 - Formation of plastic hinges due to insufficient horizontal restraint

In the case of a masonry wall supported by a beam, Hardy, S.J. & Al-Salka, M.A. (1995) studied the effect of cracks on the loaded masonry wall, concluding that vertical cracks disrupt composite action, transferring the full load to the horizontal member. Mifsud J. (2003) referenced B.S.5977: Part 1 (1981), noting that when arching occurs, the wall's weight on the beam approximates a triangular area defined by mirrored lines starting at the supports and inclined at a 45° angle from the horizontal member.

Research on composite action typically involves wall loading on lintel beams to maximize arching potential. This should be considered when analysing crack formation due to structural movement.

This interaction between the masonry wall and the underlying horizontal support element also plays a key role in determining the wall's in-plane stiffness. Stronger bonds between the masonry units enhance this stiffness, enabling the wall to better resist deformation.

Building on this, it is logical to explore the different failure mechanisms that masonry walls may experience under these conditions.

3.4. Failure Mechanisms in Masonry

Masonry building damage can occur due to either out-of-plane or in-plane failure modes (Oyguc, R., & Oyguc, E., 2017), as shown in Figure 3:19. Out-of-plane behaviour results from forces acting perpendicular to the plane of the wall. Such damage is commonly observed after earthquakes, where out-of-plane failure mechanisms often lead to wall collapse and detachment from the structure (Decanini et al, 2004). Unreinforced masonry buildings are particularly vulnerable to out-of-plane flexural failure due to the lack of sufficient steel reinforcement to resist tensile forces.

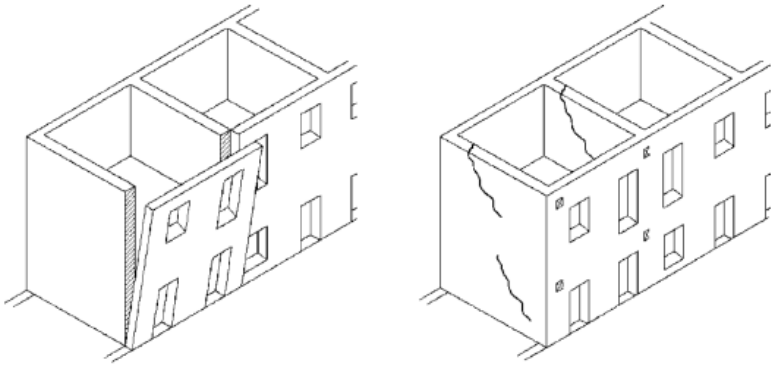

Figure 3:19 - Out-of-plane behaviour to the left and in-plane behaviour to the right

In contrast, in-plane behaviour arises from forces acting horizontally and vertically within the plane of the wall. In-plane failure mechanisms can be categorized into sliding shear, diagonal shear, and flexural failure, with flexural failure further divided into toe crushing and rocking (Oyguc, R., & Oyguc, E., 2017) as illustrated in Figure 3:20. Flexural failure by rocking occurs when the panel wall splits in the tension zone, while toe crushing results in compression zone damage. Sliding shear failure involves the panel wall sliding within its own plane due to horizontal cracks forming along the bed joints. Diagonal shear failure arises from diagonal cracks that develop along the direction of the principal stresses (Calio, I., Marletta, M., & Panto, B., 2005).

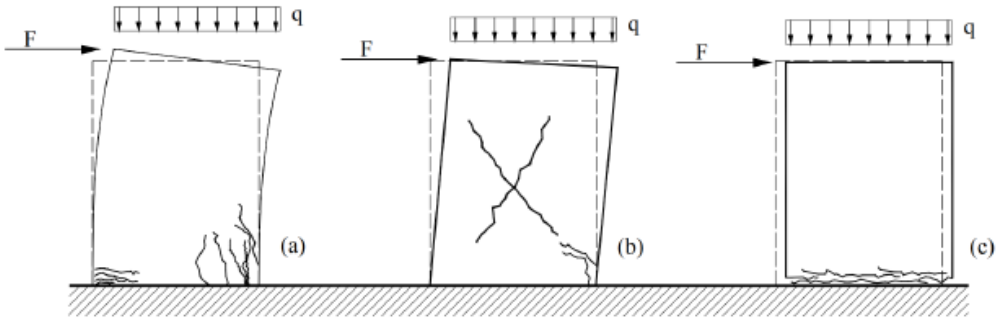

Figure 3:20 - In-plane failure mechanisms: (a) rocking and toe crushing, (b) diagonal shear, & (c) sliding shear failure.

The above examples have shown the failure mechanisms of masonry on a larger scale; however, it is also interesting to analyse the failure mechanisms of masonry on a smaller scale. For instance, if a two-block masonry assembly is considered where two blocks are joined by an intermediate mortar layer, distinct failure mechanisms can occur under tensile, compressive, and shear stresses. The behaviour of two-block masonry couplet depends on the orientation of the applied stresses within the structure. According to D'Altri et al (2020) & Lourenco, (1994) the two-block masonry couplet is susceptible to five distinct failure mechanisms, which are described below and illustrated in Figure 3:21.

One common failure mode is joint tension cracking, which occurs in the mortar joints due to tensile stresses and the constrained deformation of the mortar within the bed joints (Lourenco, P. B., & Rots, J. G., 1997), (Hendry, 1998), as shown in Figure 3:21. This type of cracking reflects the inability of the mortar to accommodate tensile forces without damage.

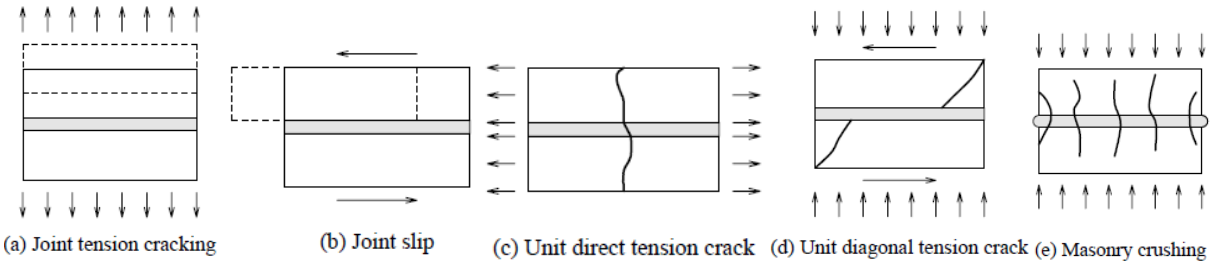

Figure 3:21 - Two-block failure mechanisms

Another important failure mechanism is joint slip, which involves sliding along a bed or head joint under low normal stress (Lourenco, P. B., & Rots, J. G., 1997), as shown in Figure 3:21. In-plane forces, such as those generated during seismic activity, can cause sections of a wall to slide along these weaker planes, particularly when vertical compressive stress and mortar quality are low (Behera, B., & Nanda, R. P., 2021), (Hendry, 1998). This failure mode is more prevalent in the upper portions of masonry buildings, where compressive stresses are reduced compared to the base. Additionally, the risk increases in these areas due to higher acceleration responses during dynamic events (Tomazevic, 2009).

Direct tension cracks typically appear as diagonal cracks that follow the bonding pattern of the masonry, often tracking along horizontal and vertical joints. These cracks may also partially split the masonry units themselves, as shown in Figure 3:21. This failure results from the tensile strength of the masonry being insufficient to resist the principal tensile stresses acting on the wall and is closely related to the material's brittleness (Behera, B., & Nanda, R. P., 2021), (Angelillo, M., Lourenco, P. B., & Milani, G., 2014).

A more severe and sudden failure mode is the diagonal tension crack, which generally occurs under compressive loading (Angelillo, M., Lourenco, P. B., & Milani, G., 2014), as shown in Figure 3:21. When masonry is subjected to uniform compression, tension cracks may develop parallel to the loading axis, indicating imminent failure (Hendry, 1998). This type of crack is particularly dangerous due to its abrupt nature and potential to cause rapid structural compromise.

Finally, masonry crushing occurs when direct tensile stresses cause the masonry units to crack and split, ultimately leading to the separation and collapse of the masonry assembly, as shown in Figure 3:21. This failure mode highlights the importance of tensile stress management within masonry elements to prevent catastrophic damage.

3.5. Conclusion

In conclusion, this chapter presented practical and technical insights into local masonry construction, as well as the general behaviour and failure mechanisms of masonry under various loading conditions. It lays the groundwork for Chapter 4, where the concepts discussed here will inform the modelling process, particularly decisions related to the constitutive model for local masonry construction.

4. Numerical Approach to Masonry Deformation

4.1. Brief Overview

Building on Chapter 3, this chapter shifts focus to the numerical modelling of local masonry construction, examining, from a modelling perspective, the concepts that have been discussed in the preceding sections.

In view of the objectives of this research, the modelling approach used is limited to the finite element method. This is because finite element modelling emerged as the most suitable option among available finite element packages. Its selection was influenced by the complexities associated with alternative packages, time constraints, and other limitations encountered when considering conducting the dissertation through experimental methods.

Different finite element modelling approaches will be discussed, along with the selection of appropriate constitutive models used to represent masonry behaviour. Finally, the limitations and challenges encountered during the modelling process will also be explored, providing a comprehensive understanding of the complexities involved in simulating masonry structures.

4.2. Modelling Strategies

In the past, the behaviour of masonry load-bearing walls was primarily evaluated through experimental testing. Over time, alternative methods have been developed, with numerical modelling emerging as a powerful tool for assessing masonry walls. Numerical modelling is often considered superior to experimentation as it overcomes the boundary limitations inherent to physical models, offering unparalleled flexibility to explore variations in size and number. Moreover, it enables engineers to analyse entire structures rather than isolated elements—an achievement that is nearly impossible through experimental methods (Lourenco, Paulo B., 1994). Numerical modelling is also highly efficient, being less time-consuming, cost-effective, and sustainable. Unlike physical testing, it eliminates the need for construction and demolition, reducing material usage and waste, making it a versatile and environmentally friendly alternative.

In structural engineering, one of the most widely used techniques for such simulations is the finite element method (FEM). FEM simplifies the stress analysis of complex structures by breaking them into smaller elements connected at nodes. These nodes allow displacement in specific directions, depending on boundary conditions and the type of element used. Each node behaves according to a ‘constitutive’ law, which relates stress to strain, and given that adjacent nodes need to satisfy compatibility (they need to move together if the material is to remain continuous), the strain relationships generate a series of simultaneous equations whose solution (in matrix form) needs to satisfy the applied boundary conditions.

For three-dimensional problems, this usually includes six degrees of freedom: translations and rotations along and around the three coordinate axes (Cook, R. D., et al., 2001). FEM supports both linear and nonlinear constitutive laws (and therefore simulations) and can incorporate several different constitutive laws for different materials—mathematical descriptions of material behaviour within the same numerical model.

Masonry structures can also be modelled using the finite element method. There are three main approaches, each balancing accuracy and computational efficiency (Lourenco P. B., 1998). Detailed micro-modelling represents each brick-and-mortar joint as a continuum, with interfaces between units and mortar treated as discontinuities. This method offers high accuracy but demands extensive input data and significant computational resources, as illustrated in Figure 4:1. Simplified micro-modelling reduces complexity by expanding brick units to include mortar thickness, with joints modelled as discontinuous interfaces. This approach lowers computational requirements while retaining critical interaction details, also depicted in Figure 4:1. In contrast, macro-modelling simplifies the structure by treating masonry as a homogenized, continuous material, disregarding the individual distinctions between blocks and joints. Although less detailed, this method minimizes model complexity and is widely adopted for practical applications, as shown in Figure 4:1.

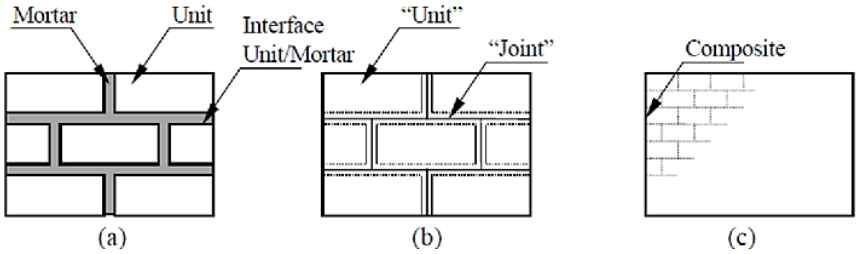

Figure 4:1 - Three modelling approaches; (a) Detailed Micro-Modelling, (b) Simplified Micro-Modelling, (c) Macro-Modelling.

In macro-modelling, joints are effectively removed from the analysis. To maintain geometric consistency, the dimensions of masonry blocks are increased by half the mortar joint thickness in both horizontal and vertical directions. This results in an equivalent material that reflects average stress–strain behaviour of the combined components. Although less precise than micro-level strategies, macro-modelling is particularly suitable when experimental data is limited or when computational efficiency is a priority (Lourenco P. B., 1998).

In macro-modelling, the input parameters required for blocks include geometry, mean compressive strength, configuration, parent material, and classification group. For mortar, only the type and compressive strength are necessary. In contrast, micro-modelling demands additional interface parameters, such as stiffness, dilation angle, and friction, which typically require laboratory testing to obtain.

Ultimately, the choice of modelling strategy involves a trade-off between accuracy and computational efficiency. While detailed micro-modelling provides greater fidelity, it demands significant resources. Macro-modelling, by contrast, offers a practical balance for many applications, especially when used in conjunction with calibrated input data and advanced FEM tools. As numerical methods continue to evolve, they offer structural engineers powerful tools to simulate, evaluate, and optimize masonry performance in a sustainable and cost-effective manner.

The success or otherwise of the numerical model therefore depends on careful choice and formulation of the appropriate material and constitutive models to accurately simulate the behaviour of the masonry construction in hand.

4.3. Elastic vs Plastic Material Model

When performing any kind of numerical modelling, a conscious decision needs to be made in terms of the type of behaviour that the model is allowed to develop and hence replicate. In this respect, the model can simulate elastic behaviour of the materials, or it can go further to allow plasticity (or irreversible deformation) to develop, the latter being much more complex to simulate. The choice between elastic and plastic (or nonlinear) material model behaviour depends on the materials being analysed, the specific objectives of the analysis, the level of detail required, and the available computational resources.

Elastic material models assume a linear stress–strain relationship, meaning that any deformation under load is fully recoverable once the load is removed. A rubber band can serve as an analogy to illustrate the behaviour of an elastic material, as shown in the Figure 4:2. These models are straightforward and computationally efficient, making them well-suited for preliminary design stages or serviceability analyses, such as checking deflections or evaluating natural frequencies (Zhang & Wang, 2012). They are often used in global structural analysis when the structure is expected to remain largely un-cracked or when stress levels are relatively low. However, elastic models have a major limitation: they cannot account for irreversible behaviour such as cracking, crushing, or permanent deformations (Resta et al, 2013). As a result, they tend to overestimate structural capacity under ultimate loading conditions and are unsuitable for detailed failure assessments.

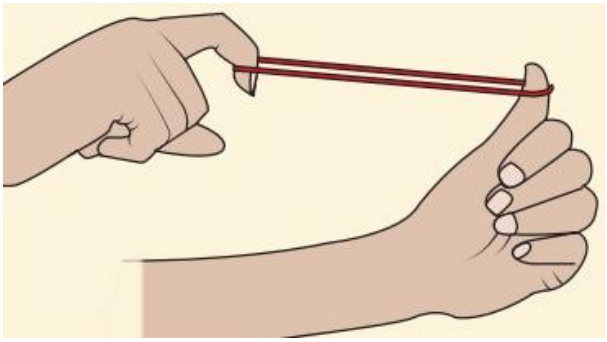

Figure 4:2 - Elastic material (rubber band)

In contrast, plastic or nonlinear material models are capable of representing the complex, inelastic behaviour of masonry under higher stress levels. These models can simulate irreversible deformation and damage mechanisms, such as cracking in tension and crushing in compression, which are typical of masonry under extreme loading or settlement (Zhang & Wang, 2012). Plastic behaviour is often based on classical plasticity theories like the Mohr-Coulomb or Drucker-Prager failure criteria, or on more advanced formulations such as plastic-damage or combined damage-plasticity models (Chisari et al, 2022). They allow for a more realistic assessment of masonry behaviour under ultimate conditions, including seismic events or accidental impact. While these models provide greater accuracy, they also require more computational effort and must be calibrated carefully against experimental data (Resta et al, 2013). This is particularly challenging in the case of masonry due to its heterogeneous and quasi-brittle nature and the limited availability of post-peak data (Resta et al, 2013).

The theory of plasticity, originally developed for metals, offers a framework that can be partially adapted to simulate the inelastic behaviour of masonry (Resta et al, 2013). In this context, the hardening law, plastic potential, and flow rule play important roles. The hardening law describes how

a material evolves after yielding, as shown in Figure 4:3. While metals typically exhibit hardening—gaining strength with continued deformation—masonry tends to soften as cracks develop (Meccanica, 2017). Thus, a modified hardening law is employed to represent the gradual loss of strength in masonry as damage accumulates (Meccanica, 2017). This is particularly relevant in simulating wall behaviour during differential settlement.

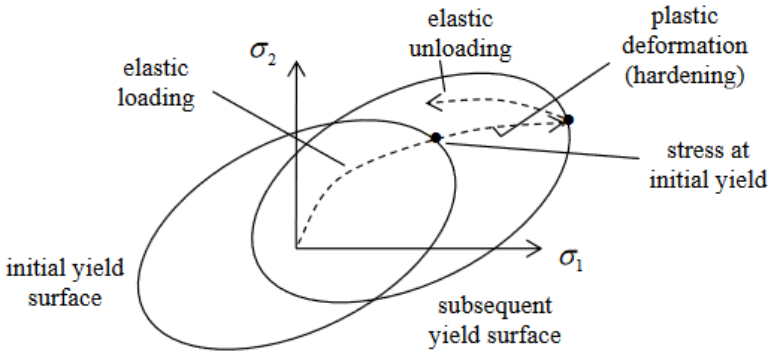

Figure 4:3 - The Hardening Law (Evolution of material after yielding)

Plastic potential is a mathematical concept used to determine the direction in which the material deforms once it yields.

The flow rule defines how plastic strain grows—both in magnitude and direction—after the material has yielded. There are two main types: the associated flow rule, where the plastic strain direction is normal to the yield surface, and the non-associated flow rule, where the strain direction is governed by the plastic potential function (Chisari et al, 2022), as shown in Figure 4:4. In materials like masonry, which behave differently in tension and compression and include frictional interactions between units and mortar, a non-associated flow rule is commonly applied (Chisari et al, 2022). This means the direction of plastic strain is not normal to the yield surface but is derived from a separate plastic potential function, as shown in Figure 4:4. Such an approach is more suitable for materials with non-symmetrical or complex deformation patterns .The latter is often preferred for masonry and similar materials because it yields more realistic results, especially by avoiding overestimation of volume change (dilation) during shear (Chisari et al, 2022). A useful analogy is pressing a sponge—depending on its internal structure and shape, it may deform in directions not aligned with the applied force. In masonry, this helps simulate how cracks propagate or how mortar joints slide as the structure adjusts to settlement (Chisari et al, 2022).

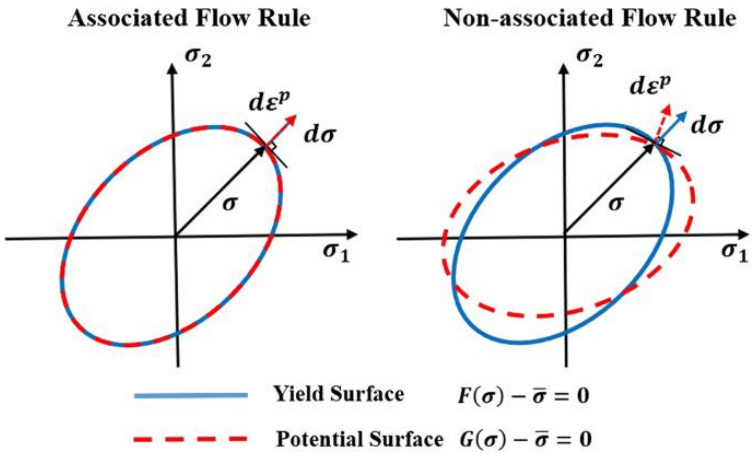

Figure 4:4 - a) Associated Flow Rule, b) Non-Associated Flow Rule

Despite the usefulness of plasticity theory, there are inherent limitations when applying it to masonry. Masonry is a composite and heterogeneous material composed of discrete units and mortar, and its behaviour is quasi-brittle, particularly under tension (Chisari et al, 2022). Classical plasticity models may not adequately capture features such as anisotropy, cracking patterns, and post-peak tensile behaviour (Meccanica, 2017). To improve accuracy in such cases, the theory of plasticity is often used in conjunction with Continuum Damage Mechanics (CDM) or Discrete Element Models (DEM), which offer enhanced modelling of damage evolution and the interaction between masonry components (Meccanica, 2017), (Zhang & Wang, 2012).

In summary, elastic models are appropriate for simplified analyses where masonry remains largely un-cracked, while plastic models provide a more realistic depiction of masonry under complex or extreme conditions. Adapting the theory of plasticity—through modified hardening laws, non-associated flow rules, and tailored plastic potential functions—enables more accurate modelling of the behaviour of masonry structures as a building experiences foundation settlement, cracking, and other nonlinear behaviour in masonry structures. However, due to the unique and brittle nature of masonry, additional modelling strategies may be necessary to fully capture its structural performance.

4.3.1. Choice of the Constitutive Model

At the core of both elastic and plastic models lies the constitutive model, which describes how materials respond mechanically under various loading conditions. Constitutive models are typically defined through stress–strain relationships, conservation laws, and kinematic constraints. The selection of a suitable constitutive model for masonry depends on its composition and failure mechanisms, which are complex and direction-dependent (Chisari et al, 2022). Unlike homogeneous, isotropic materials such as steel—where well-established laws like Hooke's Law and the von Mises yield criterion can accurately model behaviour across elastic, plastic, and strain-hardening ranges—masonry displays highly nonlinear and anisotropic behaviour, cracking in tension, crushing in compression, and behaving differently in shear (Meccanica, 2017), (Chisari et al, 2022).

Masonry, composed of blocks and mortar, presents significant modelling challenges due to its nonlinear, anisotropic behaviour and the interaction between its components. Because it is difficult to represent this behaviour with a single constitutive model. This would require a material model capable of capturing all stress states. This task is challenging due to the limited availability of comprehensive experimental data, particularly for specific construction methodologies like the local hollow concrete block masonry construction, as most studies have historically focused on clay bricks. Additionally, variability in material composition, workmanship, and construction detailing further complicates the validity of the modelling process. As a result, numerical models based on limited or generalized data often fail to fully capture the behaviour of specific masonry systems, making additional testing or the application of reverse analysis techniques essential.

Material homogenization techniques have become increasingly common to simplify macro-level modelling by treating masonry as a continuum with averaged properties, avoiding the need to model individual blocks and mortar joints. This approach also facilitates adaptation to different block sizes and mortar thicknesses without new testing campaigns. However, obtaining reliable equivalent material properties can be difficult, as individual component behaviours often change when combined, necessitating reverse analysis based on observed structural behaviour.

In practice, various modelling strategies have been employed. The direct approach, for example, uses empirical stress–strain data derived from experiments to inform numerical models. This can yield models that replicate observed behaviour well, but the specificity of test conditions often limits the generalizability of the results. Researchers such as D'Altri et al (2020) and Lourenco P. B. (1996) have highlighted these limitations and the difficulty in establishing universal constitutive laws for masonry. Moreover, treating masonry as a layered material, isolating vertical and horizontal joints, is a simplification strategy sometimes used to address its heterogeneous nature.

Challenges also arise in modelling failure surfaces and material softening, which can introduce numerical instabilities similar to those seen in materials like soft clay. Proposed solutions, such as elliptical failure surfaces, may reduce numerical issues but can also overestimate strength in certain stress regions, thereby introducing new sources of error. Additionally, the real-world variability in construction, such as inconsistent joint thicknesses and uneven block strengths, further complicates modelling efforts. These irregularities can significantly lower actual wall performance compared to numerical predictions, meaning that even accurate constitutive models may fall short if construction quality is poor.

This section emphasizes the importance of constitutive models in capturing masonry's nonlinear behaviour. Despite challenges such as material variability, techniques like homogenization and macro-modelling simplify the process. Frameworks like DDMaS (2021) (elaborated in Chapter 5) align with Eurocodes to balance computational efficiency with accuracy. The masonry add-on includes isotropic and orthotropic models to address masonry's complexities, detailed in the next section.

4.3.2. Isotropic Material Model

An isotropic material is defined as a material that exhibits the same properties in all directions. This is evident from the typical stress-strain diagrams provided by RFEM6, as shown in Figure 4:5.

For analytical purposes, masonry structures are often simplified as isotropic materials with no tensile strength. This idealized and conservative assumption can significantly simplify preliminary structural analysis, especially when material properties, such as tensile strength, are uncertain (D'Altri et al, 2020).

The rationale behind this approach is that masonry typically exhibits very limited tensile strength compared to its compressive strength, with tensile-to-compressive strength ratios often below 0.1 or even lower. While minor tensile stresses may exist locally, masonry generally behaves in a linear elastic manner up to 80–90% of its compressive strength (Angelillo, M., Lourenco, P. B., & Milani, G., 2014).

However, this "no-tension" assumption has its limitations. It cannot account for plastic or post-peak behaviour, as it models masonry as an entirely elastic material. As a result, it is unsuitable for simulating seismic responses and may inaccurately predict failure modes, given that masonry does possess some tensile strength.

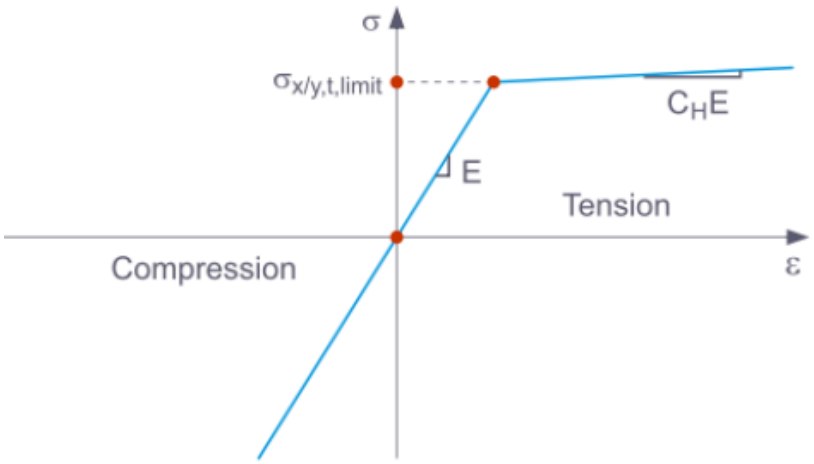

Figure 4:5 - Typical stress-strain diagram for Isotropic plastic constitutive model for masonry (RFEM6)

4.3.3. Orthotropic Material Model

An orthotropic material is defined as a material that has symmetric properties in two or three mutually perpendicular planes. Masonry construction can be described by orthotropic behaviour using a composite yield criterion, which adapts concepts from isotropic quasi-brittle materials. The Rankine criterion governs tensile behaviour (cracking in the masonry) (Lourenco P. B., 1996), while the Hill criterion governs compressive behaviour (crushing of the masonry) (Lourenco P. B., 1996), resulting in a combined yield surface, as shown in Figure 4:6. Both the Rankine and Hill criteria will be discussed in greater detail later in this section.

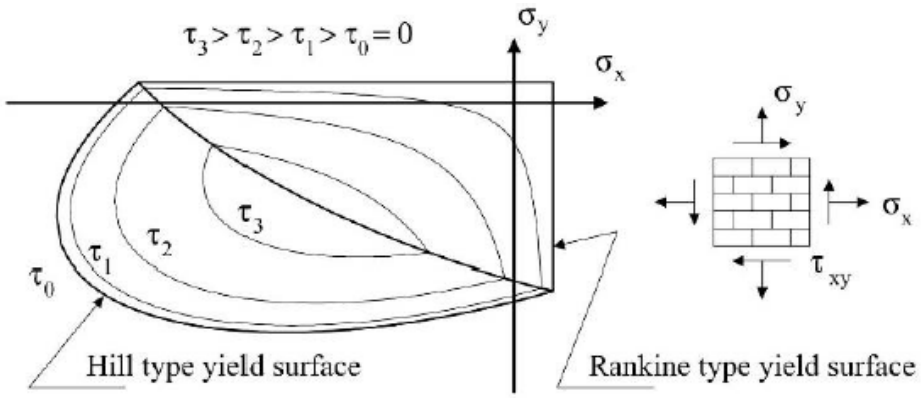

Figure 4:6 - Proposed composite yield surface with iso-shear stress lines. Different strength values for tension and compression along each material axis.

Orthotropic materials, also considered as non-linear materials, tend to have complex stress-strain relationships and are dependent on the material's loading history. The typical stress-strain diagram for a material exhibiting orthotropic behaviour is shown in Figure 4:7. Therefore, solving such problems requires an iterative approach, where equilibrium is checked at each step to ensure the material's behaviour follows its constitutive laws. In some cases, the problem's complexity or multiple possible solutions may require applying loads in small increments to find a solution (Lourenco P. B., 1996).

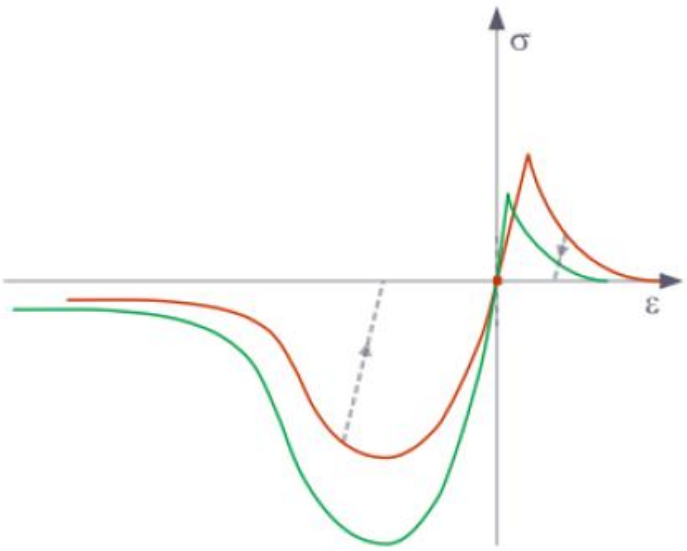

Figure 4:7 - Typical stress-strain diagram for orthotropic constitutive model for masonry (RFEM6)

The Newton-Raphson method addresses this challenge by applying loads incrementally and updating the material's tangent stiffness at each step to find a convergent solution. This method allows for constructing a load-displacement curve, showing how the material deforms under increasing loads (Cook, R. D., et al., 2001). Newton Raphson is a standard convergence technique that is used in models of this kind.

The main advantage of this material model is that it recognizes the fact that no single model can fully capture all failure modes of masonry. Thus, this model combines two models to address different aspects. The main disadvantage of this combined approach is the occurrence of points of singularity. The method assumes specific failure mechanisms for compression and tension, such as micro-level crack growth, and incorporates internal damage modelling through fracture energies in both tension and compression. This creates an energy-based model that effectively captures material behaviour (Lourenco, P. B., Rots, J. G., & Blaauwendraad, J., 1995).

The Rankine yield criterion faces difficulties when representing softening (damage) in the material. Traditional models assume isotropic (uniform in all directions) softening, but this does not fully capture how materials like masonry behave under stress, especially since softening in masonry is not uniform in all directions. A more accurate model involves "kinematic softening," which shifts the yield surface (the limit of the material's strength) in the direction of the first principal stress (the primary direction of stress). While kinematic softening improves the model, it is still not entirely realistic. For example, after a crack form in one direction, the material behaves almost plastically (permanently deformed) when loaded in the perpendicular direction (Lourenco P. B., 1996).

To avoid instability, a simpler approach is used: a single scalar value controls the softening behaviour along the two material axes. This method still considers two different fracture energies (the energy required for cracking in each direction) but leads to a more stable and practical algorithm, even if it’s less physically accurate (Lourenco P. B., 1996).

The Hill yield criterion models the material behaviour with parabolic hardening (strengthening as the material is loaded) followed by parabolic/exponential softening (weakening after the peak strength) in both stress-strain diagrams. After softening, the material reaches a residual plateau (where the material behaves plastically without further hardening). The compressive fracture energy (how much

energy the material can absorb before breaking) is defined separately for each material axis. The peak strength is assumed to be the same in both directions (isotropic hardening), followed by softening that depends on the fracture energy in each direction (anisotropic softening) (Lourenco P. B., 1996).

4.4. Conclusion

In conclusion, this chapter establishes a solid foundation for the numerical modelling approach, emphasizing the importance of modelling strategies and constitutive models in accurately capturing masonry behaviour and deformations. A clear understanding of these concepts is essential for reliably representing masonry's structural response. The insights from this chapter will directly inform the decision-making process in the Chapter 5, where these principles are applied to simulate the behaviour of local masonry structures.

5. Methodology

5.1. Brief Overview

This chapter outlines the methodology used to model an apartment block of the type referenced in Chapter 1. It begins by outlining the modelling parameters, providing the reader with a clearer understanding of the modelling methodology, followed by a detailed explanation of the modelling process.

Rather than modelling the full structure from the outset, the approach involved breaking the apartment block down into smaller, manageable stages. Each stage served as a step toward the final model, allowing for a structured and incremental development of the numerical analysis.

The chapter also discusses the challenges encountered at each stage and the decisions made to address them. This step-by-step progression facilitated a deeper understanding of the modelling software while maintaining control over the number of variables involved. By gradually increasing the complexity, the process ensured a clearer interpretation of results and a more reliable assessment of the model's behaviour.

5.2. Modelling Parameters

This section focuses on the parameters used during modelling and the choices taken during the modelling process. The information discussed below is in general and refers to the modelling of every structure, as these aspects have been used to model every structure.

Constitutive Model

Based on the discussion in Section 4.2, adopting a macro-modelling approach is a practical choice considering time constraints, the level of expertise, and the complexities associated with micro-modelling. The primary objective of this dissertation is not to achieve absolute precision but to demonstrate a solid understanding of the topic and propose practical solutions. This approach emphasizes key issues without becoming overly entangled in intricate details.

The masonry add-on provided by RFEM6, based on the Digital Design of Masonry Structures (DDMaS, 2021), plays a crucial role in modelling local masonry construction. The DDMaS framework integrates advanced digital tools to enhance masonry design and analysis, addressing challenges such as anisotropic behaviour and nonlinear responses. By employing macro-modelling techniques, it simplifies computations by treating masonry as a homogenized material while maintaining accuracy. The framework adopts a nonlinear elastic-plastic constitutive model, as described by Lourenço (1996), which combines tensile and compressive criteria to realistically simulate elastic, plastic, and failure behaviours. Furthermore, DDMaS aligns with international standards and has been validated through experimental and normative comparisons, ensuring robust and reliable applications in masonry design.

Selecting an appropriate constitutive model for masonry behaviour was challenging due to the difficulty of accurately representing its complex characteristics. The masonry adds-on provides isotropic and orthotropic modelling options, but masonry exhibits neither purely orthotropic nor isotropic behaviour. The orthotropic model, treats the masonry wall as an elasto-plastic system, providing a more accurate representation of its inherent anisotropy and directional variability compared to isotropic models, which assume uniform behaviour in all directions. This is particularly

important when considering the construction practices and errors in Maltese masonry structures, as discussed earlier. The adoption of isotropic models could produce results that deviate significantly from real-world performance, potentially leading to overestimations. Selecting a constitutive model often involves balancing realism with practical approximations to capture masonry's behaviour and failure mechanisms as accurately as possible.

Therefore, based on the preceding discussion, as well as the insights highlighted in Section 3.2 and Section 4.3, an orthotropic constitutive model emerges as the most suitable choice for simulating local masonry construction, as shown in Figure 5:1.

As shown in the Basic Material Properties on the right-hand side of Figure 5:1, the mass density value was obtained from local hollow concrete block manufacturers (Attard Bros.) (see Appendix E), while the remaining values were left as default, as recommended by the software.

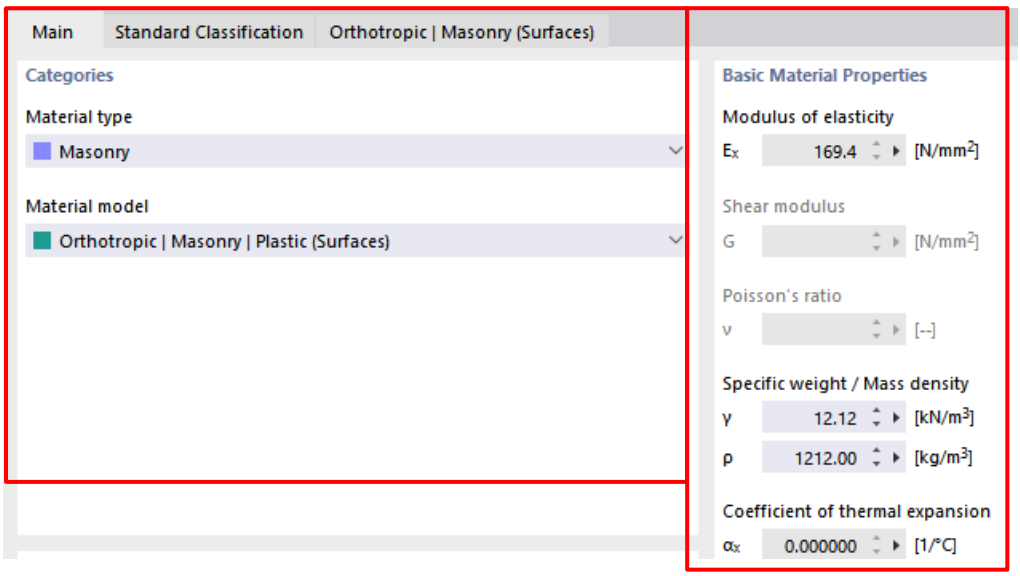

Figure 5:1 - Screenshot from RFEM6 showing the Orthotropic Material Model

The data for local masonry construction in Malta were manually input, as illustrated in Figure 5:2. It is important to emphasise that the parameter values required by the program were not arbitrarily selected but logically deduced. For instance, within the brickwork section, values were derived from EN 1996-1-1, while the mortar parameters were informed by construction practices and errors previously discussed in Section 3.2, leading to the selection of the weakest mortar. Similarly, the stone section parameters, including hollow concrete block dimensions and normalised mean compressive strengths, were sourced from manufacturers' data sheets (Attard Bros., Appendix E), whereas the horizontal compressive strength was estimated based on informed assumptions. Finally, certain options such as the partial factor were left at default, while filled head joints were deselected, reflecting the construction practices outlined in Section 3.2.

Hollow concrete blocks were used in the construction of all structures discussed in the following sections, with the exception of Ta' Kenuna Tower, which is built from local globigerina limestone blocks. Consequently, the parameters shown in Figure 5:2 vary slightly. The brickwork parameters were again derived from EN 1996-1-1, while the basic block dimensions in the stone section were measured directly during the site visit, as the tower is an older structure and its blocks are slightly larger than those typically used today. The remaining parameters within the stone, mortar, and options sections were retained as those defined for hollow concrete blocks, as illustrated in the Figure 5:2.

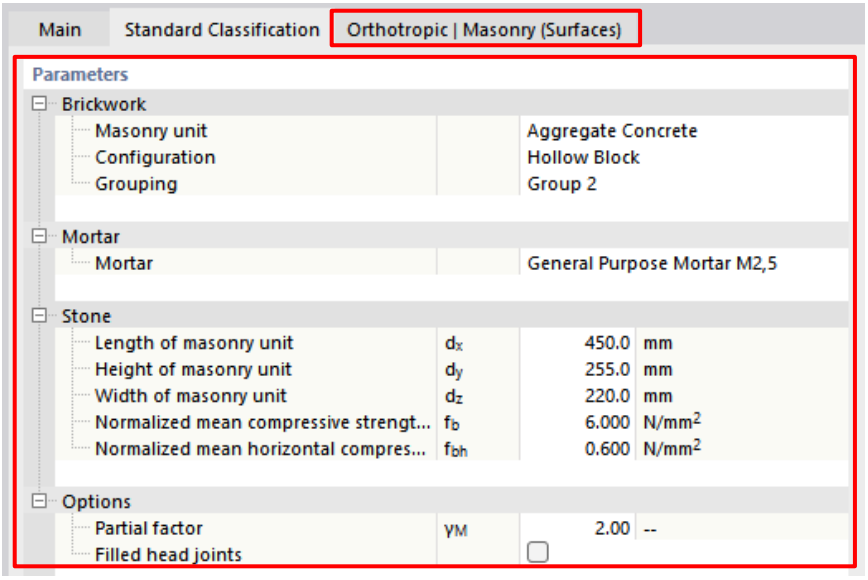

Figure 5:2 - Screenshot from RFEM6 showing the data input interface for an Orthotropic Material Model

After entering the above-mentioned properties of the mortar and block, the program automatically computed specific behavioural characteristics for the resulting homogeneous material, as shown in Figure 5:3. These properties represent an average of the combined block and mortar attributes.

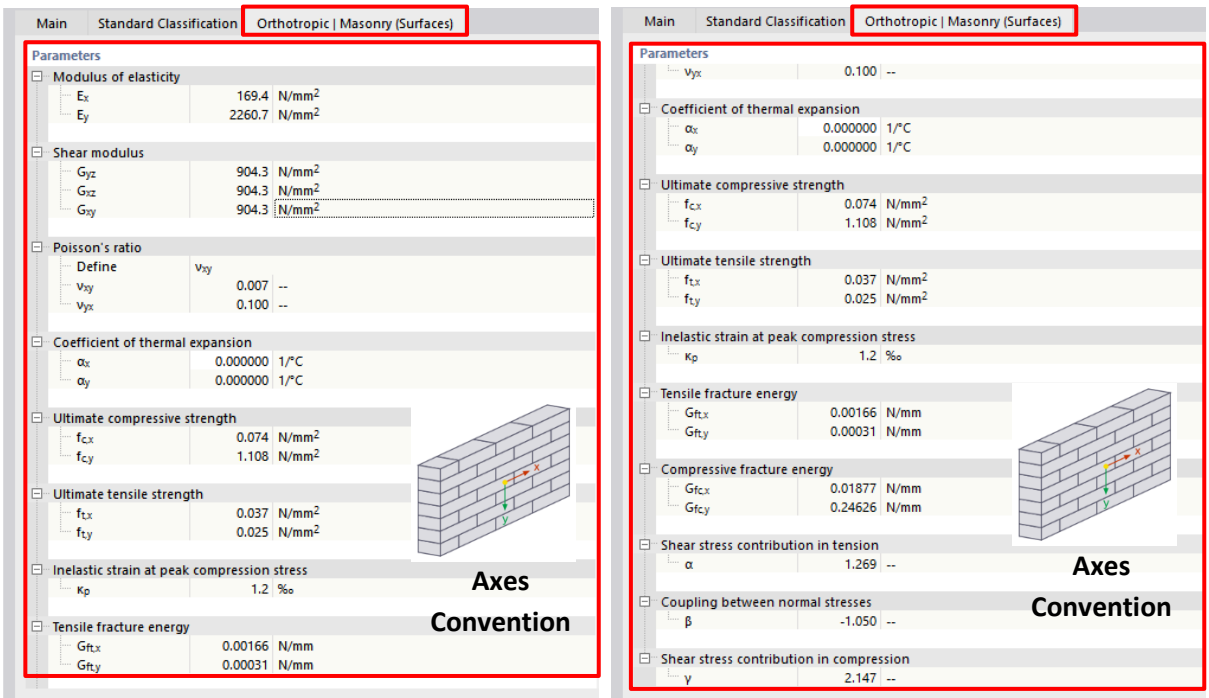

Figure 5:3 - Screenshot from RFEM6 showing the averaged properties of an Orthotropic Material Model as calculated by the program

In addition to the constitutive model selected for the masonry wall, it is important to highlight the models used for other commonly employed structural elements, such as steel beams (representing the foundation) and reinforced concrete roofs/slabs. For both elements, an isotropic material model was adopted as shown in Figure 5:5 & Figure 5:8. Figure 5:4 to Figure 5:6 highlight the properties of steel, whilst Figure 5:7 to Figure 5:9 highlight the properties of concrete.

Properties of Steel

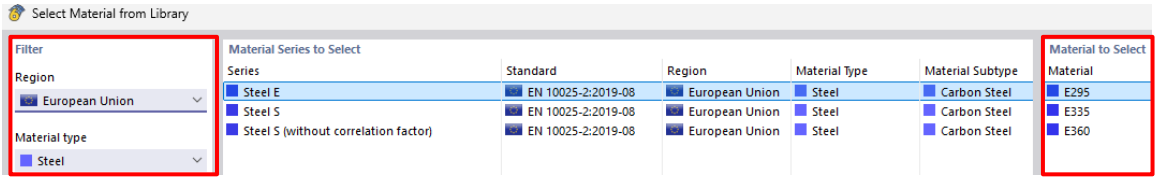

Figure 5:4 - Screenshot from RFEM6 showing the steel grade

In the Basic Material Properties section shown on the right-hand side of Figure 5:5, the modulus of elasticity, Poisson's ratio, and mass density were defined based on informed assumptions. The remaining parameters in this section, as well as those in Figure 5:6, were retained as default values.

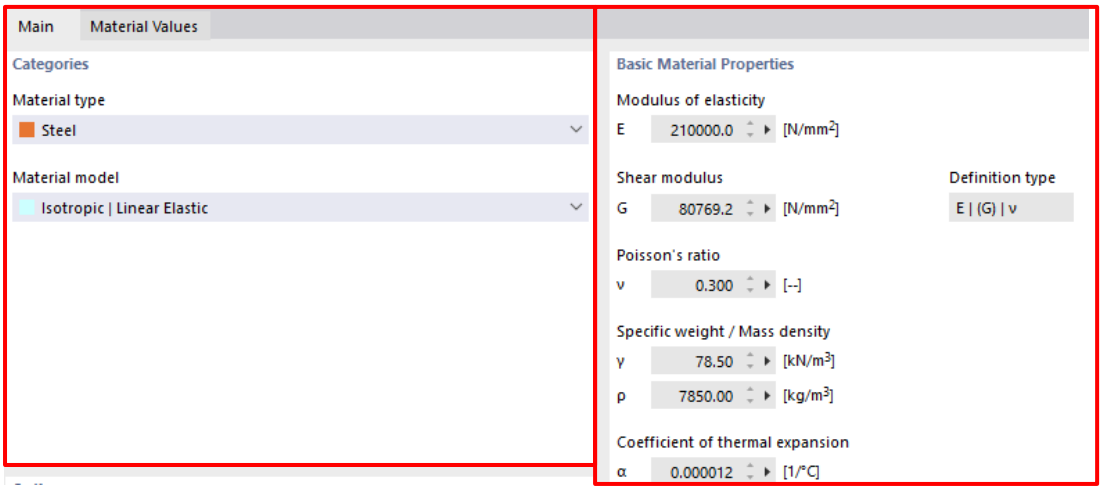

Figure 5:5 - Screenshot from RFEM6 displaying the material model and fundamental properties for steel

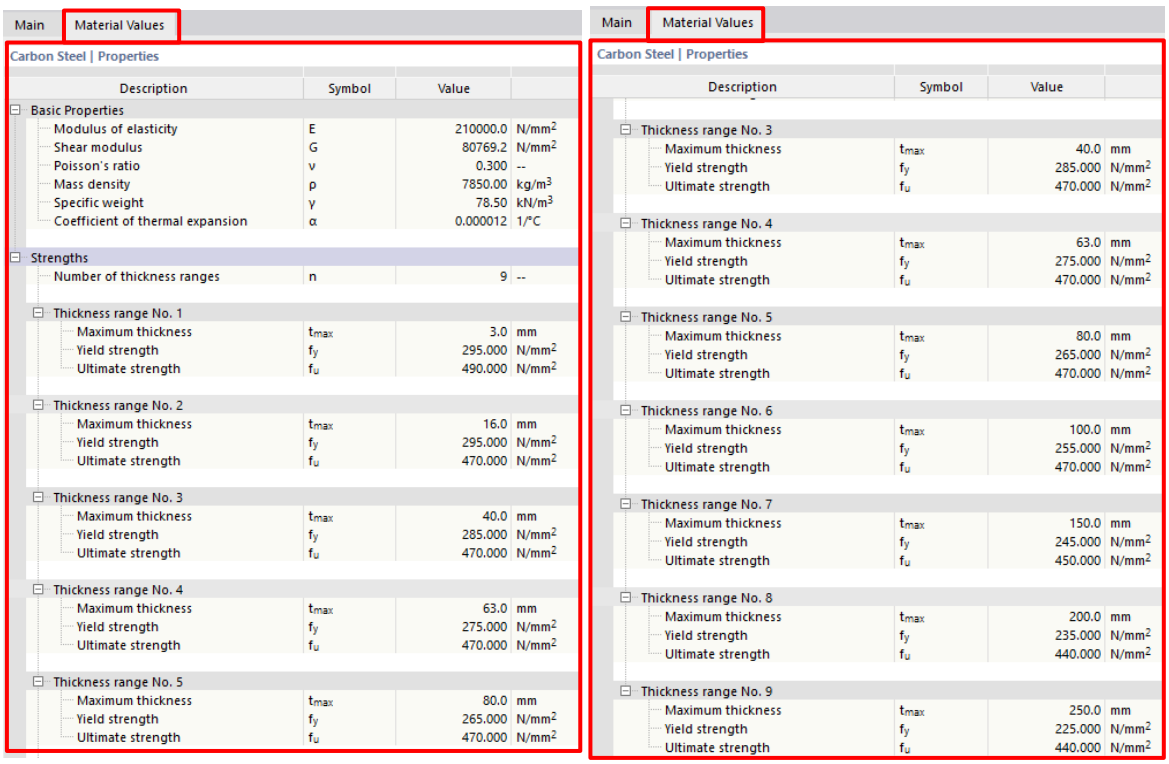

Figure 5:6 - Screenshot from RFEM6 showing default properties of carbon steel

Properties of Concrete

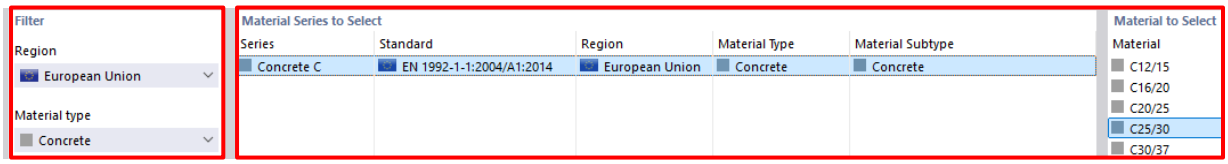

Figure 5:7 - Screenshot from RFEM6 showing the concrete grade

In the Basic Material Properties section shown on the right-hand side of Figure 5:8, the modulus of elasticity, Poisson's ratio, and mass density were defined based on informed assumptions. The remaining parameters in this section, along with those presented in Figure 5:9, were retained as default values.

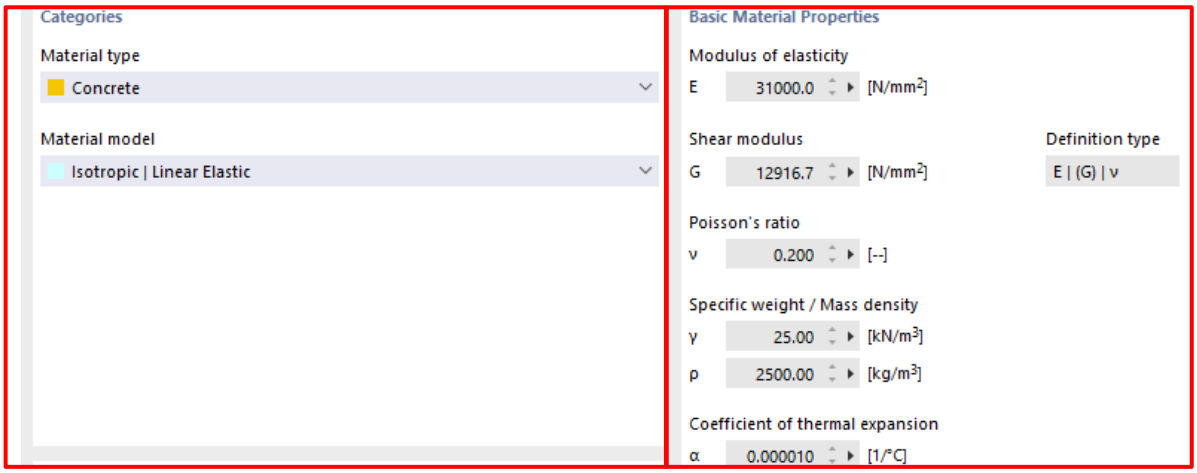

Figure 5:8 - Screenshot from RFEM6 displaying the material model and fundamental properties for concrete

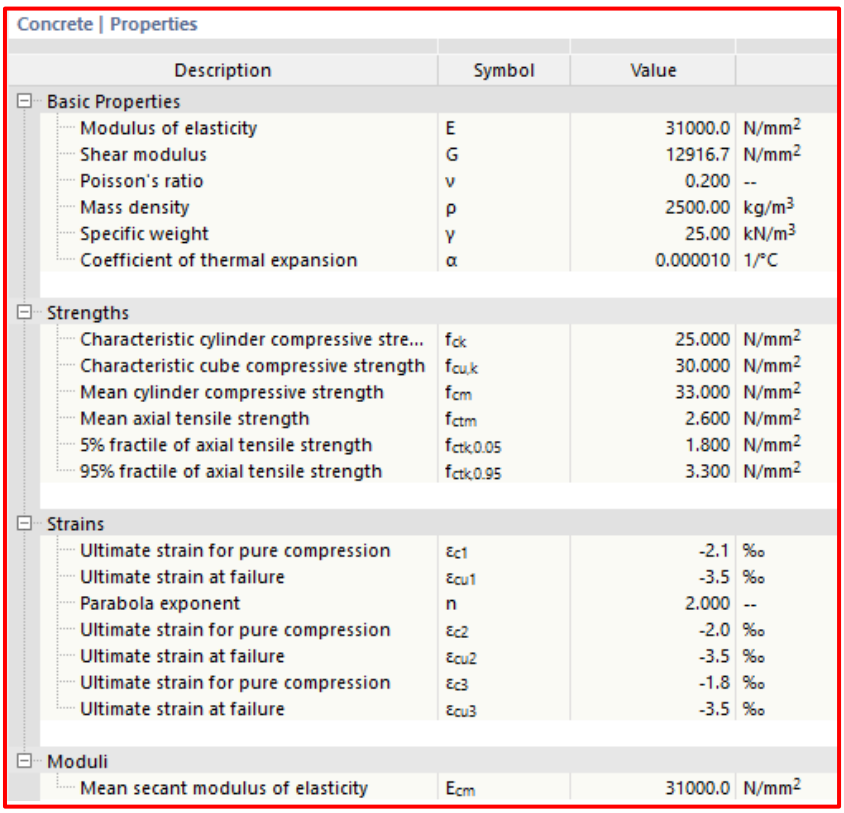

Figure 5:9 - Screenshot from RFEM6 showing default concrete properties

Mesh

The mesh used in the analysis was left at the default value suggested by RFEM6, as shown in Figure 5:10. This decision was made due to a lack of experience with numerical modelling and limited understanding of the impact of mesh size on simulation outcomes. For consistency, all models retained the default mesh size provided by the software.

Over time, it became clear that mesh size significantly affects the accuracy, efficiency, and stability of simulations. While finer meshes can improve accuracy, they come with the downside of increased computational cost. To achieve a balance, adaptive meshing is frequently utilized. This approach applies finer meshes to critical regions where rapid stress variations are expected, while coarser meshes are used in areas where stress changes are less significant. Regular mesh refinement studies are also essential to ensure that the solution remains robust and minimally affected by mesh resolution.

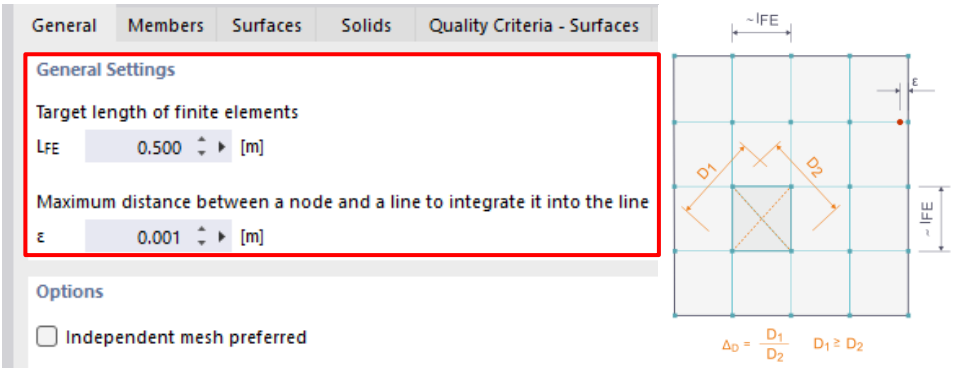

Figure 5:10 - Default mesh used for modelling

Structural elements & Support conditions

In all the modelled structures, the primary structural elements included masonry walls (constructed from hollow concrete blocks), reinforced concrete floor/roof slabs, and steel beams simulating the foundations.

The masonry walls and reinforced concrete slabs were modelled as linear surface elements (plate elements), each assigned their respective properties and thicknesses. The thickness of these surface elements varied depending on the specific type of structure being modelled. This variation in thickness, particularly for slabs and walls, will be further discussed in later sections.

In contrast, the steel beam was modelled as a linear element. In some cases, a standard beam was used; in others, a custom regular beam was used. In all cases, the steel beams served as rigid foundations supporting the masonry walls. These beams spanned across supports, which were predominantly pinned, with occasional use of roller supports. The specific support conditions adopted for each structure will also be elaborated on later.

Load Cases & Combinations

Another important topic to address is the load cases and combinations used during the modelling of the various structures, as this helps the reader better interpret the results. The analysis incorporated only two load cases: the self-weight load case, which accounted for the dead load of the structural elements, and the settlement load case, which simulated the nodal deflections applied to the

respective structures. Beyond these, no imposed or variable loads were applied, and partial safety factors were excluded from the load cases.

The decision to omit imposed or variable loads and safety factors was driven by a desire to simplify the models as much as possible. This simplification aimed to make the results more straightforward to analyse, understand, and interpret by minimizing the number of variables influencing the outcomes. Additionally, the application of imposed loads or safety factors was considered secondary to the primary objectives of this dissertation. Focusing on the fundamental aspects of the study was deemed more valuable than allocating time to these less critical factors at this stage.

The general approach to applying load combinations in the model was to first analyse the behaviour of the structure under its self-weight. Once the results were validated and found to be logical, the second load case (settlement) was applied in conjunction with the self-weight. This step-by-step method limited the number of variables introduced at any given time, enabling a clearer and more effective assessment of whether the results were reasonable.

5.3. Modelling Stage 1: Modelling a simply supported beam with an HCB wall

5.3.1. Context

The first modelling attempt focused on a simple masonry load-bearing wall, which was calibrated using a real-life case study from Malta. The selected case study was derived from ‘’The Effects of Support Movement on Local Concrete Block Construction’’, a B.E&A (Hons) undergraduate dissertation by Julian Mifsud (2012). In this dissertation, Mifsud constructed a full-scale load-bearing masonry wall and observed its behaviour as the wall was subject to differential settlement of its intermediate support. Mifsud also measured the crack widths created at different stages of this process.

This section aims to establish a foundational understanding of the software, enabling the modelling of the masonry load-bearing wall described in Mifsud J. (2012), which will be addressed later in Section 5.4. To ensure a clear and effective approach, the problem was initially simplified as much as possible. This involved starting with simple objects and progressively introducing variables to critically analyse the outcomes and evaluate their validity. This step-by-step methodology also provided valuable insights into the software's functionality. The modelling process, however, presented several challenges, as outlined below:

5.3.2. Step 1 – Modelling a simply supported steel beam subjected to its own self-weight

In this step, the steel beam is supported by a pin and a roller connection, one at each end of the beam, as shown in Figure 5:11. The bending moment, shear force diagrams, and deflection of the steel beam, subjected to its own self-weight, were verified using hand calculations. The results from the modelling closely aligned with those obtained from the hand calculations, as shown in Appendix B.

Figure 5:11 - Simply supported steel beam subjected to its self-weight

5.3.3. Step 2 – Modelling a simply supported steel beam subjected to an imposed load

Step 1 was repeated; however, an imposed load was introduced on top of the beam, as shown in Figure 5:12. The bending moment, shear force diagrams, and deflection results obtained from the modelling closely matched those derived from hand calculations, as shown in Appendix B.

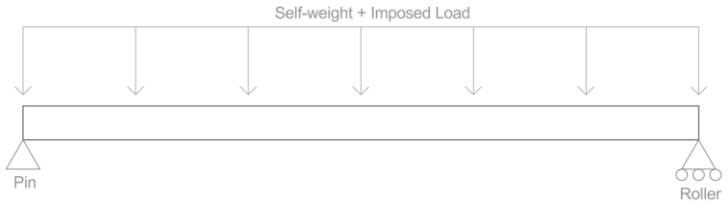

Figure 5:12 - Simply supported steel beam subjected to its self-weight & an imposed load

5.3.4. Step 3 – Modelling a simply supported beam subjected to a masonry wall loads

In this step, the same beam and support conditions were used; however, the beam was loaded with an HCB wall instead of an imposed load, as shown in Figure 5:13. The bending moment, shear force diagrams, and deflection of the steel beam under the wall's load were compared with hand calculations. The results obtained from the modelling were significantly different from the hand calculations, indicating that the beam and wall were not behaving as intended. During this phase, the behaviour of the wall and beam was studied to identify factors affecting the overall "system." The main issues encountered during this process are outlined in Section 5.3.4.1.

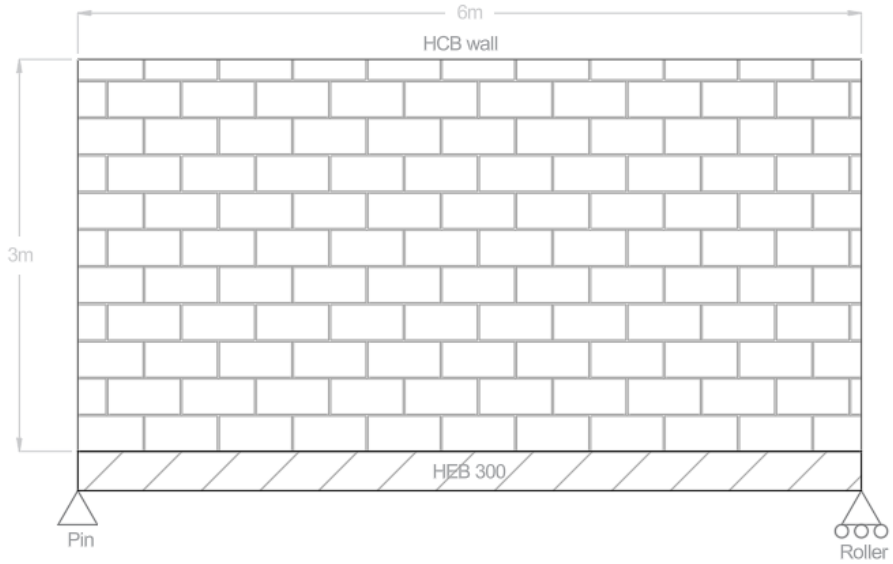

Figure 5:13 - Simply supported beam subjected to the load of a masonry load-bearing wall

5.3.4.1 Modelling Challenges

This section briefly outlines the main challenges encountered during the modelling process to provide context for understanding the methodology and its foundation. A detailed discussion of all modelling challenges is available in Appendix A.

Two primary issues arose during the modelling process. The first involved the beam element supporting the masonry wall. Initially deemed unnecessary, the results revealed that without the beam element, the masonry wall behaved like a "jelly," with supports penetrating the wall, as shown in Figure 5:14. This demonstrated the beam element's critical role in the model.

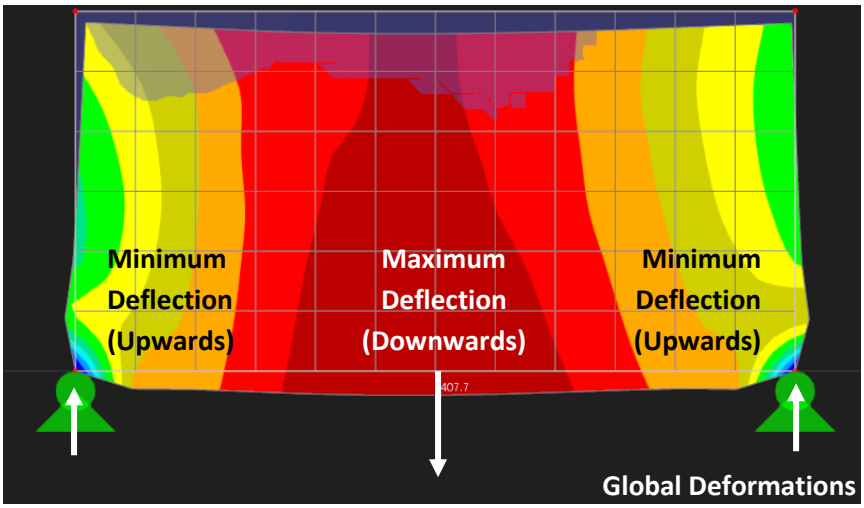

Figure 5:14 - Masonry wall supported by nodal supports at both ends

The second issue emerged after introducing the beam element, as the software treated the beam and masonry wall as a single object, altering the masonry wall's behaviour and preventing proper analysis. The solution was to implement a line release, allowing independent behaviour of the masonry wall, as shown in Figure 5:15.

To aid the reader's understanding, it is important to briefly explain the concept of a line release and its application within this dissertation. Essentially, a line release enables the model to be decoupled along a specific line. In this context, it will be used to separate the wall surface from the beam element, effectively decoupling their behaviours. This allows the wall and beam to act independently by releasing specific translational and rotational constraints.

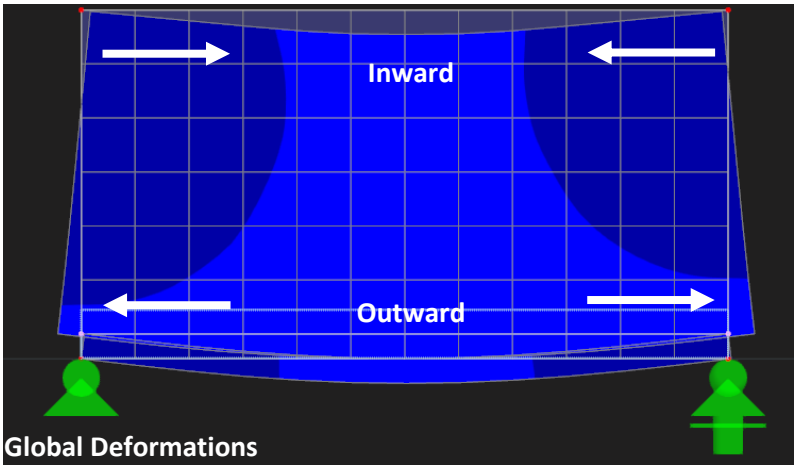

Figure 5:15 - Independent behaviour of the masonry wall and the steel beam

5.3.4.2 Conclusion on the above-mentioned issues

The most realistic results were obtained by supporting the steel beam with a pin and a roller at each end and applying a line release to decouple the wall and beam. This allowed for nearly independent behaviour, with only longitudinal translation released and a small spring constant (0.001kN/m²) modelling an elastic hinge between the two elements.

5.4. Modelling Stage 2 – Modelling the wall set-up in Mifsud (2012)

5.4.1. Context

The modelling process described in Section 5.3 served as a foundation and preparatory work for this section and the subsequent sections, increasing familiarity with numerical modelling and the software.

The wall setup described in Mifsud J. (2012) forms the foundation of this dissertation, as it is essential for calibrating and validating the numerical model against the full-scale experimental model used in that study. Given its significance, it is logical to present the results and discussion of this wall setup in this section.

This stage focuses on explaining and modelling the set-up used in Mifsud J. (2012). To avoid repetitions only the details will be discussed. The setup adopted in Mifsud J. (2012) consisted of a masonry load-bearing wall made from local hollow concrete blocks supported by steel beams. The steel beams were supported by hydraulic jacks placed at both ends of the wall and at 1/3 of the wall's length. The central jack was intended to simulate ground settlement by producing vertical displacement at a constant rate, as shown in Figure 5:16 & Figure 5:17.

Since the set-up discussed in Section 5.3.4, is very similar to the one used in Julian Mifsud's dissertation, the knowledge presented in Section 5.3, has been adopted for this modelling stage. However, the only difference in this stage is the inclusion of an intermediate support, which led to the issues described below:

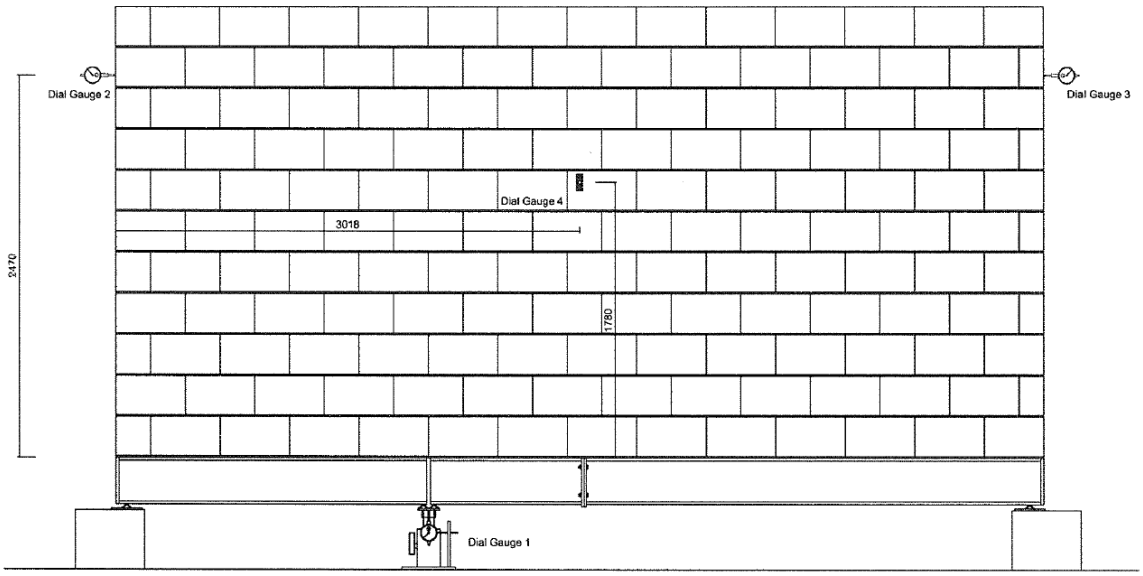

Figure 5:16 - The wall set-up outlined in (Mifsud J. , 2012)

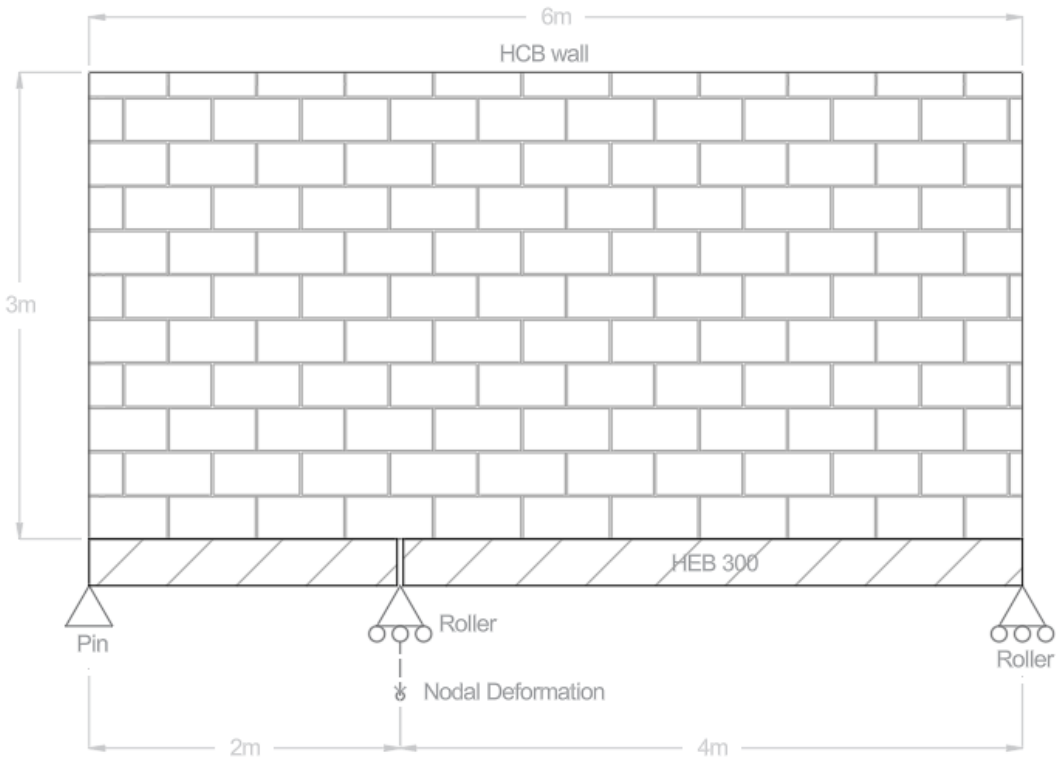

Figure 5:17 - A schematic diagram of the wall configuration adopted for the modelling process

5.4.2. Modelling Challenges

Issue 1 – Intermediate Support

Originally, the intermediate support was planned to be a pin support. However, it was noted that if the support were designed as a pin connection, the wall would be restricted from moving laterally, which would not provide an accurate representation of the results Therefore, a roller support was used instead, as illustrated in Figure 5:18.

Issue 2 - Beam to beam interaction

The two beams used by Julian to support the wall were released at their ends, where they meet and are supported by a common central support, as shown in Figure 5:18. This was important because it allowed the two beams to behave independently, rather than as a single, unified beam. The end releases involved freeing all rotations, ensuring that as nodal deformations occurred, the ends of the beams were able to rotate independently.

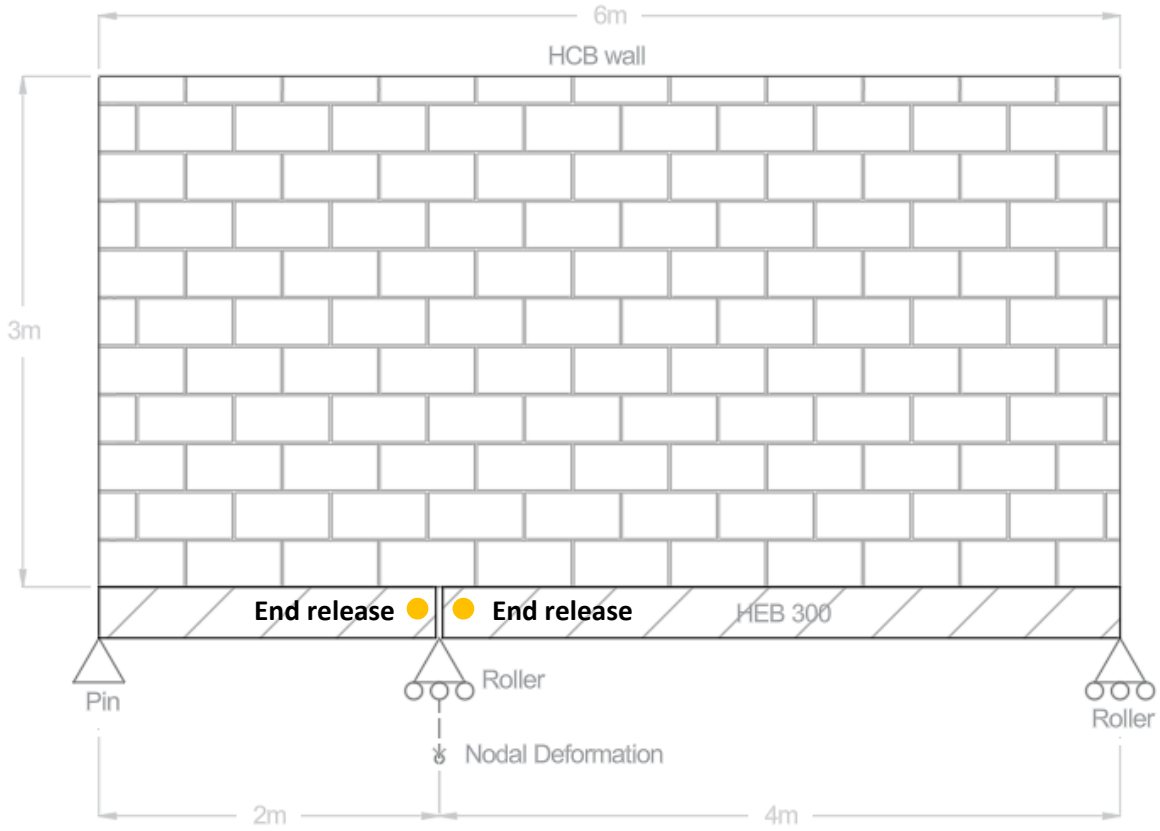

Figure 5:18 - The final diagram of the wall set-up modelled in the software

5.4.3. Results and Discussion

When analysing the results of this numerical model, three key aspects have been considered. First, the maximum plastic strains are examined, revealing the degree and distribution of strain within the wall. This analysis highlights areas where cracks are most likely to form and identifies regions where the severity of cracking is higher compared to others. Second, the principal stresses are assessed to understand the type and magnitude of stress experienced by the wall. Lastly, the deformations undergone by the wall during settlement are evaluated. Together, these aspects provide a comprehensive understanding of the behaviour of the masonry wall under nodal deformation from multiple perspectives.

Maximum Plastic Strain

Graphically, plastic strains are represented by several overlapping arched contours in the RFEM6 programme. The greater density of the strain contours on one side is clearly visible (Figure 5:19), which is attributed to the fact that the intermediate support is offset to one side. Each contour corresponds to a specific strain range, with the uppermost contours indicating lower strain values and the lowermost contours indicating higher strains. This pattern is expected, as the region with the highest strain is closest to the point of nodal deformation and, consequently, is experiencing the most severe cracking, as shown in the Figure 5:19.

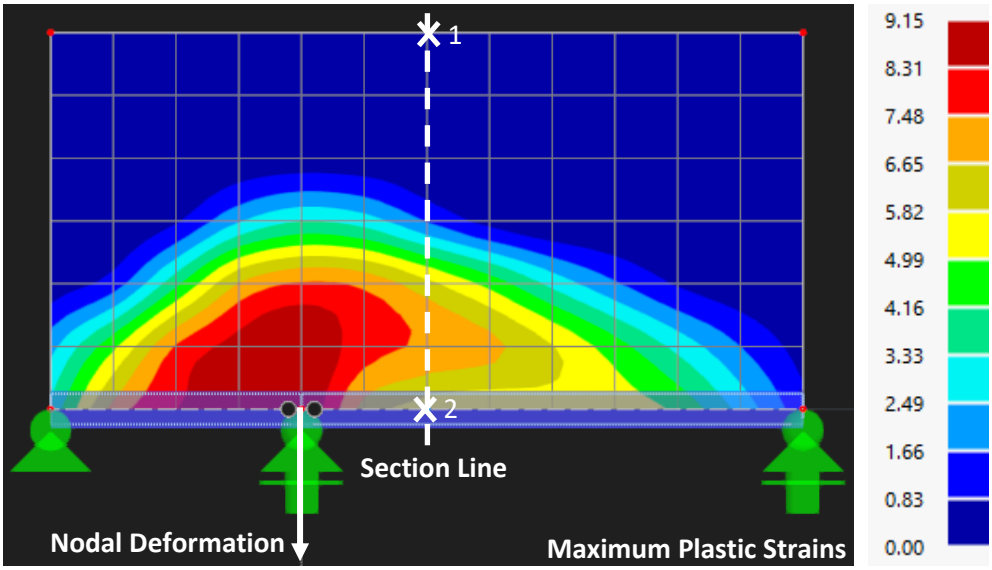

Figure 5:19 - Maximum plastic strains experienced by the wall

The wall is partially in the elastic stage and partially in the plastic stage, as illustrated by the coloured contour plot in Figure 5:19.The dark blue areas at the sides indicate regions under compression, while the red areas highlight zones experiencing the highest tension. The gradient of colours between these extremes represents the transition of the wall material from elastic to plastic behaviour.

A section line through the wall confirms that the total strain comprises both elastic and plastic components. This is validated by comparing the maximum plastic strains, which show only plastic deformation, with the maximum total strains, which include both elastic and plastic contributions (Figure 5:20). The close match between these diagrams indicates that while both types of strain are present, plastic strains dominate, with elastic strains being minimal.

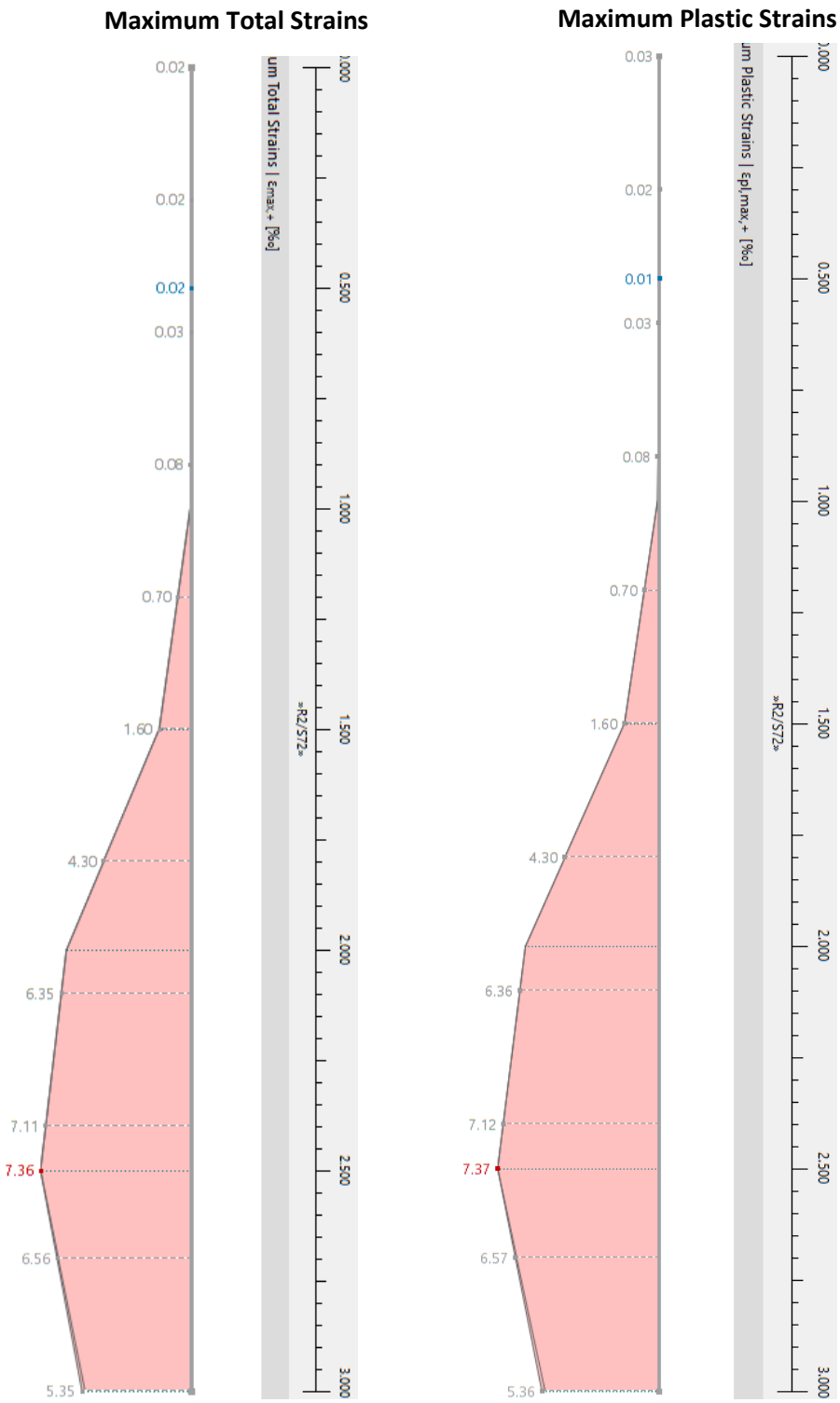

Figure 5:20 - 1)Maximum Total Strains and 2)Maximum Plastic Strains

The presence of plastic strains in certain areas of the wall indicates that these regions have exceeded the elastic limit and entered the plastic stage. These plastic strains are irreversible, signifying significant and permanent damage. If the wall's state during the plastic stage were to be traced on the stress-strain curve defined by the orthotropic constitutive model used in the analysis, it would have surpassed the peak and be situated within the plastic region, as marked in Figure 5:21. It is important to note that the cross mark on the curve serves as an indicative representation of the wall's behaviour and should not be interpreted as an exact position.

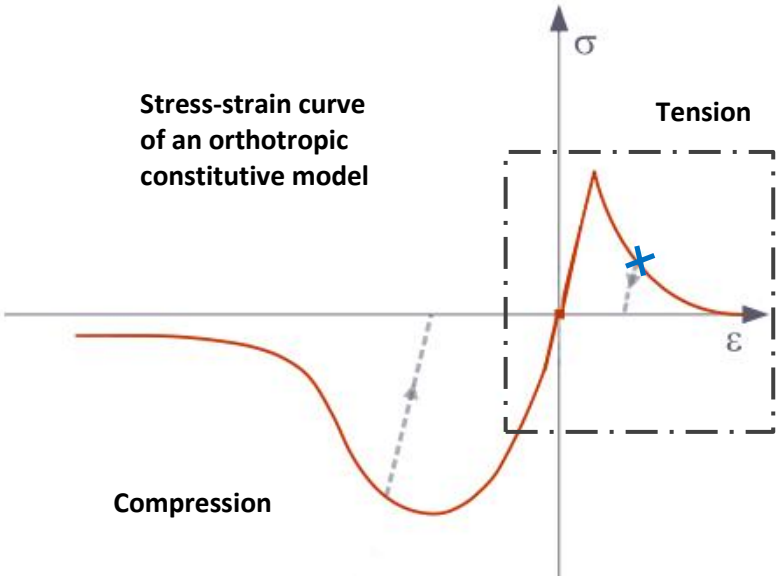

Figure 5:21 - The position of the masonry wall within the stress-strain curve according to the selected constitutive models

Moreover, Figure 5:22 visually supports and clarifies the previous argument concerning the total strains (the sum of elastic and plastic strains) recorded along the section line through the wall, as shown in Figure 5:20.

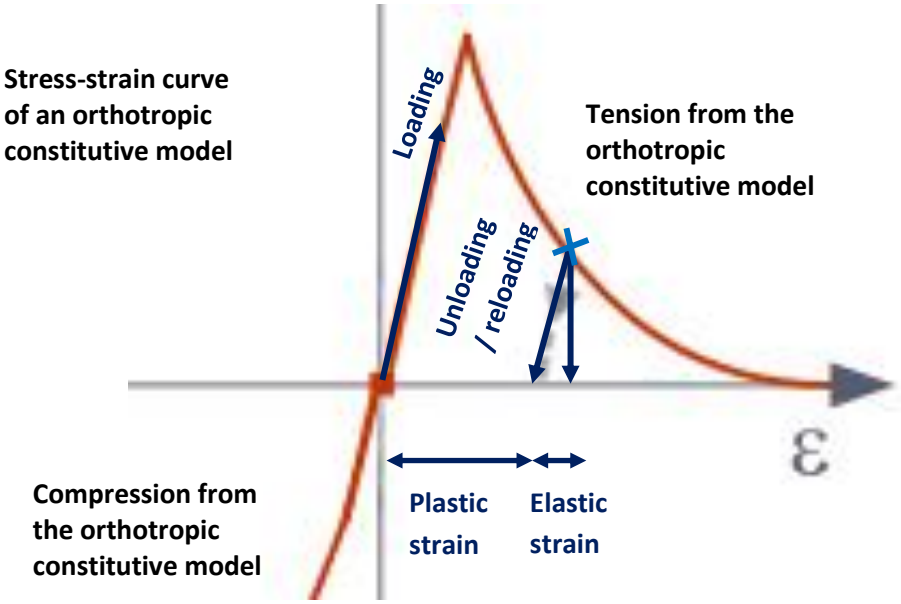

Figure 5:22 - Explanation of plastic and elastic strain on the orthotropic constitutive model's stress-strain curve

A transverse section through the centre of the wall reveals that the maximum plastic strains are relatively low near the top of the wall (x = 0 m), and extend approximately 1 meter downward (Figure 5:23). However, the plastic strains increase more rapidly between x = 1 m and x = 3 m, corresponding to the lower section of the wall (Figure 5:23). In fact, the plastic strain distribution diagram shows that plasticity begins to develop approximately one-third of the way down from the top of the wall.

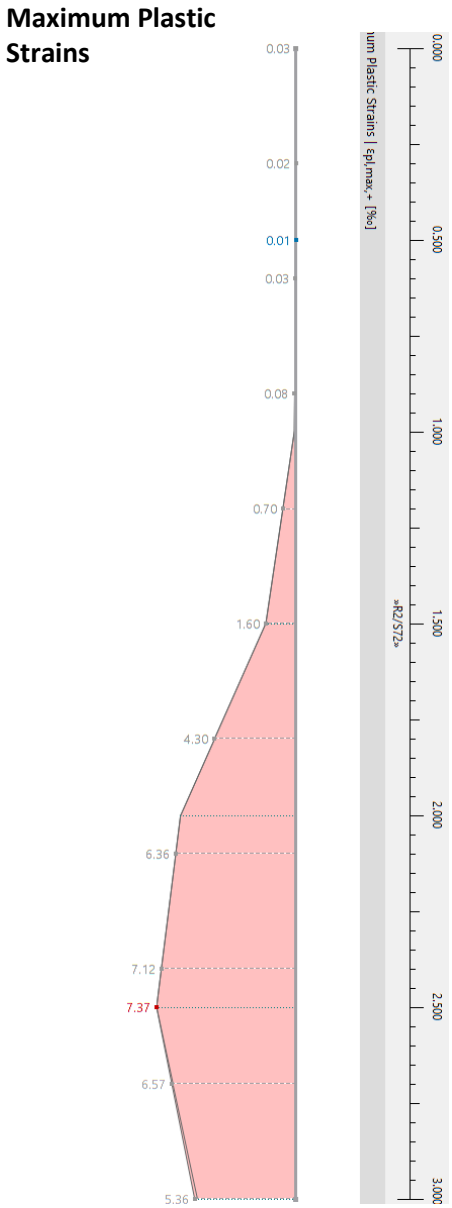

Figure 5:23 - Maximum plastic strain distribution through a wall section

The increase in plastic strain is not linear; instead, it accelerates sharply, reaching a maximum near the bottom of the wall, close to its point of contact with the beam, as shown Figure 5:23. In this region, individual cracks tend to widen and merge, forming continuous, irreversible cracks, which may eventually lead to the detachment of this section from the rest of the wall. At this stage, the possibility of restoring the wall becomes extremely limited.

It is crucial to distinguish between failure in the Serviceability Limit State (SLS) and the Ultimate Limit State (ULS), as they are often misunderstood. Failure under the SLS indicates the appearance of cracks, but it does not imply that the wall is unstable or at imminent risk of collapse. Over time, however, these cracks can propagate and widen until the ULS is reached—at which point the wall is no longer considered stable and may be on the verge of collapse.

Moreover, it is important to evaluate damage within the broader context. The severity of wall damage is typically assessed based on multiple factors, including the number and width of cracks, the significance of the building, and subjective human judgement—all of which play a critical role in this evaluation, as discussed in detail in Section 2.3.

Principal Stresses

The principal stress distribution of the wall (Figure 5:24) clearly indicates that the wall transitions from an elastic zone (governed by Hooke's Law), through a transition zone, and into a plastic zone. The upper portion of the wall is subjected to compressive stresses, with the highest values occurring at the top. These compressive stresses gradually decrease and reduce to zero at approximately one-quarter of the wall's height (measured from the top), marking the location of the neutral axis (Figure 5:24). Below this point, the wall experiences only tensile stresses. It is also important to note that the transition from compression to tension is not abrupt but follows an almost linear gradient across the neutral axis, as shown in Figure 5:24.

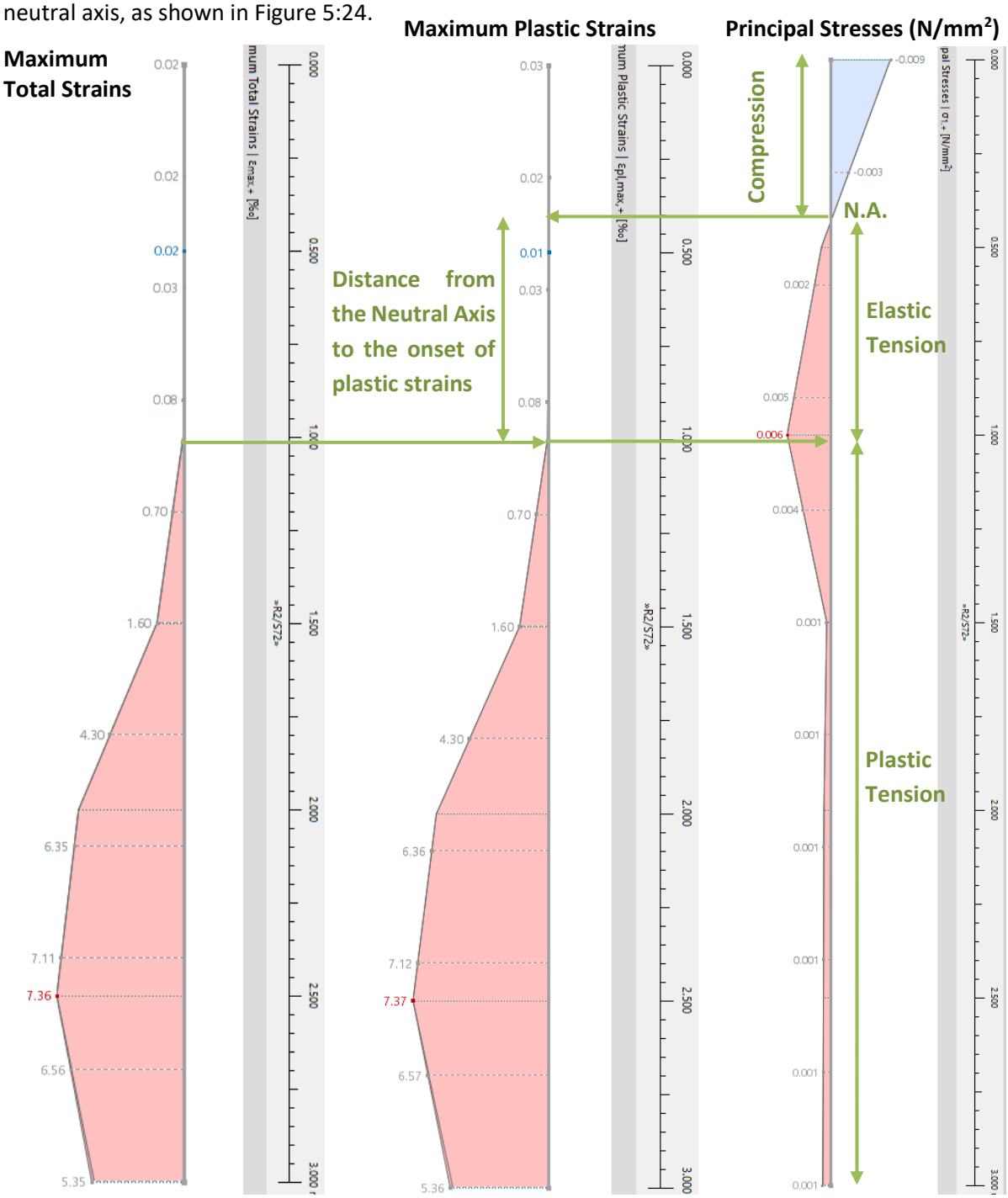

Figure 5:24 - Analysis of the results by observing: 1) Maximum Plastic Strains & 2) Principal Stresses through a wall section

It is important to distinguish between two types of tension within the wall: elastic and plastic tension. This distinction becomes evident when comparing the principal stress distribution with the maximum plastic strain diagram (Figure 5:24). Elastic tension develops in the region between the neutral axis—identified in the principal stress diagram—and the point at which plastic strains become significant, as illustrated in the maximum plastic strain diagram. Although plastic strain initiates at the top of the wall, its magnitude there is negligible. A more pronounced increase in plastic strain is observed beginning at approximately one-third of the wall's height, measured from the top edge, as shown in Figure 5:24.

This comparison clearly demonstrates that the neutral axis does not coincide with the onset of plastic deformation (Figure 5:24). Instead, there exists a tension zone where the material behaves elastically before transitioning into the plastic range. This observation highlights the progressive nature of the material's response under load, transitioning from reversible (elastic) deformation to irreversible (plastic) strain, as shown in Figure 5:24.

Therefore, the principal stresses (Figure 5:24) confirm that the wall exhibits both elastic and plastic behaviour, with its total strain comprising both components rather than being exclusively one or the other, as previously discussed.

Another consideration is that a section through the numerical model of the wall reveals the stress distribution within the wall, as illustrated in Figure 5:25. This distribution closely resembles the stress pattern of an arch subjected to an eccentrically applied point load (Figure 5:25). Although no external loads other than the wall's self-weight have been applied, the presence of nodal deformation effectively mimics the impact of such a point load on the arch.

A notable comparison reveals a similarity between the transition from compressive to tensile stresses in an arch subjected to an eccentrically applied point load—positioned similarly to the nodal deformation in the wall—and the principal stresses observed in the wall model, as shown in Figure 5:25.

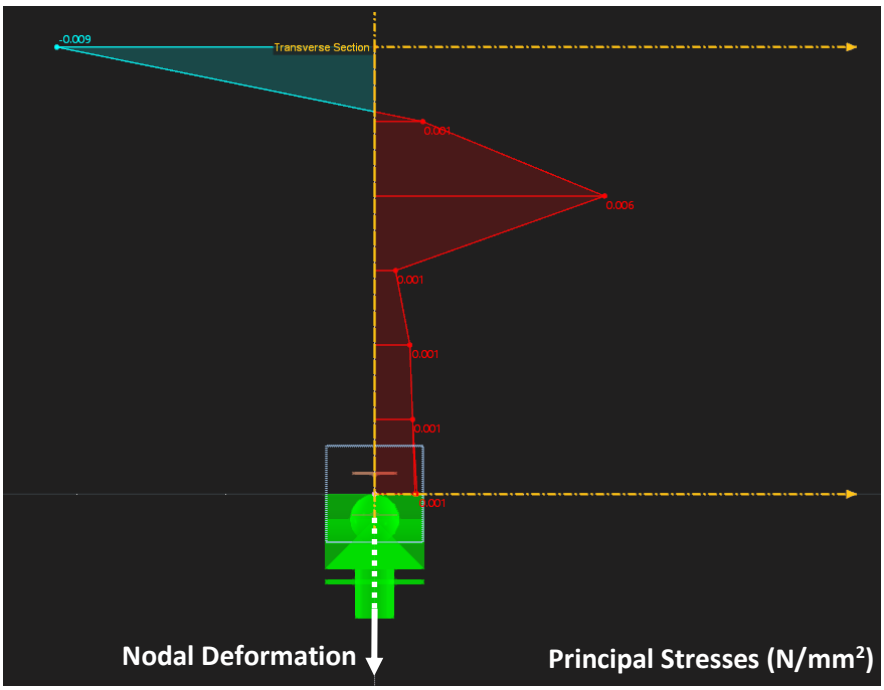

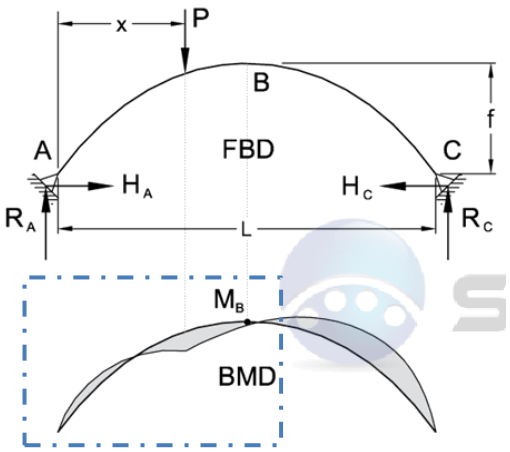

Figure 5:25 - 1)Section through the wall showing the principal stresses, 2)Stresses in an arch

Global Deformation

The global deformation pattern of the numerical model provides a clear visualisation of the damage sustained by the wall during nodal deformation. As settlement progresses, the wall gradually follows the downward displacement of the central support, as shown in Figure 5:26. With increasing nodal deformation, tensile stresses develop within the wall, initially causing the formation of small, isolated cracks. As these tensile stresses intensify, the cracks begin to widen and coalesce, eventually forming larger, more significant fractures.

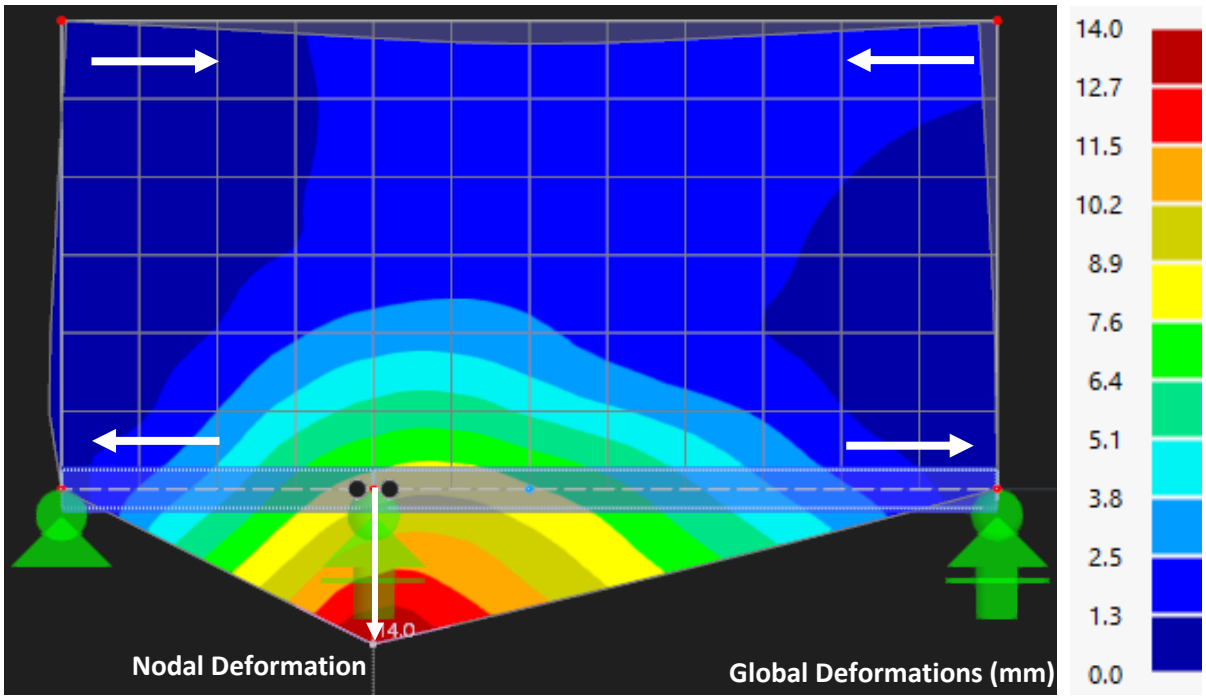

Figure 5:26 - Deformations experienced by the masonry wall

It is also important to observe that the global deformation remains relatively uniform from the top of the wall to approximately mid-height. However, a sharp increase in deformation is noted in the lower half of the wall. This observation aligns with the initiation of plastic strains at roughly one-third of the wall's height (measured from the top), indicating that the upper portion of the wall remains within the elastic range and does not undergo plastic deformation. As a result, the most significant deformations occur in the lower region, where plastic behaviour is dominant, as shown in Figure 5:26.

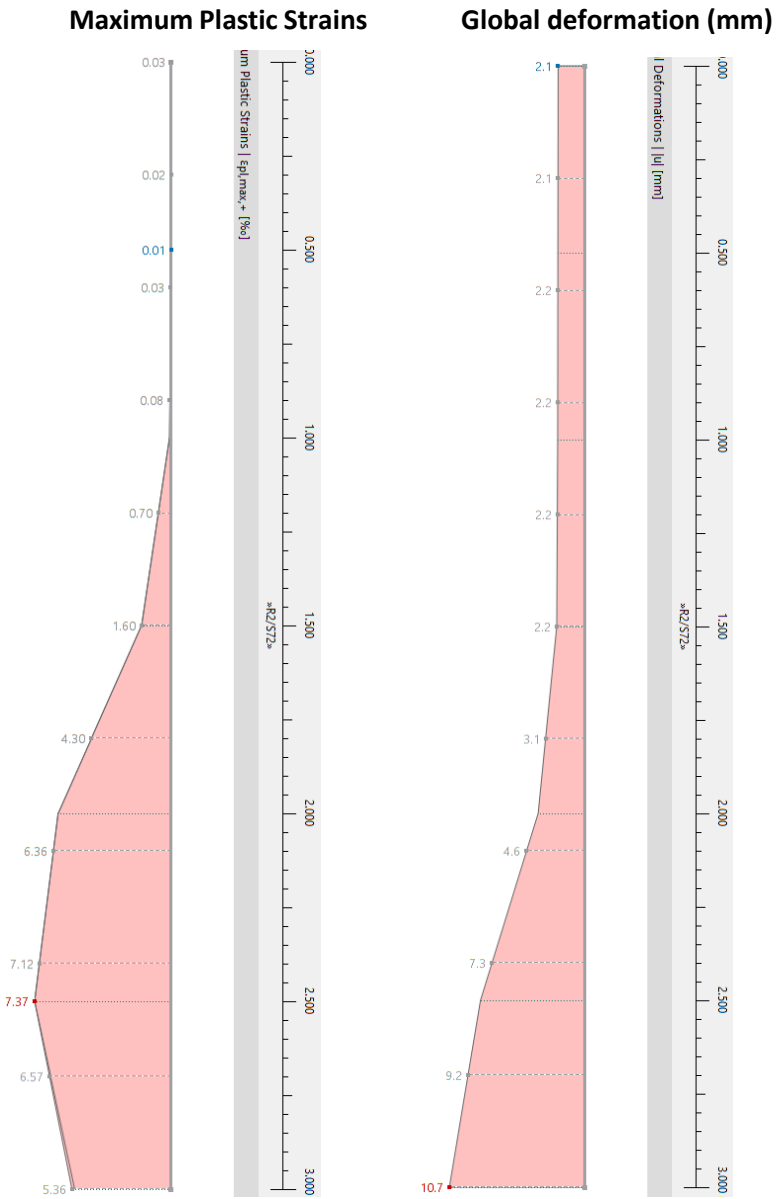

Figure 5:27 - Analysis of the results by observing: 1) Maximum Plastic Strains & 2) Global Deformations through a wall section

This is expected, as the base of the wall, where it interfaces with the beam, is the closest point to the applied nodal deformation and therefore experiences the highest strain concentrations. While it may appear counterintuitive that the plastic strains are not maximal at the very bottom of the wall, even though global deformation peaks there, this can be explained by the material's behaviour in the plastic range. According to the elasto-plastic constitutive model, once the material yields, even minimal additional stress can result in disproportionately large deformations, as shown in Figure 5:27.

In parallel, the wall begins to exhibit bending behaviour as nodal deformation progresses. This is evident from the deformation pattern: the top corners of the wall bend inward, while the bottom corners displace outward, closely resembling the behaviour of a beam under bending, as shown in Figure 5:26.

Ultimately, this process leads to the development of an arched thrust line spanning between the end supports, as shown in Figure 5:26. Structural failure occurs when plastic hinges form along this arch, rendering the wall unstable and leading to collapse. The formation and behaviour of this arch mechanism are further discussed in Section 3.3.1.

5.4.4. Comparison of Results

In this section, the results of the model that have been discussed in Section 5.4.3, will be compared to the results obtained from the experimental testing on the model set-up found in Mifsud J. (2012). There are a lot of important results and observations that have been highlighted in Mifsud J. (2012), however it is impossible to discuss all the results in this dissertation, and hence, only the most relevant observations and results will be discussed.

A direct comparison between the numerical model and the experimental results presented by Mifsud (2012) was carried out, albeit to a limited extent. In Mifsud's study, measured crack widths were reported, whereas in the present study this was not feasible, and only strains could be recorded. Consequently, the comparison was instead based on the observed crack formation patterns. The results show reasonably good agreement between the experimental findings and the numerical model, with the cracks reported by Mifsud (2012) aligning well with the formation of eccentrically arched strain contours. Moreover, the height of the arch (measured from the beam) is very similar, as shown in Figure 5:28. One can argue that the numerical model of the wall did not fully capture all the cracks experienced by the wall, as 'crack 8' from Mifsud J. (2012) is not shown in the plastic strains of the numerical model. One reason for this is since in RFEM6, macro modelling is used, where an equivalent material is used as a substitute to the masonry wall made from mortar and blocks. This means that some accuracy is lost, and thus and to capture all the cracks, discrete element modelling is required.

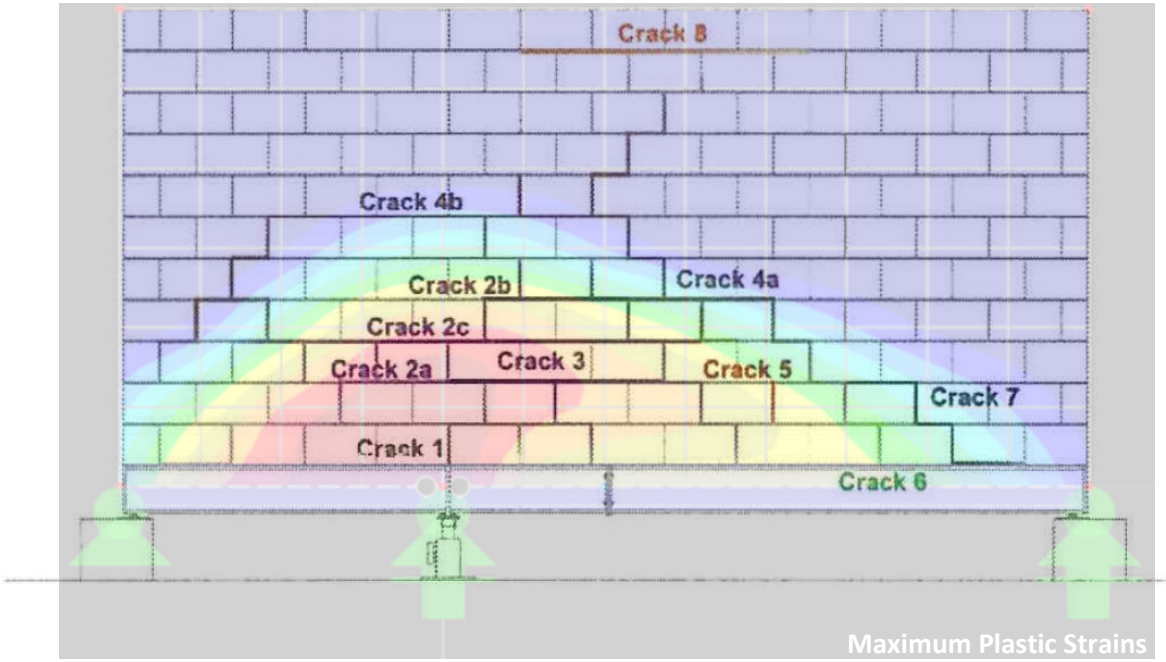

Figure 5:28 - Crack formation in the wall setup described by (Mifsud J. , 2012) superimposed over the Maximum Plastic Strains experienced by the numerical model

Mifsud J. (2012) points out that the widest cracks and most frequent cracks appear in areas with the most critical relative rotation. If the two support beams undergo the same nodal deformation at their contact point, the shorter beam will experience a greater rotation than the longer beam, assuming compatibility is maintained, and the nodal deformation is shared by both contact ends. In fact, Mifsud J. (2012) states that in elevation, the cracks over the longer span are narrower than those over the shorter span. This is also evident from the plastic strains exhibited in the wall, as the arched strain contours are offset to one side and peak closer to the shorter beam rather than the longer beam, as shown in Figure 5:28.

Mifsud J. (2012) argues that a rotation considered critical for one span may not be critical for another. For instance, achieving the same crack width requires the short span to undergo only half the rotation of the long span. This means that even though the long span rotates less, it can still fall into a worse damage category because the span is longer. In the numerical model, however, this is challenging to visualize, as the cracks are not explicitly depicted. Instead, the arched strain contours appear less dense (more spaced out) on the left side and denser (less spaced out) on the right side, hinting how limited rotation can still generate considerable strains in the wall, as shown in Figure 5:29.

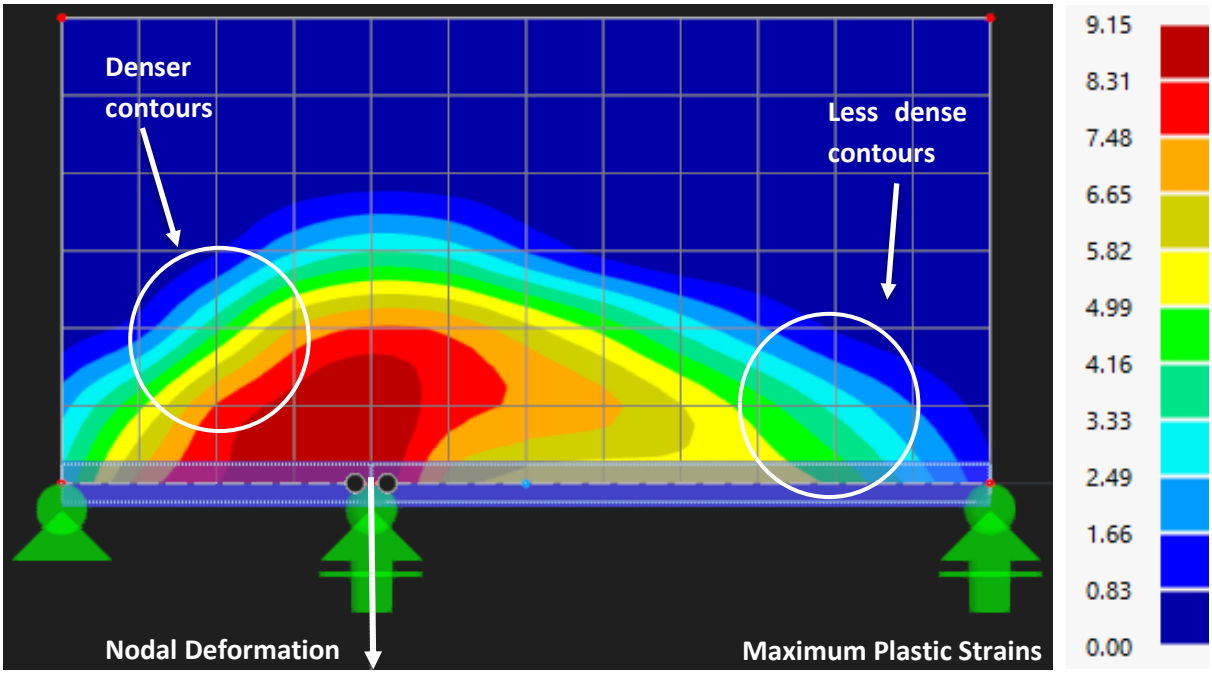

Figure 5:29 - Arched contours in the regions of Maximum Plastic Strain

Apart from that, when looking at the analysis of the results conducted by Mifsud J. (2012), it was stated that, ''As the shallow beam bends, the lower courses push outwards and the upper wall edges tilt inwards. This is shown when recording the values of dial gauges 2 and 3''. The use of dial gauges when trying to understand the deformation experienced by the wall is crucial as it is very difficult to capture this type of deformation with the naked eye. The deformation explained by Mifsud J. (2012) is in agreement with the deformation experienced by the numerical model, as illustrated in Figure 5:30 and as already discussed in Section 5.4.3.

Comparison of the in-plane displacement values recorded by the dial gauges 2 and 3 in Mifsud J. (2012) and the same value from the numerical model indicates some discrepancies. The values of dial gauge 3 in Mifsud J. (2012) and the numerical model seem to be very close to each other, however, the values of dial gauge 2 do not. This is clearly illustrated by comparing the readings of dial gauges 2 and 3 in Figure 5:30 & Figure 5:31. In Figure 5:31, dial gauge 2 records a greater plane displacement than dial gauge 3, whereas in Figure 5:30, the opposite is observed.

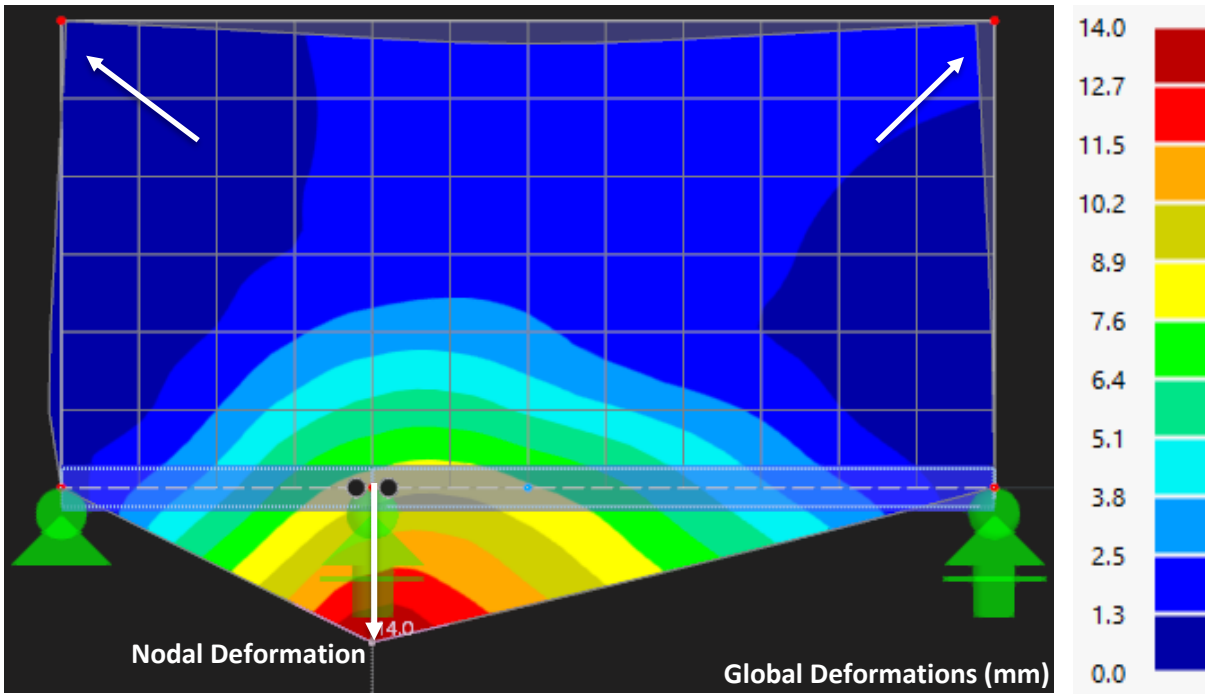

Figure 5:30 - Deformations exhibited by the masonry wall

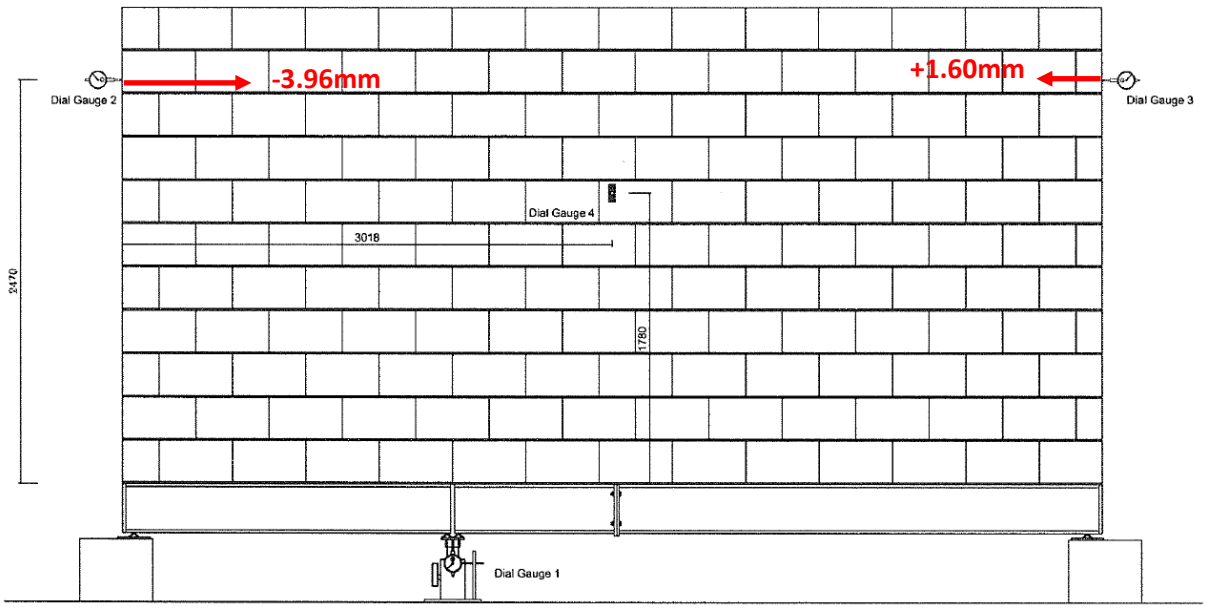

Figure 5:31 - Plotting the plane displacements measured by the dial gauges in (Mifsud J. , 2012)

This is unexpected, as the numerical model aligns with the real-life case study in some respects but shows considerable discrepancies in others. In reality, given that the shorter beam should experience more severe rotations, one would expect the displacement values to be greater on that side.

It can be concluded that the results obtained by Mifsud J. (2012) are more reliable than the results obtained by the numerical model. The discrepancy observed cannot be attributed to the model's setup, as the model geometry functions correctly on one side but not the other. Therefore, the main reason for this discrepancy is contributed to the use of macro-modelling, where an equivalent material has been used, and thus some accuracy may be lost as well. The use of macro modelling is very useful to understand the overall behaviour; however, it shows limitations when trying to achieve this type of accuracy.

There is an alternative interpretation of the deformations observed in the numerical model, in contrast to what was previously explained. Consider that the wall can be conceptually divided into two sections at the location of the nodal deformation. If we assume that this nodal deformation occurs and the wall segments are free to tilt, the left segment will rotate clockwise (towards the right), while the right segment would rotate anticlockwise (towards the left). Given that the nodal deformation is eccentrically located towards the left, the right wall segment possesses a greater mass. As the right wall tilts, it tends to exert a lateral force, pushing the left segment further in the same direction it is already tilting. This interaction results in overall distortion of the wall system, as shown in Figure 5:32. This could explain an apparent inconsistency: although it was expected that the portion of the wall resting on the short-span beam would undergo the most significant rotation, the model shows that it actually experienced the least deflection. In contrast, the upper portion of the wall on the right-hand side exhibited greater deflection, likely due to the lateral force imposed by the more massive, tilting right segment.

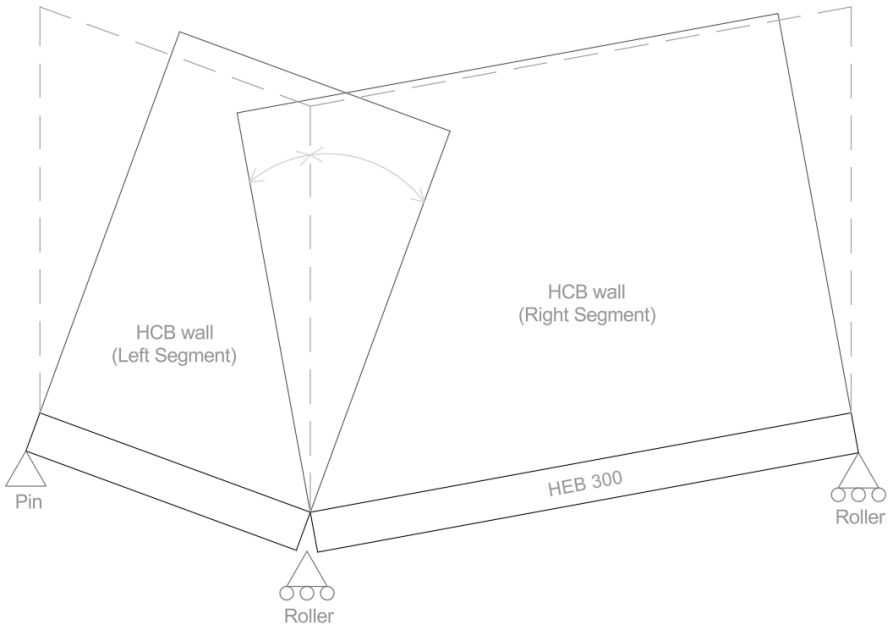

Figure 5:32 - Distortion experienced by the masonry wall

Another important observation that should be made is that part of the wall closest to the nodal deformation experiences the greatest degree of tensile stress and therefore the strain in that region is considered to be the highest when compared to the strains in other parts of the wall. This was exhibited both by the numerical model where the arched red contour was at the location of the nodal deformation as well as in the observations by Mifsud J. (2012) stating that ''Cracks 1,2,4 exceeded the serviceability limit category. Crack 5 remained quite unaltered throughout the tests and could be either the result of drying shrinkage of the finish, the effect of a 4m span serviceability deflection or some minor structural movement''. In fact, cracks 1,2,4 are very close to the location of the nodal deformation, whilst crack 5 is further away from the nodal deformation and thus the effect of the nodal deformation is 'less effective', thus the strain in that area is much less and as a result the crack width is not considerable and was unaltered during the gradual nodal deformation. This means that there is also agreement between the results of the two models, once again. This is illustrated in Figure 5:33.

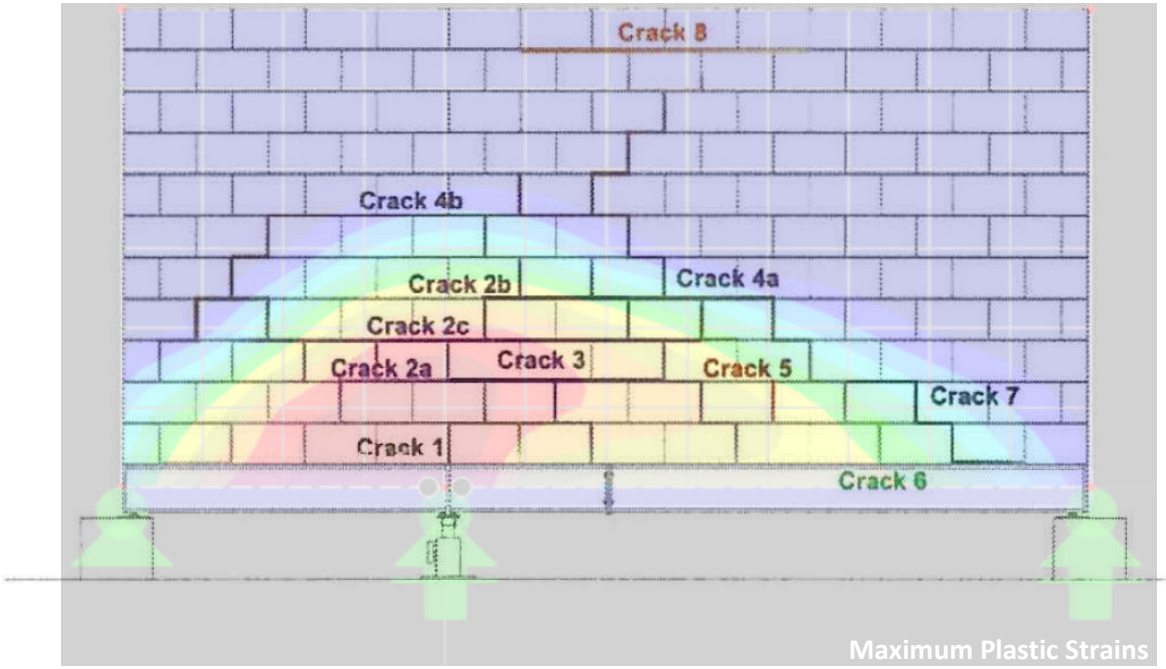

Figure 5:33 - Crack formation in the wall setup described by (Mifsud J. , 2012) superimposed over the Maximum Plastic Strains experienced by the numerical model

Mifsud J. (2012) also added that ''one can notice that cracks 2 and 3 form quite abruptly when considering their first noticeable crack width in contrast with the other cracks.'' This behaviour is expected due to the proximity of these cracks to the point where nodal deformation was applied. Consequently, the tensile stress near the applied nodal deformation develops at a faster rate.

5.5. Modelling Stage 3 – Modelling a room

5.5.1. Context

In this stage, the transition from a planar 2-D structure to a full 3-D structure was attempted. A single-storey room (measuring 8m in length, 4m in width, and 3m in height) was modelled, as shown in Figure 5:34. Similar to the previous models, the walls of this room were constructed from hollow concrete blocks, while the roof was made from reinforced concrete. The masonry walls forming part of the room are assumed to be supported by strip foundations.

A nodal deformation was applied to one corner of the room, with the aim of studying the overall deformation of the room and the formation of stresses in the walls. Modelling a room presents different challenges compared to those encountered in Sections 5.3 & 5.4, and these are listed as follows;

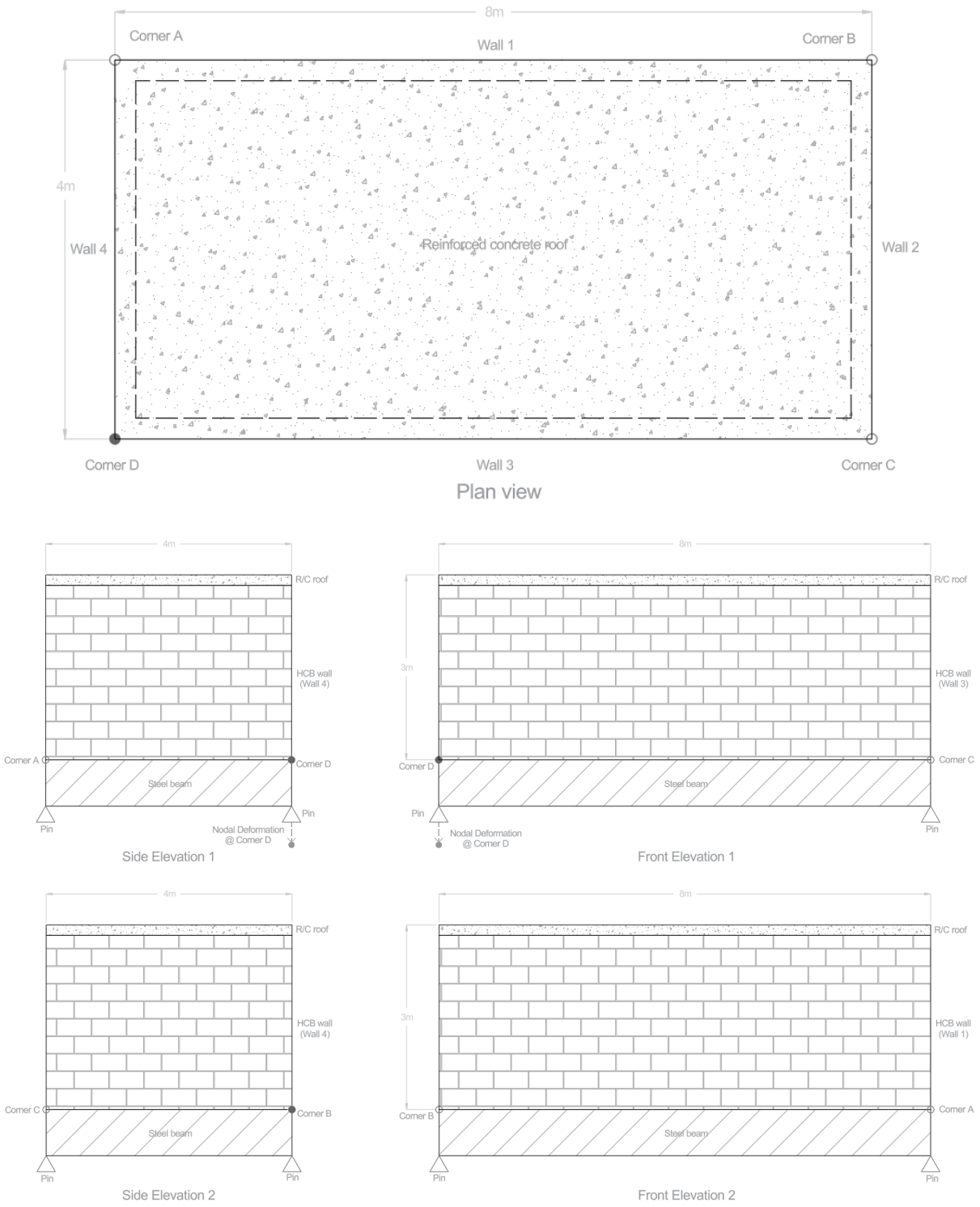

Figure 5:34 - Drawings of the single-storey room

5.5.2. Modelling Challenges

Issue 1 (Release between strip footing (beam) and wall)

A line release has been applied between the wall and the strip footing, allowing independent behaviour between the two structural elements. This is because, in reality, a damp-proof course layer is typically spread on top of the strip footing, resulting in complete separation of the two elements, as shown in Figure 5:35. As a result, the wall is allowed to move longitudinally.

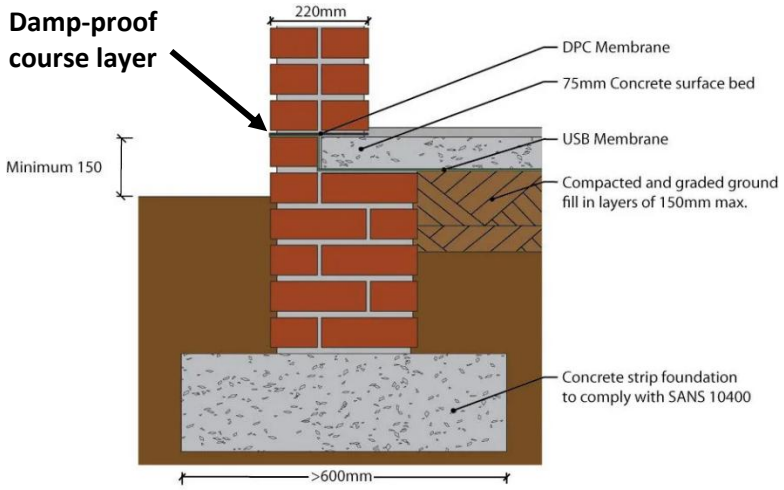

Figure 5:35 - The damp-proof course separating the strip footing from the wall

Issue 2 (Release between roof slab and wall)

A line release between the walls and the roof slab has been applied, assuming that no reinforcement from the masonry block wall is embedded in the slab, as shown in Figure 5:36. The slab is simply cast and supported by the wall, with no direct connection between the wall and the roof slab—only contact due to the slab resting on the wall. Any lateral loading applied to the slab is counteracted by the frictional force between the underside of the slab and the wall.

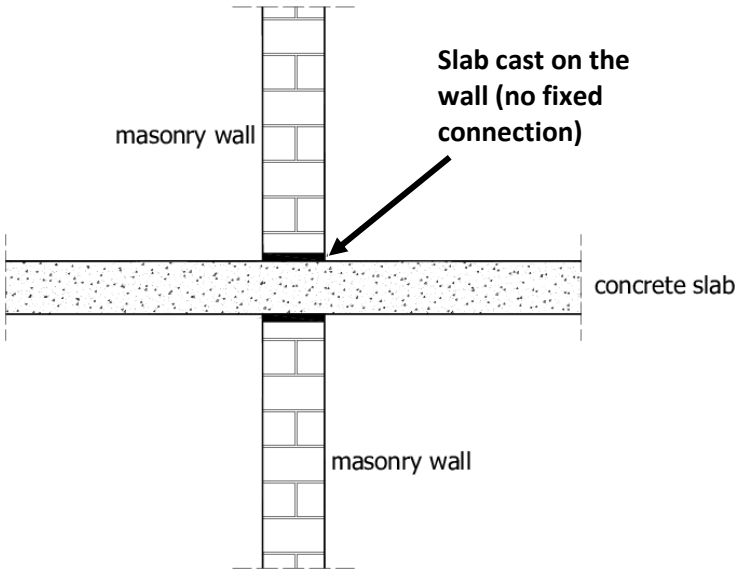

Figure 5:36 - Reinforced concrete roof casted on the masonry walls

Issue 3 (Release between orthogonal walls)

No release has been applied between orthogonal walls, as the walls are tied to each other, and movement is restricted due to the corbelling action between the masonry units from the orthogonal walls, as shown in Figure 5:37. In structural theory and finite element analysis, this concept is known as compatibility. It means that when a structure bends, stretches, or moves, the connected ends must move in a way that ensures the structure behaves as a single, continuous system.

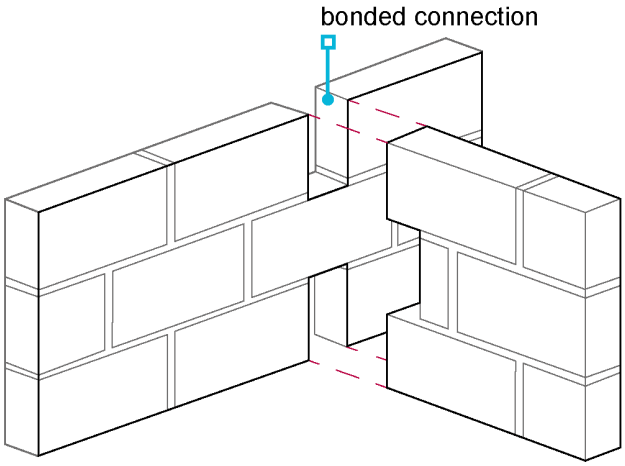

Figure 5:37 - Corbelling between orthogonal masonry walls

Issue 4 (Release between strip footing supporting orthogonal walls)

No release has been applied at the interface where the strip footings meet. This is because the strip footings supporting the overlying orthogonal walls would be cast as a single structural element, as shown in Figure 5:38. Additionally, it does not make sense for orthogonal strip footings to be unconnected, considering that the overlying supported walls are connected by the corbelling of the blockwork. If the orthogonal strip footings were not connected, it would undermine the purpose of the corbelling in the walls.

Figure 5:38 - Strip footing beneath the overlying structure

Issue 5 (Support)

Originally, a pin line support was chosen to support the overlying structure based on the fact that, due to the self-weight of the wall and the frictional force between the strip foundation and the ground material, the strip will not experience longitudinal movement, meaning the strip will not slide in the direction of settlement. Also, a line support was preferred over nodal supports at the intersection of the beams, as in reality the strip is continuously supported by the ground material.

However, the main issue with using the line support is that it would have been complex to analyse and interpret the formation of strains in the wall. This is because there is no guarantee that the formation of strains is solely due to the nodal deformation, or if other variables are influencing it. Therefore, to simplify the approach and limit the number of variables, the preferred solution consists of using very stiff beams that support the wall without bending under the imposed self-weight of the wall, as shown

in Figure 5:39. This ensures that any strains experienced by the wall are solely generated by the nodal deformation. This eliminates the possibility of strains forming in the wall because of bending in the beam.

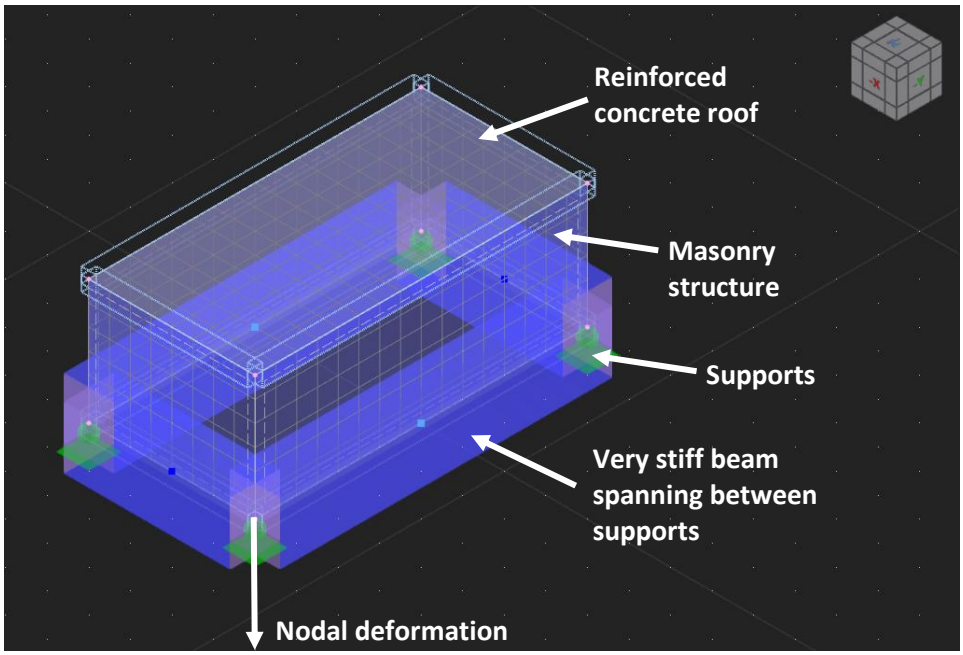

Figure 5:39 - 3D model of the room's structure

The advantage of this solution is that the use of very stiff beams achieves the same effect as if the beam were supported by a line support, as theoretically, the beam will not deflect due to its considerable stiffness. Thus, the simply supported beam behaves as a continuously supported beam. Apart from that, this approach provides a clearer understanding of strain formation when the wall undergoes nodal deformation, eliminating other variables that could affect the behaviour of the wall, such as strain development in the wall resulting from beam bending caused by insufficient stiffness.

The stiffness required for the beam was determined using the equation for the maximum deflection of a beam under a uniformly distributed load, representing the masonry wall. To meet the stringent stiffness requirements, a custom rectangular solid steel beam was selected, as standard steel beams may not provide sufficient rigidity. The moment of inertia, derived from the deflection formula, was used to calculate the necessary dimensions for the beam to achieve the desired stiffness.

5.5.3. Modelling of Ta Kenuna Tower (Real Life Case Study)

5.5.3.1 Context

To provide context, it is essential to explain the reasoning and decision-making process behind this approach. Until now, the calibration has been performed on a 2D planar wall, based on the work of Mifsud J. (2012). However, no calibration or validation had yet been conducted for a 3D structure. Given that the room model shared several characteristics with the Ta' Kenuna Tower—such as similar plan dimensions, simple prismatic structure, and masonry construction—it was logical to attempt modelling this real-life tower, whose performance is well-documented, akin to the approach taken by Mifsud J. (2012). This proved to be an effective exercise in validating and calibrating the numerical model, significantly enhancing the research's overall value.

As this model forms a foundational element of this dissertation, serving to calibrate and establish the reliability of the numerical model against a real-life structure, the results of the Ta' Kenuna Tower analysis will be presented and discussed in this section.

5.5.3.2 Historical Background

Ta' Kenuna Tower, named after *kenur* (a place where signal fires were lit), was built in 1848 during Queen Victoria's reign and Governor Richard More O'Ferrall's time as one of Malta's three semaphore stations. Its strategic location in Gozo provided clear visibility for transferring messages between towers, facilitating telegraph communication between Malta and Gozo. Though it was only used for twelve years before becoming obsolete due to technological advances, the tower remained significant. After falling into disrepair and suffering damage during WWII, it was restored in 1998 by Maltacom (now GO plc) and repurposed for modern telecommunications (Meilak, 2021). Today, it houses technology for cellular, paging, data, and maritime services, once again serving as a vital communications hub for the Malta-Gozo link, as shown in Figure 5:40.

Figure 5:40 - Ta' Kenuna Tower

5.5.3.3 Recent Structural Interventions

The intervention is a self-supporting structure that avoids any physical impact on the historic tower. It features a single inclined column as its core, supporting all floors and a copper-clad roof that appears to float above the tower, allowing sky views and maintaining visual separation through large, glazed areas. The design preserves the tower's original fragmented silhouette while referencing its historic signalling framework. All modern services and installations are integrated within the new structure without affecting the old fabric.

5.5.3.4 Geotechnical related issues

The tower stands on a cliff composed of Upper Coralline Limestone overlying Blue Clay. Prolonged exposure of the clay to natural elements has led to ongoing ground movement, evidenced by visible ground cracks near the cliff edge that have progressively widened into tension fissures, indicating continued lateral displacement. In addition to these fissures, further cracking has been observed inland

on both the eastern and western sides of the structure, as shown in the Figure 5:41. These cracks are narrower than those at the edge, suggesting that the damage is spreading inward. It is therefore assumed that similar subsurface cracking exists beneath the structure, potentially forming a continuous fracture line between the eastern and western cracks.

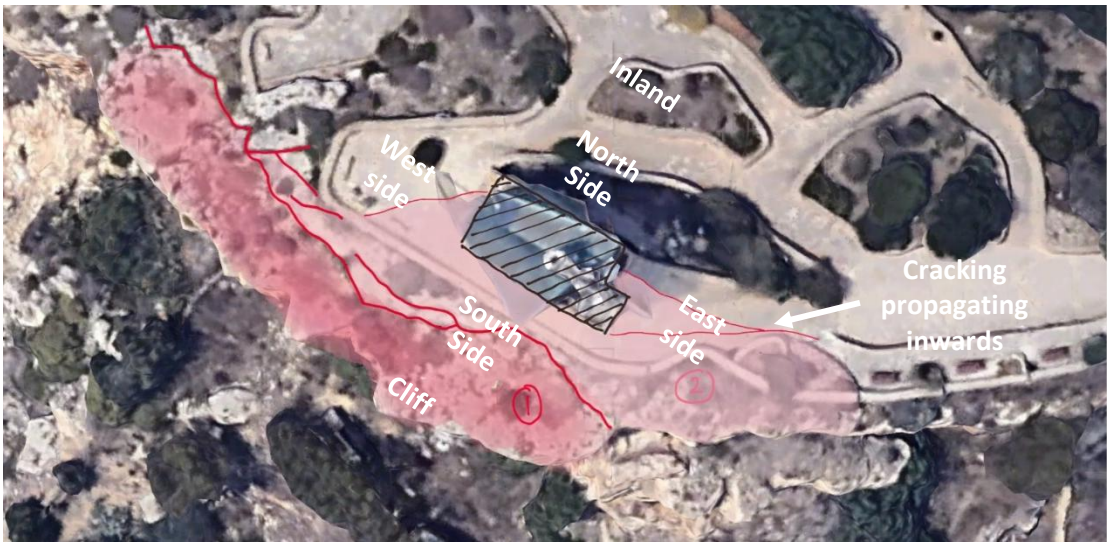

Figure 5:41 - Cracking in the ground: 1)Thick red lines indicate wide tension fissures near the cliff edge, 2)Thin light red lines represent narrower cracks beneath the structure

The wider tension fissures at the cliff edge are expected, as the unsupported edge is more susceptible to progressive widening over time. This ongoing movement gradually undermines the cliff's stability, eventually leading to edge failure and exposing the underlying rock wedge that supports the tower. As this process continues, the cliff edge retreats inland, triggering a recurring cycle of cracking and collapse, as illustrated in the Figure 5:42.

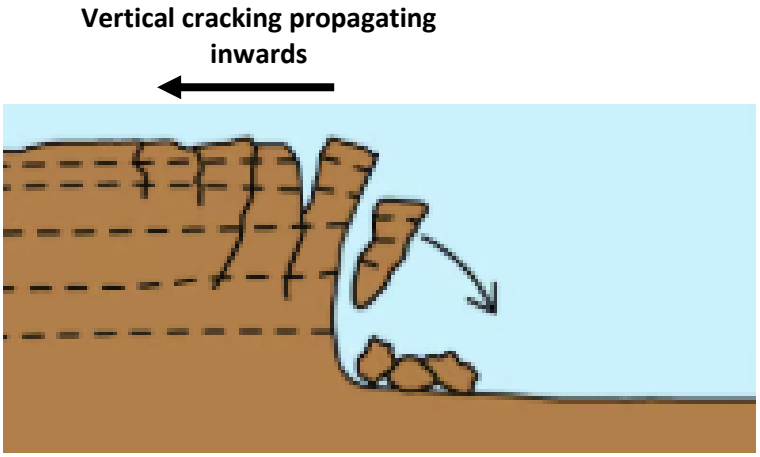

Figure 5:42 - Cracking in the ground near the cliff edge

This geological activity directly affects the stability of the masonry structure above. Uneven ground movement beneath the tower causes differential settlement, resulting in strains and cracks within the masonry walls. Mapping the visible ground cracks on site is essential to determine which parts of the structure are shifting. Observations show that most of the structure lies over the cracks on the eastern and western sides, indicating it is subject to movement, while a smaller portion remains stationary, as shown in Figure 5:41. This indicates that the structure is undergoing horizontal movement, resembling a form of lateral spreading of the foundation.

5.5.3.5 Modelling Challenges

This section highlights the key similarities and differences between the room model in Section 5.5.2 and Ta Kenuna Tower model.

There are a few differences and similarities between the model of the room and the model of Ta' Kenuna Tower. One difference is that the tower is constructed using local solid Globigerina limestone blocks, rather than hollow concrete blocks. Wall thicknesses vary between 0.65 m and 0.3 m, as shown in Figure 5:43 (or within the scaled drawings provided in Appendix C). Another difference is that the tower has no roof (Figure 5:45), as a recent intervention has introduced a self-supporting steel structure that does not impose any load on the existing masonry walls. Another difference is that the existing apertures in the tower have also been included in the model, as on site it was observed that cracks have developed at or near these openings, as shown in Figure 5:43**.**

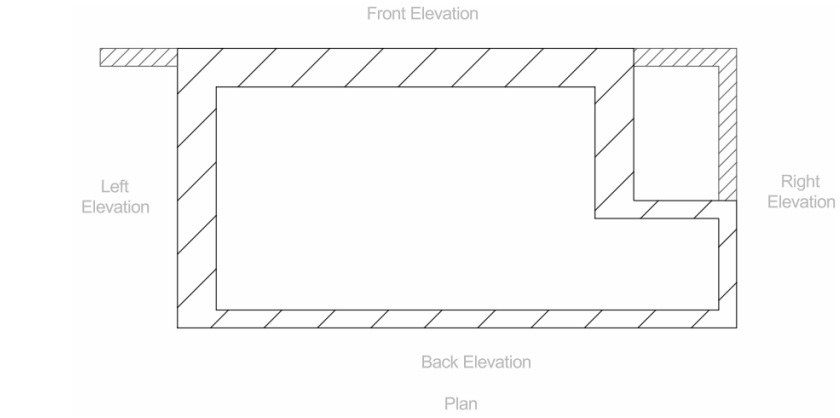

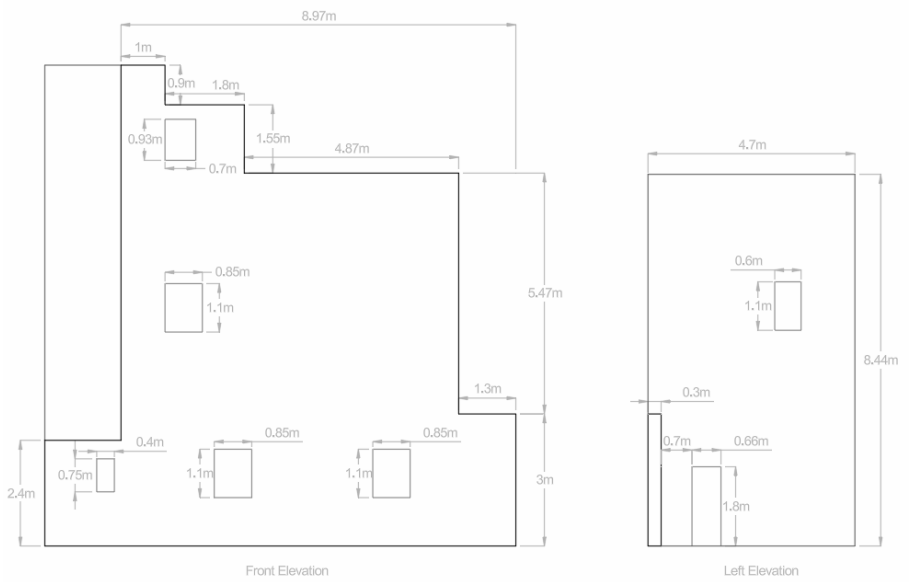

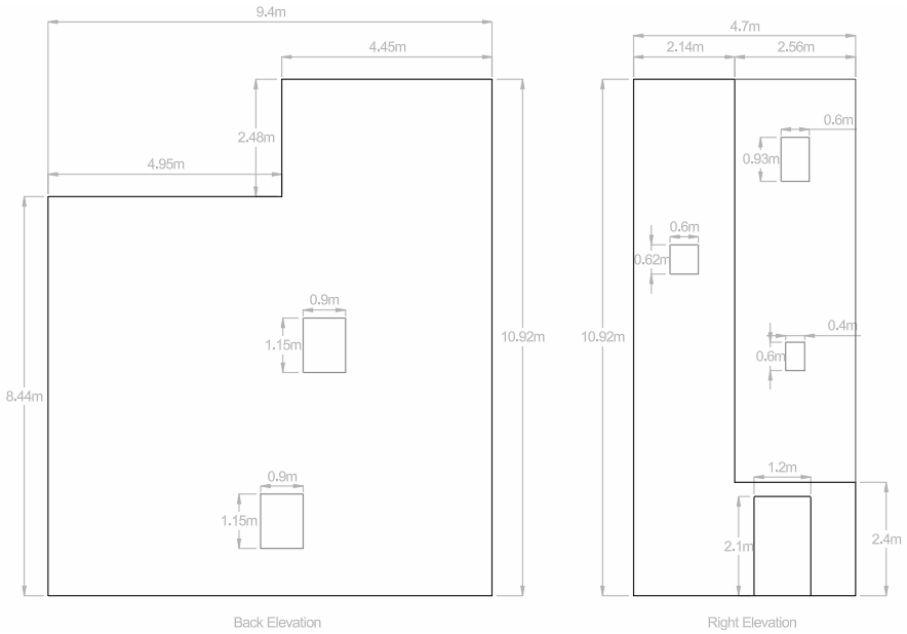

Figure 5:43 - Drawings of Ta' Kenuna Tower

The key distinction lies in the type of nodal deformation: while the room model in Section 5.5.2 undergoes vertical nodal deformation, the tower experiences horizontal nodal deformation. As detailed in Section 5.5.3.4 , ground crack mapping confirms that the structure is undergoing horizontal movement, with most of it in motion while a portion remains stationary, as shown in Figure 5:44. Consequently, unlike the room model, horizontal nodal deformation must be applied to more than one corner of the tower to accurately reflect its behaviour, as shown in Figure 5:44.

Additionally, the mapping of cracks and site photographs proved useful in identifying which supports should be assigned nodal deformation in the model, as well as estimating the angle at which this horizontal deformation should be applied, as shown in Figure 5:44. The deformation values were determined through a trial-and-error approach, as the objective of the exercise was not to calculate the exact nodal deformation experienced by the structure.

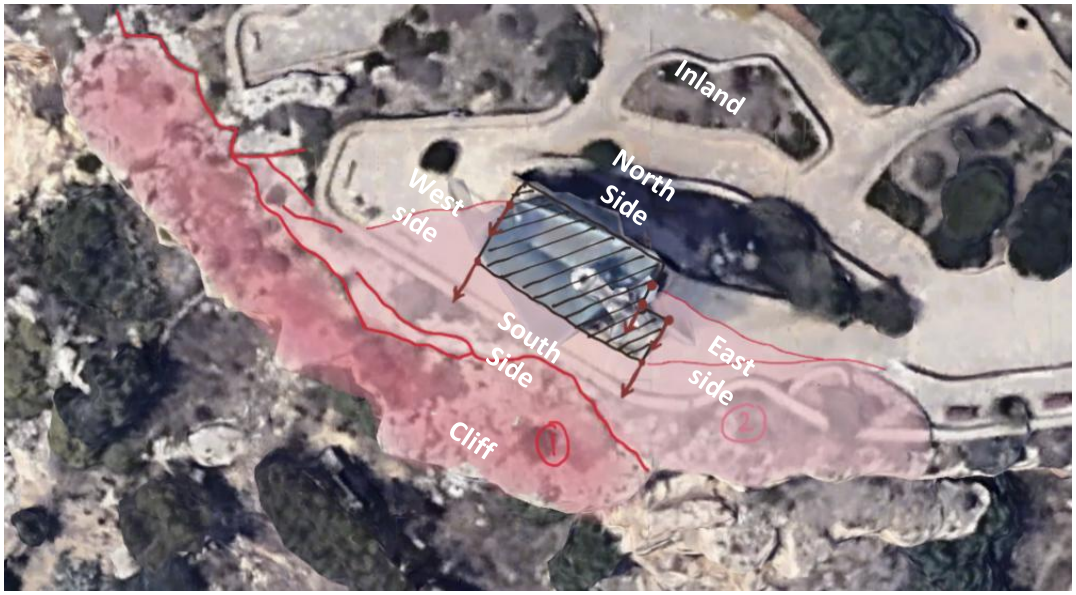

Figure 5:44 - Ground crack mapping and locations within the structure where nodal deformations are applied

On the other hand, the first similarity is that the foundation concept remains unchanged: the masonry walls are supported by very stiff beams, which are pin supported at their ends, mimicking the existing foundation system beneath the actual tower (Figure 5:45). Also, to simulate pin connections, rotational releases were applied at the ends of the beams, preventing moment transfer. This avoids the introduction of hogging moments into the masonry walls, which could exacerbate deformation. Another similarity is that a line release was introduced between the masonry walls and the supporting beams, allowing independent behaviour of the two components and preventing unintended composite action (Figure 5:45). The final similarity is that no releases were applied between orthogonal walls, ensuring compatibility and enabling the walls to function together through tying action (Figure 5:45).

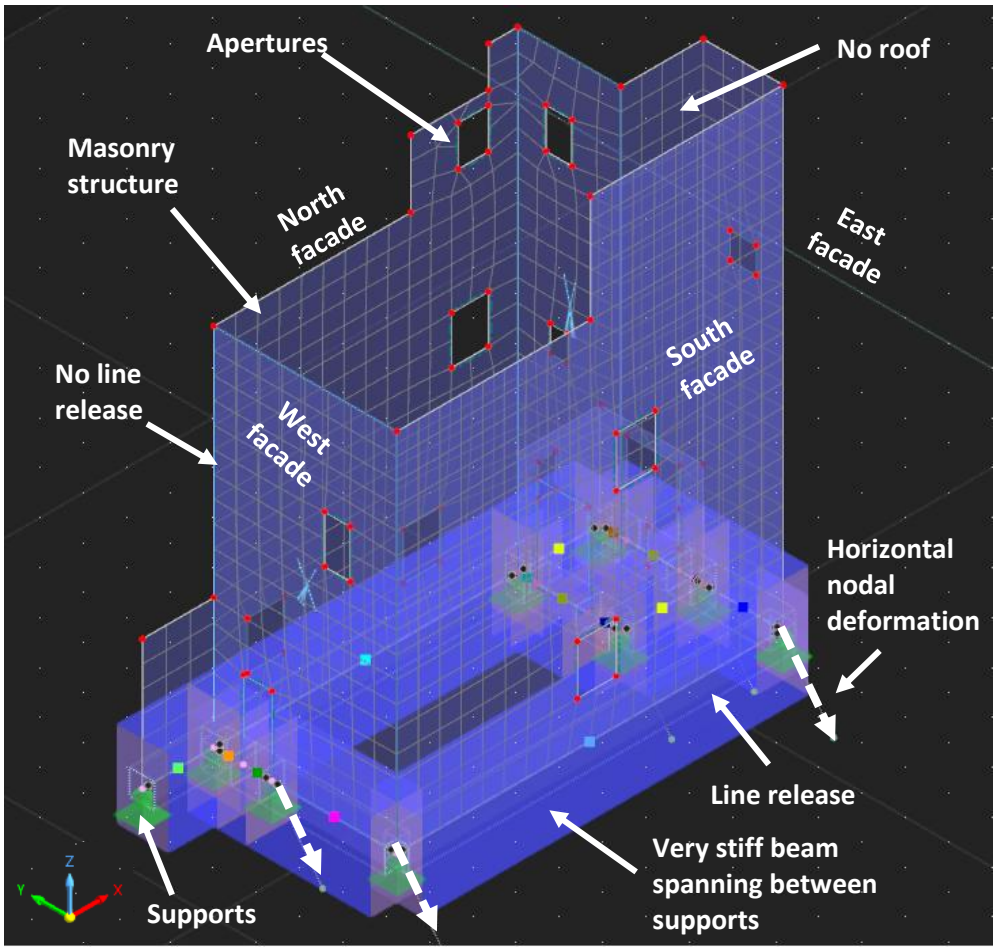

Figure 5:45 - 3D model of Ta' Kenuna Tower

5.5.3.6 Results and Discussion

When analysing the results of this numerical model, two key aspects were considered. First, it was crucial to understand and visualize the overall deformations experienced by the structure due to the nodal deformations. Second, it was important to compare the cracks observed in the real-life structure with the numerical model's results, focusing on the maximum plastic strains.

Global Deformations

From the global deformations of the numerical model, appears that the façades located above the wedge of rock—moving outward toward the cliff edge—are also displacing outward. This suggests that these façades are being pulled along by the movement of the underlying rock wedge, as shown in Figure 5:46. This behaviour is logical: due to their self-weight, the façades rest directly on the wedge and therefore follow its displacement, unable to resist the motion independently.

In contrast, the façades located on stable ground (i.e., not subject to rock movement) also exhibit outward displacement. However, in this case, the movement is not driven by ground motion, but rather by corbelling and structural interconnection between orthogonal masonry walls. These walls tie the South and North façades together by the frictional and cohesive forces acting between the masonry units and the mortar, so as the front façade moves outward, the resultant shear stress exerts a pulling force on the rear masonry walls, causing them to displace as well, as shown in Figure 5:46.

Since the applied horizontal nodal deformation was at an angle—neither strictly along the x-axis nor the y-axis—the global deformation pattern shows movement in both directions. This gives the impression that the structure is being stretched diagonally, in the direction of the applied nodal deformation. Consequently, the front façade appears to tilt outward in that direction, further supporting the observation of diagonal displacement, as shown in Figure 5:46.

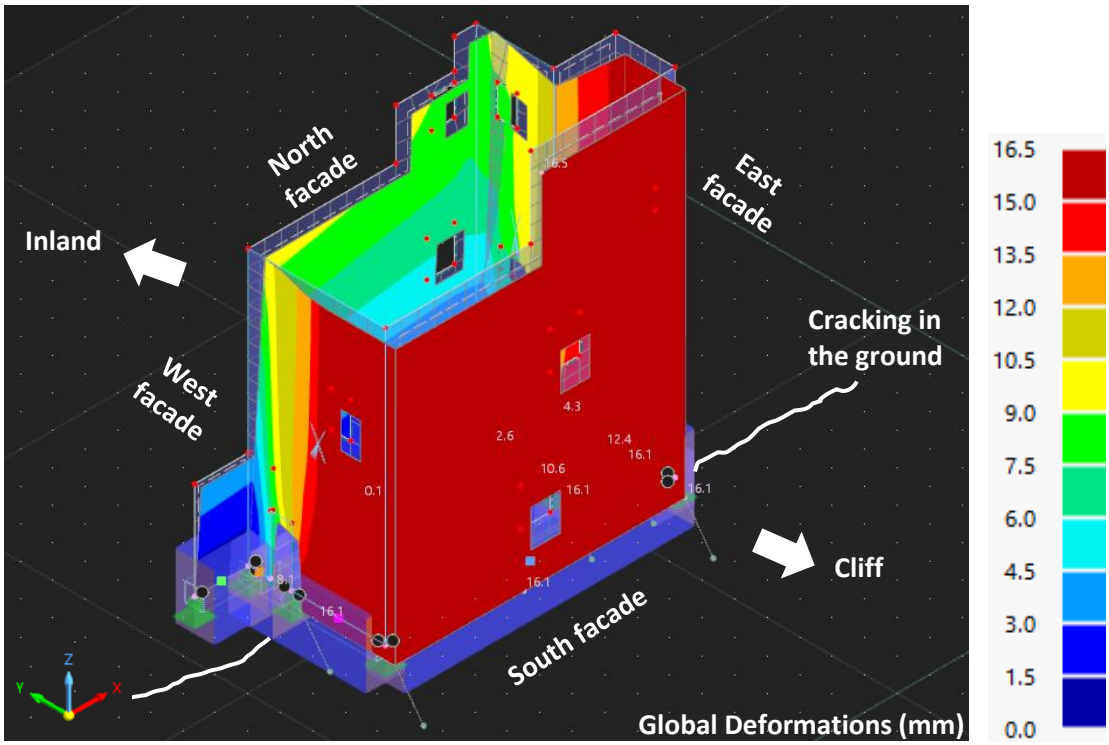

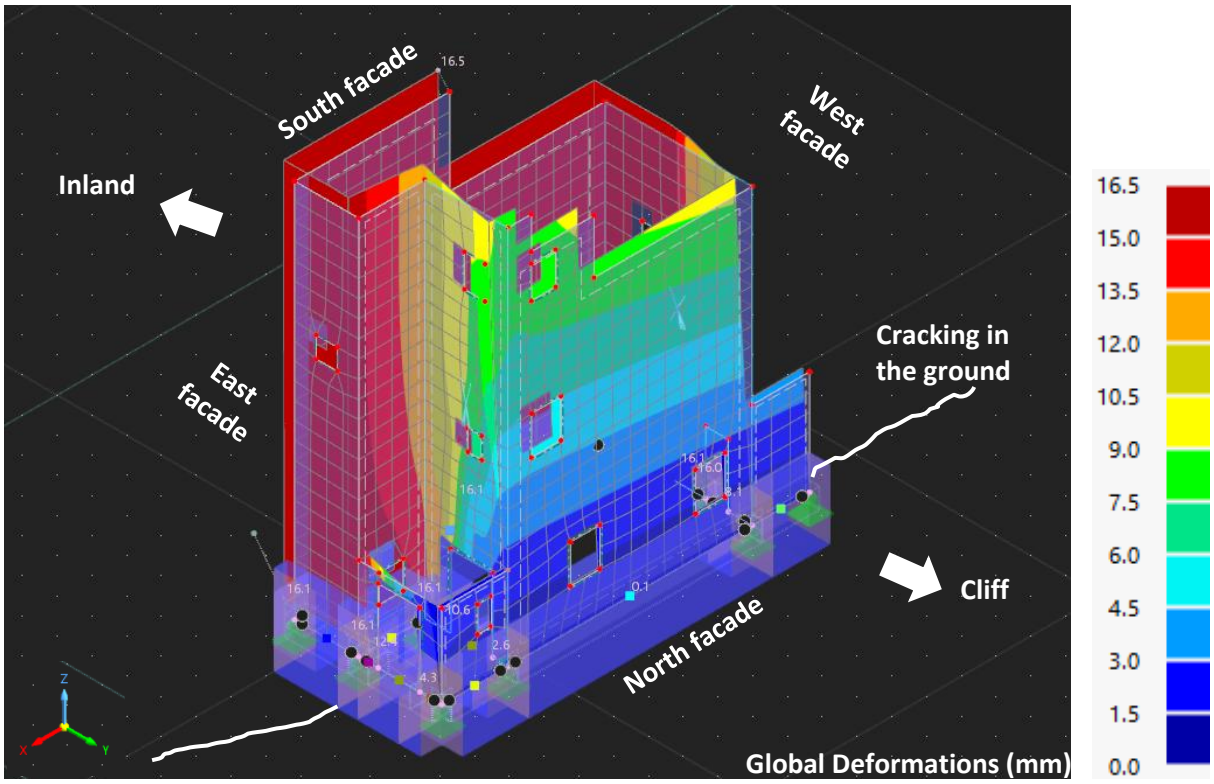

Figure 5:46 - Global Deformation of Ta' Kenuna Tower model from different views

Another important observation is the impact of this diagonal stretch on the apertures (windows and openings) within the façades, as illustrated in Figure 5:46. On the South façade, while the windows move in tandem with the façade, the apertures themselves remain largely unaffected, showing no significant distortion or deformation. This indicates that the forces pulling the structure apart are more uniform and do not cause significant local shear strain (Figure 5:46). In contrast, the east and west façades display visible aperture distortions. As the façades displace outward, the apertures become stretched and deformed, with the greatest distortions occurring near the nodal deformation application point (Figure 5:46). Apertures higher up, farther from this applied force, experience minimal impact. Additionally, the North façade tilts as it is pulled by the front and side walls, resulting in slight deformation of its apertures (Figure 5:46). However, these deformations are less pronounced compared to those observed on the side façades.

It is worth noting that the magnitude of the applied nodal deformation in the model is greater than the deformations currently observed on site, as shown in Figure 5:47, Figure 5:48 and Figure 5:49. This is not problematic, as the model still serves a dual purpose: it allows comparison with existing damage observations and helps predict where further deformation might develop in the real-life structure under worsening ground conditions.

Maximum Plastic Strain

So far, only a few cracks have been observed on the structure, and these are primarily located near the apertures. In the examples below, photographs taken during the site visit—focusing on the East and West façades—are compared with the results from the numerical model to assess the model's reliability.

By examining the regions of maximum plastic strain in the model, a clear correlation can be seen between the simulated results and the cracking patterns observed on site, as illustrated in Figure 5:47 and Figure 5:48. This similarity indicates that the numerical model is accurately capturing the structural behaviour. Furthermore, the model provides insight into how further cracking is likely to evolve under the effect of further ground movement, offering a valuable predictive tool for future damage assessment and mitigation.

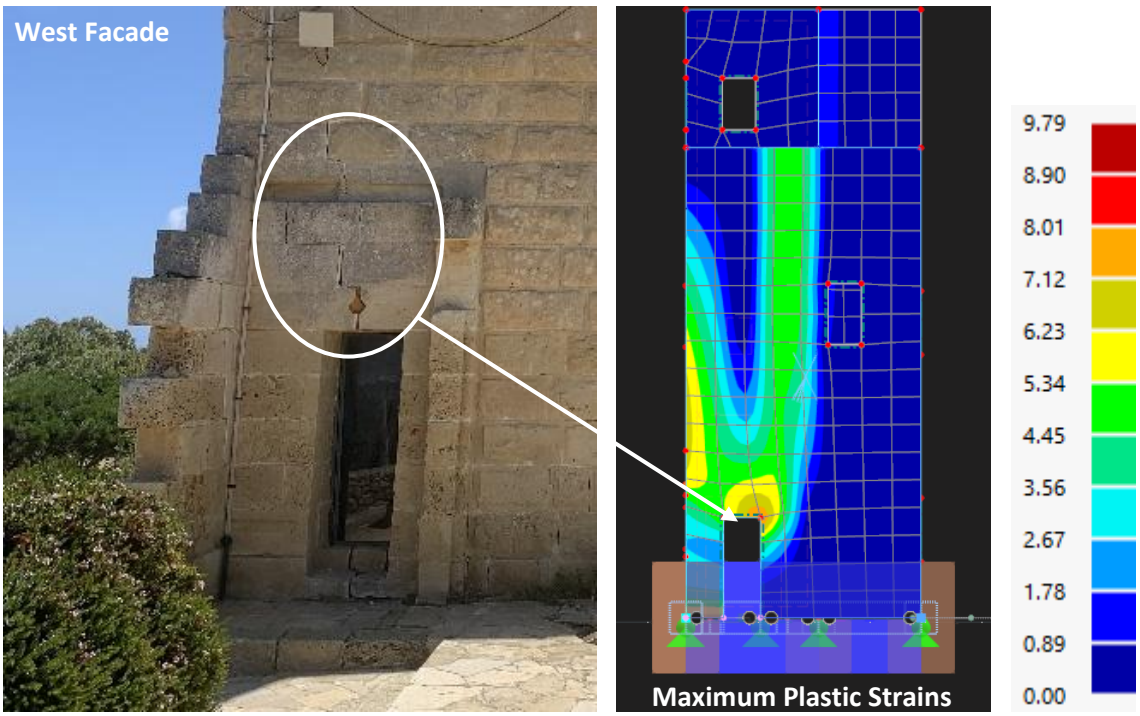

Figure 5:47 - Comparison between the numerical model and observed on-site cracking

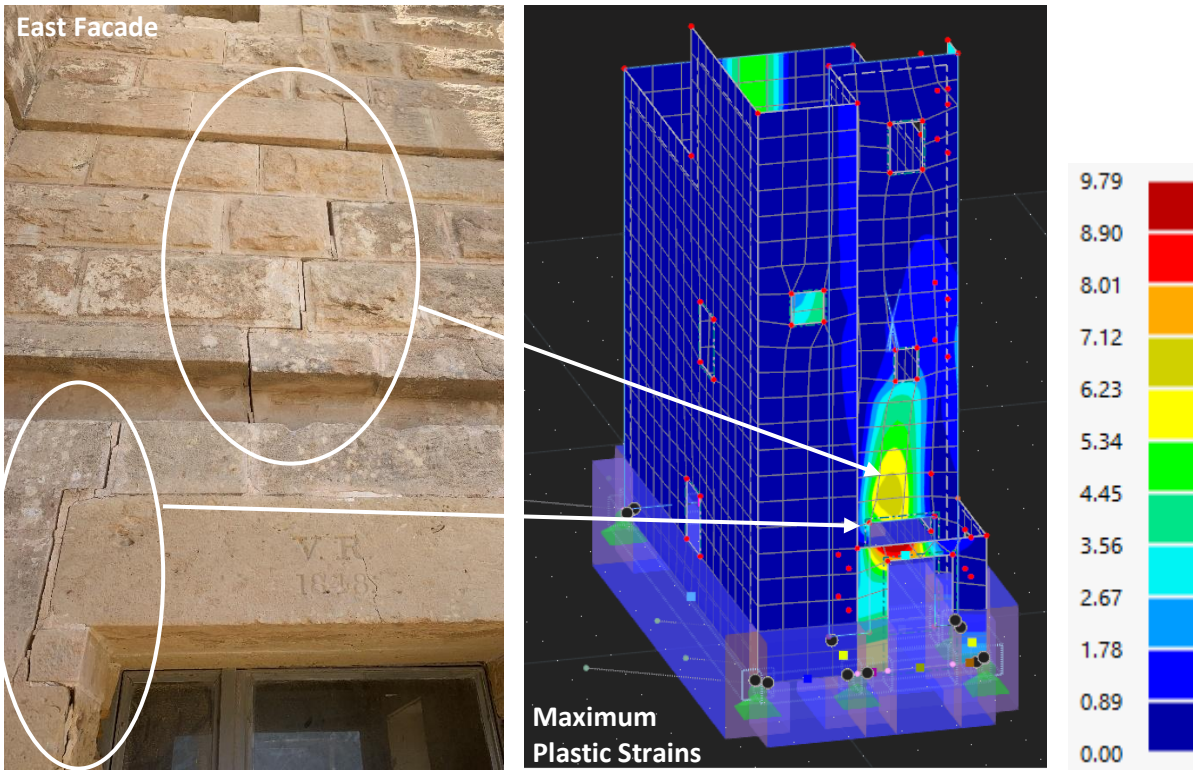

Figure 5:48 - Comparison between the numerical model and observed on-site cracking

On the other hand, the numerical model did not predict the cracking observed near the aperture on the back façade, even though such damage is clearly visible on site, as shown in Figure 5:49. This does not indicate that the model is inaccurate or unreliable in representing the structural behaviour. Rather, it reflects the fact that the nature of the damage on the back façade differs from that of the East and West façades.

As previously discussed, the East and West façades appear to be undergoing diagonal stretching in the direction of the applied nodal deformation, whereas the back façade is primarily experiencing tilting. This tilting behaviour is captured by the numerical model, which shows that the upper portion of the back façade is subjected to more significant displacement compared to the lower portion.

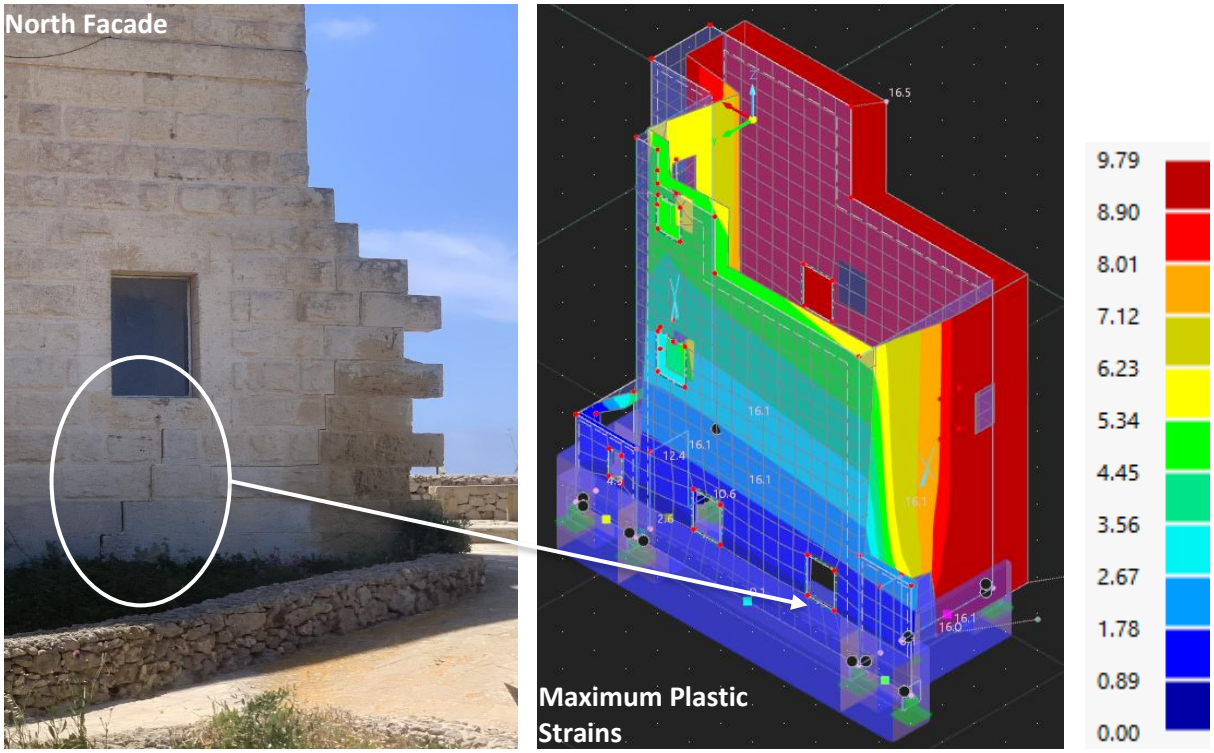

Figure 5:49 - Comparison between the numerical model and observed on-site cracking

Therefore, it is reasonable to conclude that the crack near the aperture on the back façade is likely a result of this tilting action, rather than the diagonal tension observed on the side façades. The difference in damage mechanisms explains why the crack was not captured in the same way within the model.

5.6. Modelling of a Typical Apartment Block

5.6.1. Context

Finally, after verifying the methodology using both 2-D planar and 3-D models in comparison with real-life structures, sufficient confidence in the modelling technique was established. This enabled the exploration of numerical modelling for an entire apartment block.

Given the complexity of the apartment block compared to the structures discussed in previous sections, this section has been subdivided into smaller segments. Each segment focuses on a specific aspect of the apartment block, providing the necessary context and background to enhance the reader's understanding and improve overall clarity.

5.6.2. Spatial Layout & Selection Criteria

This section is divided into two parts. The first part focuses on the selected typical apartment block, presenting its design and discussing the spatial layouts of its various floors. The second part explains the rationale behind choosing this specific design.

It is important to note that the layouts shown below and in the Appendix D (to scale) are not direct copies. Instead, they are based on research into typical apartment layouts in Malta, using plans sourced from the Planning Authority website. Key features and common elements identified during this research were combined and synthesized into a single representative drawing.

A typical apartment block consists of several distinct floor types (Figure 5:50). At the lowest level, there is an underground basement. Above this lies the ground floor, which typically houses maisonettes. Overlying the maisonettes are additional apartment floors, the number of which varies based on local planning regulations. Finally, at the topmost level, a penthouse is located. The following sections provide a detailed overview of the spatial layout of each floor type (Figure 5:50).

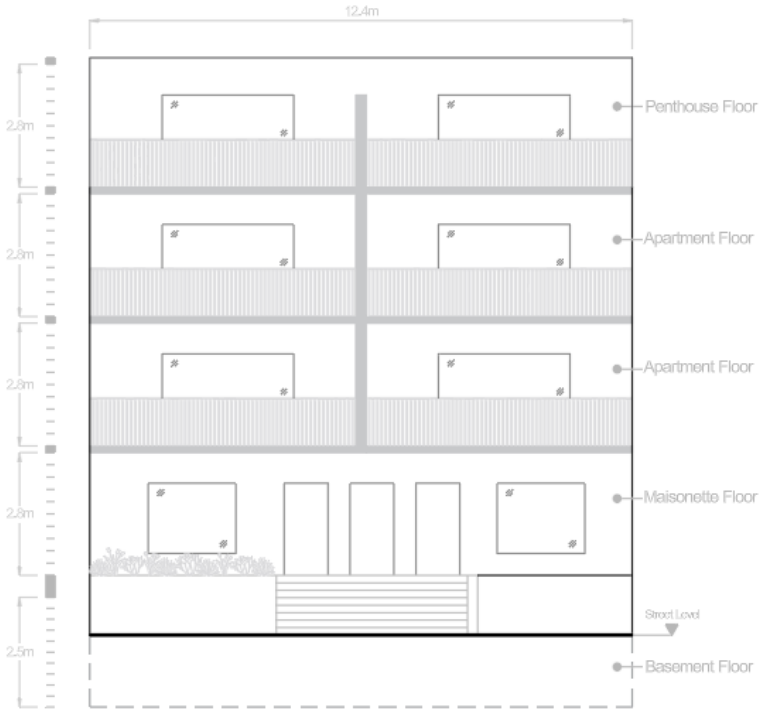

Figure 5:50 - Elevation view of a typical apartment block

Basement (Underground) – Level -1

The basement, located at Level -1, is accessed via a ramp (Figure 5:51). The layout of this floor includes a series of garages positioned on the west and north sides, with a wide corridor opposite the garages on the east side (Figure 5:51). This corridor facilitates vehicle manoeuvring for entry and exit from the garages (Figure 5:51). Adjacent to the ramp, on the left side, there is a lift and a storeroom. The storeroom is typically situated beneath the front garden and staircase at the ground floor level (Figure 5:51). Due to this placement, the storeroom has a reduced internal height, making it suitable for storage purposes. The basement is designed to maximize the number of garages within the available space, ensuring efficient use of the area.

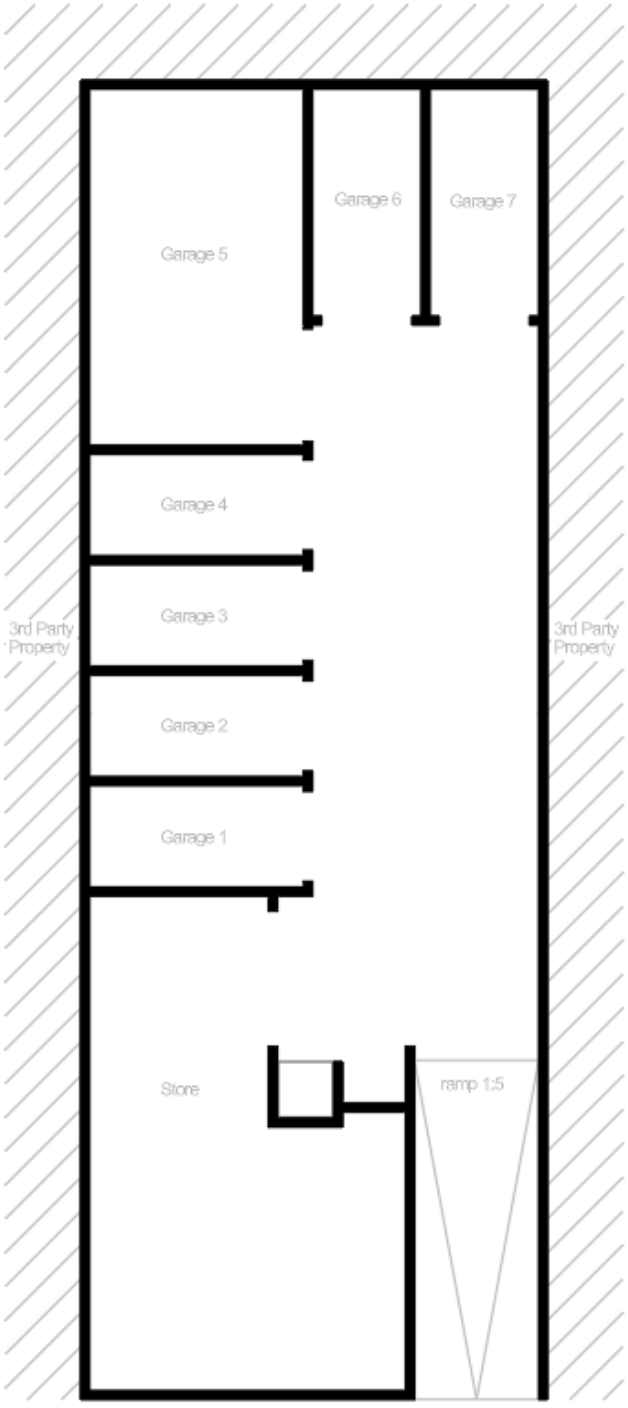

Figure 5:51 - Typical basement floor layout plan

Maisonettes (Ground Floor – Level 0) & Apartments (Level 1 to Penthouse)

The maisonettes on the ground floor (Level 0) and the apartments above them share a similar spatial layout (Figure 5:52). However, the maisonettes differ in having separate entrances, while access to the apartments and penthouse is provided through a common area, including a staircase and lift (Figure 5:52). The spatial layout for these floors begins with an entrance that opens into a combined kitchen, dining, and living area, which occupies the largest portion of the floor. A narrow corridor connects this main area to the bedrooms and bathrooms. Central to the design is a large shaft that facilitates ventilation and accommodates ductwork for the bathrooms and ensuites (Figure 5:52).

While the layouts of the maisonettes and apartments are nearly identical, there are a few distinctions. For instance, slight variations exist in the walls surrounding the core, which houses the staircase and lift (Figure 5:52). Additionally, the apartment floors typically feature narrow balconies at both the front and back, which are absent in the maisonettes (Figure 5:52). Since the spatial layout of the apartment floors remains consistent across levels, further repetition is unnecessary.

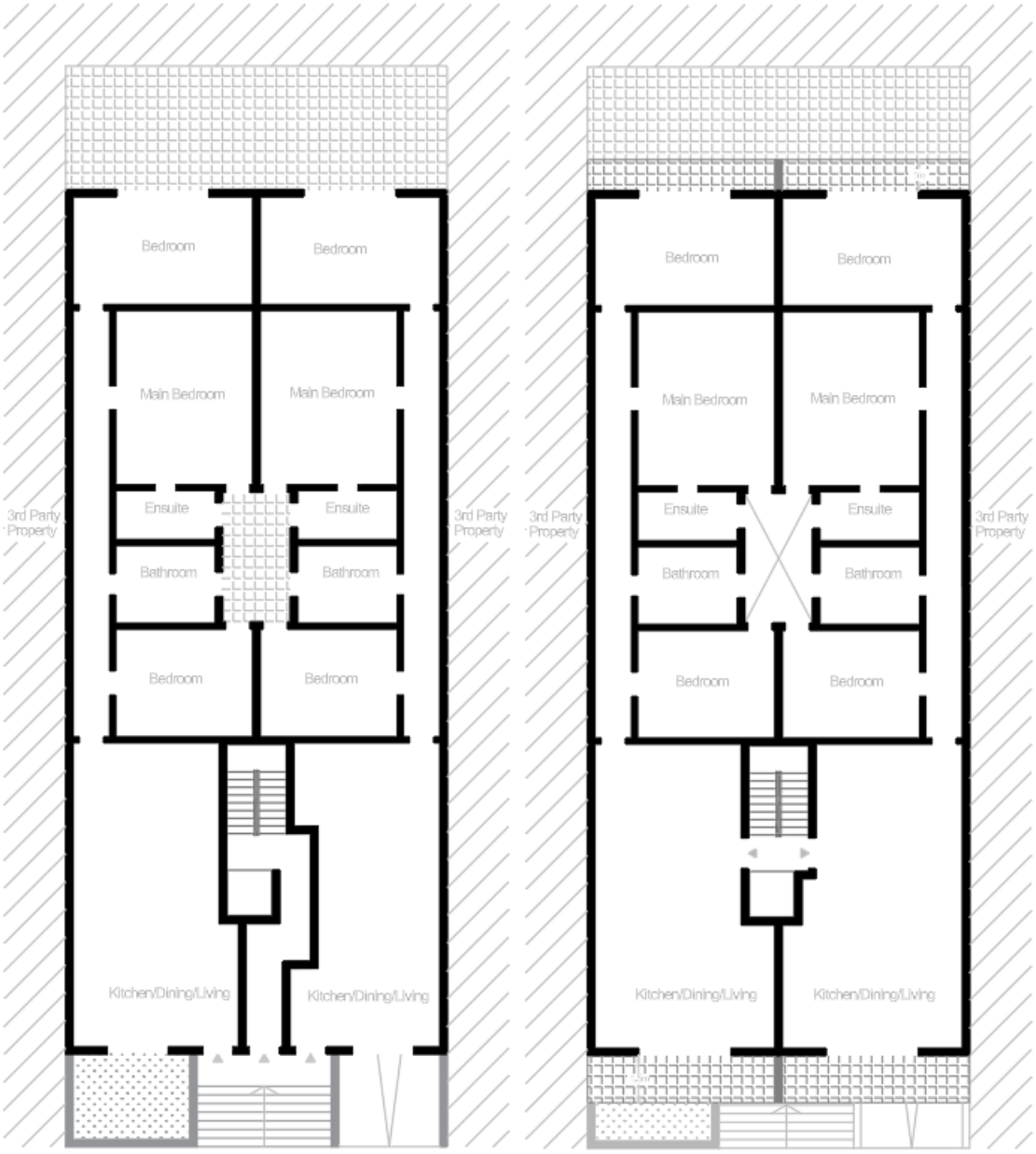

Figure 5:52 - 1)Typical maisonette floor layout plan, 2)Typical apartment floor layout plan

Penthouse – (Top Most Floor)

The penthouse, located at the topmost floor, mirrors the general spatial layout of the apartments but incorporates setbacks at the front and back, which reduce its overall floor area (Figure 5:53). The front setback creates a spacious terrace that is often used as an outdoor living area, while the back setback forms a smaller balcony (Figure 5:53). Despite the reduced built-up area, the penthouse retains the same number of rooms as the apartments below. To achieve this, the room sizes, particularly the kitchen, dining, and living area, as well as the two rear bedrooms, are slightly smaller (Figure 5:53). While the penthouse maintains the overall layout consistency of the maisonettes and apartments, its unique setbacks introduce additional outdoor spaces and slightly modified room dimensions (Figure 5:53).

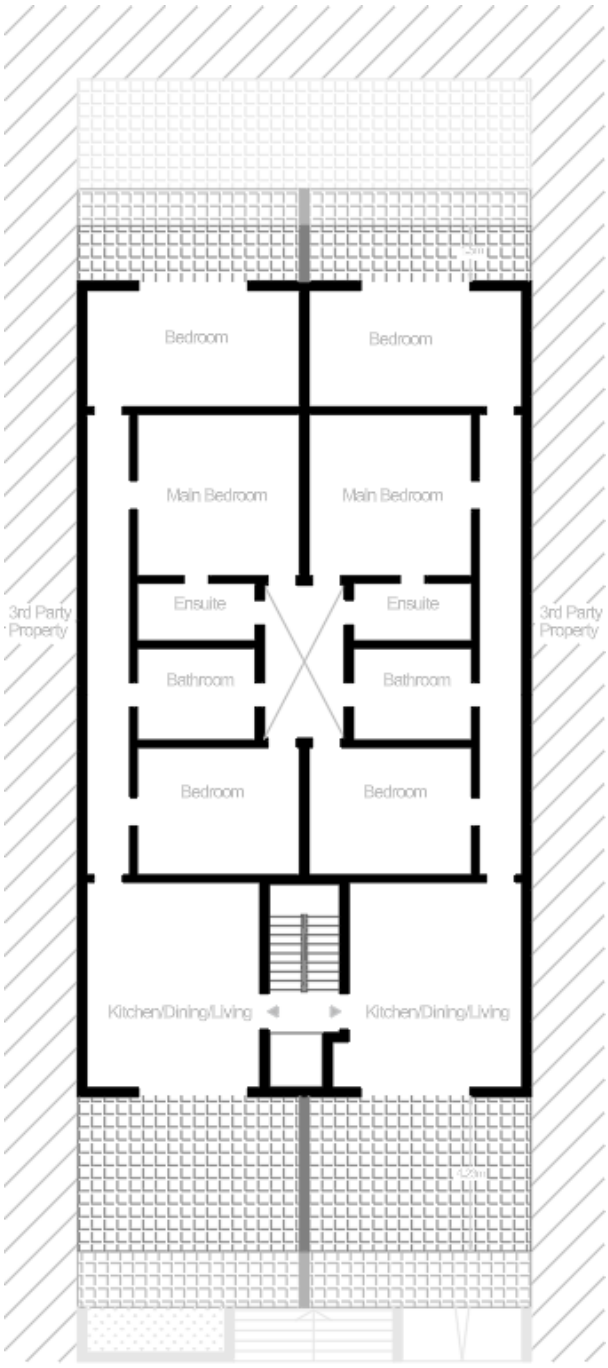

Figure 5:53 - Typical penthouse floor layout plan

Selection Criteria

Research was conducted on residential buildings commonly constructed in Malta to ensure the modelled structure accurately reflects local architectural and structural characteristics, particularly in terms of layout. The selection process was guided by several carefully chosen criteria:

- A rectangular plot layout
- Apartments consisting of three bedrooms
- Access to an underground basement
- Inclusion of a penthouse
- Adjacent Apartments with central mirror layout

These criteria were selected with the dual aim of reflecting typical Maltese construction practices and facilitating the modelling process. For example, a rectangular and vertically symmetrical layout simplifies the geometry and reduces modelling complexity. The choice of three-bedroom apartments with adjacent apartments having a central mirror layout was based on the larger size of these blocks, which enhances the development and visibility of strain patterns, facilitating easier study of structural behaviour.

Including a basement was considered essential due to its distinct layout compared to the upper floors. This difference necessitates a transfer slab, creating a soft story and significantly impacting the overall structural response— a design feature uncommon in other countries, where structural frames are typically used. Consequently, the basement leads to significant deformations and strain throughout the entire structure. Similarly, incorporating a penthouse was important, as its slightly varied layout introduces additional variation in load paths and structural behaviour, enhancing the realism and comprehensiveness of the model.

5.6.3. Construction Methodology

As highlighted in Chapter 1, evolving residential building typologies in the Maltese Islands have significantly impacted the structural and geotechnical aspects of masonry construction. This section explores these developments, providing a foundation for understanding the construction methodologies of the local industry. These concepts will contextualize the construction approach for the selected typical apartment block.

Structural Aspects

The first key issue to address is the definition of local masonry construction, which traditionally refers to structures built using blocks bonded with mortar. Historically, terraced houses and villas were primarily constructed with local Globigerina limestone blocks, while hollow concrete blocks were reserved for secondary elements, as illustrated in Figure 5:54. In contrast, modern apartment blocks predominantly use hollow concrete blocks, with Globigerina limestone now mainly serving decorative purposes, as shown in Figure 5:54.

Figure 5:54 - Traditional terraced houses built using locally Globigerina limestone blocks, and modern apartment blocks built using locally Hollow Concrete Blocks (HCB) respectively

One of the most critical structural concerns lies in the continued use of hollow concrete blocks as load-bearing elements. Unlike globigerina limestone, which is solid and has relatively higher compressive strength, hollow blocks are weaker and less suited for high-load conditions. This becomes increasingly problematic as apartment blocks grow in height compared to traditional low-rise buildings. Moreover, in most cases, the walls are unreinforced and single-skin, exacerbating the risk of cracking, crushing, or instability, especially under vertical and lateral loads.

Another critical concern in local masonry construction is the absence of structural frames in many apartment blocks, which rely solely on unreinforced masonry (URM). Unlike terraced houses, apartment blocks typically have more floors and generate significantly higher loads, making the inclusion of a structural frame essential for stability and proper load distribution, as shown in Figure 5:55. URM, being brittle and lacking ductility, is particularly vulnerable to seismic activity and wind loading, especially in taller buildings. Without reinforced frames, there is no effective lateral load-resisting system, and lower walls bear excessive vertical stress, significantly increasing the risk of failure.

URM structures are also more susceptible to differential settlement, which often leads to cracking. In the absence of a frame to help distribute loads or restrain movement, these effects become more pronounced. Additionally, URM construction limits architectural flexibility and complicates any future modifications or extensions.

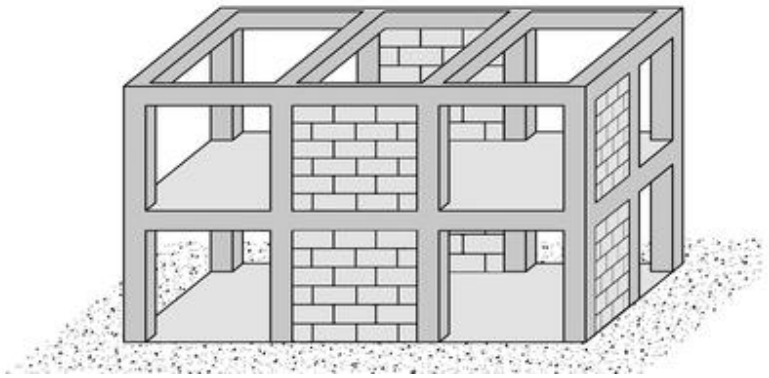

Figure 5:55 - Concrete-reinforced frame infilled with masonry wall

Another important issue, unrelated to masonry construction itself, is the floor layout and load path of apartment blocks. The internal layouts of modern apartment blocks have introduced new structural challenges. Open-plan designs with minimal internal walls are now common, resulting in longer slab spans and irregular load distribution, which increase the risk of stress concentrations. Furthermore, internal partition walls are often positioned based on apartment configurations rather than structural alignment, leading to two significant issues.

First, corridors frequently run alongside long, unbraced walls that lack cross-wall support, reducing their stiffness and stability. Second, discontinuities in the load path are particularly evident between the ground floor (often a maisonette) and the basement, where the layouts differ completely from the typical floors above. This requires the use of a transfer slab, a thick reinforced slab that redirects the load from misaligned walls above to supporting elements below. While functional, this solution introduces a form of soft storey, which is structurally undesirable due to its vulnerability to lateral forces and potential for uneven deformation.

This contrasts with older terraced houses, where the load path was typically direct and consistent. Where discontinuities occurred, supporting beams were introduced to carry the load of upper walls, maintaining structural integrity.

Geotechnical aspects

The foundation design of any structure in Malta is inherently influenced by the islands' geology, which comprises five main sedimentary rock formations: Lower Coralline Limestone, Globigerina Limestone, Blue Clay, Greensand, and Upper Coralline Limestone, as shown in Figure 5:56. Each formation exhibits distinct geotechnical characteristics, which have historically shaped construction practices across the islands.

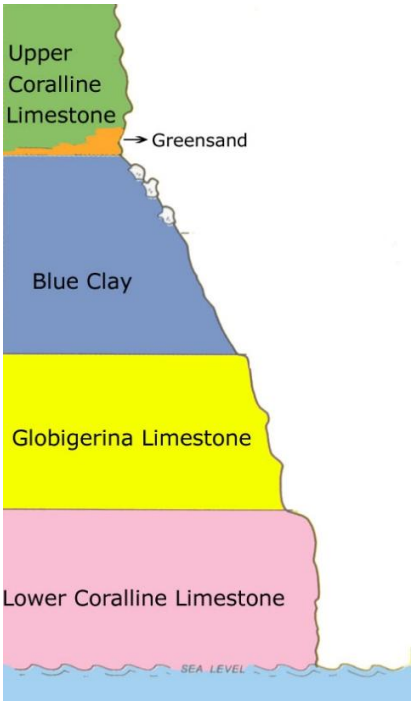

Figure 5:56 - Geological formation of the Maltese Islands

Over time, natural geological processes have exposed different strata at the surface. Traditionally, sites with problematic ground conditions—such as the soft Blue Clay or highly fractured Lower Globigerina

Limestone—were typically avoided. Builders favoured areas underlain by stronger rock formations, relying on the ground's natural strength to support structures, as shown in Figure 5:57. Foundations were commonly shallow and consisted of thick masonry walls that distributed the load over a broad area, effectively reducing ground pressure. This method was particularly suitable for low-rise traditional buildings, where structural loads were relatively light and advanced foundation systems were unnecessary.

Figure 5:57 - Masonry walls constructed directly on the rock

However, the situation has changed significantly in recent decades. Due to rising property values and the scarcity of developable land, avoiding geo-technically challenging sites is no longer a feasible option. Moreover, modern buildings tend to be larger, taller, and more complex than traditional masonry structures, placing greater demands on the ground. As a result, thorough geotechnical investigations and engineered foundation solutions are now essential for safe construction. Contemporary techniques such as pad and strip footings, raft foundations, piles, and anchors have been successfully employed to address a variety of ground conditions, as shown in Figure 5:58. While this dissertation does not aim to examine each of these methods in detail, it highlights the shift in foundation practices within local masonry construction and outlines the adaptive strategies used in different scenarios.

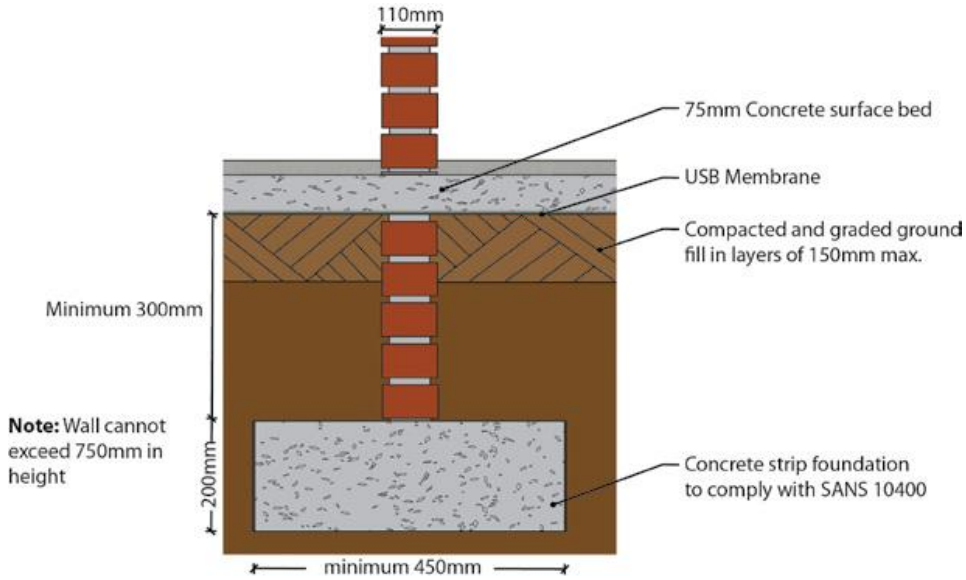

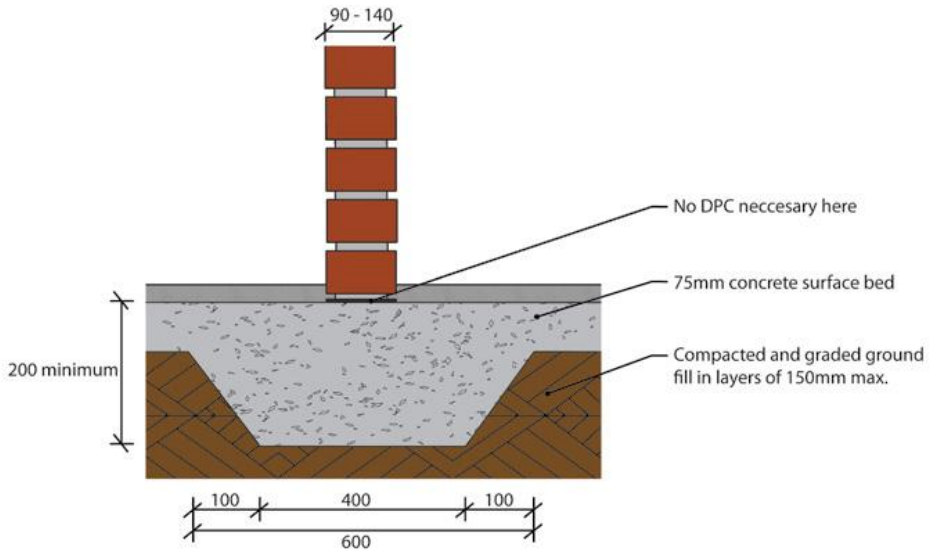

Figure 5:58 - An example of masonry wall supported by a strip foundation and a raft foundation respectively

Beyond the selection of appropriate foundation types, the Maltese construction industry is currently facing a broader and more pressing geotechnical challenge: ground movement and settlement. In Malta's dense urban fabric, where buildings are often constructed directly adjacent to one another, settlement in one structure can jeopardize the stability of neighbouring buildings. Additionally, excavation and construction activities—particularly along roads lined with properties on both sides—can cause damage to nearby structures. This makes detailed geotechnical assessments, monitoring, and settlement analysis increasingly critical.

Accordingly, this dissertation focuses on the impact of structural settlement and the ways in which ground movement affects both individual buildings and their surroundings in the context of Malta's evolving construction landscape.

Construction Process

Before delving into the construction process, it is important to outline the preliminary procedures. If the site includes an existing structure, such as a traditional terraced house, it is carefully demolished. Similarly, excavation is conducted with caution to maintain the stability of neighbouring structures, which may flank the site on both sides.

The construction process begins with laying the foundation. The basement floor construction follows, starting with the basement's bottom slab and masonry walls. A thick, reinforced concrete transfer slab is then constructed to serve as the basement roof. This transfer slab plays a crucial role in transferring the imposed loads of the overlying structure to the basement's masonry walls when a direct load path is not present.

Subsequent construction involves building the walls of the maisonette floor atop the transfer slab, followed by its reinforced concrete roof. This process is repeated for each of the upper apartment floors and concludes with the construction of the penthouse floor.

5.6.4. Modelling Challenges

This section discusses the challenges encountered during the modelling of the selected typical apartment block structure and the decisions made to address them.

Issue 1 - Boundary conditions

It is important to discuss the construction process that has been considered for the construction of the apartment block. The construction typology that was considered for the apartment block consisted of a single-skin wall system, where the floor slab is supported directly by the wall. In this case, the masonry wall is constructed on top of the slab, making it discontinuous due to the interruption caused by the floor slabs, as shown in Figure 5:59. This typology is preferred over other typologies as it is a very common construction method in Malta, and it is simpler to model compared to other options.

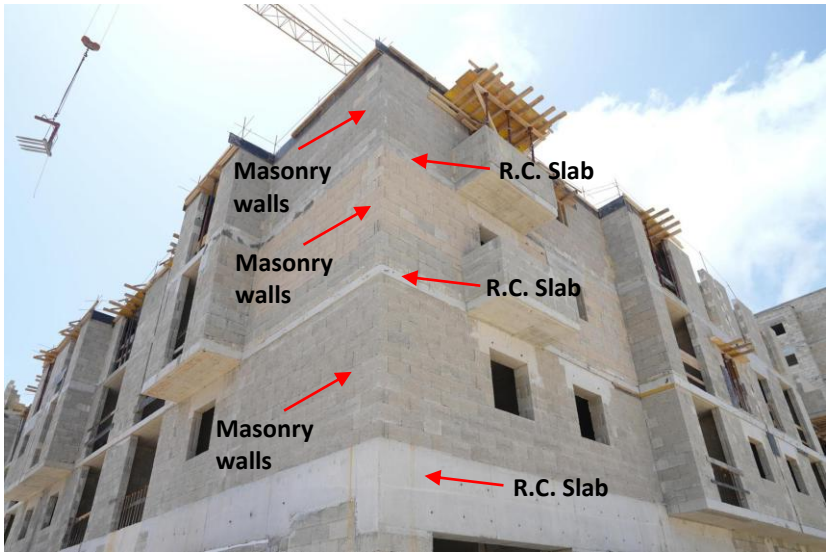

Figure 5:59 - Construction of a typical apartment block, where the masonry wall is discontinuous due to the presence of a floor slab directly supported by the wall

Issue 2 - Supports & Foundation

The approach described in Section 5.5.2 was adopted here as well. A very stiff beam was placed beneath the basement walls to prevent bending under their self-weight. This ensured that any strain in the walls was solely due to imposed nodal deformations, avoiding artificial strain from beam deflection.

However, the perimeter wall of the basement, located on the right side in the plan view, extends approximately 30 meters, as shown in Figure 5:60. For such a long span, no single beam is sufficiently stiff to serve this purpose without deforming. To address this, the beam was divided into shorter segments, each less than 5 meters long, with supports placed at their ends, as shown in Figure 5:61. This segmentation ensured that the beams remained stiff enough to prevent bending-induced strain in the wall.

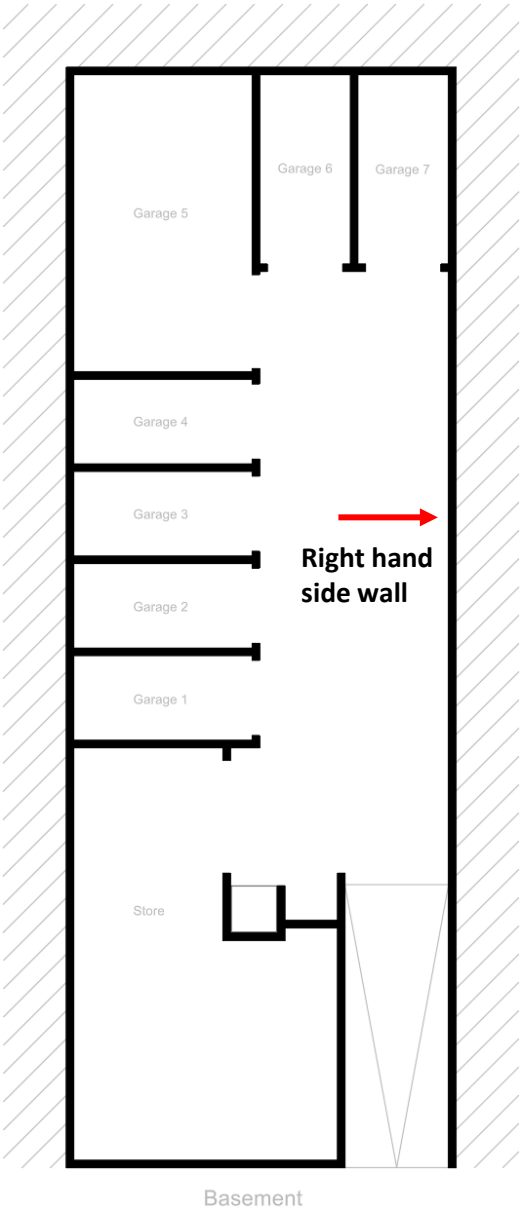

Figure 5:60 - Long-span masonry wall at the basement level

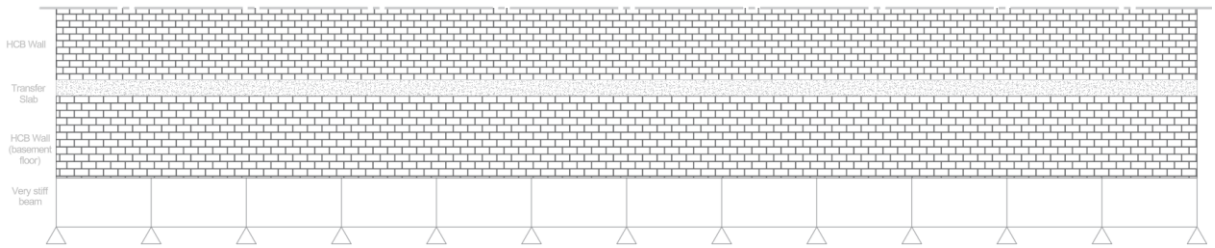

Figure 5:61 - Beam supporting the long-span masonry wall divided in shorter segments

The beams representing the strip footings were initially modelled as moment-connected, causing them to behave as a single continuous beam (Figure 5:62). However, during the simulation of the apartment block, differential nodal deformation caused one end of the beam to deflect downward, while the other end induced a hogging moment on the wall above (Figure 5:63). As a result, the wall followed this hogging behaviour, arching upward in an unrealistic manner.

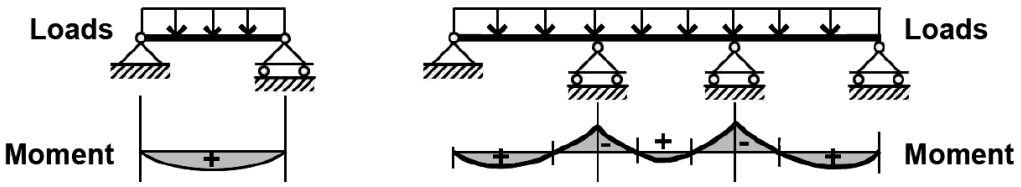

Figure 5:62 - Bending Moment Diagrams of a pin-ended beam & continuous beam

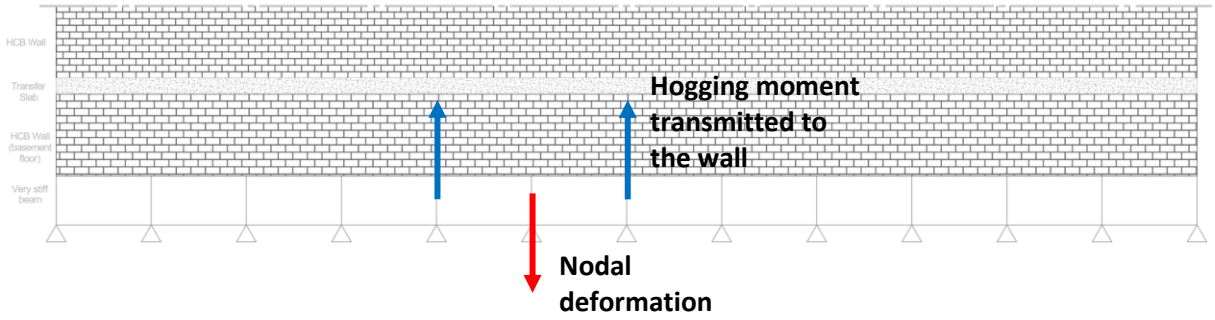

Figure 5:63 - Moment connected beams supporting the masonry wall

This response does not accurately reflect real-world conditions. In reality, strip footings beneath masonry walls do not develop significant hogging moments, as the self-weight of the wall counteracts such effects. When part of the strip undergoes vertical deformation while another part remains restrained by the wall's weight, cracking or localized yielding would typically occur instead of inducing a hogging response in the wall.

To more accurately replicate this behaviour, the ends of the beams in contact were released to create pin connections (Figure 5:64). This adjustment simulates the 'plastic hinge' effect observed in the strip footing during vertical deformation, preventing the transfer of bending moments to the wall and resulting in a more realistic structural response.

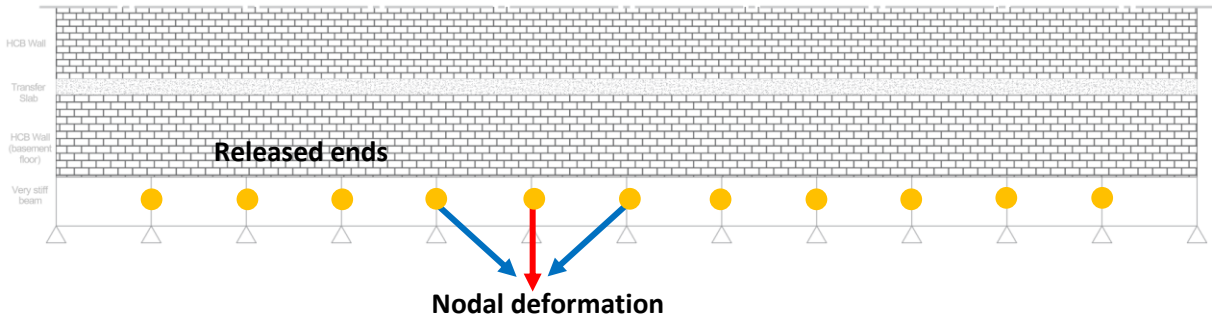

Figure 5:64 - End releases applied to the ends of beams in contact

Additionally, the very stiff beams simulating the strip footings were supported by pin supports, which allow rotation about the x and y axes but prevent translation. This setup enables structural deformation, a key focus of this study.

Also, similarly to what has been already mentioned in Section 5.5.2, a line release has been between the masonry walls and the strip footing as well as between the masonry walls and the concrete slab, as shown in Figure 5:65.

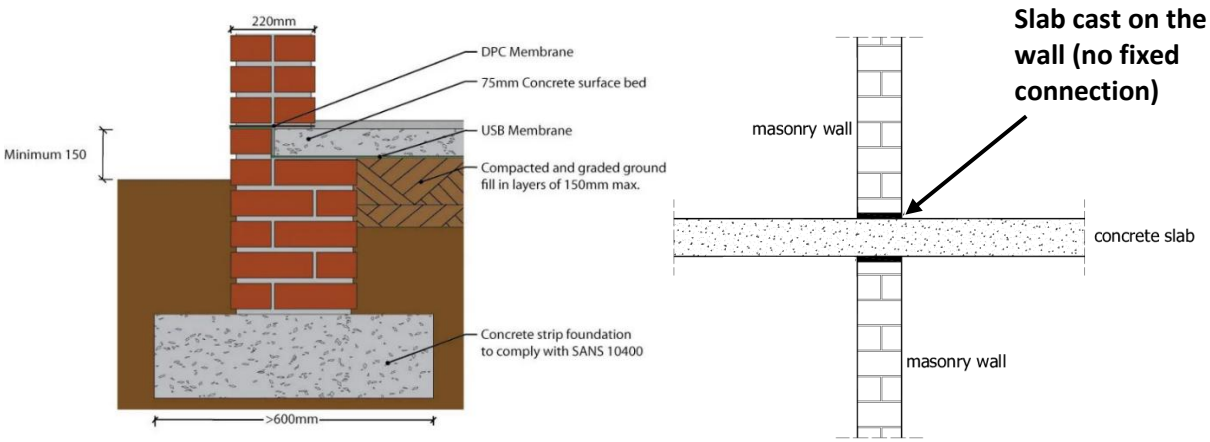

Figure 5:65 - Application of the line release between the masonry wall and the strip foundation & the masonry wall and the reinforced concrete roof

Issue 3 - Walls in the Basement Floor

In the basement level, walls were removed in areas where garage access doors are located. Keeping these walls without accounting for the openings would unrealistically increase the overall stiffness of the structure. On the other hand, modelling the walls with large apertures would render them structurally ineffective, as they would contribute little to the overall stability. Therefore, to more accurately reflect real conditions, these wall segments were omitted from the model, as shown in Figure 5:66.

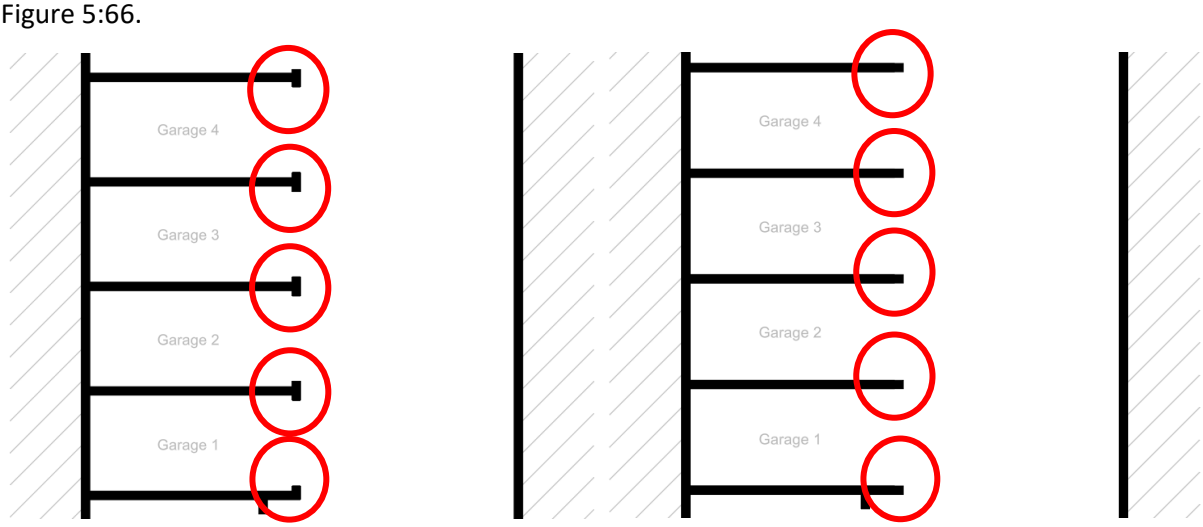

Figure 5:66 - Masonry walls with large apertures were omitted from the model

Issue 4 - Transfer Slab

A transfer slab was introduced to redistribute the loads from the ground floor maisonettes to the basement garages, due to the drastic change in layout between the basement floor and the ground floor apartments resulting in a lack of direct vertical load path where walls are not vertically aligned, as shown in Figure 5:67. To effectively perform this function, it must be thicker than conventional reinforced concrete slabs.

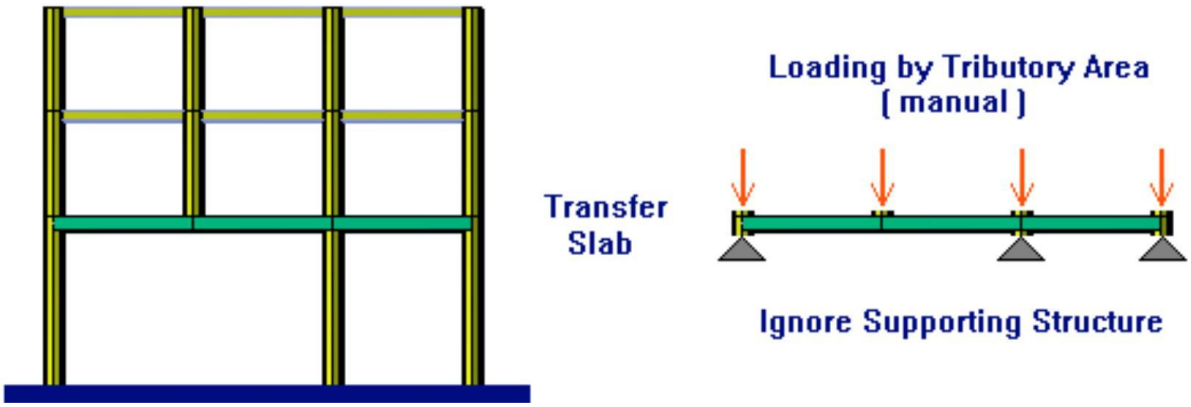

Figure 5:67 - Transferring the loads from the upper floors to the lower floors via a transfer slab

Issue 5 - Initial tilting of the structure

During the structural modelling process, it was observed that the building exhibited tilting about the x-axis under its own self-weight. When additional variable loads were applied to the slabs, or when an extra floor was introduced, the model produced an unstable numerical solution.

Although the upper floors—including the penthouse—share nearly identical layouts, with only minor setbacks at the front and back façades and a slightly recessed internal wall, the primary variation in layout plan occurs at the basement level. At this level, a significant stiffness imbalance exists between the left and right sides of the plan. The left side is noticeably stiffer than the right, causing the structure to tilt toward the less stiff right-hand side, as shown in Figure 5:68.

This behaviour stems from a long single-skin masonry wall on the right, which supports loads from the upper floors but is connected only at one end, providing limited lateral restraint. In contrast, the corresponding masonry wall on the left benefits from orthogonal garage walls, which significantly increase its lateral stiffness and provide effective restraint, as shown in Figure 5:68.

During modelling, out-of-plane deformation was observed in the right-hand masonry wall. This initially seemed unexpected, but was later attributed to the large compressive forces imposed by the overlying structure. Given that the wall is single-skin, its slenderness and lack of lateral support made it vulnerable to out-of-plane instability.

To validate the behaviour described above, the orthogonal garage walls on the left side were mirrored onto the right side, as illustrated in Figure 5:68. This adjustment confirmed the hypothesis: the inclusion of orthogonal walls effectively prevented tilting, resulting in uniform settlement of the structure. These orthogonal elements provided effective restraint by reducing the unbraced length of the walls and enhancing their out-of-plane stability. It is important to clarify that the pink walls mirrored onto the right side were included solely as a test case to investigate whether the unsupported, long-spanning wall on the right side was the primary cause of the initial tilting of the structure.

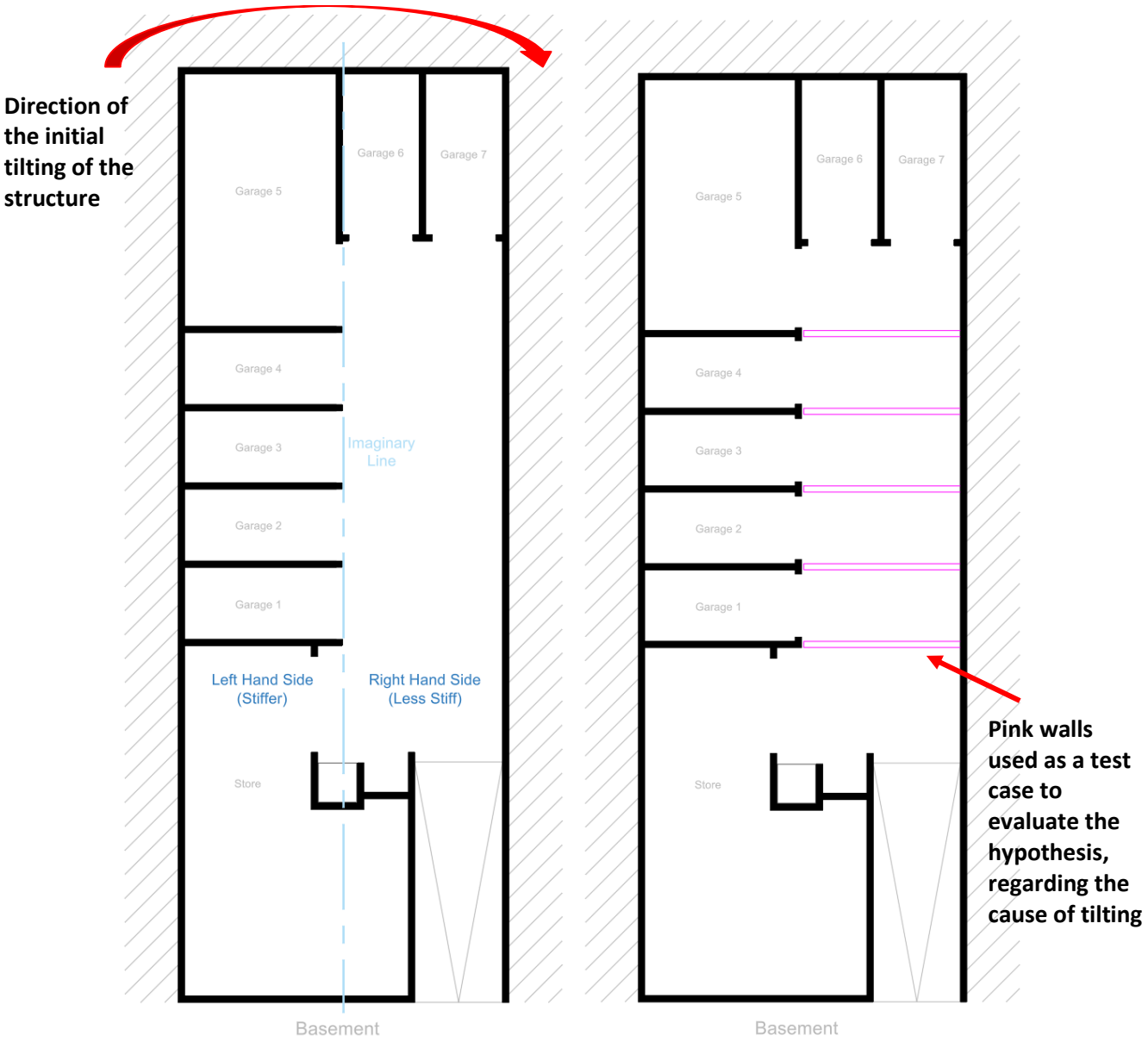

Figure 5:68 - The first image illustrates the variation in structural stiffness and the direction of tilt indicated by the red arrow, while the second image highlights the mirroring of the orthogonal walls shown in pink

Since the structure is tilting under its own self-weight, interpreting the results becomes challenging, as it is difficult to distinguish between actual nodal deformation and instability caused by layout-induced asymmetry. Therefore, it is crucial to eliminate this self-induced tilting and ensure the structure is properly stabilised before applying additional loads or boundary conditions.

Two primary solutions were explored to address the structural issues, each offering unique benefits and challenges. The first approach incorporated masonry piers along the longer wall sections, such as the right-hand side, to act as lateral stiffeners (Figure 5:69 & Figure 5:70). This effectively reduced the unbraced length and slenderness ratio, significantly minimizing deformation and promoting near-uniform settlement. However, the need for floor layout modifications made this approach less desirable (Figure 5:70). Finally, a double-skin wall was introduced along the longer wall sections, increasing the moment of inertia and reducing out-of-plane deflection under compression (Figure 5:70). This solution produced the most uniform settlement and, crucially, preserved the existing floor layout, making it the preferred option over masonry piers (Figure 5:70).

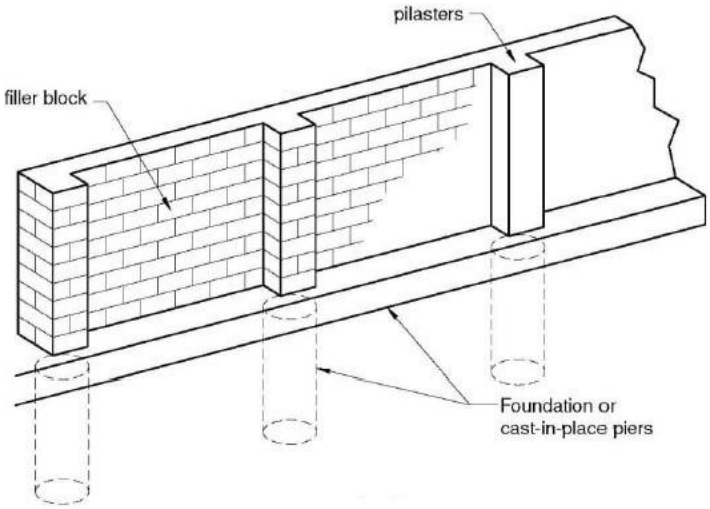

Figure 5:69 - Masonry piers in traditional masonry construction

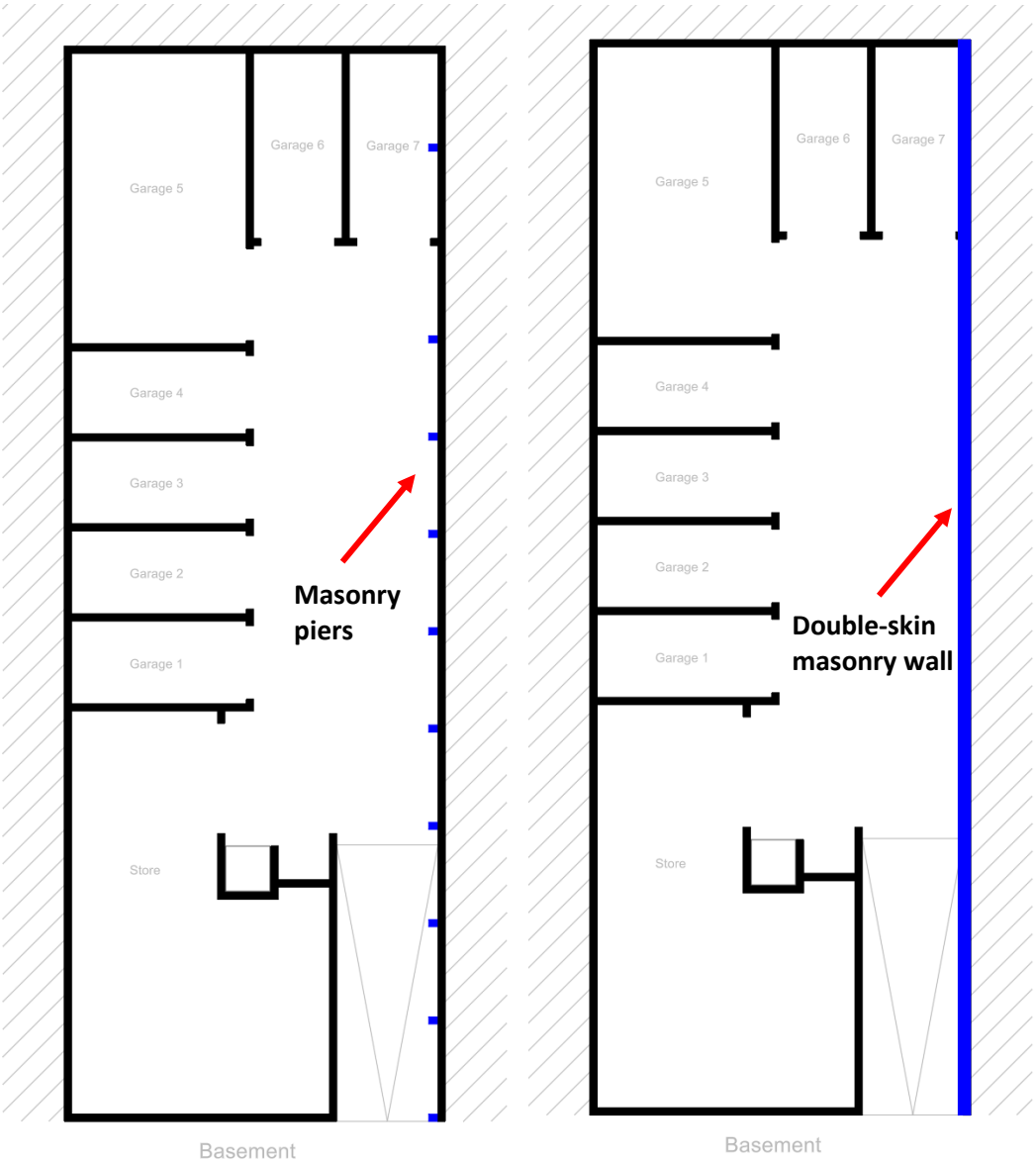

Figure 5:70 - The first image illustrates the implementation of the first solution, where masonry piers are added within the long-spanning wall. The second image depicts the second solution, featuring a double-skin wall replacing the original single-skin wall.

When the structure was modelled with a double-skin wall on the right-hand side, that side became significantly stiffer—more so than the left-hand side. As a result, the structure tilted toward the left, effectively reversing the original direction of tilt (Figure 5:71). While this adjustment resolved the issue on one side, it created a new issue on the opposite side.

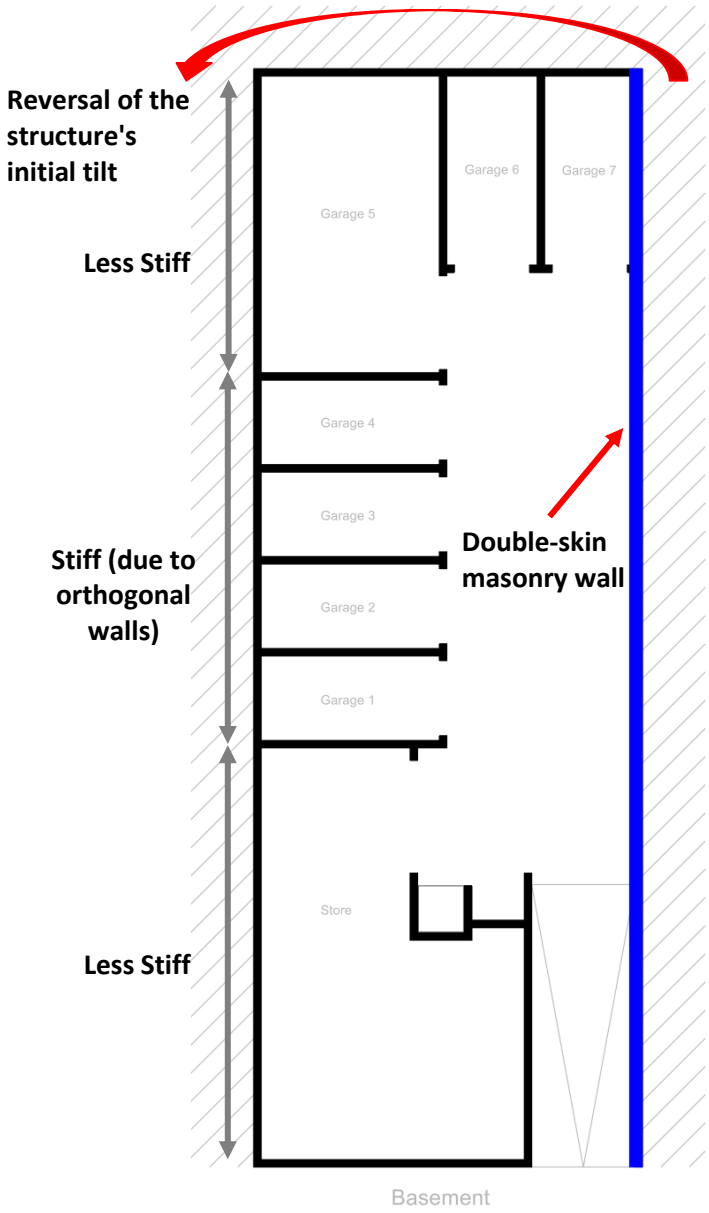

Figure 5:71 - The implementation of the double-skin wall on the right-hand side reversed the structure's original tilt

A closer examination revealed that the left-hand wall was inherently stiff at its centre due to the presence of orthogonal walls but was less stiff at its ends, where longer spans lacked such support (Figure 5:72). To address this, double-skin walls were introduced at the ends of the left-hand wall, while the central section was left as a single-skin wall, as it was already adequately stiff (Figure 5:72). This modification reduced the overall tilting but did not eliminate it entirely, with a slight tilt still occurring in the same direction. This was likely because the central section, although supported by orthogonal walls, remained less stiff than the now-reinforced ends due to its single-skin construction, as shown in Figure 5:72.

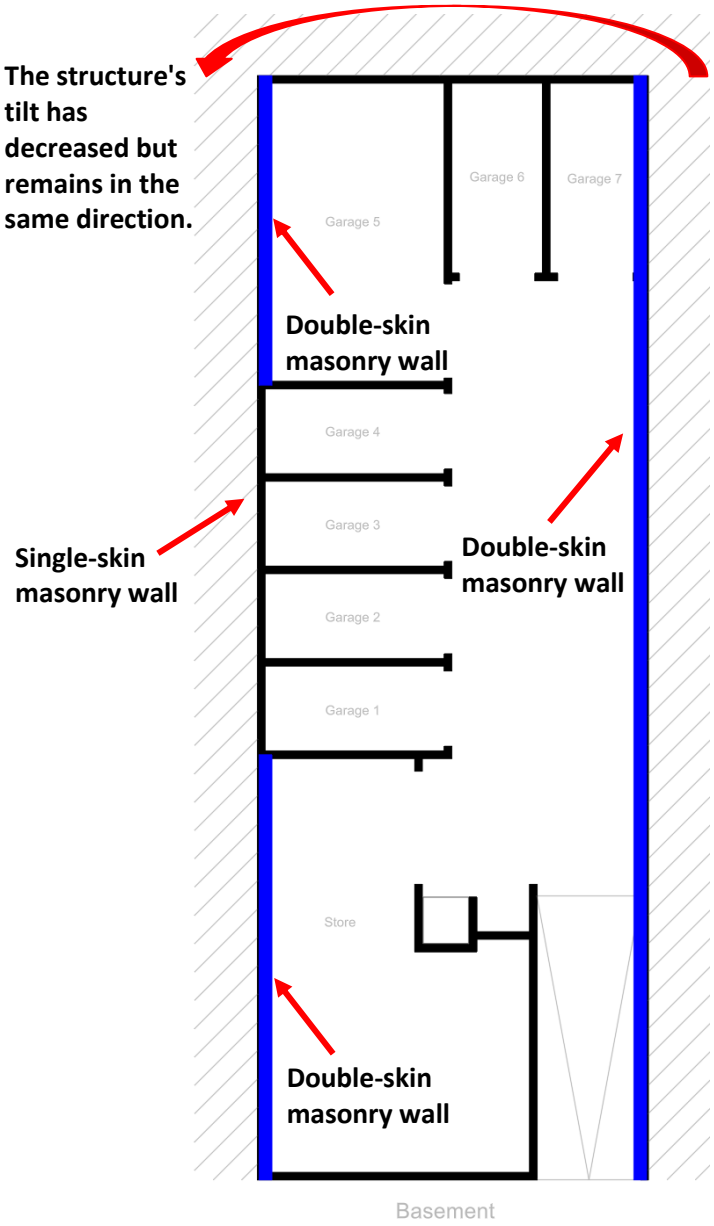

Figure 5:72 - The use of double-skin walls (blue) for long-spanning walls, while retaining single-skin walls (black) for shorter spans

Subsequently, the central portion was also converted to a double-skin wall in an attempt to balance the structure (Figure 5:73). However, this modification caused the tilt to shift in the opposite direction (Figure 5:73). This cycle of adjustments ultimately led to the tilt oscillating from one side to the other, without achieving the intended structural balance or stability

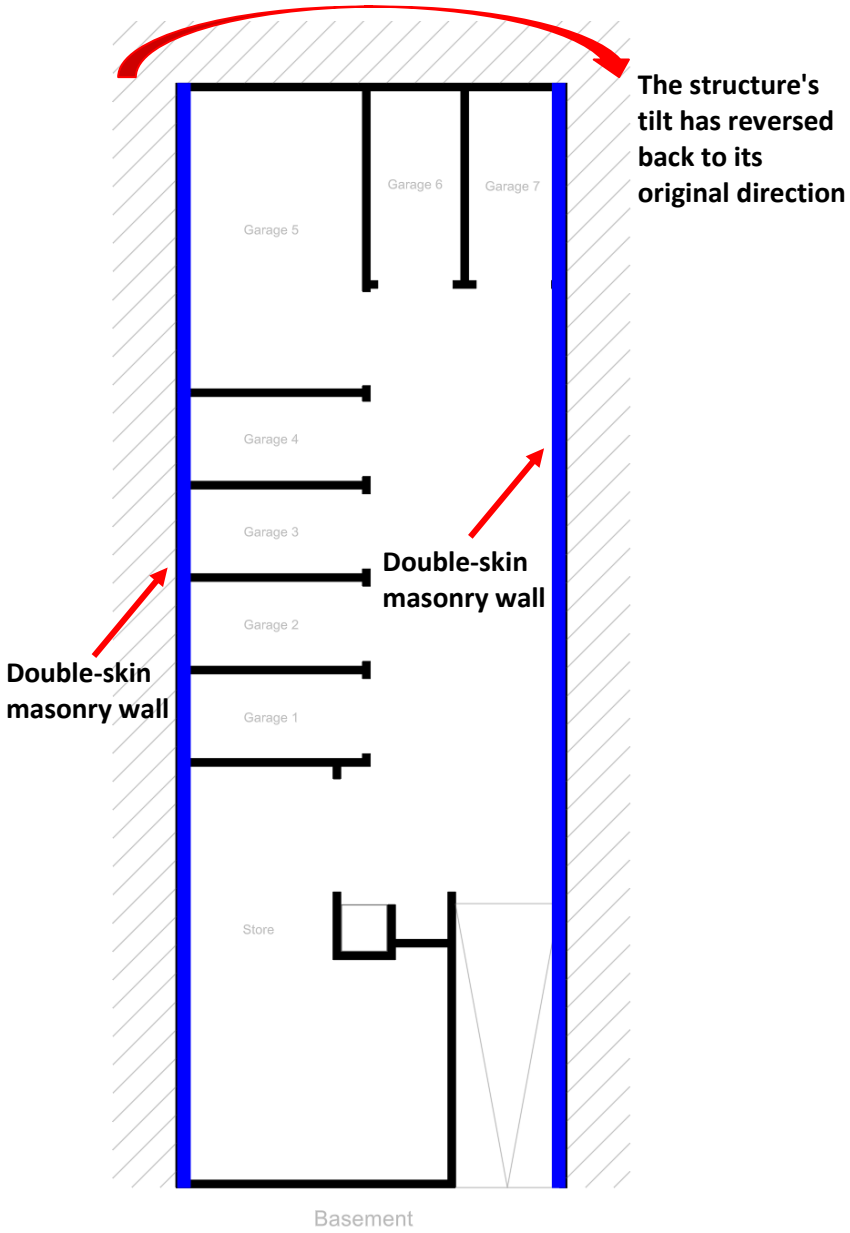

Figure 5:73 - Replacing the single-skin wall in the central region of the left-hand side wall with double-skin walls

As a result of the tilting of the structure under its own self-weight, no imposed variable load could be added to the structure, and it also dictated the number of floors that could possibly be applied, as additional loads would have increased tilting of the structure, making it even more unstable then already is.

Issue 6 - Nodal deformation

Also, the nodal deformations were applied to both internal and external walls because the internal garage walls bear the heaviest loads, while the external walls may experience settlement due to roadworks or activity in neighbouring structures.

6. Results and Discussion

6.1. Introduction

After modelling the various setups described in Chapter 5, the results will be analysed and interpreted in this chapter to determine their validity and alignment with expectations for each setup outlined in the previous chapter.

6.2. Modelling of a simply supported beam subject to masonry wall loads

The first two modelling steps in Sections 5.3.2 & 5.3.3, involving a steel beam subjected to its self-weight in the first step and an additional imposed load in the second, will not be discussed here due to their straightforward nature. However, these models are presented in Appendix B. This section focuses exclusively on the beam subjected to loads imposed by a masonry wall.

This model analyses the behaviour of a beam, specifically to determine whether the beam and wall are acting as a single unit or independently. This verification ensures that the model's results are consistent with expected behaviour, thereby supporting the validity and reliability of further modelling.

Due to the self-weight of the wall, the steel beam experienced bending, shear, and deflection. The values of the bending moment, shear force diagram, and deflection of the beam were compared with hand calculations, as shown in Appendix B. The results were close, but not fully accurate, as shown in Figure 6:1, Figure 6:2 & Figure 6:3. This comparison was done by treating the self-weight of both the wall and the beam as a uniformly distributed load on the beam.

One main reason for the slight difference between the hand calculations and the results obtained from the model is probably due to the line release. It was noted that the application of the line release did not fully achieve the intended separation between the behaviour of the wall and the beam. Although the bending moment and shear force diagrams of the beam were still slightly influenced by the interaction with the wall surface, they were very close to what would be expected for a simply supported beam, though not typical in the strictest sense.

However, given the time limitations and the scope of this dissertation, the model and the application of the line release were deemed sufficient. The results were close enough to the expected behaviour to be considered reliable for the purposes of this study.

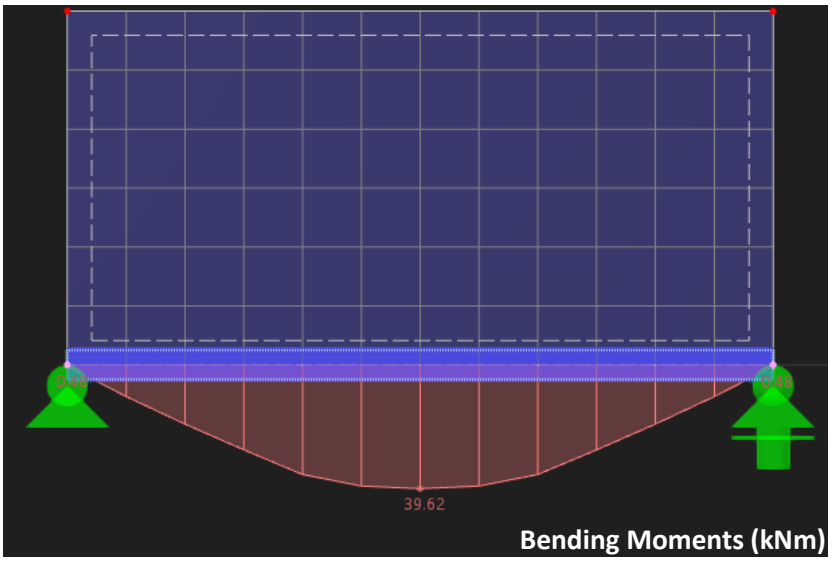

Figure 6:1 - Bending Moment Diagram of the steel beam

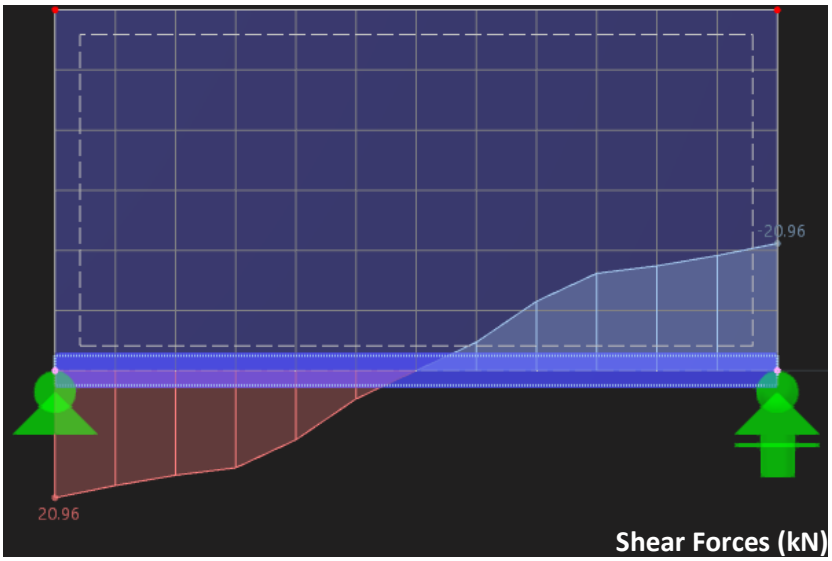

Figure 6:2 - Shear Force Diagram of the steel beam

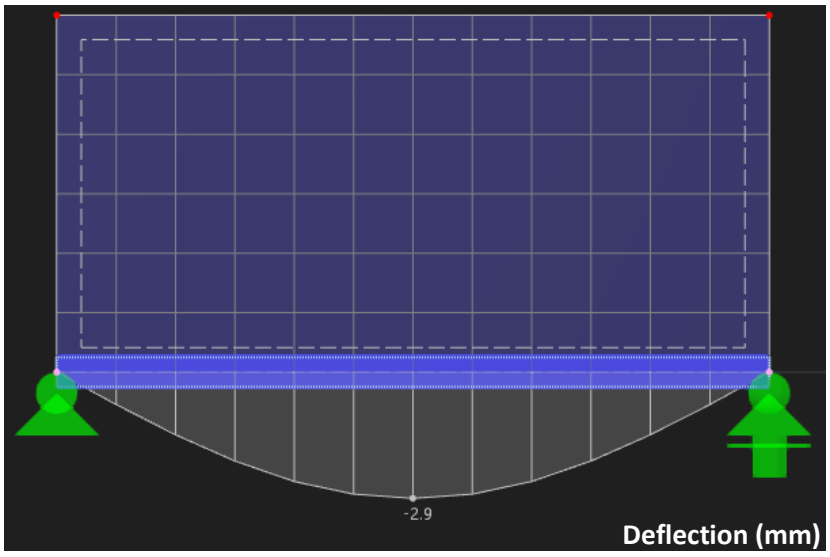

Figure 6:3 - Deflection of the steel beam

6.3. Modelling of a room

To aid understanding, a labelled plan view of the room is provided, indicating the corner where settlement was applied and identifying the walls referenced in the discussion, as shown in Figure 6:4.

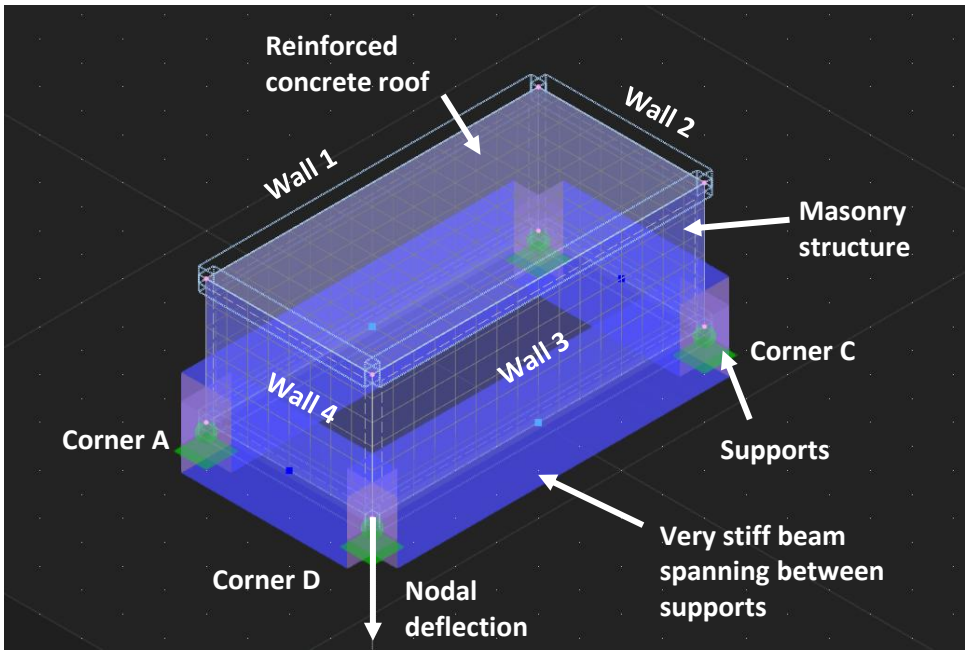

Figure 6:4 - Labelled 3D view of the room model

When analysing the results of this numerical model, three key aspects have been considered. First, the global deformations provide a clearer visualization and understanding of the structure's overall behaviour. Next, the focus shifts to examining the underlying factors causing these deformations by analysing the basic and principal plastic strains.

Global Deformations

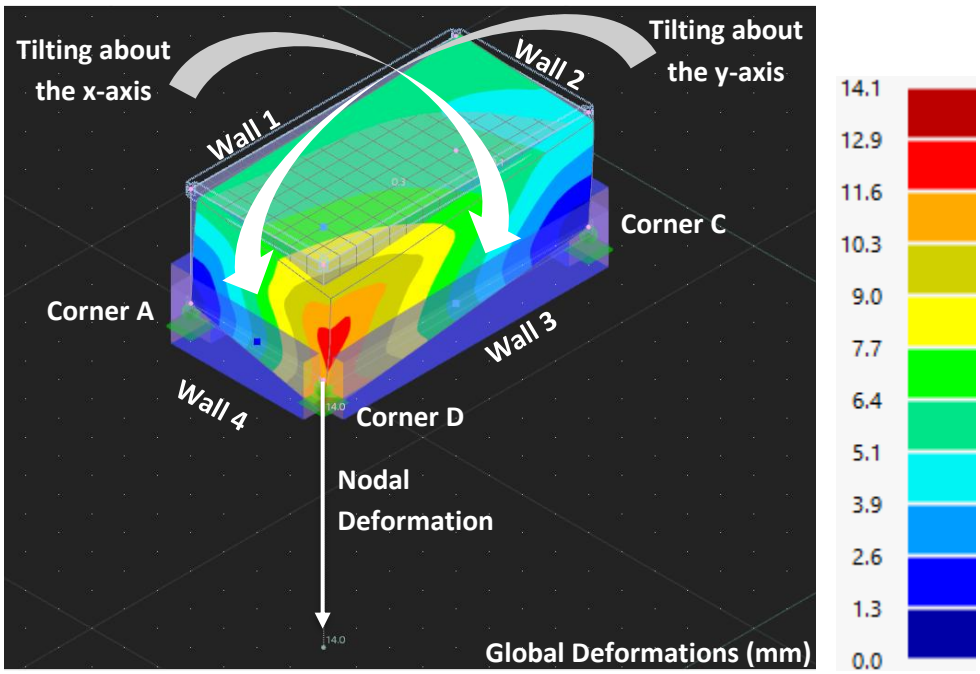

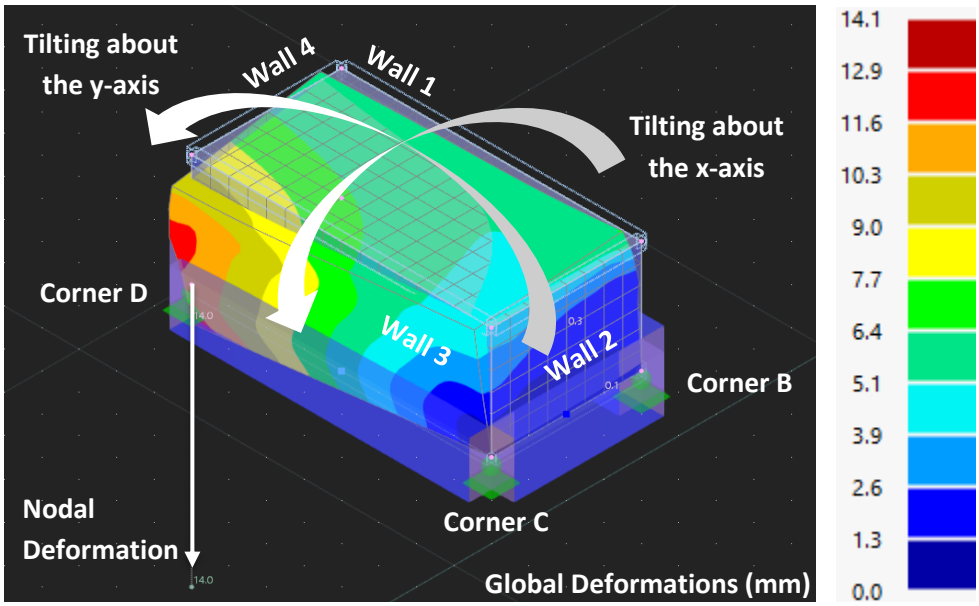

Figure 6:5 - Global Deformations experienced by the room model

To better understand the overall deformations experienced by the wall, it is important to analyse the global deformations. As corner D undergoes nodal deformation, the structure distorts in various ways. The room experiences distortion as it experience tilting in both the x and y directions (global axes), which is expected since the nodal deformation is located at corner D. Tilting in both axes gives the impression that the room is unstable, as the walls seem to move out of their plane as illustrated in Figure 6:5. Also, the room undergoes further distortion, as corner D experiences vertical displacement as it follows the nodal deformations, while the opposing corner (corner B) experiences an upward displacement, as shown in Figure 6:6.

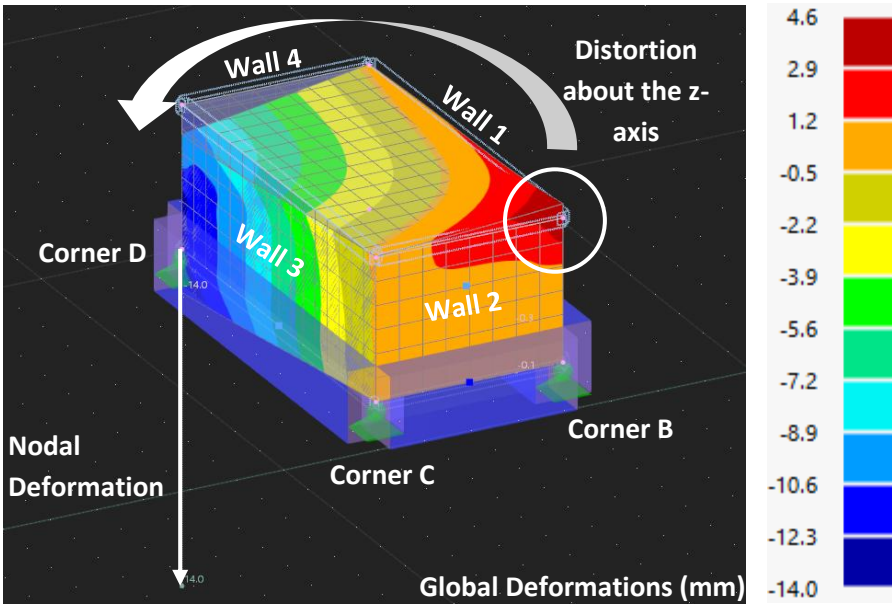

Figure 6:6 - Further deformation observed in the room model

Although this may seem unusual, this behaviour is actually observed in reality. To understand this, it is important to note that the roof slab follows the deformations of the walls. This behaviour is particularly evident in areas where the roof slab is relatively thin for its span and unsupported by internal walls, such as the washroom slab. During construction, the roof is cast directly on top of the top course of

the wall, and there is a tendency for the top course to become "glued" to the concrete roof. As the roof has a large span, it tends to sag, pulling the uppermost course that is in contact with it, which can lead to the observed deformation in Figure 6:6.

Principal Plastic Strains

The analysis will centre on two key components of the Principal Plastic Strains: the angle and the maximum plastic strains. Before diving into the results, some background context will be provided to help better interpret the findings.

To predict where cracks might form, it is important to first identify the main directions in which the material is stretched or compressed, known as the principal stress directions. Using the Mohr circle, these stresses can be translated into normal and shear stresses on various planes within the material. This process helps determine the most likely locations and directions for cracking.

In particular, the angle (α^{+}) represents the direction of the principal tensile strain (the main stretching direction). By analysing this angle, we can understand how the structure deforms and identify probable crack directions, since cracks often form perpendicular to the maximum tensile strain. From Figure 6:7, the strain trajectories are arched and spread across a wide area, indicating that deformation and stress are not confined to one spot but affect a larger portion of the structure.

Additionally, the maximum plastic strain contours follow the same arched pattern as the strain trajectories (Figure 6:7), suggesting that the structure deforms by stretching diagonally. Consequently, cracks are also likely to form along these diagonal paths. This observation aligns with the earlier description of the room's deformation, which appears unstable due to out-of-plane deformation caused by the nodal deformation.

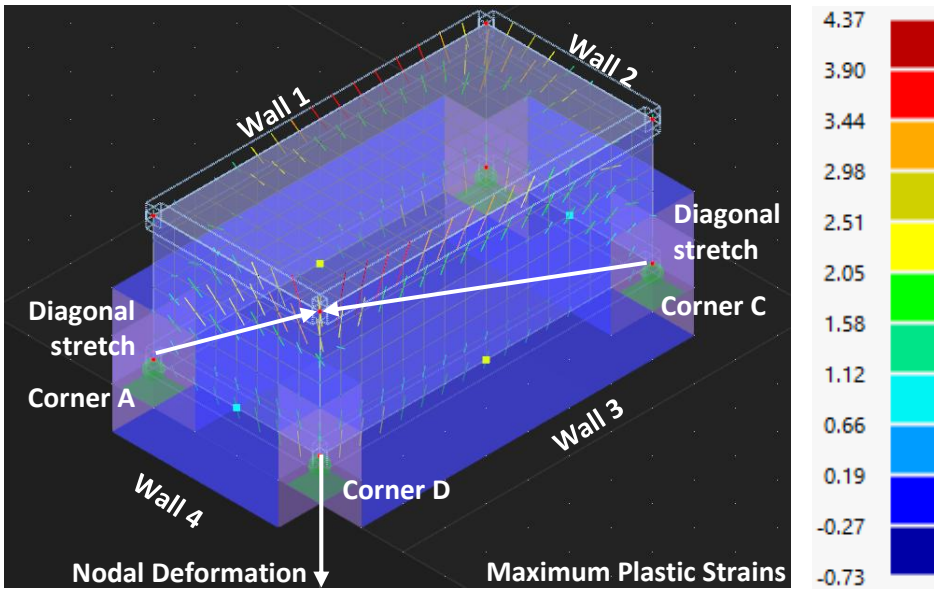

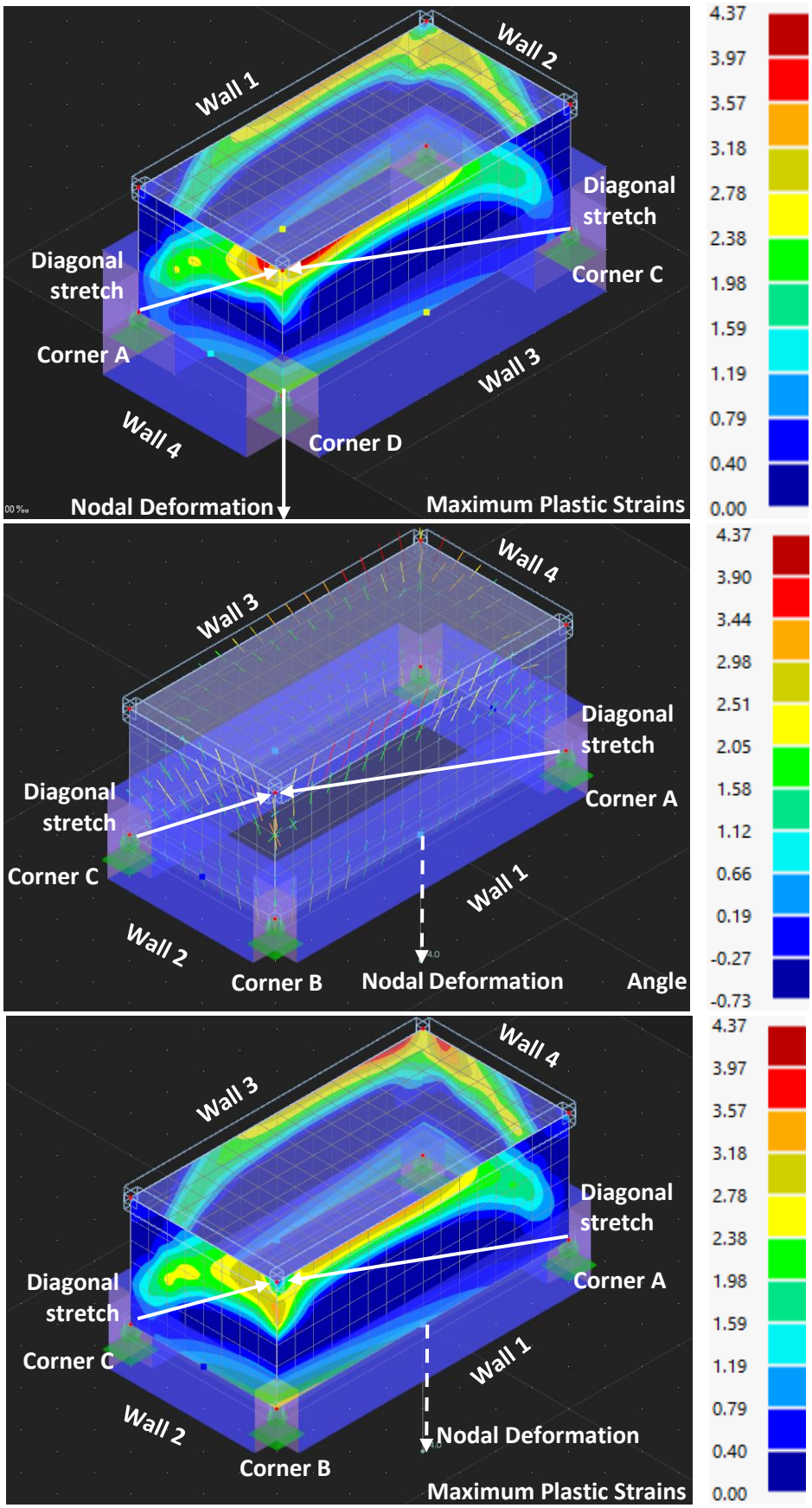

Figure 6:7 - Comparison of the results for the Angle & Principal Plastic Strains by the room model from different perspectives, analysed individually

The observations of the room structure based on the principal plastic strains can be linked to the theory of plasticity, which is particularly useful in such cases. As discussed earlier in Section 4.3, the theory of plasticity explains how materials undergo permanent shape changes when subjected to stresses beyond their elastic limits. In structural terms, this means identifying where and how parts of the material deform permanently and do not return to their original shape. The principal plastic strains highlight these zones of irreversible deformation.

Basic Plastic Strains (local x-axis - Plastic strains corresponding to the local axes of the surfaces)

This section will be divided into two parts. The first part will expand on the discussion of principal plastic strains. The second part will shift focus to a different perspective, analysing another set of results that illustrate the deformation experienced by the structure and applying these findings to a hypothetical practical scenario.

Building on the discussion of principal plastic strains, the basic plastic strains are relatively simpler to interpret. Another way to identify where cracks will form is by examining the shear basic plastic strains. These strains also support the hypothesis of diagonal cracking, as the same contours observed under basic plastic strain in the x-axis appear in the shear-based plastic strain contours, as shown in Figure 6:8.

It is important to note that the majority of the strains formed in the walls are plastic, meaning most of the room is exhibiting irreversible cracks. This is primarily due to the degree of nodal deformation, the aspect ratio, and the thickness of the walls, among other factors related to the construction and composition of the walls themselves.

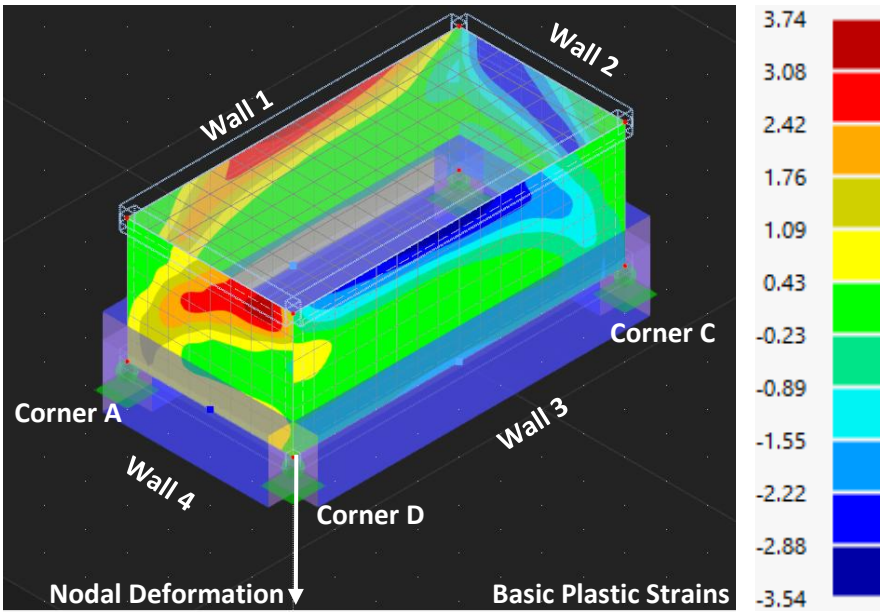

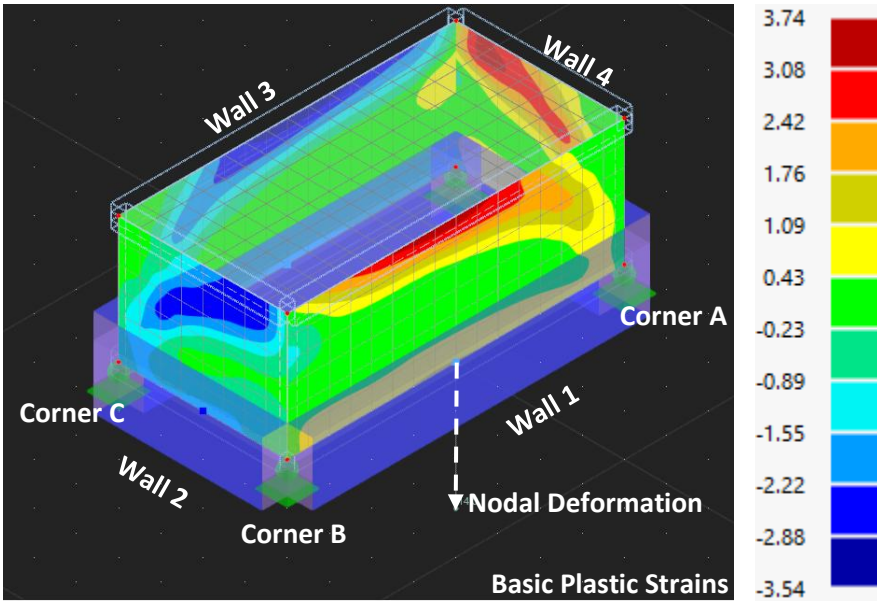

Figure 6:8 - Basic Plastic Strain experienced by the room model

Beyond analysing the overall deformations experienced by the room and understanding the underlying behaviour driving these changes, it is crucial to examine the areas where strains are likely to develop as the structure undergoes settlement. This analysis will start by discussing basic plastic strains. It will then shift to interpreting these findings in practical terms, considering their potential implications for a real-life room structure subjected to settlement.

Hypothetically, and based on comparisons with Mifsud J. (2012) real-life case study, zones of plastic strain (Figure 6:9) can indicate areas where masonry joints are pulled apart due to nodal deformation, leading to irreversible deformations and crack formation. Notably, plastic deformation is observed in all four walls, though the severity of deformation varies (Figure 6:9).

A common observation is that plastic strains often appear inclined, suggesting the formation of diagonal cracking within the walls (Figure 6:9). The analysis indicates that both major and minor cracks may develop, as evidenced by the strain contours of varying colours on the walls (Figure 6:9). Red strain contours highlight regions experiencing the greatest tension, making them the most susceptible to significant cracking. Other strain contours, though less critical, may also lead to minor cracks. Strain, defined as the change in length relative to the original length, suggests that even lower-critical areas could experience minor cracking.

Applying this interpretation to a hypothetical real-life room structure subjected to nodal deformation at the same corner reveals intriguing insights. It is argued that the results might be influenced by the corbelling between orthogonal masonry walls, which affects the structural performance. While this analysis does not directly address corbelling—since the numerical model does not simulate it—it emphasises the possible effects of restraint developed at the corner of orthogonal walls, implying enhanced rigidity at these intersections.

Two potential effects of corbelling-related restraint are identified. First, without corbelling to tie the walls together, walls 3 and 4, located closer to the nodal deformation, would likely experience settlement, while walls 1 and 2 might remain largely unaffected. However, strain contours show that walls 1 and 2, though not directly influenced by the nodal deformation at corner D, still exhibit strain (Figure 6:9). This suggests that the tying action of corbelling transfers some deformation forces to walls

1 and 2, with wall 1 being pulled away by wall 4 as it undergoes nodal deformation. Similarly, a comparable effect occurs between walls 2 and 3 (Figure 6:9).

The second effect focuses on the formation of strain contours and the cracks themselves. Without the corbelling action, the behaviour of the masonry walls might differ significantly. Corbelling likely plays a role in moderating how the structure deforms. For example, wall 1 may aid in restraining wall 4, preventing it from fully following the nodal deformation (Figure 6:9). Consequently, corbelling between masonry walls appears to contribute to the overall stability of the structure, preventing it from falling apart.

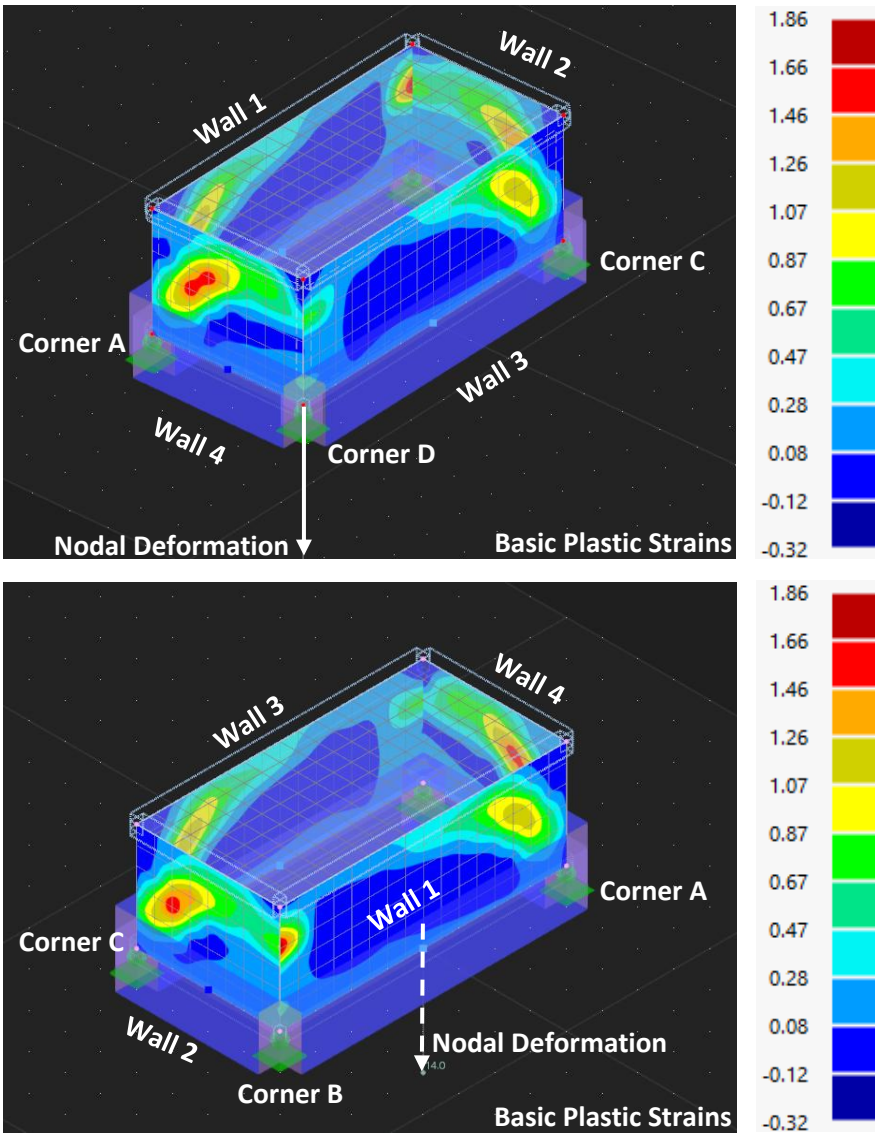

Figure 6:9 - Basic Plastic Strains exhibited by the room model

6.4. Modelling of a Typical Apartment Block

During the modelling process of the apartment blocks, several important insights were observed prior to the analysis of the final results. These observations, along with the analytical and critical evaluation of the outcomes, provide valuable perspectives for the actual construction of apartment buildings.

As discussed in Section 1, the construction sequence was modelled by considering different runs of the same basic numerical model but with an increasing number of floors. The structure began exhibiting

signs of tilting even during partial stages of construction. This early tilting contributed significantly to the overall instability of the model, particularly as additional floors were added, variable residential loads applied, and nodal deformations introduced. These factors collectively increased the degree of tilt to the point where the structural stability was compromised.

This outcome was contrary to initial expectations. It was assumed that displacements would manifest only after the full structure had been modelled and loaded. However, in practice, structural displacement may occur either during or after construction, depending heavily on the properties of the underlying ground material.

For example, when a structure is founded on fine-grained soil, such as clay, displacement can occur both during construction and after its completion. The weight of the structure compresses the clay, causing a reduction in its volume. This process leads to settlement and potential structural movement, which may persist post-construction. Conversely, if the structure is built on a hard rock stratum, it behaves in a drained condition. In such cases, any displacement tends to occur during construction. These movements can often be corrected or compensated for by construction crews as the work progresses, resulting in a final structure that appears unaffected, despite early-stage adjustments. A well-known example of this is the Tower of Pisa. During its construction, builders noticed that the structure was beginning to tilt. In an attempt to counteract the lean, they adjusted the masonry by constructing one course with greater height on the side experiencing the tilt and a smaller course on the opposite side.

It is also crucial to acknowledge that the modelled structure represents a standalone scenario. While the layout of each floor is based on a typical apartment configuration, the isolation of the model does not fully capture real-world behaviour. In reality, apartment blocks are often constructed in urbanized environments, where adjacent buildings provide lateral confinement and support. This external bracing reduces the likelihood of out-of-plane deformation in basement wall by utilising surrounding structures as stabilising elements. Indeed, it is common for the stability of a building to partially rely on neighbouring structures. When these adjacent buildings are later demolished, the central structure may lack the lateral support necessary to remain stable, resulting in unexpected damage or failure. The corollary to this observation is that adjacent buildings are often stressed by the adjacent buildings under construction, leading to damage and therefore complaints from the adjacent third parties.

It could be argued that structural tilting during construction is not a widespread issue. However, this argument should be approached with caution and informed judgment. The absence of past failures does not negate the underlying risks, much like Russian roulette—a perilous gamble where extreme risks can lead to severe consequences. While structural tilting may not typically result in fatalities, complacency in addressing such risks is unwise. In Malta, the rarity of such failures is often due more to a fortunate circumstance than to proactive risk mitigation.

For the purpose of this exercise, the interpretation of structural behaviour during settlement will be further discussed. As mentioned in Section 5.6.4, two external and one internal nodal deformations have been applied. To address the tilting issue identified in the model, a double-skin wall with considerable length has been included at basement level, within the model. This improvement aims to enhance wall stiffness and reduce overall structural tilting. However, minor tilting remains present, indicating that the model may not yet be fully reliable for predicting damage due to settlement. Nonetheless, it offers a useful starting point for understanding deformation patterns and identifying areas most susceptible to strain, even during construction.

Additionally, this section examines the deformations experienced by the structure during staged construction using phased modelling. This approach allows for the analysis of how the addition of each new floor affects the overall structural behaviour, particularly its impact on the levels below as the building progresses.

It is important to note that, because the typical apartment block structure is more complex than the previously modelled structures, the approach to analysing and interpreting the results will differ slightly. Instead of examining individual results sequentially, the focus will be on building cohesive arguments to explain the structure's behaviour, using multiple results simultaneously to support each argument.

6.4.1. Phased Construction Approach

By modelling the structure at each stage of construction, this analysis offers a clear understanding of how the building behaves before the application of nodal deformations.

Basement floor only

Based on the basement model alone, the transfer slab appears to experience the greatest deformations in areas with large unsupported spans, such as the storeroom, the corner garage, and the vehicular manoeuvring space in front of the garage doors, as shown in Figure 6:10. Additionally, the orthogonal walls forming the garages are already showing signs of deformation and plastic strain, indicating the onset of out-of-plane deformation, as shown in Figure 6:11.

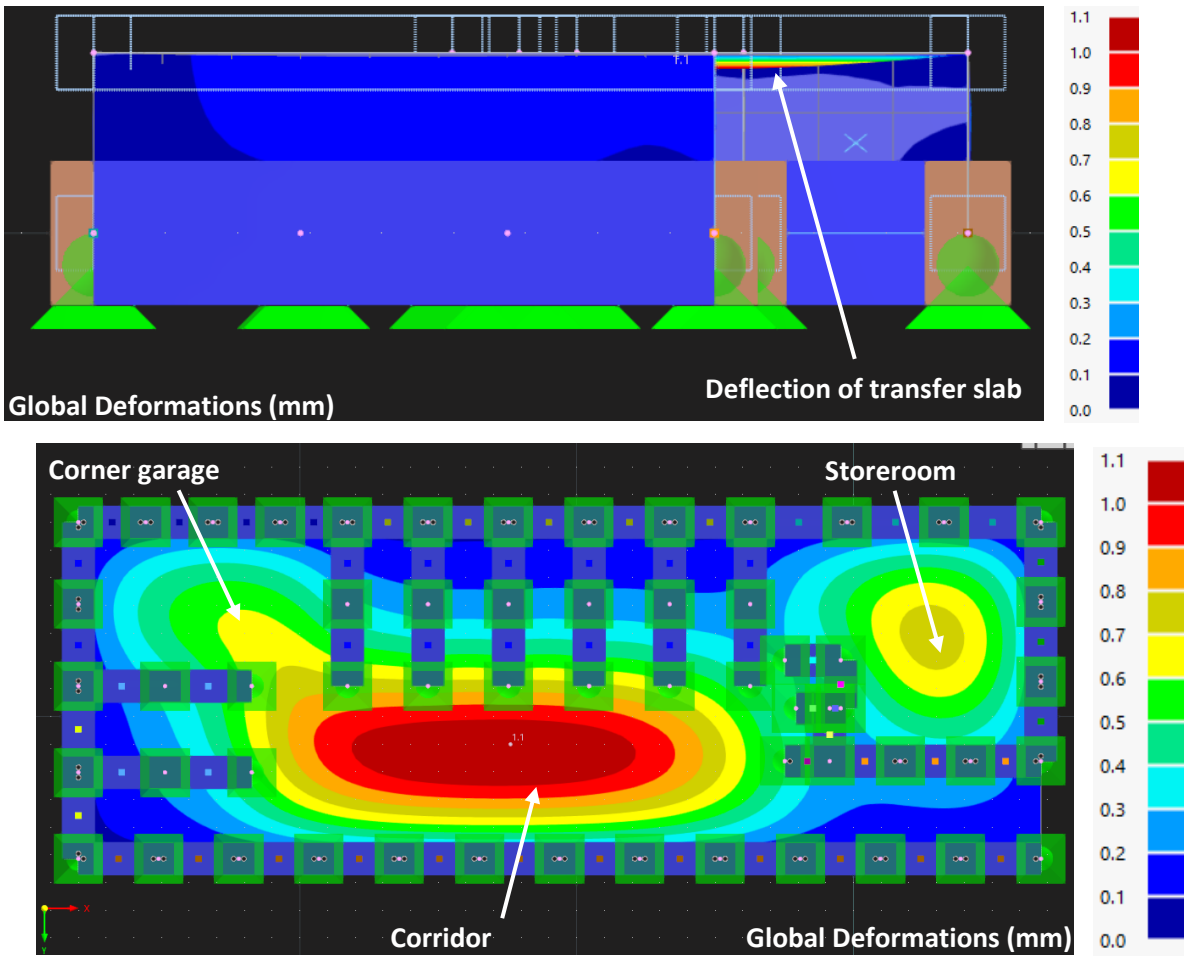

Figure 6:10 - Different views showing the deflections of the transfer slab across different regions

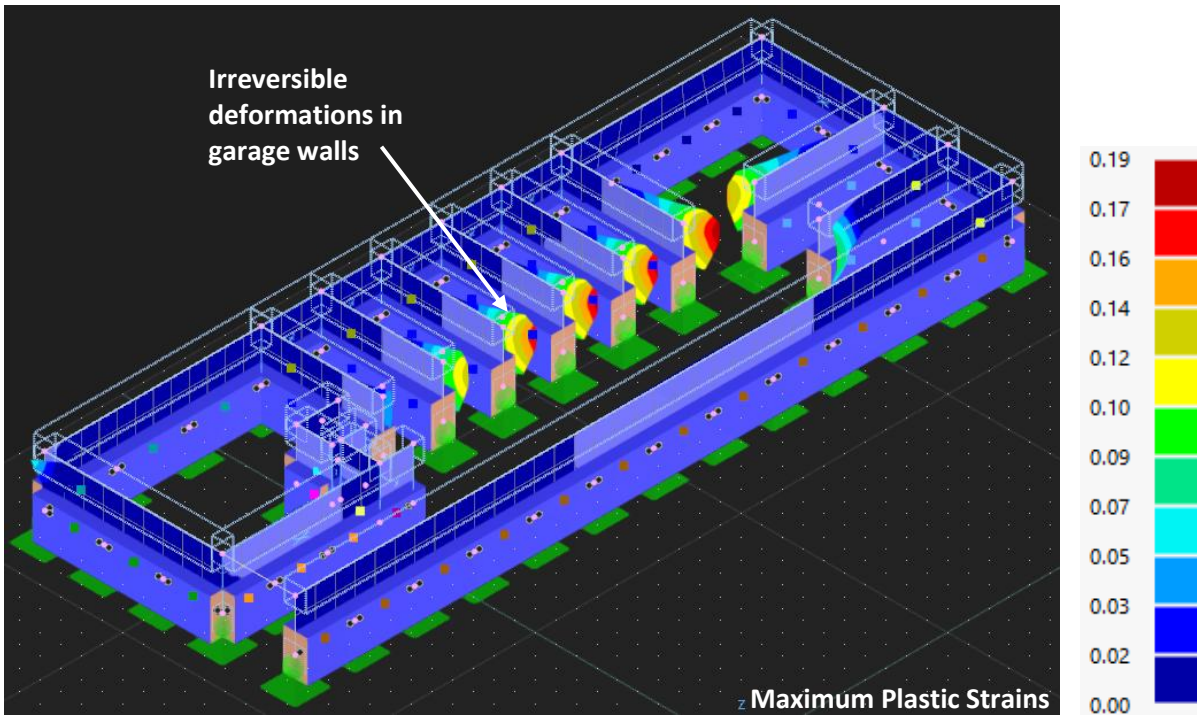

Figure 6:11 - Deformations in garage walls

Basement Floor + Ground Floor

With the addition of the ground floor above the basement, the deformations observed in the initial model changed slightly, but not entirely as expected. It was anticipated that the deflections in the transfer slab would increase due to the added vertical loads from the ground floor walls. However, the actual behaviour is influenced by how the structure is constructed. Specifically, the perimeter walls of the ground floor apartment apply loads along the slab's edges, effectively restraining further deflection. As a result, the transfer slab behaves similarly to a beam with fixed ends and thus limiting the deflections aligning with this structural analogy, as shown in Figure 6:12.

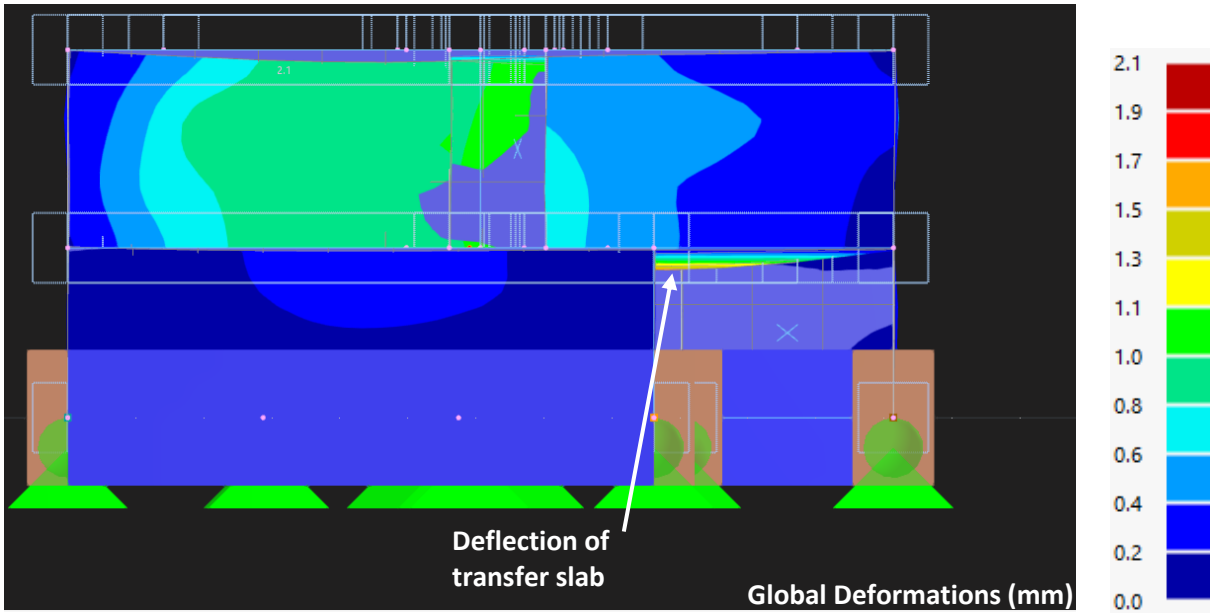

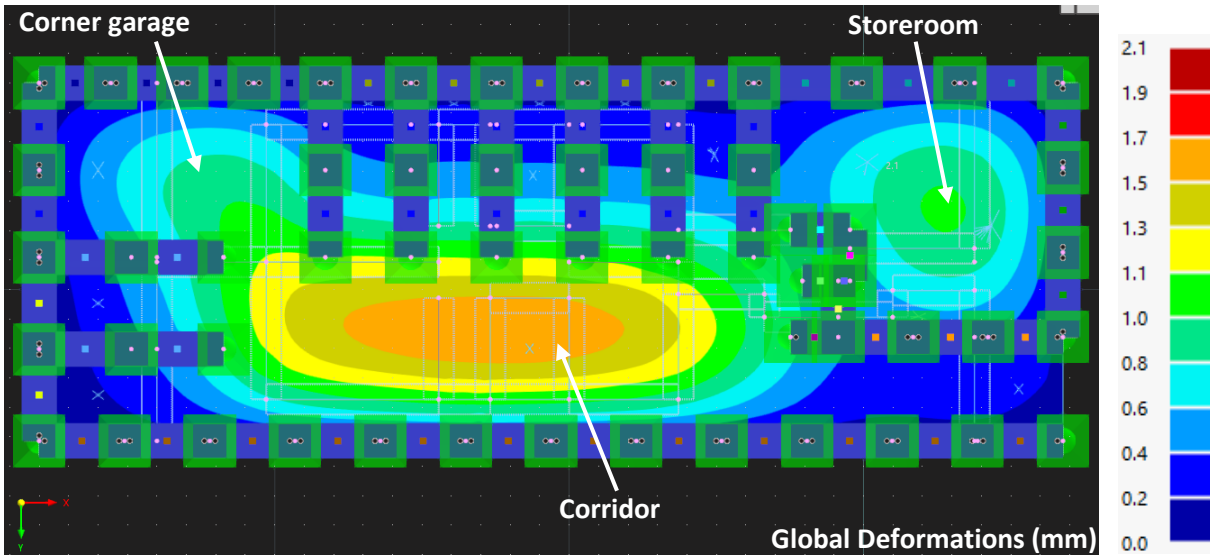

Figure 6:12 - Different views showing how the transfer slab is deflecting

Nevertheless, in areas where the transfer slab had already experienced significant deflections, the newly constructed walls above these zones follow the slab's deformation due to their self-weight. As these walls sag with the slab, cracks begin to form within them, as shown in Figure 6:13.

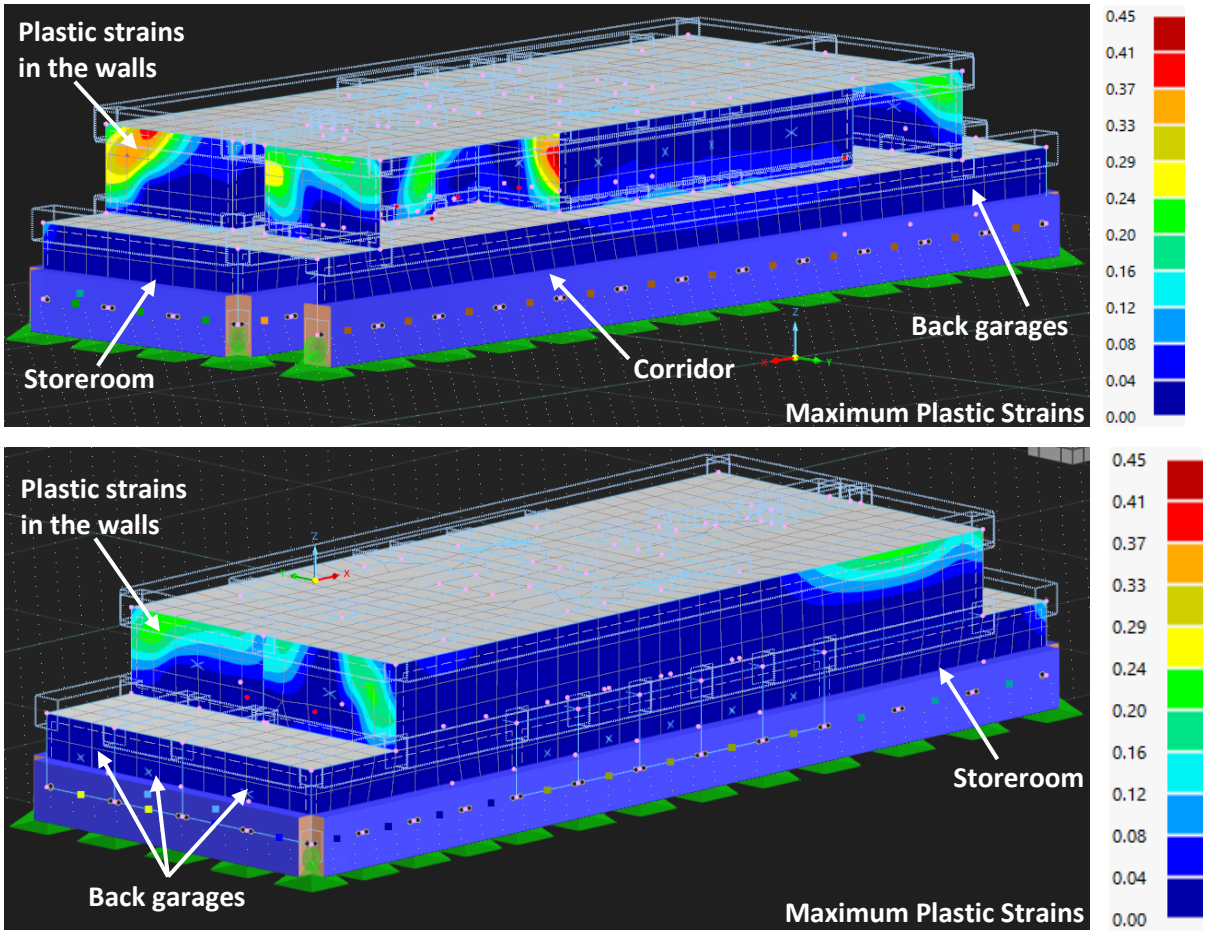

Figure 6:13 - Maximum plastic strains observed in the walls of the ground floor apartments

Because the transfer slab spans a large unsupported area—particularly the vehicle manoeuvring corridor—it channels significant compressive loads to the long wall on the right-hand side. This wall is

further burdened by vertical loads from the perimeter masonry walls of the upper floors. As a result, it begins to exhibit out-of-plane deformation due to the combined compressive forces, as shown in Figure 6:14. Also, the deformation and plastic strain observed in the orthogonal garage walls during the basement-only stage persist even after the addition of the ground floor, as shown in Figure 6:14.

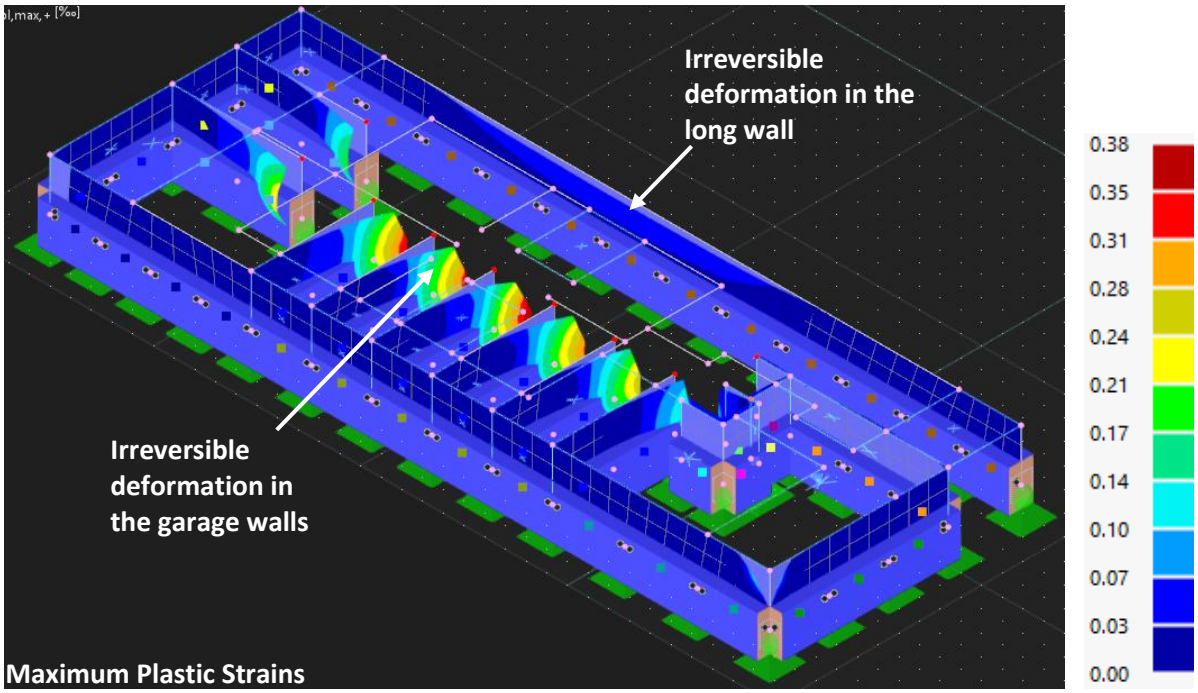

Figure 6:14 - Maximum Plastic Strains exhibited in the basement walls

It is also important to note that the roof slab of the ground floor apartment, which spans large unsupported areas, experiences considerable deflection as well—mirroring the behaviour of the basement transfer slab, as shown in Figure 6:15.

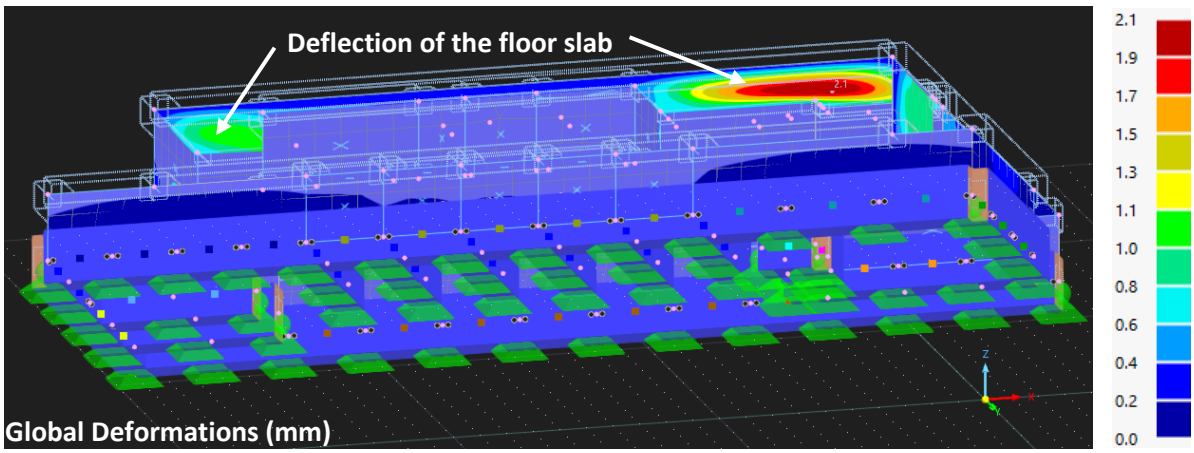

Figure 6:15 - Deflection of the floor slab

Basement Floor + Ground Floor + First Floor

With the addition of another floor, all previously noted observations remain valid and will not be repeated here. Notably, the overall structure now exhibits a very slight tilt. This is expected, given that the added structural elements at the first-floor level have increased both the deflection of the transfer slab—particularly in the corridor area—and the out-of-plane deformation of the right-hand basement wall, as shown in Figure 6:16.

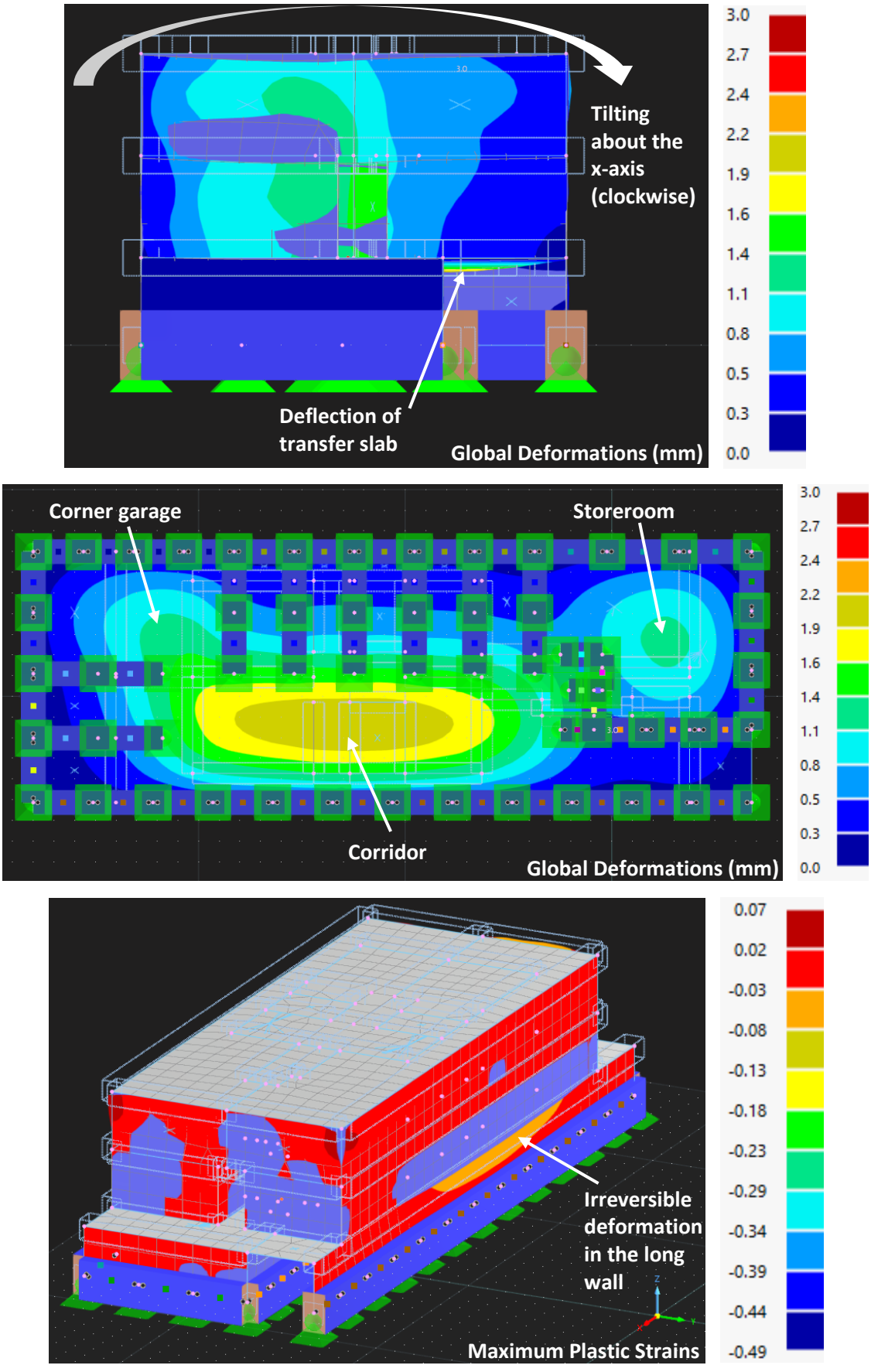

Figure 6:16 - Deformations & Maximum Plastic Strains exhibited in the basement floor walls and the transfer slab

Conclusions

The model did not permit the addition of further floors beyond this point, as the structure became unstable. This outcome aligns with earlier observations indicating that the structure was already exhibiting signs of instability, such as minor tilting in the scaled deformation results. It is reasonable to conclude that the addition of further floors would have amplified this tilting and exacerbated the instability. Moreover, introducing additional floors into an already unstable model would not be meaningful, as it would compromise the integrity of the analysis.

Nevertheless, the observations discussed thus far provide a solid understanding of the structural behaviour. This serves as a strong foundation for interpreting the results presented in the following sections.

6.4.2. Behaviour of the Apartment block under self-weight

The results of the numerical model under the structure's self-weight indicate that the apartment block is experiencing significant deformations, primarily due to tilting about the x-axis toward the side where the garage walls are located, as shown in Figure 6:17. This behaviour is attributed to the basement floor's layout, which differs from that of the overlying floors. The asymmetrical arrangement of the basement floor, results in varying stiffness across the plan, contributing to the observed structural response.

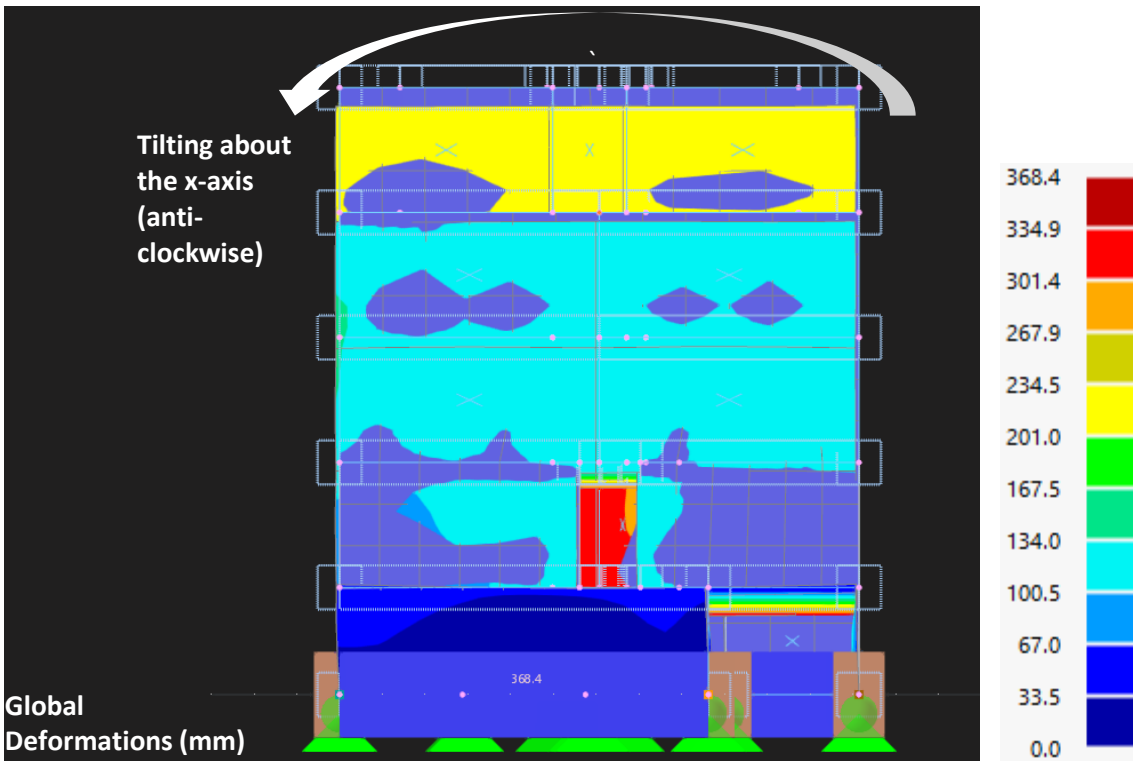

Figure 6:17 - Tilting of the structure

An analysis of global deformations and maximum plastic strains reveals that the orthogonal walls on the left-hand side of the basement, forming the garage walls, are undergoing plastic strains and exhibit deformations in both in-plane and out-of-plane directions, as shown in Figure 6:18. This observation aligns with the direction of the overall tilt, which occurs towards these walls. Additionally, the orthogonal walls and the central region of the long wall on the right-hand side—where these

orthogonal walls connect—are constructed as single-skin walls. As such, these areas demonstrate notable deformations and strain due to their reduced stiffness.

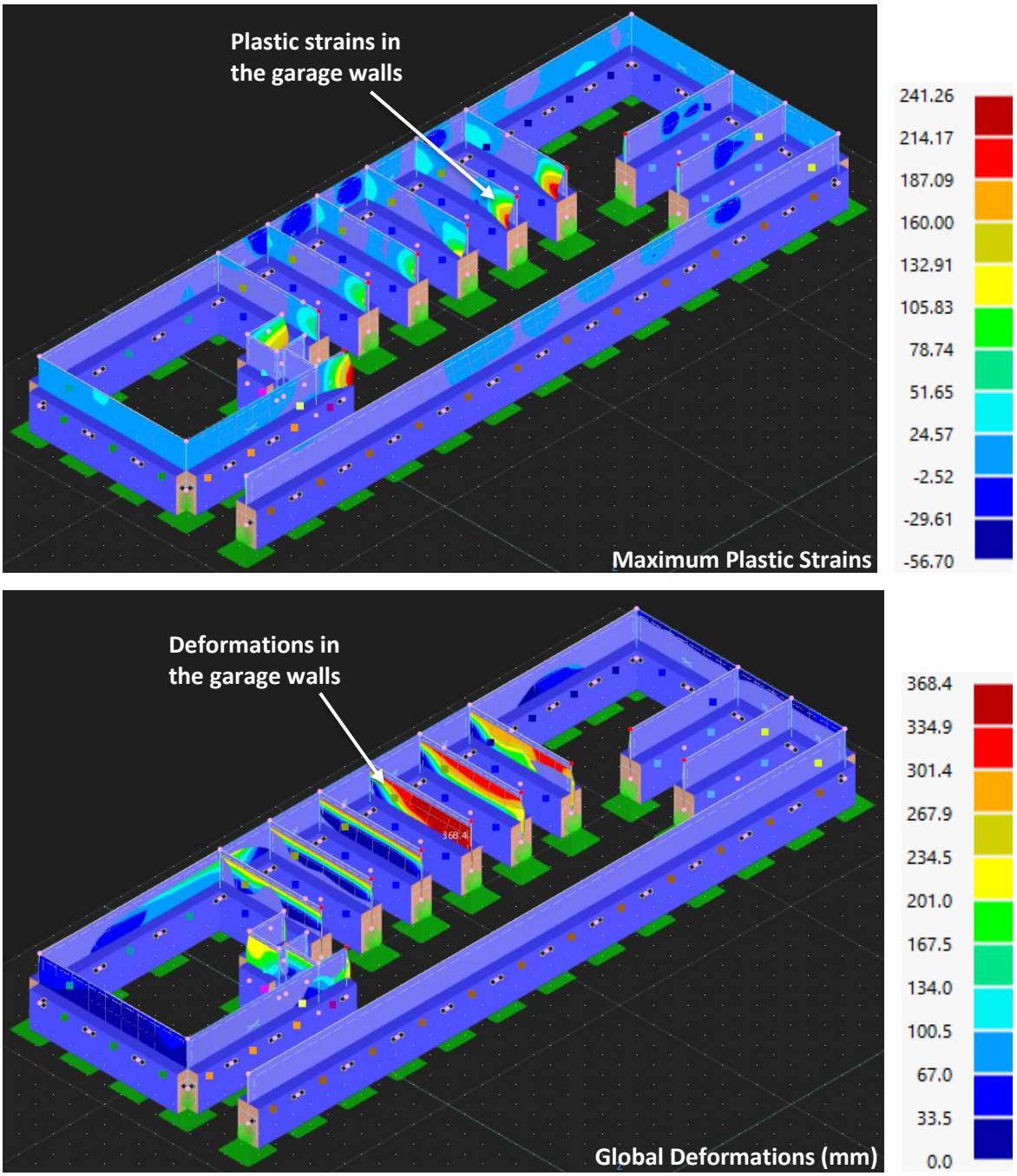

Figure 6:18 - Maximum plastic strain and deformations exhibited in the basement floor walls

Another contributing factor is the presence of an internal aisle in the basement garage to accommodate vehicular movement. This aisle introduces a structural discontinuity, as it results in a lack of vertical support beneath the transfer slab. Consequently, the slab spans the full length of the garage without intermediate support, leading to significant deflections, clearly reflected in the global deformation results, as shown in Figure 6:19.

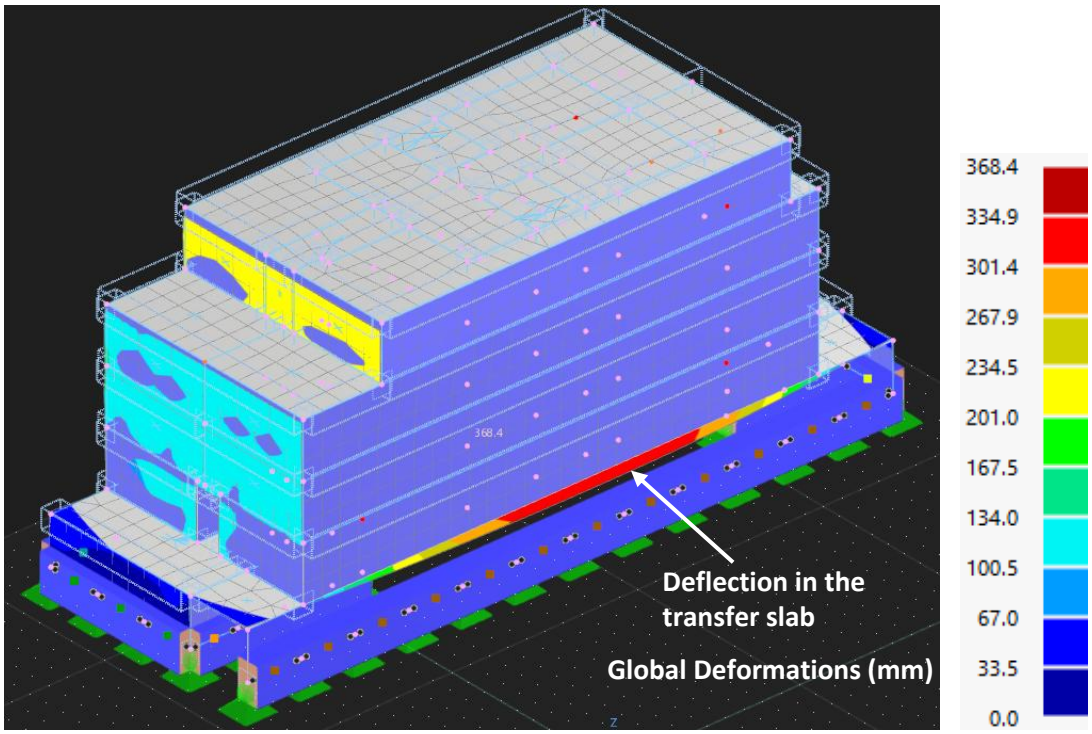

Figure 6:19 - Deflection of the transfer slab

Combined, these issues on both the left and right sides of the basement result in widespread deformation throughout the structure. Notably, the critical zones in the above-ground apartment levels appear to be located at the centre of the apartments, as shown in Figure 6:20 & Figure 6:21. This is expected, as the central area is the most heavily loaded. Moreover, due to the lack of internal support, the basement transfer slab behaves similarly to a simply supported beam. In such a configuration, maximum vertical deflections occur at mid-span—precisely where the structure is most loaded from the overlying floors. This explains why walls and slabs in the central region of the apartments are the most critically affected.

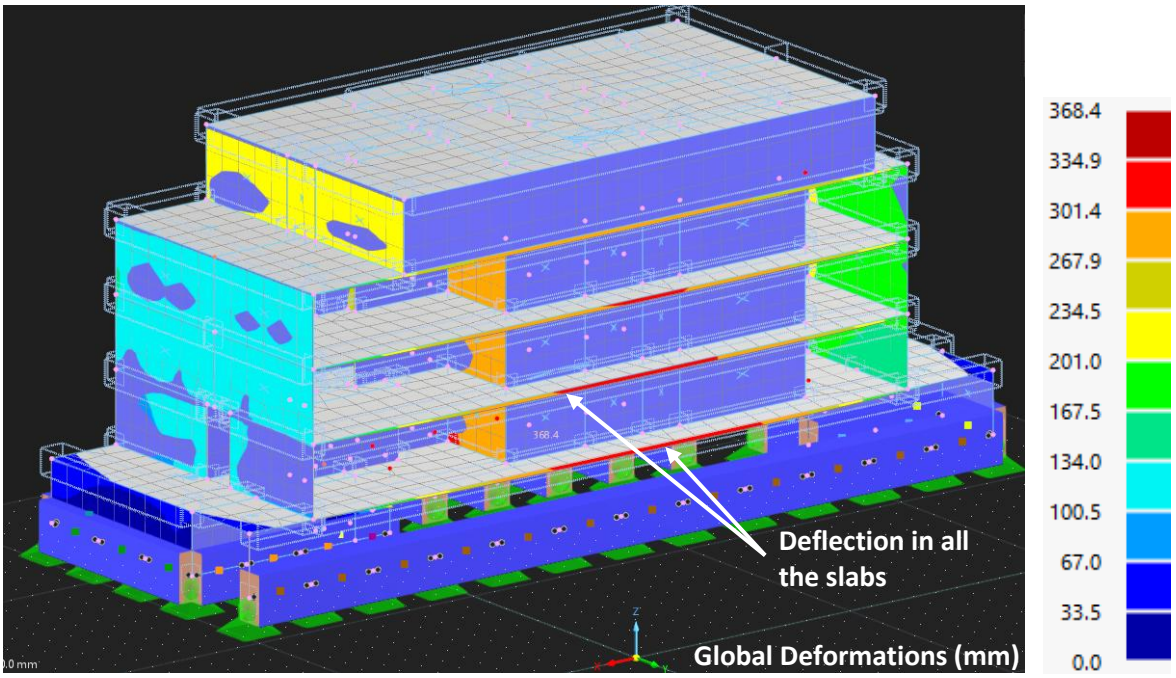

Figure 6:20 - Deflections of the floor slabs

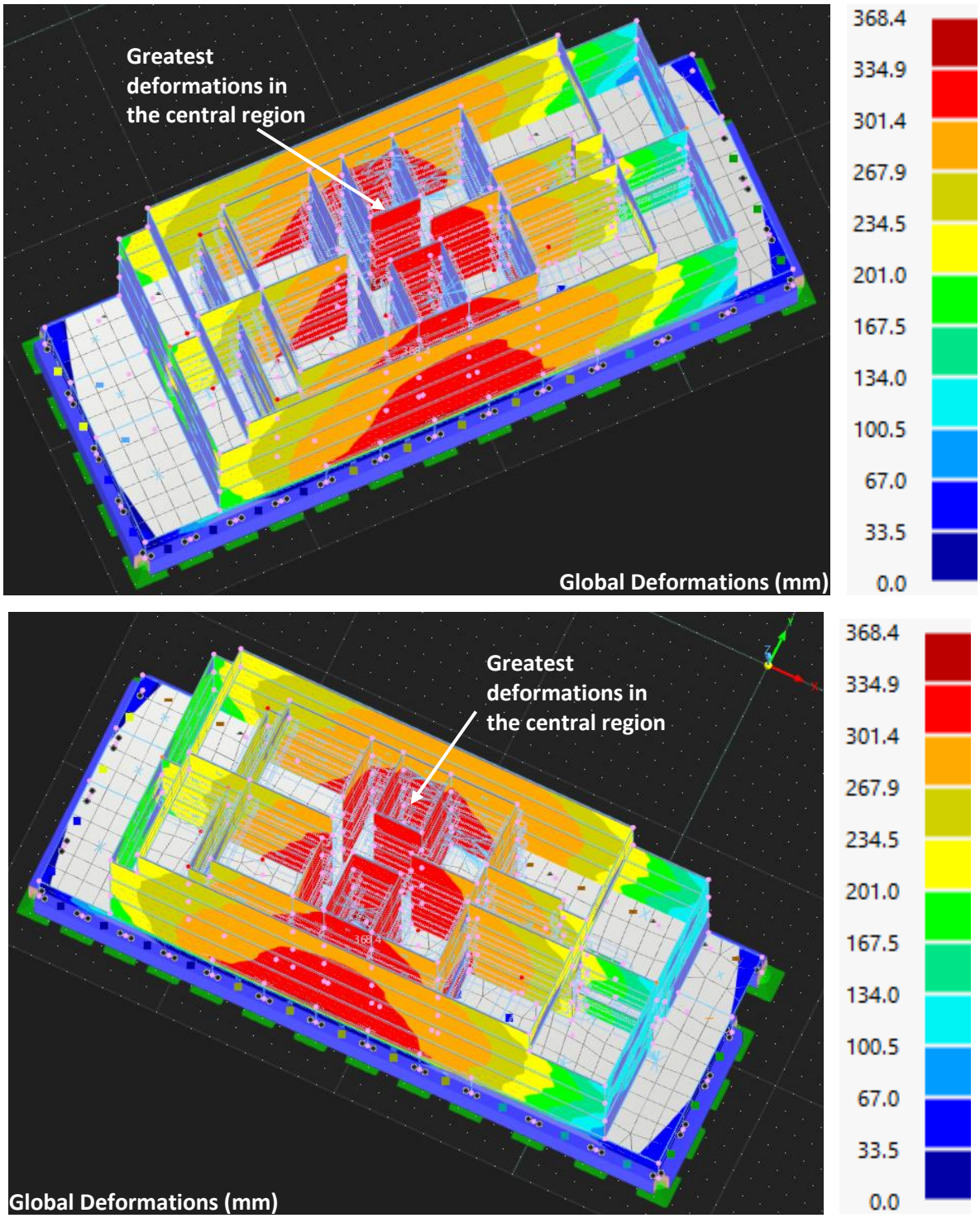

Figure 6:21 - Deformations observed in the central region of the structure

Additionally, on the right-hand side of the basement, the transfer slab is supported by a single long wall without any internal supporting walls beneath it. This results in all vertical loads being transferred directly to that wall, placing it under considerable stress. The plastic strain results suggest that this wall is approaching out-of-plane deformation, as shown in Figure 6:22. A similar condition exists along the long wall on the left-hand side, where the spans supporting the slab are also extensive, increasing the risk of structural instability, as shown in Figure 6:22.

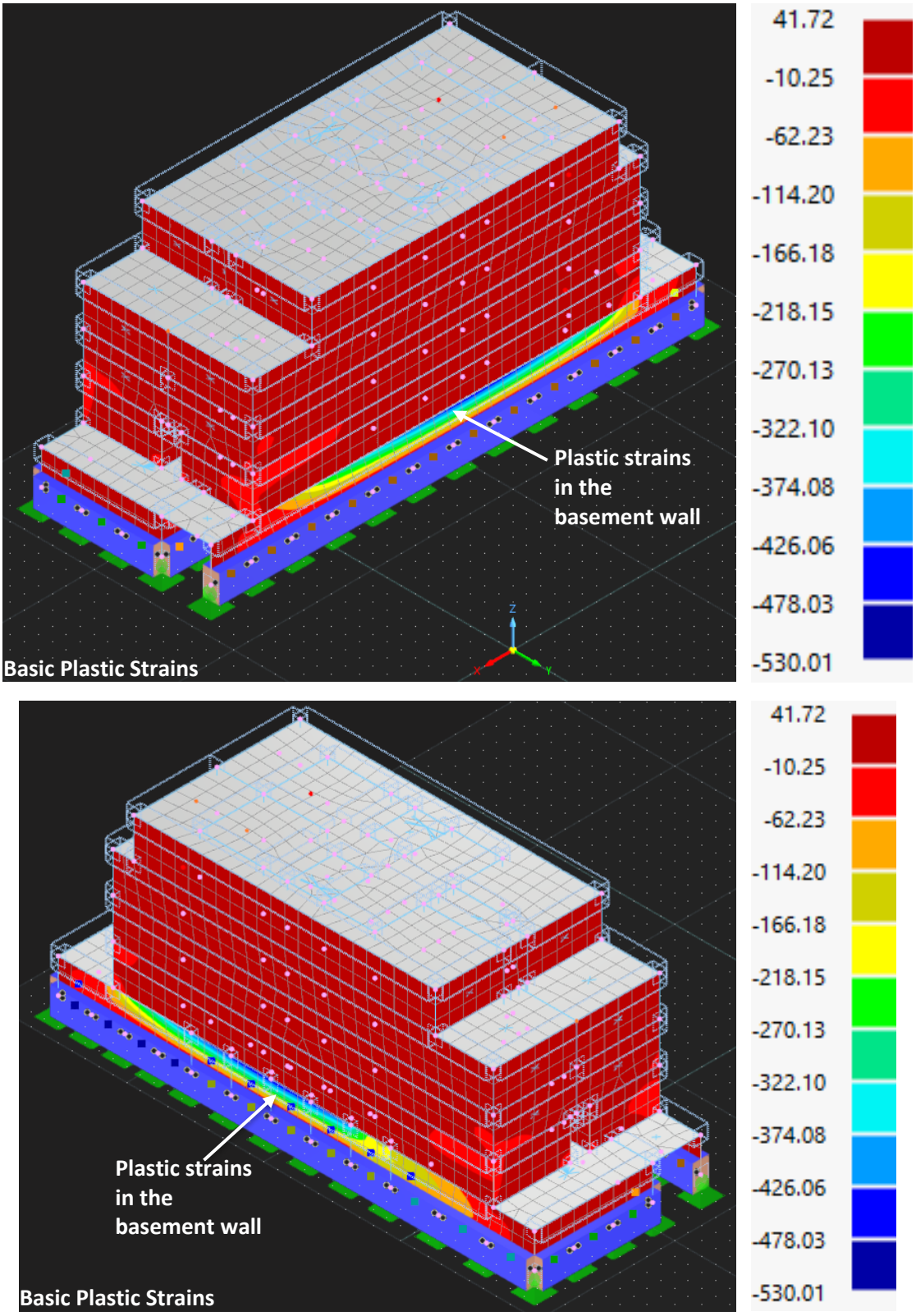

Figure 6:22 - Plastic strains exhibited in the basement walls

Another important consideration is that the long walls at the basement level, which appear to be deforming, are causing deformation in the masonry walls of the apartment floors they support. This observation is also confirmed by the global deformation results of the structure, as shown in Figure 6:23.

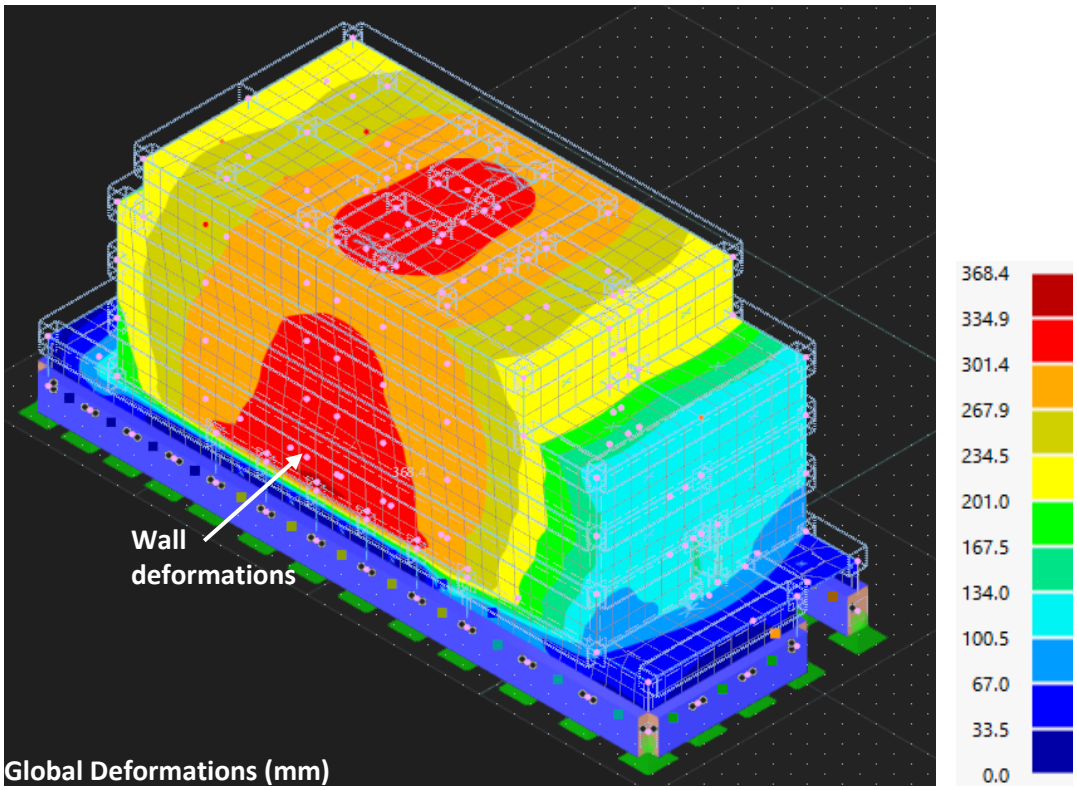

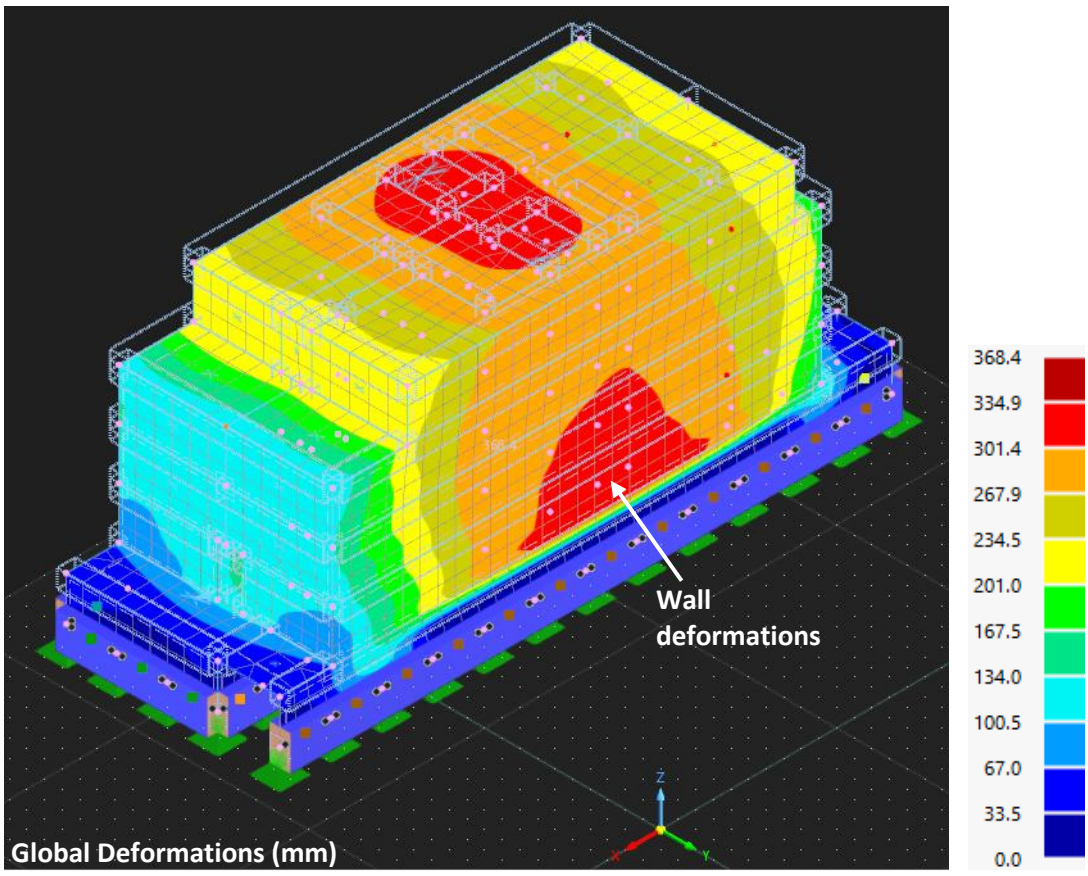

Figure 6:23 - Global deformations experienced by the structure

While other walls within the structure are also subject to stresses and deformations, these are less severe compared to the critical regions discussed above.

6.4.3. Applying a Nodal Deformation along the Longitudinal Side

The block was initially observed to be tilting under its own self-weight. To simulate potential settlement caused by excavation or construction works on a neighbouring property, a nodal deformation was applied to the sides of the structure, as shown in Figure 6:24.

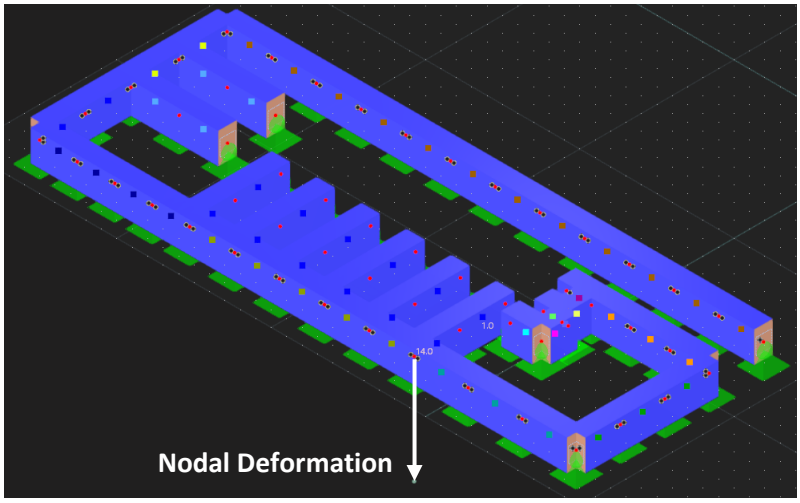

Figure 6:24 - Location where the nodal deformation is applied

Upon applying the nodal deformation, the structure began tilting in the opposite direction to its original lean, as shown in Figure 6:25. This outcome was unexpected, as it was anticipated that the structure would continue to deform in the same direction as the original tilt.

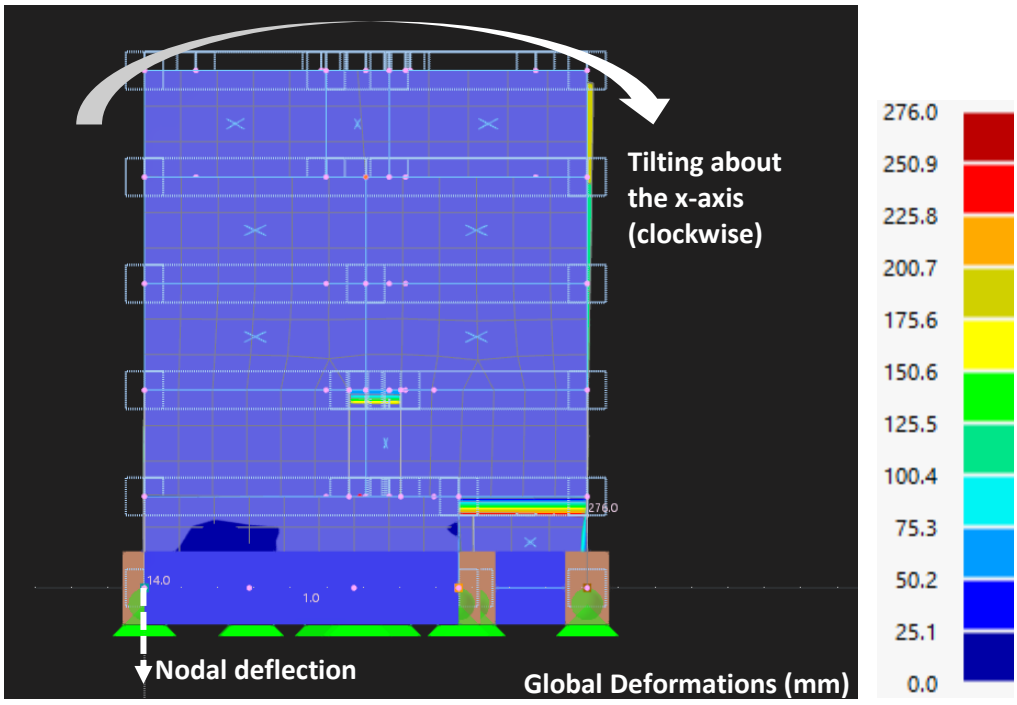

Figure 6:25 - Tilting of the structure

However, applying a nodal deformation to a specific part of the structure alters the internal force equilibrium throughout the entire system—not just at the affected node. Even when the applied deformation is in the same direction as the original tilt, it can relieve or redistribute internal stresses in such a way that the structure rebalances and tilts in the opposite direction. For instance, if the

deformation causes a key load-bearing element to soften or further deform, load may be redistributed to stiffer elements, resulting in a reversal of the tilt.

As a consequence, the tilt on the left-hand side has decreased, while the tilt on the right-hand side has increased (Figure 6:26). This redistribution of load has reduced deformation and strain in the left basement wall, as the load previously acting on it has been transferred to the right basement wall (Figure 6:26). Correspondingly, strain and deformation in the right basement wall have increased. Due to this new tilt direction, the floor slabs appear to be inclined toward the right-hand basement wall, concentrating more force on it and intensifying its deformation. Consequently, the walls supported by this basement wall also experience increased deformation (Figure 6:26).

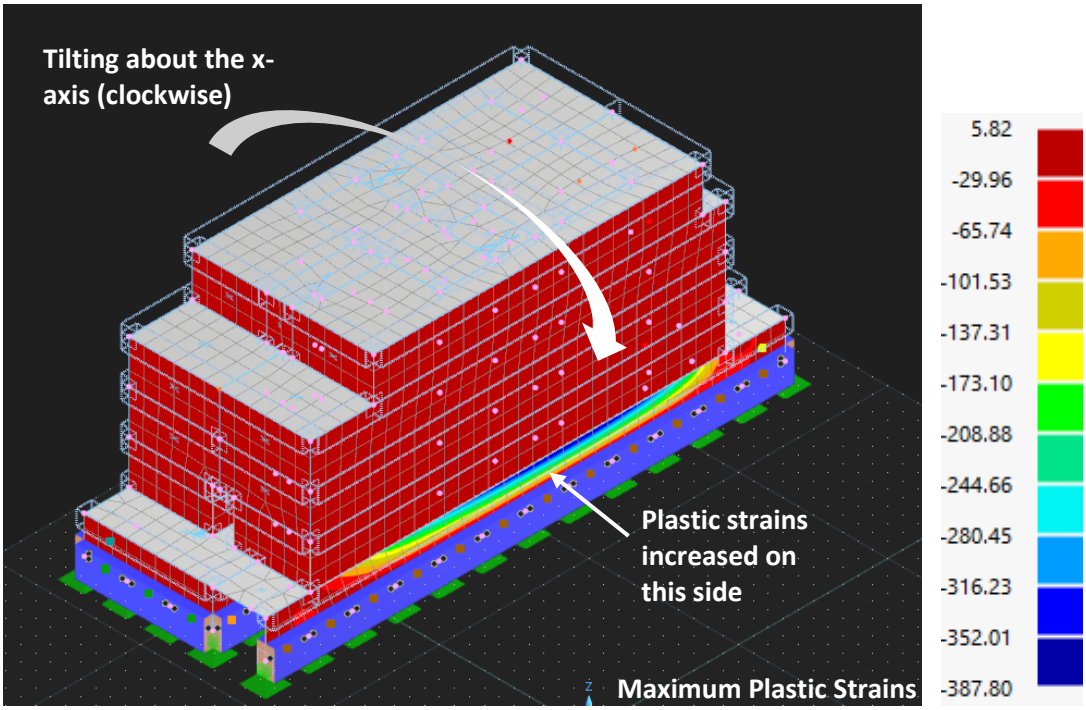

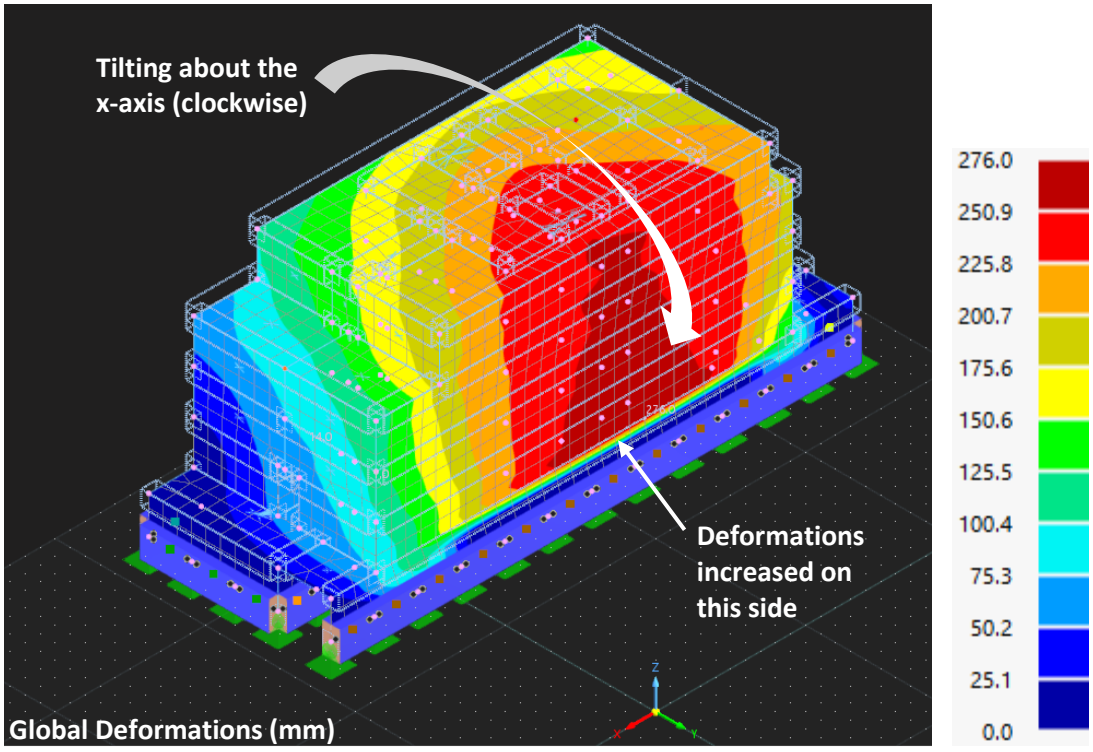

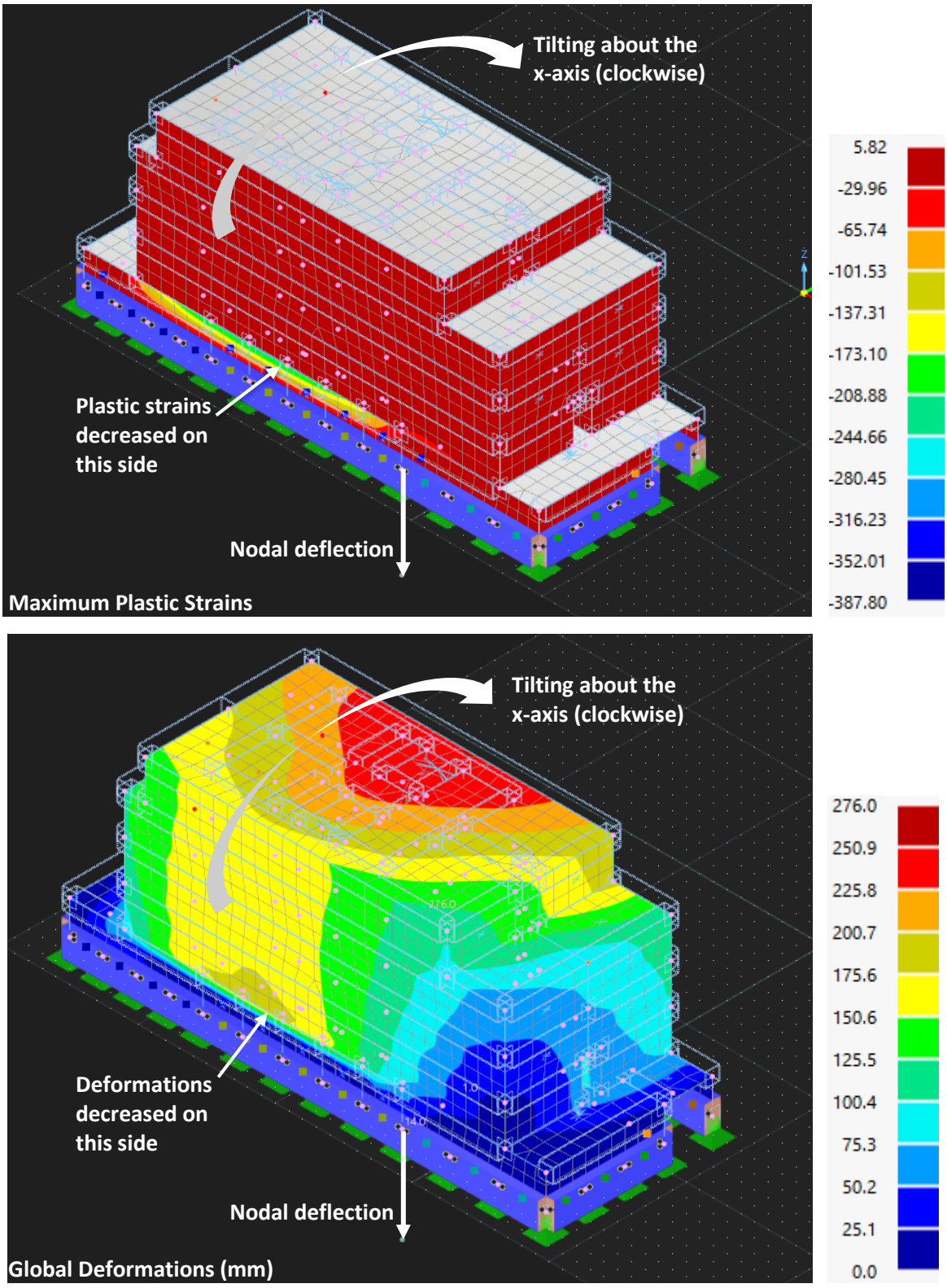

Figure 6:26 - Comparison of the results for the Global Deformations & Maximum Principal Plastic Strains by the apartment block model from different perspectives, analysed individually

Although the central areas of the apartment block remain the most critical, as discussed in Section 6.4.1 , the shift in tilt has caused these critical regions to move slightly toward the right-hand side of the slabs, as shown in Figure 6:27. This is consistent with the new deformation pattern, as the critical areas now align with the direction of tilt.

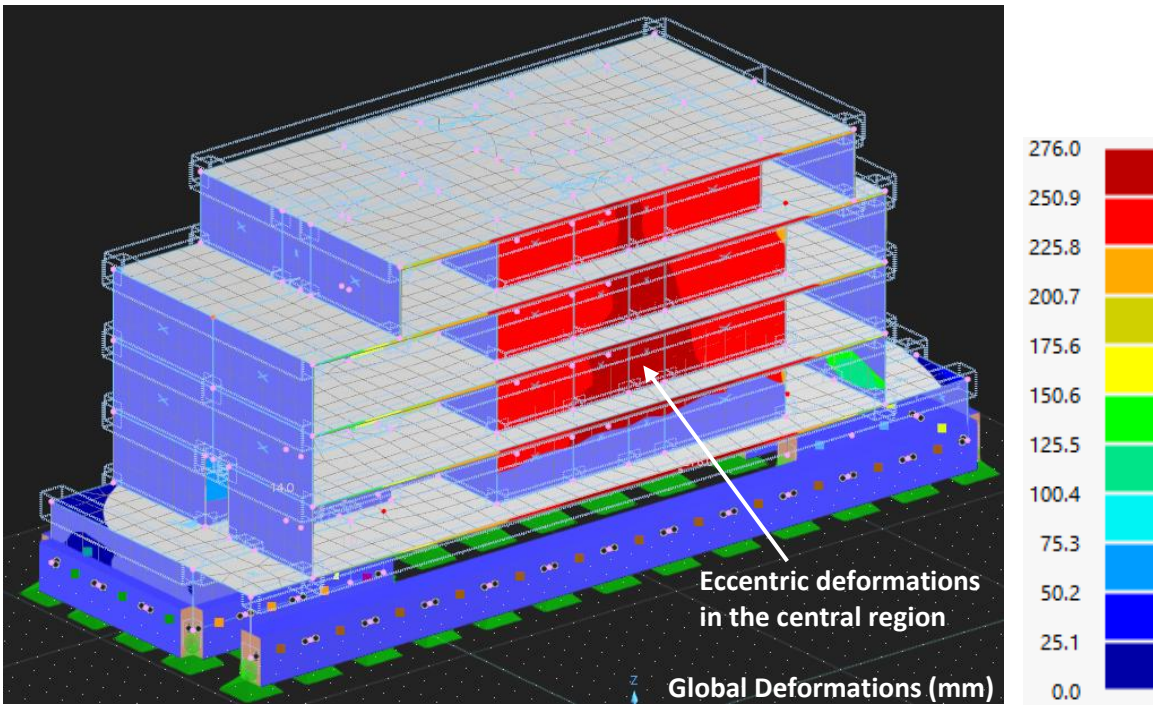
276.0
250.9
225.8
200.7
175.6
150.6
125.5
100.4
75.3
50.2
25.1
0.0
Eccentric deformations in the central region
Global Deformations (mm)

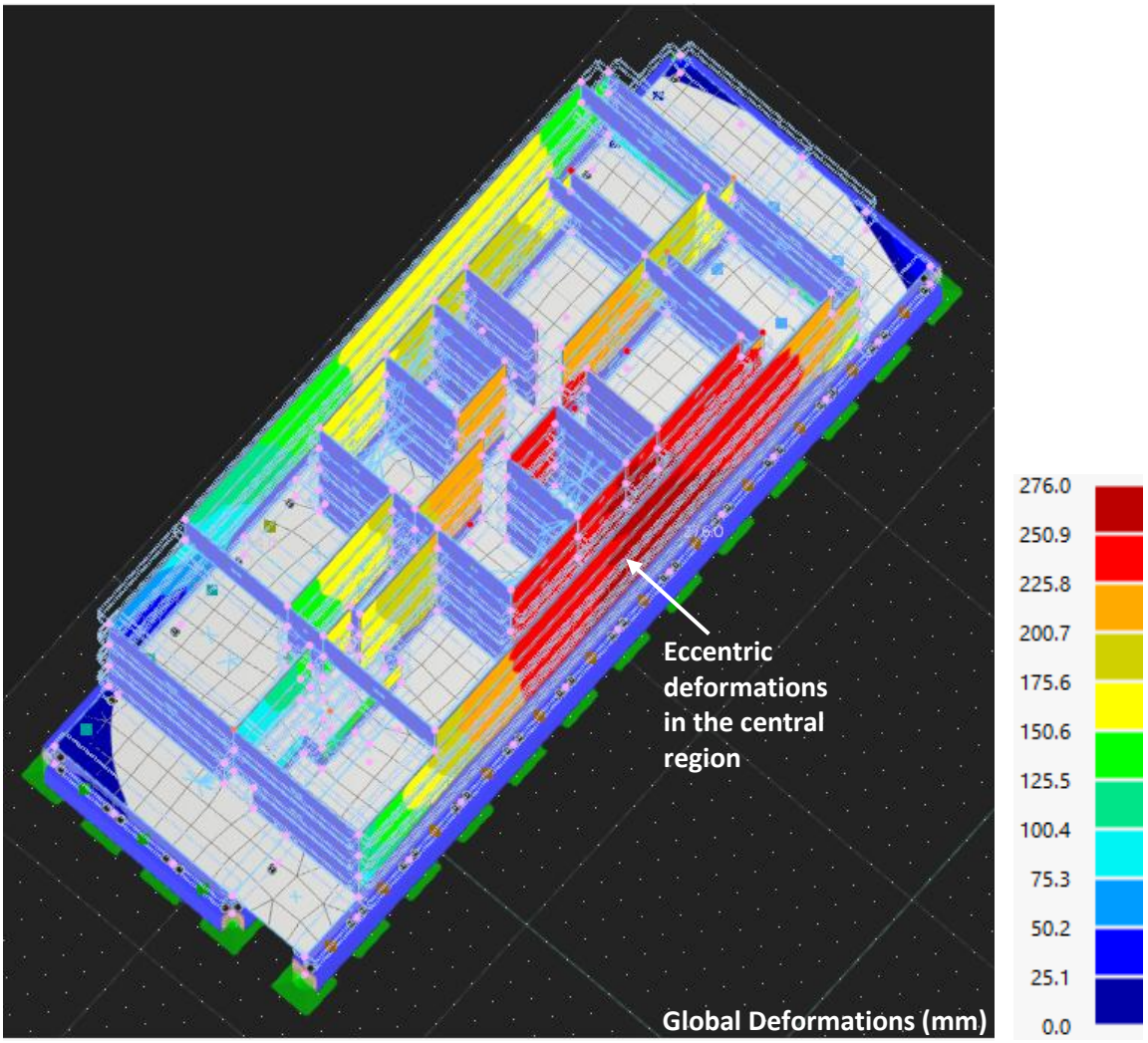
276.0
250.9
225.8
200.7
175.6
150.6
125.5
100.4
75.3
50.2
25.1
0.0
Eccentric deformations in the central region
Global Deformations (mm)

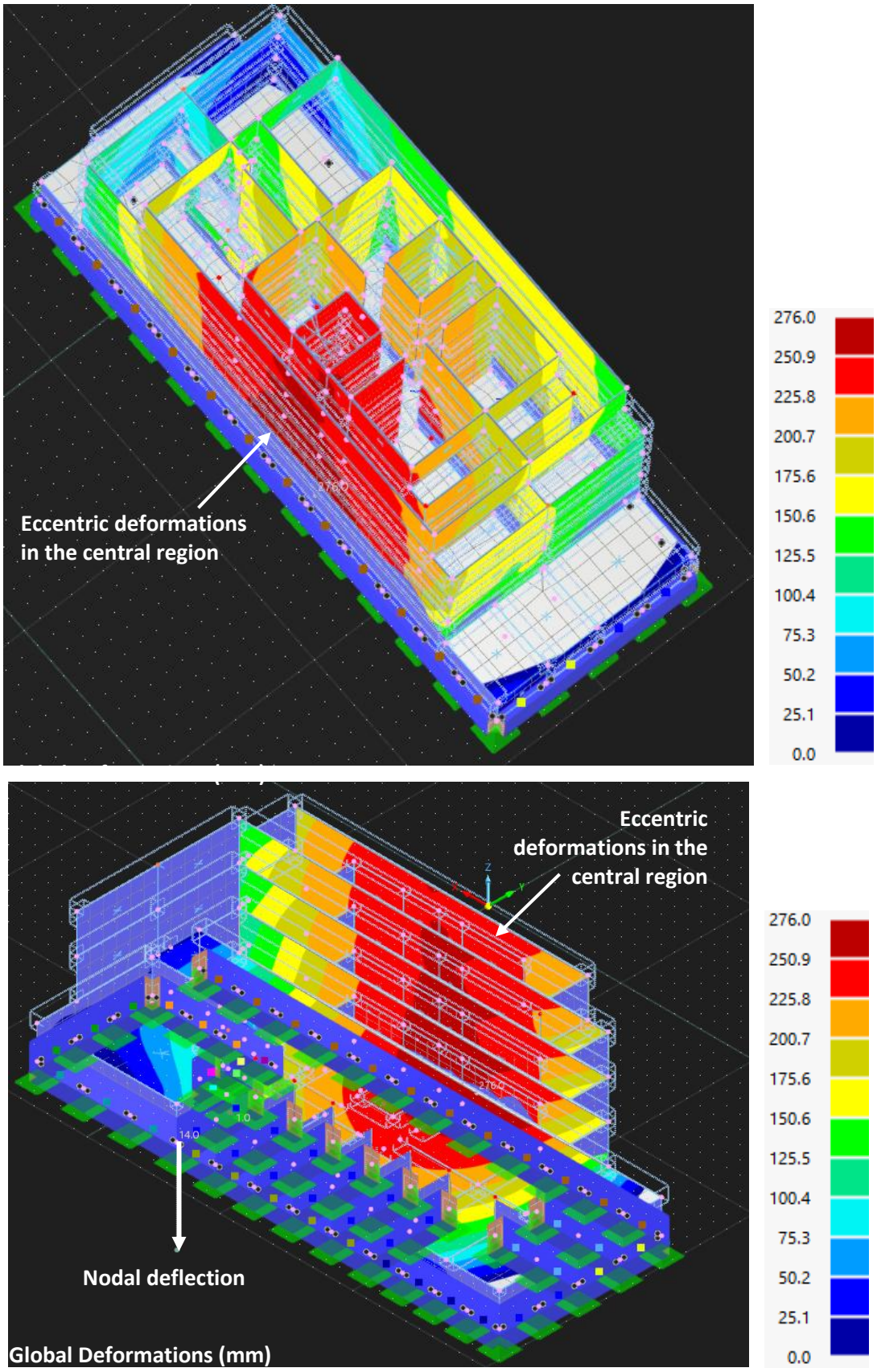

Figure 6:27 - Deformations observed in the central region of the structure, from different views

Furthermore, as previously explained in Section 6.4.1 , the orthogonal walls forming the garages also experience deformation and plastic strain in this model.

6.4.4. Applying Nodal Deformation on the Frontal Side

The nodal deformation was applied to the shortest side (front side) of the apartment block to simulate potential ground settlement resulting from excavation or construction works along the adjacent road, as shown in Figure 6:28.

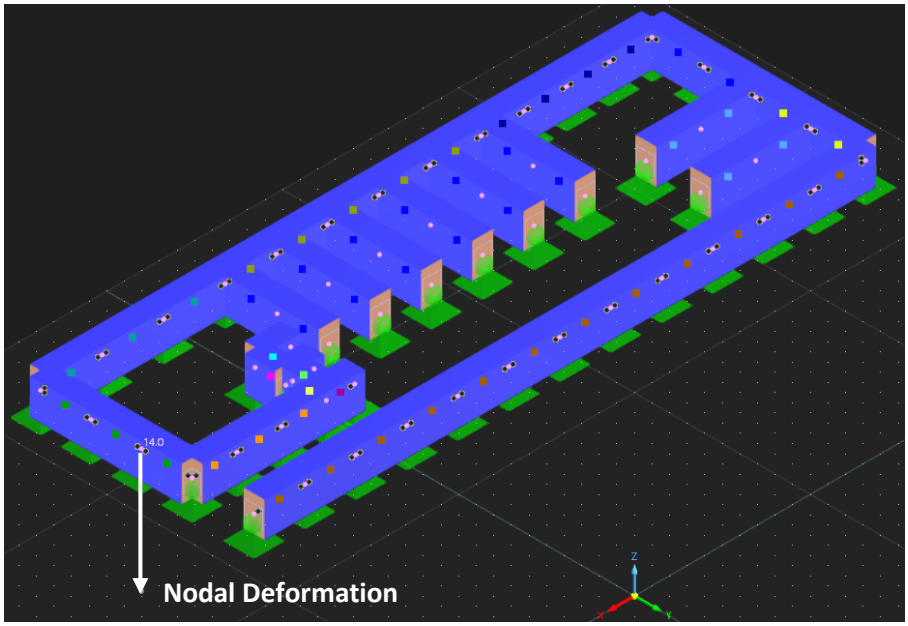

Figure 6:28 - Location where the nodal deformation is applied

The global deformation results indicate that the impact of this nodal deformation is not particularly critical in this scenario. While there are some slight differences compared to the deformations caused by self-weight alone, the overall structural behaviour remains largely similar. To avoid redundancy, only the changes observed will be discussed—any aspects not mentioned can be considered unchanged.

Although the structure continues to exhibit tilting towards the left-hand side, the degree of tilt has slightly reduced due to the applied nodal deformation. This is logical, as long as the structure behaves monolithically. When one side settles, the rest of the structure tends to follow, resulting in a reduction in overall tilt—similar to the way a table stabilises when a shorter leg settles further into the ground. In fact, the global deformations shown in Figure 6:29 indicate that the deformations on the left hand side of the structure are very similar to those on the right hand side, thus the structure seems to be balanced.

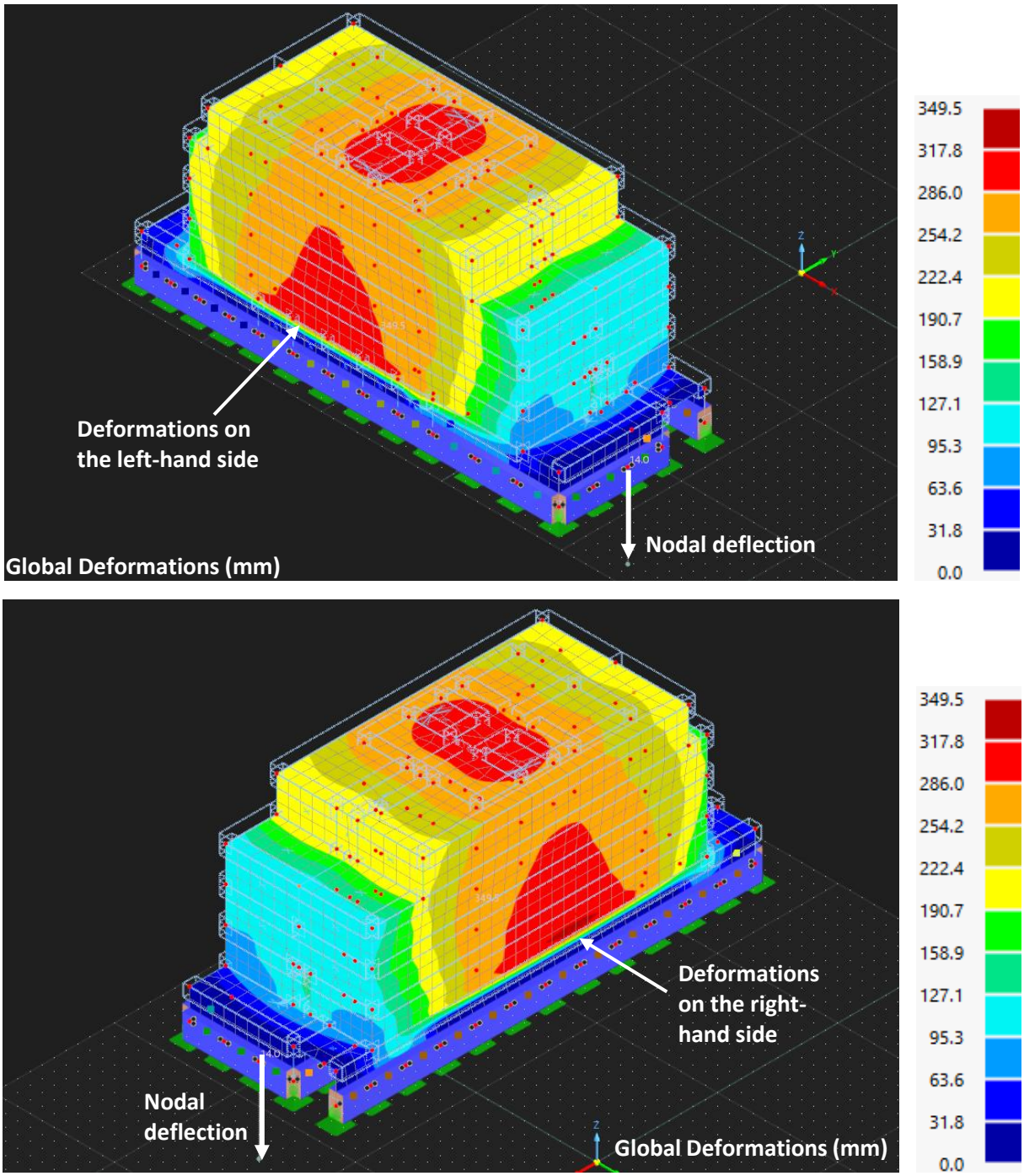

Figure 6:29 - Global Deformations experienced by the structure

As the tilt decreases, the load previously concentrated on the left-hand wall is reduced. This, in turn diminishes the deformation in the basement wall, resulting in decreased deformations in the overlying masonry walls.

However, since the tilt has diminished, some of the load has effectively been redistributed. The load alleviated from the left-hand basement wall has now been partially transferred to the basement wall on the right-hand side and to the orthogonal walls forming part of the garage layout. This is reflected in the plastic strains results, which show a slight increase in strain and deflection in the right-hand basement wall, as illustrated in Figure 6:30.

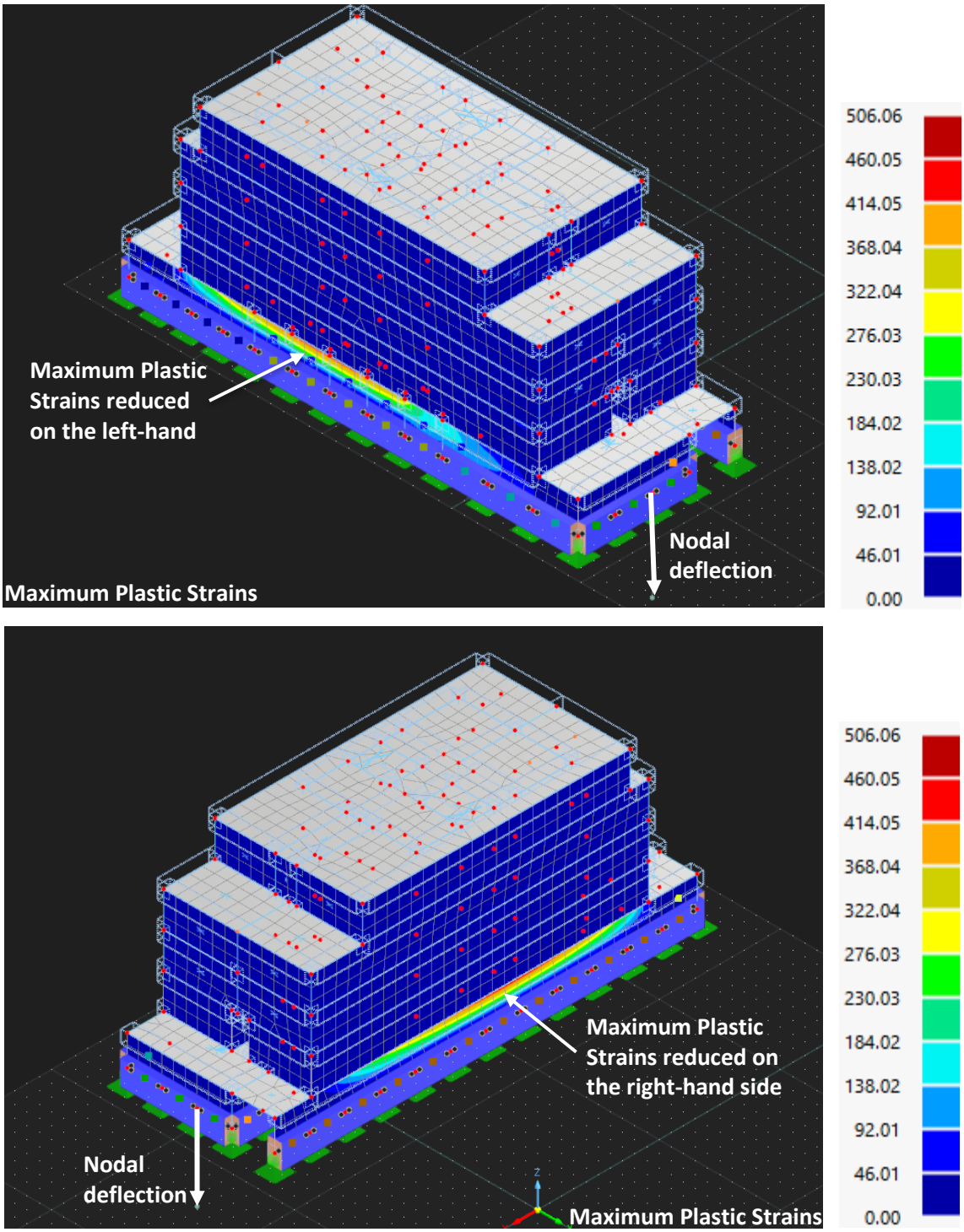

Figure 6:30 - Different views showing the structure's Maximum Plastic Strains

6.4.5. Applying Nodal Deformation to Internal Walls

In this case, the nodal deformation was applied to an internal garage wall (Figure 6:31), as these walls are subject to significant loading from the overlying floors. It was anticipated that this internal nodal deformation would help mitigate the structural tilt—similar to correcting a wobbly table by adjusting a shorter leg.

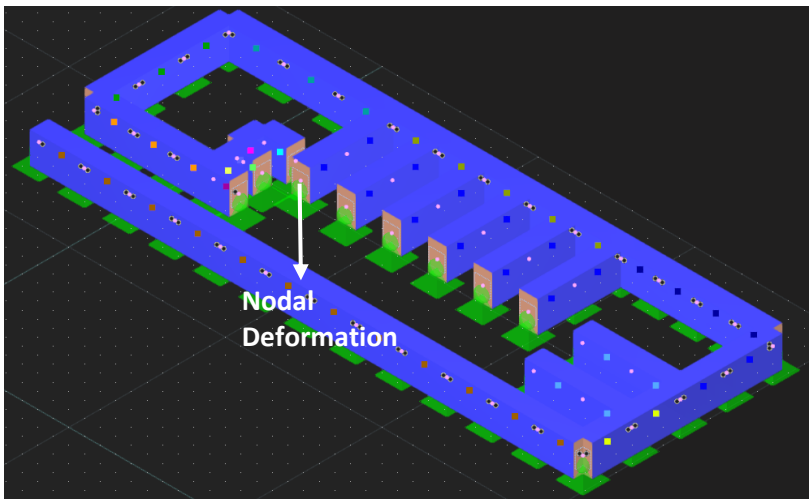

Figure 6:31 - Location where the nodal deformation is applied

However, the results indicate that the nodal deformation had minimal impact on the overall structural response. When compared to the deformation under self-weight alone, as discussed in Section 6.4.2 the global deformation results show only negligible differences. The overall behaviour of the structure remains largely unchanged, as shown in Figure 6:32. Therefore, to avoid redundancy, the results will not be discussed in detail here, as they have already been adequately covered in Section 6.4.2.

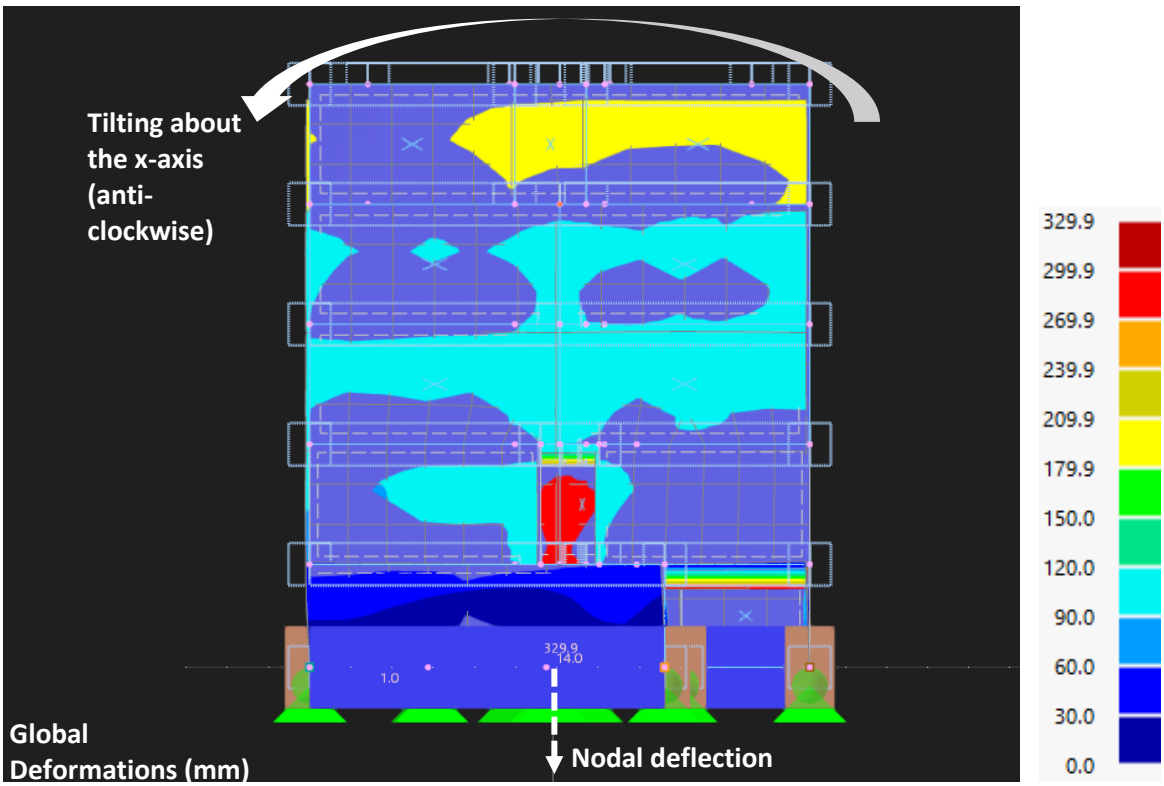

Figure 6:32 - Global Deformations experienced by the structure

6.4.6. Further Discussion on the Typical Apartment Block

In this section, further discussion based on the results and observations presented in Section 6.4, will be discussed. This discussion will serve as a two-fold function, where it should target the current construction practices as well as the current construction methodology, serving as an eye opener of what should be avoided and what could cause considerable damage.

Impact of excavation

Excavation generally impacts a structure's stability, as previously discussed. The degree of this effect depends on the excavation's location. It is important to note that, due to time constraints, nodal deformation was applied to only one point along both the longitudinal and frontal sides in this study. Consequently, there may be other points along these sides where applying nodal deformation could have a greater impact on the structure's stability.

From the results discussed, it is evident that the structure's stability was most significantly affected when nodal deflection (excavation) occurred on the longitudinal side. While this outcome was anticipated, it is concerning because excavations on the longitudinal side are common in local construction practices.

In conclusion, construction planning, preparation, and geotechnical studies should be prioritized as highly as other project aspects, if not more. During the excavation stage, architects bear the responsibility of ensuring the stability of adjacent structures—often inhabited by people—and the safety of workers within the excavation site.

To achieve this, construction planning and geotechnical studies must be integrated at the project's inception rather than treated as afterthoughts. Addressing these considerations early on can prevent delays, disappointments, and potential fatalities.

Use of Transfer Slab

A key challenge with this structure stems from the significant discrepancies between the basement floor plan and the plans of the overlying floors. This variation disrupts the load path, necessitating the use of a transfer slab to redirect the loads from the upper floors to the basement.

For professionals working with multi-storey buildings, it is crucial to recognise the detrimental effects of non-direct load paths and drastic changes in floor plans on overall structural stability. Ideally, structures should be designed with direct load paths to enhance stability. However, achieving this can be difficult in many cases.

When a direct load path is not feasible, an alternative recommendation is to reconsider the structural solution. For example, adopting a structural frame with masonry infill walls or reinforced masonry construction could be more effective. These alternatives provide better stability compared to the common local approach for apartment blocks, which typically involves unreinforced masonry structures combined with a transfer slab to address non-direct load paths.

Basement Layout Floor

The basement floor plan is asymmetrical due to the presence of garages on one side and a vehicle manoeuvring corridor on the other. This asymmetry causes uneven plan stiffness, primarily resulting from the long, unstiffened wall of the manoeuvring corridor. Such walls, like other single-skin masonry walls in the basement, are significant structural weaknesses because their considerable length makes

them prone to deformation. A similar issue with long, unstiffened walls is also observed in the apartment floors, particularly along the corridor walls.

Another major structural concern arises from the vehicle manoeuvring corridor, which creates a large unsupported span for the transfer slab. Originally designed to address non-direct load paths and to bear significant loads from the overlying floors, the transfer slab now suffers substantial deflections due to inadequate support, further undermining the building's structural stability. This problem is not limited to the basement; large unsupported slab areas are also common in apartment floors, especially in modern open-plan layouts.

To address these challenges, it is recommended to design layouts with minimal variations in stiffness across the plan. When uniform stiffness is difficult to achieve, solutions such as introducing masonry piers or double-skin walls can help balance and even out stiffness, particularly in areas like the basement. These measures would also serve to stiffen long, unstiffened walls. Additionally, limiting the span of unsupported slab areas wherever possible is crucial. When this is not feasible, alternative structural systems should be considered to meet the structural demands effectively. Proactively addressing these issues can enhance structural integrity and lead to safer, more reliable designs.

Critical zones

The identification of critical zones in a typical apartment block subjected to nodal deformation is an essential and frequently discussed topic. A key consideration is not which individual apartment is most susceptible to settlement but rather which areas within the apartment block are the most structurally critical. In the discussion below, the apartment block will be considered as a single unified structure.

From the results already discussed, one notable observation is that the central area of the apartment block emerges as the most critical zone. This criticality is further influenced by the application of nodal deformation along the longitudinal side of the structure. If excavation occurs adjacent to the apartment block, causing the structure to tilt (as previously explained), the critical zone remains central but shifts slightly toward the direction of the tilt.

As highlighted in the results, the central critical zone arises primarily due to the large unsupported span of the transfer slab. This slab carries the heaviest load from the multiple floors above, leading to significant deformation regardless of the type of nodal displacement applied. Consequently, the walls of the above-ground apartments supported by the transfer slab exhibit the greatest deformations in this zone.

To conclude, addressing a crucial question: the penthouse is the apartment most adversely affected compared to others. This is due to a significant portion of its floor area being located within the central critical zone. In contrast, larger apartments on lower floors extend beyond this zone, with their frontal and rear areas experiencing less critical effects.

7. Conclusion

7.1. Concluding Remarks

The primary aim of this dissertation is to investigate the structural behaviour of unreinforced masonry walls and structures using numerical modelling. This section provides a concise summary of key insights gained from each model, highlighting lessons learnt and their relevance to both the construction industry and future research. The intention is to reflect on both personal challenges encountered during the modelling process and the broader implications of these findings, in order to inform better practices and avoid repeating past mistakes.

Modelling of a typical apartment block

This was undoubtedly the most challenging structure to model, primarily due to the significant difference in scale compared to the previously modelled structures. However, from a modelling perspective, there were no major differences, as the same functions and approaches were applied.

Technically, the results obtained from this model were particularly important. It is crucial to remain critical and analytical when interpreting model results, especially when the structure exhibits erratic behaviour, as in this case. Results should always be considered within the specific context of the modelled scenario to ensure accurate interpretation. For example, the slight tilting observed may stem from the numerical solution itself and the fact that the structure was modelled as a standalone element, whereas in reality it is constructed between existing adjacent structures.

A critical conclusion derived from the observations discussed in Section 6.4.6 highlights the need to modernize local construction practices and methodologies to align with contemporary construction typologies. Without such evolution, structures may fail to serve their intended purposes, increasing the risk of structural failures and potentially leading to tragic consequences, including loss of life. This underscores the urgency of bridging the gap between traditional methods and modern standards.

Equally significant is the necessity to transform prevailing attitudes and approaches toward local construction on two crucial fronts. Firstly, the local construction industry cannot advance meaningfully if projects prioritize profit maximization at the expense of structural integrity and the overall quality of life provided by the built environment. Such a profit-centric focus diminishes the emphasis on safety, durability, and functionality, undermining long-term sustainability.

Secondly, there must be a fundamental shift in how construction is approached, moving away from complacency to a more deliberate and thoughtful planning process. Each decision, from design to execution, should be carefully evaluated for its potential impacts and repercussions. This proactive mindset can prevent many avoidable mistakes, which, when compounded, can significantly compromise a structure's stability and reliability.

By addressing these aspects, the construction industry can achieve a balance between modern innovation, safety, and practicality, paving the way for more resilient and purpose-fit structures.

General

While this dissertation focuses on the structural behaviour of masonry structures subjected to gradual and controlled settlement, it does not address the stiffness of the underlying ground material in detail. Although the structures are founded directly on the ground, soil-structure interaction was not the

primary concern. Instead, the objective was to isolate and study the response of unreinforced masonry elements to settlement.

In most of the models developed, only the masonry structures themselves were considered. Variables such as the size and location of openings, wall aspect ratios, and overall room dimensions were intentionally excluded to maintain focus on fundamental behavioural patterns.

Overall, numerical modelling has proven to be a reliable method, as the simulated deformations closely aligned with damage observed in real-life structures. Macro-modelling, in particular, was well-suited to the scope of this study, enabling a clear understanding of how masonry walls respond to settlement.

A key takeaway from this dissertation lies in the modelling approach itself. One of the most important lessons has been the value of simplification—carefully selecting the most critical aspects of a structure while omitting unnecessary complexity. This is especially challenging with limited experience, but it became evident that overly detailed models often lead to unexpected or inaccurate results. This experience has underscored the importance of balance between simplicity and accuracy in structural modelling.

One of the key lessons from the modelling process was the importance of patience and taking time to understand the software before starting. It is essential to break problems into smaller steps, allowing for clearer analysis of individual variables. Critically evaluating results—through logical reasoning or hand calculations—is crucial rather than accepting software outputs at face value.

Modelling the wall set-up in Mifsud J. (2012)

As previously mentioned, the modelling of the wall in Mifsud J. (2012) was preceded by several smaller steps, which helped build a solid foundation of understanding. Consequently, the function of every element used in the final wall model was well understood. This made interpreting the results more straightforward, as each decision was part of a logical and methodical process.

From a technical perspective, several insights were gained about the modelling process itself. However, tackling different stages and challenges throughout the process provided valuable opportunities to experiment with the software and explore how various tools could be applied to different modelling objectives. The gradual transition of the wall from a stable state to an unstable one—progressing through the serviceability limit state and ultimately reaching the ultimate limit state—was particularly useful in visualising and understanding the deformation behaviour during settlement.

Another key technique used in this dissertation was simplifying the modelled structure and comparing it with a more basic version. This approach not only validated the accuracy and reliability of the results but also enhanced the modeller's understanding of the structural behaviour.

This comes from a practical point of view, one key piece of advice for everyone in the construction industry is to give proper importance to the masonry construction process, which is often overlooked. Many assume it's simply a matter of laying blocks on mortar, but in reality, it involves critical details—such as alignment, joint filling, reinforcement, and mortar quality—that significantly affect the structural behaviour. Often, the economic factor and construction speed are treated as the main priorities; however, these should be considered secondary. The primary concern must always be the safety and well-being of those who will live or work within the structure, as well as the long-term durability and performance of the building.

Three-dimensional model of a room

Understanding the construction process of a typical room was essential in recognising how specific construction methods influence structural behaviour. In this model, local construction practices were considered, where unreinforced masonry walls were simulated without mortar-filled voids or embedded reinforcement connecting the walls to the slab or strip foundation. As a result, the structural elements behaved independently. The modelling results clearly demonstrate how such a construction method significantly reduces the overall stiffness of the structure, thereby potentially compromising its stability.

It would have been both wiser and safer if Malta had adopted lessons from the seismic experiences of other countries, many of which have transitioned to reinforced masonry or moment frame systems to ensure adequate stiffness and structural integrity. However, economic constraints continue to influence local construction practices, limiting the feasibility of such improvements.

One notable observation was the influence of corbelling between masonry walls. The restraint provided by the corbelling action can increase the overall stiffness of the room. This construction practice serves as an example to emphasize and highlight the potential of reinforced masonry and moment frames in further enhancing the structural stability of such systems, a concept previously discussed.

In modelling the room, a stiff beam was used in place of a typical strip foundation. As the foundation design was not the primary focus, this simplification helped avoid unnecessary complications. Simplifying real-life structures for modelling purposes emerged as a recurring and essential strategy throughout this dissertation. It requires both experience and a solid understanding of the system being modelled, as well as the foresight to predict how a simplified model will behave.

Finally, modelling the room as a 3D structure greatly aided in visualising its deformation under settlement. Until this stage, only 2D structures had been analysed, making it difficult to anticipate how a room would deform in three dimensions. This exercise clearly illustrated the differences in behaviour between 2D and 3D structural systems.

Modelling of Ta' Kenuna Tower

The modelling of Ta' Kenuna Tower proved to be a valuable exercise, as the results could be directly compared to the deformations observed in the real-life structure—similar to the approach taken in Mifsud J. (2012) with the wall model. Beyond this, it offered the opportunity to engage with a real-world problem, which required a thorough understanding of the structural issues before commencing any modelling. Mapping the cracks observed on-site revealed that only half of the structure was displacing, suggesting that multiple nodes were moving. Unlike previous models that focused on vertical settlement, Ta' Kenuna Tower exhibited horizontal displacement, making it fundamentally different from earlier case studies—despite essentially being a simple prismatic structure.

From a modelling standpoint, only a few changes were made when transitioning from the earlier room model to the Ta' Kenuna Tower model, as both shared a similar basic setup. The key differences lies in the direction of displacement, the use of local globigerina limestone blocks, and the absence of a reinforced concrete roof in the tower.

The outcomes from this model highlighted the uniqueness of the structure. The deformation modes and resulting behaviour differed significantly from those in previous models, offering an opportunity

to apply familiar modelling functions in new ways and still achieve different results. This reinforced the importance of adapting techniques to suit the specific characteristics of each structure and provided further insights into structural behaviour under varying conditions.

From a practical point of view, it was observed that all the cracking within the structure—also reflected in the model—originated very close to apertures. This was expected, as the corners of apertures are areas of high stress concentration. Therefore, when designing apertures in buildings, especially in masonry load-bearing structures, it is essential to consider their structural implications—including their size, frequency, and placement within the wall—not solely their architectural role.

Another important consideration for designers is the choice of construction materials, particularly when using local globigerina limestone or hollow concrete blocks. These materials differ significantly in their physical and mechanical properties, resulting in distinct structural behaviours and variations in the indoor environment they create. A structure built with hollow concrete blocks will behave differently from one constructed with globigerina limestone. While this decision is often driven by cost-efficiency and profit, structural stability and long-term performance must need to be given the due importance.

7.2. Improvements to Methodology

This section outlines several limitations encountered when modelling masonry in RFEM6 during the analysis of different structures, which are discussed below:

Masonry properties related issues

The first issue focuses on the normalized mean horizontal compressive strength of the masonry unit (f_{bh}), as this is difficult to determine in an accurate and precise manner. An educated estimate assumes that the normalized mean horizontal compressive strength of the masonry unit is approximately 10% of the normalized mean compressive strength of the masonry unit, but this is not supported by experimental data, especially in the context of local masonry construction.

The second issue focuses on the hollow concrete block construction, were a general-purpose mortar with a compressive strength of 5 N/mm² is typically used. However, due to the issues mentioned in Section 3.2.5, it is unlikely that the mortar achieves this strength. Based on experience, it is highly probable that the compressive strength of the mortar does not exceed 2.5 N/mm², which is the lowest compressive strength option available for masonry in RFEM6.

Dependence on Mesh Size

The accuracy of the model is influenced by the mesh size, as smaller mesh sizes can better capture localized phenomena. For instance, regions with large strains are more likely to develop cracks, and the model's ability to identify these areas depends on the mesh resolution. Therefore, finer mesh sizes yield results that are closer to experimental data, at the expense of large differences in computational time.

Use of Macro-Modelling

One issue is that RFEM6 employs macro-modelling, representing the masonry wall as a homogeneous material with properties derived from averaged characteristics of both the mortar and masonry units. Consequently, RFEM6 does not provide precise stress and strain values and fails to accurately capture the heterogeneous nature of a real masonry wall. However, for the purposes of this dissertation,

RFEM6 is suitable as the focus is on understanding the overall structural performance of masonry rather than achieving fully accurate modelling, which lies beyond the scope of this study.

Another limitation of RFEM6 is that it only provides information on the stresses, strains, and deformations experienced by the masonry. It cannot predict crack formation, crack propagation sequences, or crack widths. Users must infer potential crack locations from the strain contours. To obtain such detailed insights, alternative modelling techniques, such as discrete element modelling, are required.

An additional challenge related to macro-modelling is the interaction between the masonry wall and the steel beam. While this interaction was addressed for the purposes of this dissertation, a more accurate approach would involve modelling the friction between the two structural elements. Again, this level of precision would necessitate the use of advanced techniques, such as discrete element modelling.

Measuring deformations

The software does not permit direct measurement of surface deformations relative to the original model at user-specified points, making it difficult to evaluate the deformation experienced at specific locations.

Instability of the model

In general, when attempting to run an unstable structure, a common error that appears is: 'The stiffness matrix is singular.' A key limitation of the software is that it does not provide guidance on where the issue lies within the structure. The error message is too generic, making it time-consuming to identify the root cause, especially in complex models.

7.3. Recommendations for Future Research

Understanding the influence of variables such as apertures' size, wall finishes, wall dimensions, inclusion of head joints, and boundary conditions is crucial in predicting the behaviour of masonry structures under settlement. These factors collectively determine the structural integrity and performance of masonry structures when subjected to ground movements.

Apertures such as windows and doors play a significant role in altering the behaviour of masonry structures during settlement. Examining their impact on a typical apartment block can highlight how these openings contribute to stress concentration and potential failure zones.

The behaviour of advanced or alternative masonry materials, such as geo-polymer bricks and lightweight concrete blocks, under settlement conditions is an emerging area of research. Investigating these materials' performance can lead to the development of innovative solutions that enhance the resilience of masonry structures to settlement-induced stresses.

The type of bricks and blocks used in masonry construction influences the wall behaviour under settlement conditions. Investigating how different materials respond to settlement can provide valuable guidance for selecting construction materials suited to varying site conditions.

Structural factors, such as the embedment of reinforcement between walls and slabs or between foundations and walls, significantly affect masonry wall behaviour under settlement. Analysing these

factors can provide strategies to improve structural integration and reduce vulnerability to settlement-induced deformation and damage.

Examining the performance of various structural and foundation systems, particularly frame systems, under settlement conditions is essential. For example, the same apartment block can be analysed by incorporating a frame system to assess its behaviour. Such studies not only highlight the comparative advantages of different systems but also provide valuable insights into designing structures that better accommodate settlement movements. Additionally, they can expose defects prevalent in modern local construction practices, paving the way for targeted improvements.

Comparing the effects of settlement on traditional structures, such as terraced houses, and historic systems with modern structures, like apartment blocks, can reveal key differences in their response mechanisms. These comparisons can inform the adaptation of modern engineering practices to preserve heritage structures while enhancing the resilience of contemporary buildings.

The effects of different settlement types and non-ideal nodal deformations, such as non-vertical and non-horizontal displacements, are critical factors in assessing masonry performance. Understanding these effects can improve predictive modelling and the development of construction practices that mitigate the impact of non-ideal settlement scenarios.

Comparing the accuracy of micro-modelling and macro-modelling approaches is essential to determine the most effective method for analysing masonry structures. While micro-modelling provides detailed insights at a granular level, macro-modelling offers a broader perspective suitable for large-scale simulations. Understanding the trade-offs between these approaches can help in selecting the appropriate method for specific scenarios.

8. References

Angelillo, M., Lourenco, P. B., & Milani, G. (2014). *Masonry behaviour and modelling.*

Bazant, Z. P., Xi, Y., & Reid, S. G. (1991). *Statistical size effect in quasi-brittle structures: I. Is Weibull theory applicable?*

Behera, B., & Nanda, R. P. (2021). *In-plane shear strengthening of brick masonry panel with geogrid reinforcement embedded in bed and bed-head joints mortar.*

Boone S.J. (2001). *Assessing construction and Settlement-Induced Building Damage.*

Boscardin M.D. & Cording E.G. (1989). *Building response to excavation-induced settlement .*

Burhouse, P. (1969). *Composite action between brick panel walls and their supporting beams.*

Burland J. B. & Wroth C. P. (1974). Settlement of Buildings and Associated Damage. *Allowable and differential settlement of structures, including damage and soil-structure interaction*, (pp. 611-654).

Burland J.B. (1995). *Assessment of risk of damage to buildings due to tunneling and excavation.*

Calio, I., Marletta, M., & Panto, B. (2005). *A simplified model for the evaluation of the seismic behaviour of masonry buildings.*

Chisari et al. (2022). *Anisotropic plastic-damage model for 3D nonlinear simulation of masonry structures.*

Cook, R. D., et al. (2001). *Concepts and applications of finite element analysis 4th edition.*

D'Altri et al. (2020). *Modeling strategies for the computational analysis of unreinforced masonry structures: review and classification.*

DDMaS. (2021). *DDMaS - Digitizing the design of masonry structures.*

Decanini et al. (2004). *Performance of masonry buildings during the 2002 Molise, Italy, earthquake.*

Dhanasekar, M., Page, A., & Kleeman, P. (1985). *The failure of brick masonry under biaxial stresses.*

Dickinson P.R. & Thornton N. (2006). *Cracking and Building Movement.*

EN1997-1. (2004). *Eurocode 7: Geotechnical Design - Part 1: General rules (Annex H).*

Finno R.J. (2005). *Evaluating Damage Potential in Buildings Affected by Excavations.*

Franzius J.N. (2003). *Behaviour of building due to tunnel induced subsidence.*

Geddes J.D. (1991). *Building response to excavation-induced settlement.*

Hardy, S.J. & Al-Salka, M.A. (1995). *Composite action between steel lintels and masonry walls.*

Hendry, A. W. (1998). *Structural masonry.*

Hilsdorf, H. K. (1969). *Investigation into the failure mechanism of brick masonry loaded in axial compression.*

Hordijk, D. (1991). *Local approach to fatigue of concrete.*

Institution of Structural Engineers. (1989). *Soil-structure interaction - The real behaviour of structures.*

Little M.E.R. (1969). *Symposium on design for movement in buildings.*

Lourenco, P. B. (1996). *Computational strategies for masonry structures.*

Lourenco, P. B. (1998). *Experimental and numerical issues in the modelling of the mechanical behaviour of masonry.*

Lourenco, P. B., & Rots, J. G. (1997). *Multisurface interface model for analysis of masonry structures.*

Lourenco, P. B., Rots, J. G., & Blaauwendraad, J. (1995). *Two approaches for the analysis of masonry structures: micro and macro-modeling.*

Lourenco, Paulo B. (1994). *Analysis of Masonry Structures with interface elements.*

Lynch, G. (1994). *Brickwork History, Technology and Practice Volume 1;.*

McNary, W. S., & Abrams, D. P. (1985). *Mechanics of masonry in compression.*

Meccanica. (2017). *A 3D mesoscale damage-plasticity approach for masonry structures under cyclic loading.*

Meilak, D. (2021). Retrieved from https://www.nadurparish.com/buildings-at-nadur/kenuna-tower/

Mier, J. (1984). *Strain-softening of concrete under multiaxial loading conditions.*

Mifsud, J. (2003). *Load Paths in Masonry Construction: An emperimental investigation of hypotheses.*

Mifsud, J. (2012). *Effects of Support Movement on Local Concrete Block Construction.*

Oyguc, R., & Oyguc, E. (2017). *2011 van earthquakes: lessons from damaged masonry structures.*

Polshin D.E. & Tokar R.A. (1957). Maximum allowable non-uniform settlement of structures. *4th Int. Conf. on Soil Mech. and Found. Eng, Vol 1*, (p. 402).

Potts D.M. & Addenbrooke T. (1997). *A structure's influence on tunneling-induced ground movements.*

R.Dickinson, P. (2004). *Cracking and Building Movement.*

Resta et al. (2013). *Non-Linear Finite Element Analysis of Masonry Towers by Adopting the Damage Plasticity Constitutive Model.*

Rosenhaupt, S. (1962). *Experimental study of masonry walls on beams.*

Schembri, G. (1989). *Investigation on the Composite Action between a masonry wall and its supporting R.C. beam.*

Skempton A.W. & MacDonald D.H. (1970). Allowable settlement of buildings. *Proc. Inst. Civ. Engrs. Part III, Vol 5*, (pp. 727-768).

Smith, S. & Riddington. (1977). *The Composite behavior of elastic wall-beam systems.*

Son M. & Cording E. (2005). *Estimation of Building Damage Due to Excavation-Induced Ground Movements.*

Thorburn S. & Hutchinson J.F. (1985). *Underpinning.*

Timoshenko S. (1947). *Strength of Materials, Part 1.*

Tomazevic, M. (2009). *Shear resistance of masonry walls and eurocode 6: shear versus tensile strength of masonry.*

Vonk, R. (1992). *Softening of concrete loaded in compression.*

Zhang & Wang. (2012). *Elasticity, Damage and Plastic Analyses of Masonry.*

9. Appendix A

As already explained in Section 5.3.4.1, this Annex provides a detailed discussion of the issues encountered during the modelling process mentioned in that section.

Issue 1.0 (Beam element/Nodal support)

Initially, the beams were considered unnecessary and were therefore removed and replaced with nodal supports, as shown in Figure 9:1. This caused the wall to behave as if it were "jelly," leaning downwards under its self-weight. Additionally, the nodal supports appeared to penetrate through the wall due to the dead load. Consequently, the areas of the wall surrounding the nodal supports exhibited high concentrations of stress.

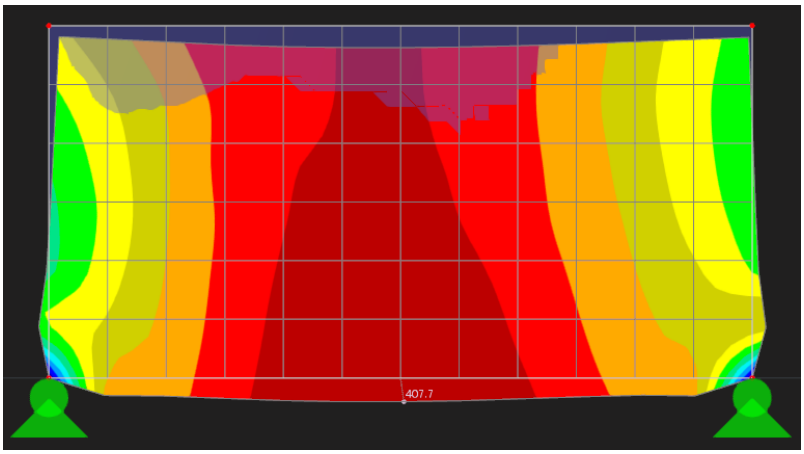

Figure 9:1 - Masonry wall supported by nodal supports at both ends

Issue 1.1 (Replacing the nodal supports by a line support)

The nodal supports were replaced with a line support, as shown in the Figure 9:2. Applying a line support with an imposed line deformation proved to be a promising solution. However, it appeared to bypass the interaction problem between the wall and the beam, and the setup tested by Mifsud J. (2012) was being modified. Furthermore, since the ultimate goal of this dissertation is to model apartment blocks, the interaction between slabs and walls would still need to be addressed. Therefore, it made sense to tackle this issue during the initial stages.

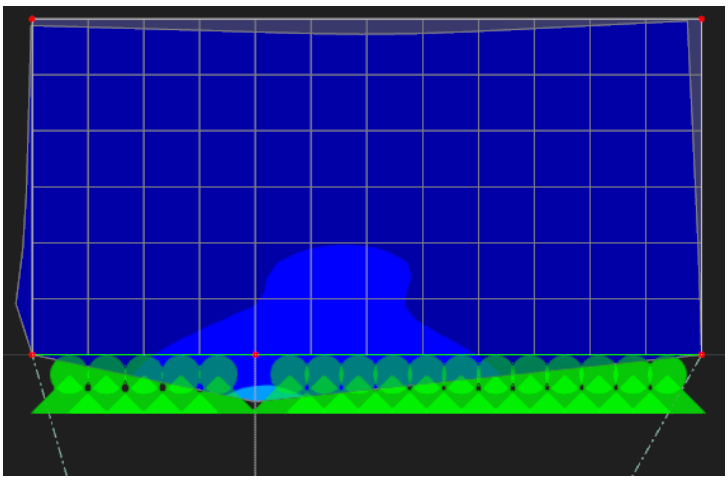

Figure 9:2 - Masonry wall supported by line supports

Issue 2 (Interaction between the beam and the wall)

The next step was to introduce a steel beam beneath the wall to provide support, preventing the "jelly-like" behaviour of the masonry wall observed in Issue 1, Figure 9:1 above.

The beam was modelled as a 3D beam element, while the wall was represented as a 2D planar surface supported by the beam. The main issue encountered was that the program treated the beam as an integral part of the masonry wall. Consequently, the bending moment and shear force diagrams exhibited by the beam indicated that it was not behaving as a simply supported beam with the imposed wall as its load, as shown in Figure 9:3 & Figure 9:4.

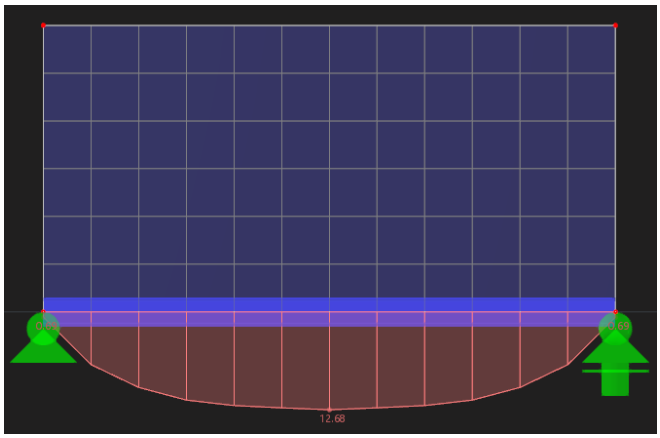

Figure 9:3 - Bending Moment Diagram of the steel beam

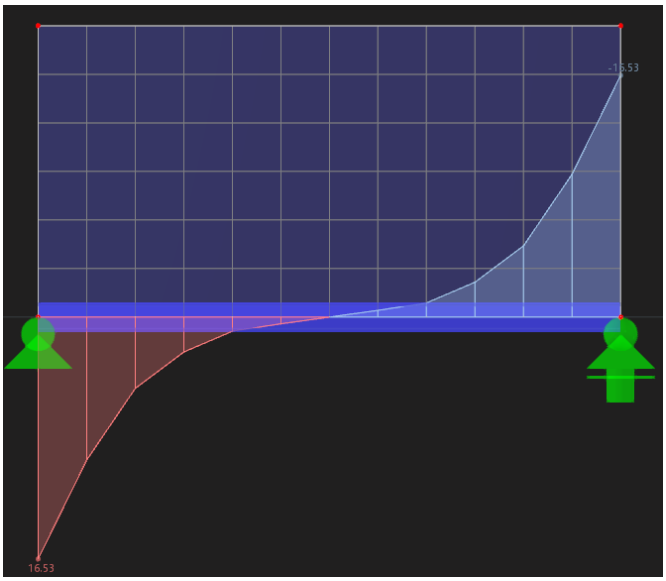

Figure 9:4 - Shear Force Diagram of the steel beam

The interaction between the beam and the wall proved to be a particularly challenging issue to resolve. Several attempts were made to address it, as outlined below:

Issue 2: Solution 1 (Tension elements)

The use of elements that do not resist tension allowed for the separation between the beam and the wall, as shown in Figure 9:5, Figure 9:6 & Figure 9:7. These elements are based on linear elastic constitutive models, where the presence of tension leads to a disconnection between the two elements. This type of solution did not work out as planned as it is evident from the bending moment

diagrams, shear force diagrams and deflection of the beams (Figure 9:5, Figure 9:6 & Figure 9:7), and also it would have been very labour-intensive if applied to the apartment blocks.

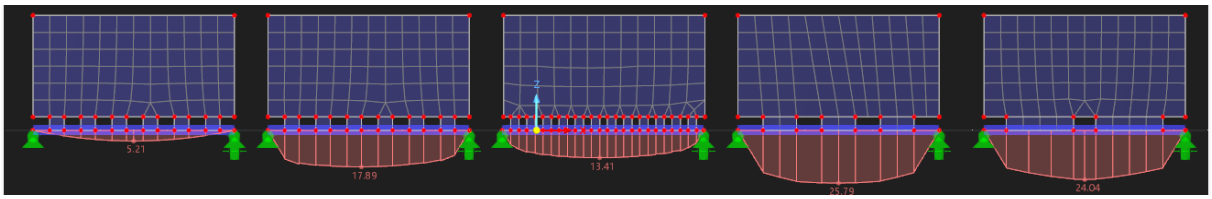

Figure 9:5 - Bending Moment Diagrams of the steel beams with no-tension elements applied at the beam-to-wall interface

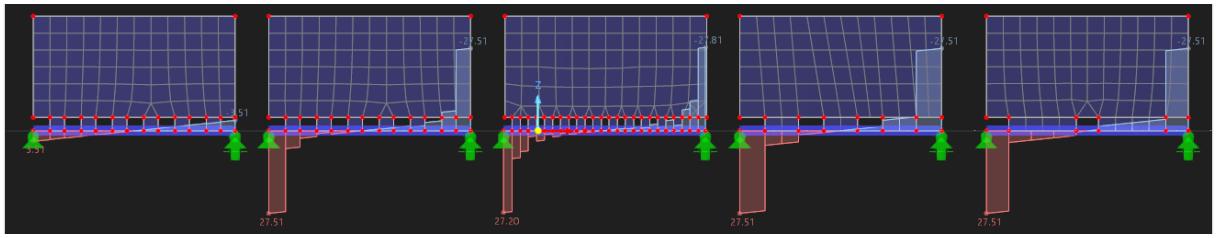

Figure 9:6 - Shear Force Diagrams of the steel beams with no-tension elements applied at the beam-to-wall interface

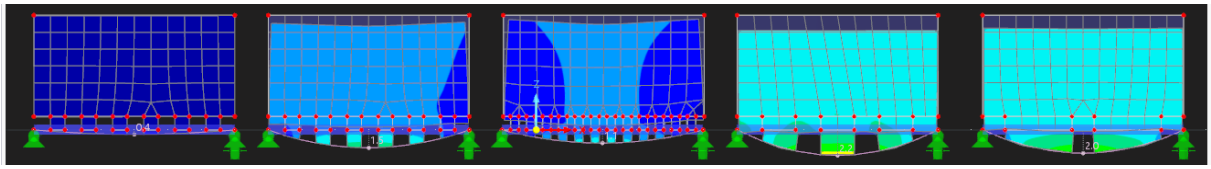

Figure 9:7 - Deflection of the steel beams with no-tension elements applied at the beam-to-wall interface

It was identified that the most effective method to separate two elements and allow for independent behaviour is the use of a line release. Initially, due to limited experience in numerical modelling, it was incorrectly assumed that a line release could only be applied between two surfaces. Consequently, the steel beam was modelled as a flat steel plate with an equivalent section modulus, enabling the application of a line release at the interface with the wall. However, implementing the line release proved challenging.

Issue 2: Solution 2.0 (Line Release) - three scenarios were considered, as follows;

1. Longitudinal and vertical release – The application of the release resulted in the wall and beam behaving independently, as shown in Figure 9:8 & Figure 9:9— to the extent that the beam exhibited bending while the wall translated downward out of plane. Furthermore, the beam's deflection appeared unaffected by the loading effect of the wall.

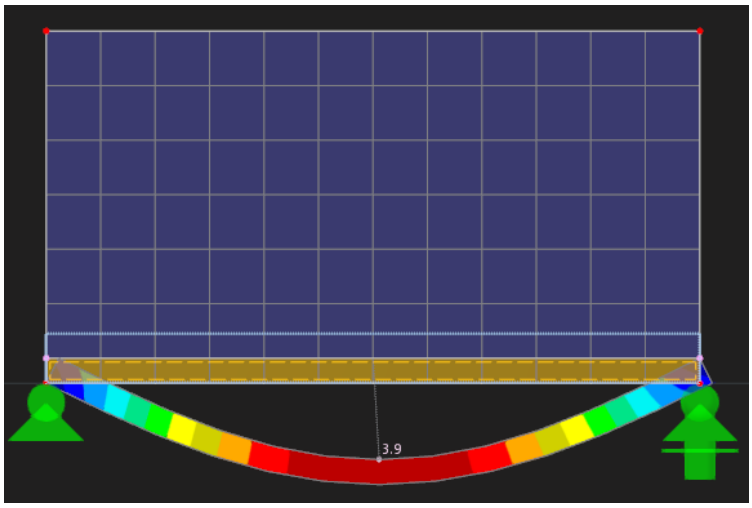

Figure 9:8 - Deflection of the steel plate

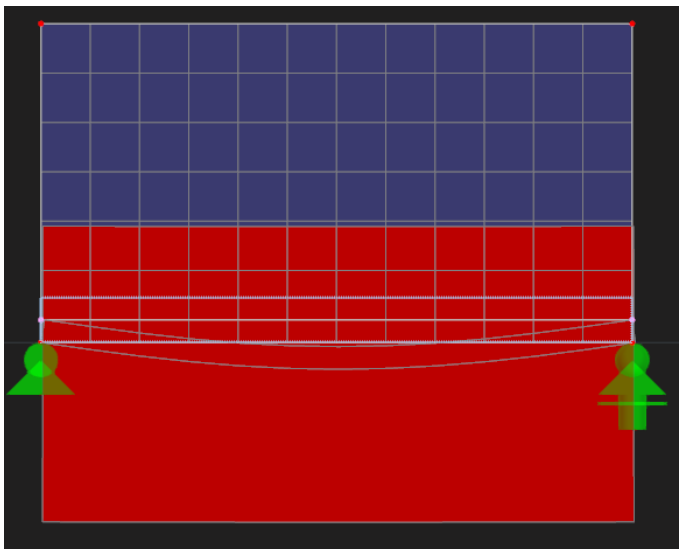

Figure 9:9 - Abnormal vertical translation of the masonry wall

2. Vertical release only – When applying this release, the wall and the beam behaved independently, exhibiting similar behaviour to the previous scenario, as shown in Figure 9:10 & Figure 9:11.

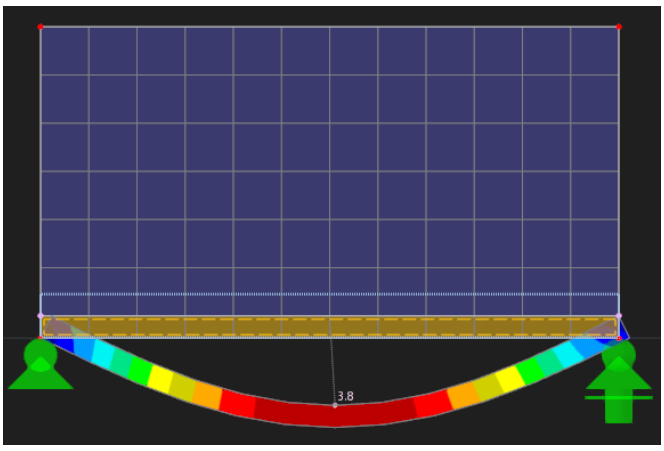

Figure 9:10 - Deflection of the steel plate

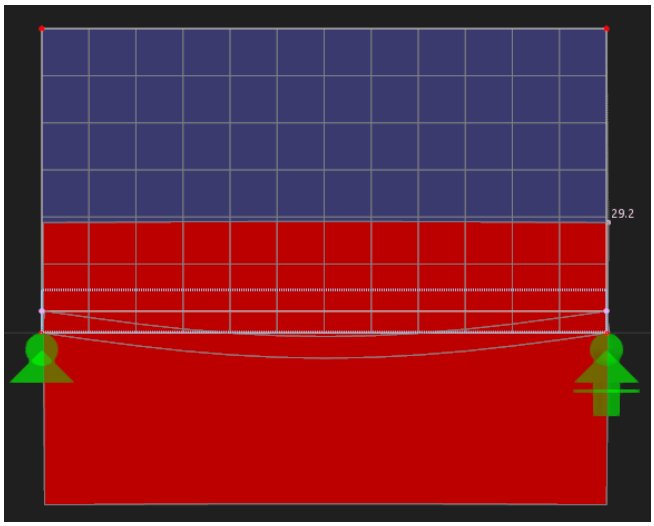

Figure 9:11 - Abnormal vertical translation of the masonry wall

3. Longitudinal release only – The application of this release produced different results, with the wall behaving more realistically, as shown in Figure 9:12. The wall was stable on its own, without the need for supports. Additionally, the wall experienced bending, with the bottom edges displacing outwards and the upper edges displacing inwards.

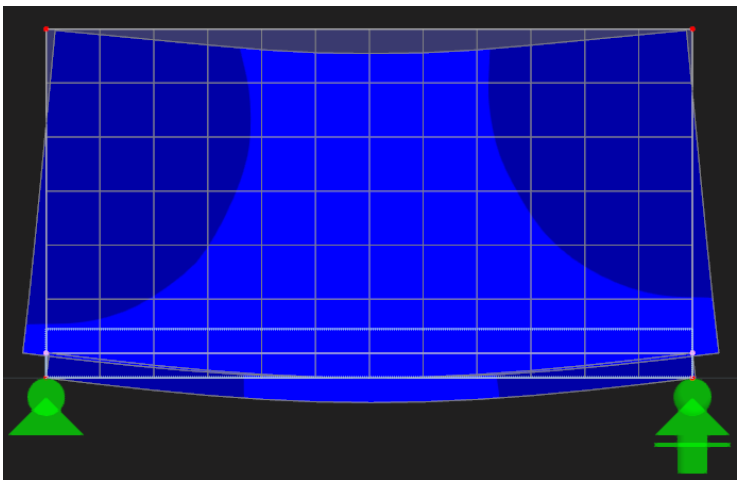

Figure 9:12 - Deflection of both the beam and the wall

The most reliable result was obtained when only the longitudinal release was applied, as shown in the Figure 9:12. This outcome is reasonable, as in reality there is longitudinal friction between the steel beam and the wall.

However, despite the longitudinal release closely resembling real-world behaviour, the results still showed the wall deforming in an unexpected manner. Specifically, the wall is intended to bend inward at the top and outward at the bottom, but not to such an exaggerated extent. Therefore, another attempt was made by modifying the line release to restrict the outward displacement of the wall's bottom edges, as described below:

Another variation of the line release was to partially apply the release between the wall and the beam. Since the bottom edges of the wall appeared to be moving outwards beyond the support, the proposed solution involved applying a partial release. Specifically, small portions of the wall (0.2m from each end) were left unreleased, while the middle part of the wall (5.6m) was released. However, this

approach resulted in the wall deforming at the released sections, while remaining fixed to the beam at the unreleased sections, where the beam and the wall behaved as a single element. As a result, the final deformation resembled that of a "jelly" more than the realistic behaviour of a masonry wall, as shown in Figure 9:13.

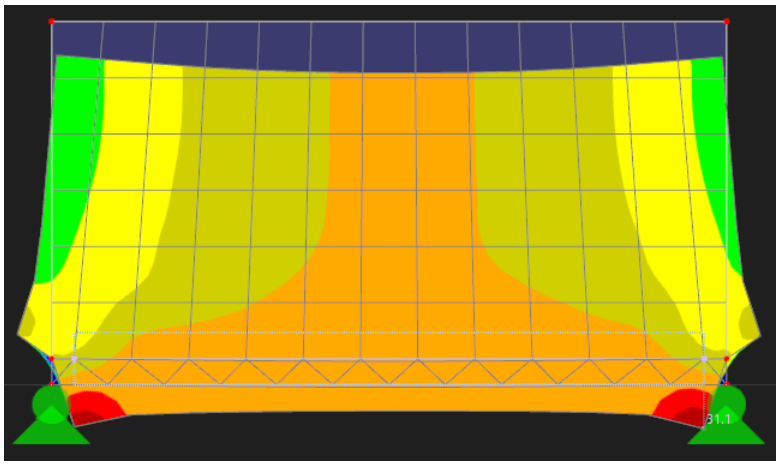

Figure 9:13 - Applying a partial line release at the beam-to-wall interface

The results obtained from this model also appeared unrealistic, as the wall exhibited strange and unexpected behaviour. As shown in Figure 9:13, the wall deflects in the released regions while remaining fixed to the beam in the unreleased areas, resulting in an inconsistent and unrealistic response. In comparison, the results shown in Figure 9:12—where only the longitudinal release was applied—appear more reasonable.

After extensive analysis, it was noted that the deformation results in Figure 9:12 were slightly exaggerated due to the deformation scale being set greater than 1, which visually amplified the displacements. Nevertheless, the application of a longitudinal release remains the most reliable and accurate approach so far.

With increased familiarity in using the line release tool, it became evident that the initial assumption—that a line release only functions when applied between two surfaces—was incorrect. In fact, the release also works effectively when applied between a beam element and a wall. Moreover, the line release feature allows for the adjustment of the spring constant coefficient and the use of non-linear criteria to more accurately simulate frictional interaction between the two elements.

<u>Issue 2: Solution 2.1 (Line Release + Varying the spring constant)</u>

Additionally, RFEM 6 allows the user to assign a spring constant coefficient to the selected type of release. This spring coefficient mimics the interaction between the wall and the beam, acting as an elastic hinge between them. It was observed that the value of the spring coefficient did not significantly affect the interaction between the wall and the beam, as shown in Figure 9:14, Figure 9:15 & Figure 9:16. However, when comparing the bending moment, shear force diagrams, and deflection obtained from the model with the results from hand calculations, the results were close when the spring coefficient was very small, such as 0.001kN/m^2.

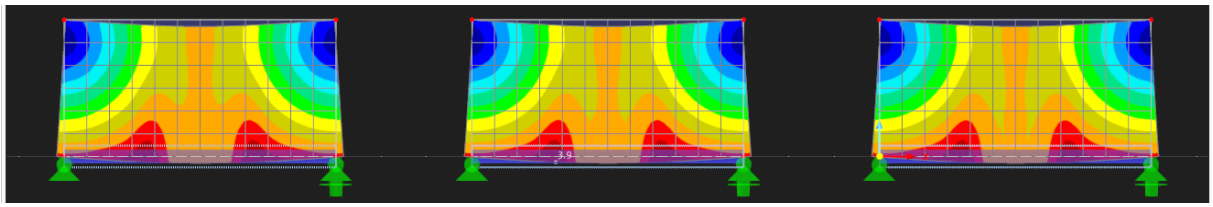

Figure 9:14 - Deformations of the masonry wall under varying spring coefficients

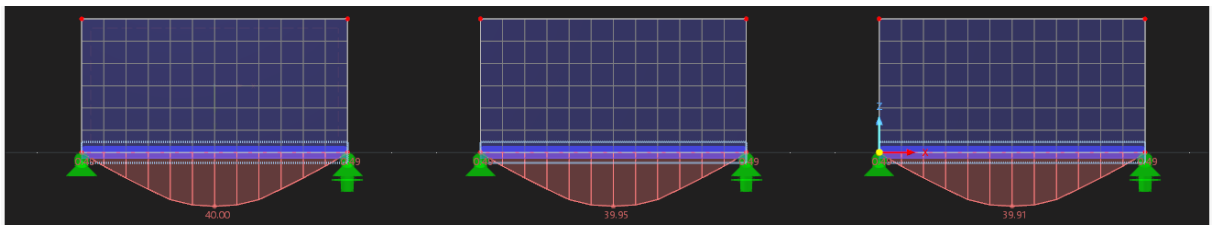

Figure 9:15 - Bending Moment Diagram of the steel beams under varying spring coefficients

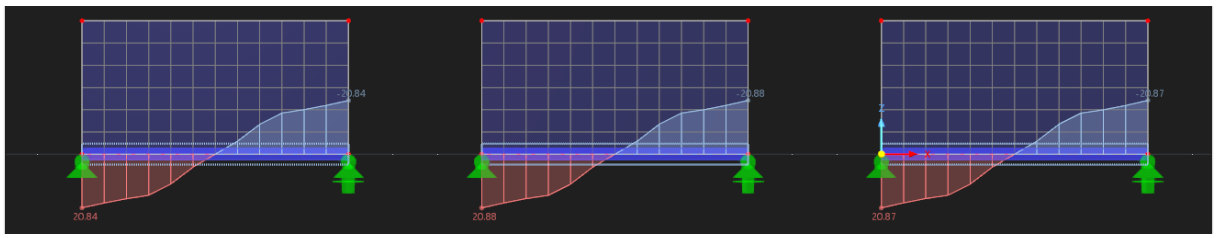

Figure 9:16 - Shear Force Diagram under varying spring coefficients

Issue 2: Solution 2.2 (Line Release + Non-linear criterias)

The factor contributing to the independent behaviour between the two elements is the interaction between the steel beam and the masonry wall. This interaction is primarily governed by the frictional coefficients of both the steel and the masonry wall. Controlling this frictional interaction using the longitudinal release is challenging, as it lacks accuracy.

RFEM 6 also offers the option to apply nonlinearities to the line release, allowing for better control over the release and potentially leading to more realistic results. One of the most relevant nonlinearities for this dissertation is the friction nonlinearity.

This nonlinearity allows for control over the friction between the wall and the beam. The user can specify the plane in which friction is present and adjust the value of the friction coefficient. Various friction nonlinearities were tested to examine their effect on the longitudinal translation release. The results are as follows:

1. Non-linearity criteria – Friction Vz, Friction VyVz, and Friction Vy+Vz exhibited similar behaviour, characterized by the wall experiencing deformations due to bending in the simply supported beam, as shown in Figure 9:17. The bending moment, shear force diagrams, and beam deflection were also very similar across these criteria.

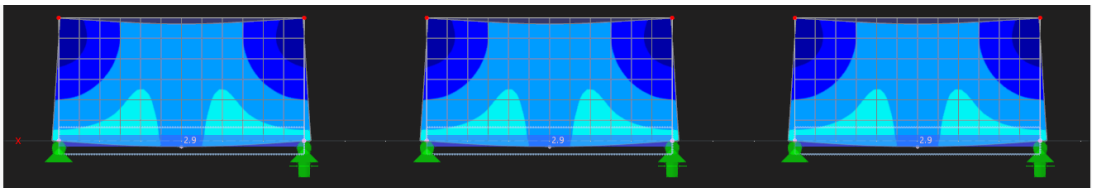

Figure 9:17 - Deformations of the masonry wall under Friction Vz, Friction VyVz, and Friction Vy+Vz

2. Non-linearity criteria – Friction Vy exhibited different behaviour, with the wall moving laterally out of the plane of the beam, as shown in Figure 9:18. However, the bending moment, shear force diagrams, and beam deflection were very similar to the results obtained from the other frictional nonlinearities.

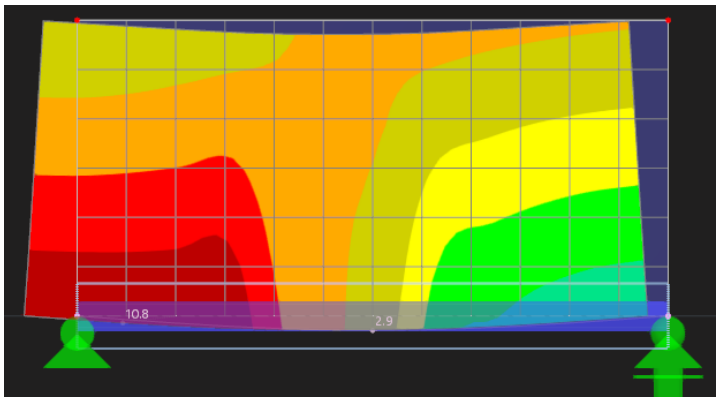

Figure 9:18 - Deformations of the masonry wall under Friction Vy

3. Other non-linear criteria were also tested, such as the "Fixed if positive" condition. However, when this criterion was applied, the beam and the wall began to behave independently, leading to numerical instability in the solution. To address this issue, supports were added at the upper edges of the wall to stabilize the model. However, the application of this non-linear criteria resulted in the wall and beam behaving independently, as shown in Figure 9:19— to the extent that the beam exhibited bending while the wall translated downward out of plane

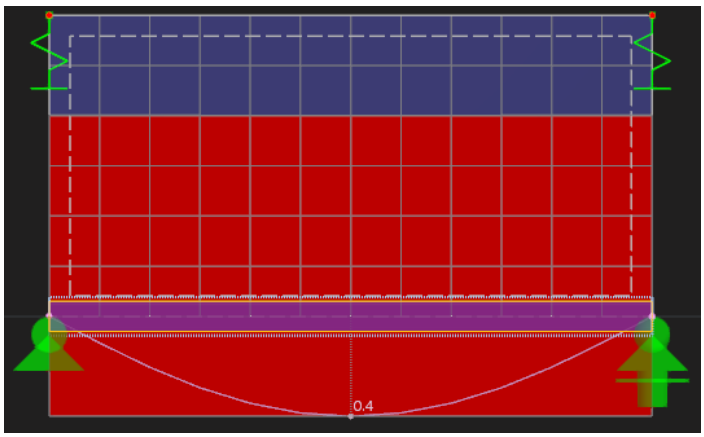

Figure 9:19 - Deformations of the masonry wall under Fixed if positive

L-Università ta' Malta

CALCULATION SHEET

Dissertation - Appendix B

Subject: Beam subjected to its own self-weight

Made by: Stewart Aquilina **Date:** 25/6/2025

Unless stated otherwise, all references are to EN 1993-1-1:2005

Data related to the Beam :	HEB 300	
Yield Strength (f_y) =	355	N/mm^2
Area of Section (A) =	149	cm^2
Second moment of area (I_{yy})=	25170	cm^4
Height (h) =	300	mm
Breadth (b) =	300	mm
Web Thickness (t_w)=	11	mm
Flange Thickness (t_f)=	19	mm
Root fillet radius (r) =	27	mm
Plastic Section Modulus ($W_{pl,y}$) =	1870	cm^3
Weight of beam (G) =	117	kg/m
Span of beam =	6	m

Loads:

Self-weight of beam (unfactored) =	1.17	kN/m

Bending capacity of beam cross-section:

For a simply-supported beam:

$M_{Ed} = WL^2/8$

$M_{Ed} = 5.27$ kNm

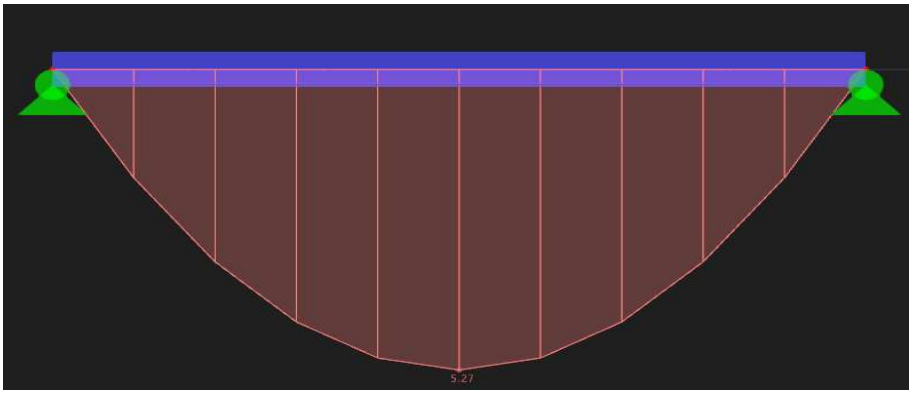

Shear capacity of beam cross-section:

For a simply-supported beam:

V_{Ed} =	WL/2	
V_{Ed} =	3.51	kN

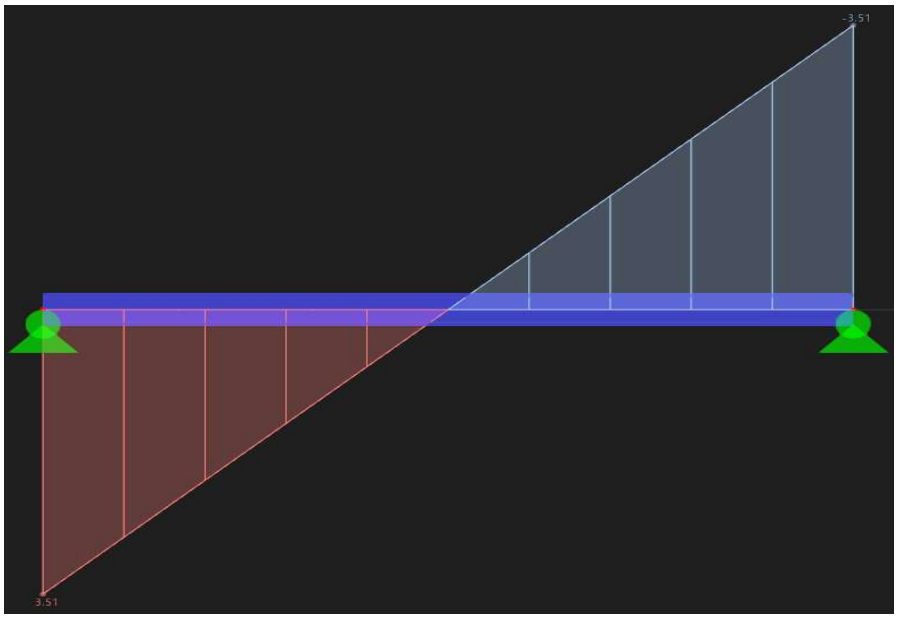

Vertical deflection of beam at mid-span:

$$\delta_{max} = \frac{5wL^4}{384EI}$$

w =	1.17	kN/m
L =	6000	mm
E =	210000	N/mm^2

δ_{max} =	0.37	mm

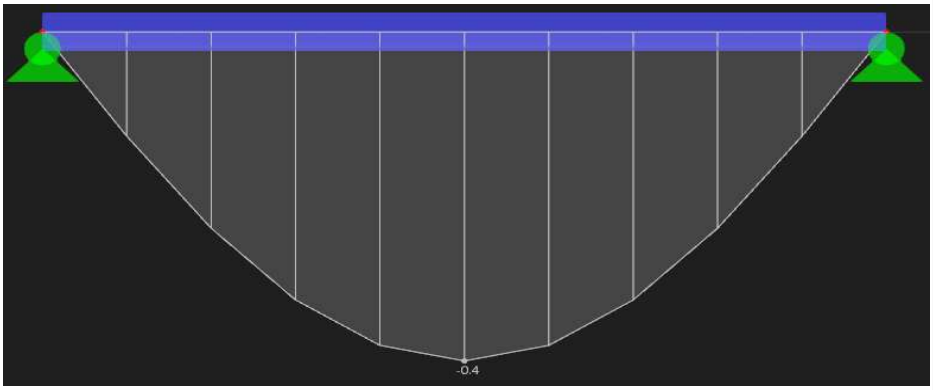

L-Università ta' Malta

CALCULATION SHEET

Dissertation - Appendix B

Subject: Beam subjected to self-weight and imposed loads

Made by: Stewart Aquilina | **Date:** 25/6/2025

Unless stated otherwise, all references are to EN 1993-1-1:2005

Data related to the Beam :	HEB 300	
Yield Strength (f_y) =	355	N/mm^2
Area of Section (A) =	149	cm^2
Second moment of area (I_{yy})=	25170	cm^4
Height (h) =	300	mm
Breadth (b) =	300	mm
Web Thickness (t_w)=	11	mm
Flange Thickness (t_f)=	19	mm
Root fillet radius (r) =	27	mm
Plastic Section Modulus ($W_{pl,y}$) =	1870	cm^3
Weight of beam (G) =	117	kg/m
Span of beam =	6	m
Loads:		
Imposed Load =	10	kN/m
Self-weight of beam =	1.17	kN/m
Total Unfactored Load =	11.17	kN/m

Bending capacity of beam cross-section:

For a simply-supported beam:

M_{Ed} = $WL^2/8$

M_{Ed} = 50.27 kNm

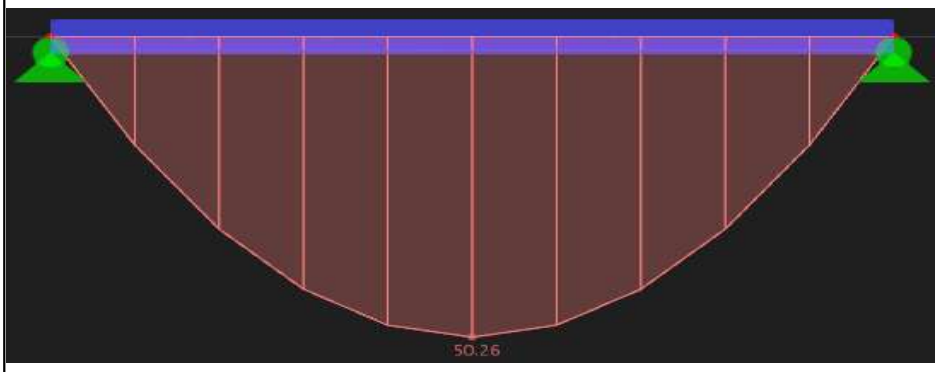

Shear capacity of beam cross-section:

For a simply-supported Beam:

V_{Ed} =	WL/2	
V_{Ed} =	33.51	kN

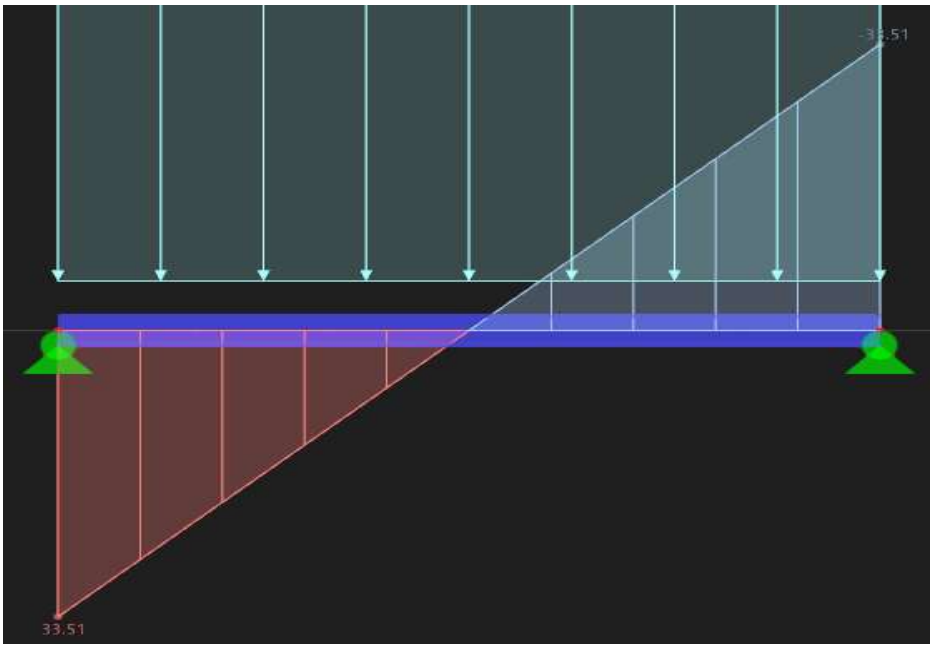

Vertical deflection of beam at mid-span:

$$\delta_{max} = \frac{5wL^4}{384EI}$$

w =	11.17	kN/m
L =	6000	mm
E =	210000	N/mm^2

δ_{max} =	3.57	mm

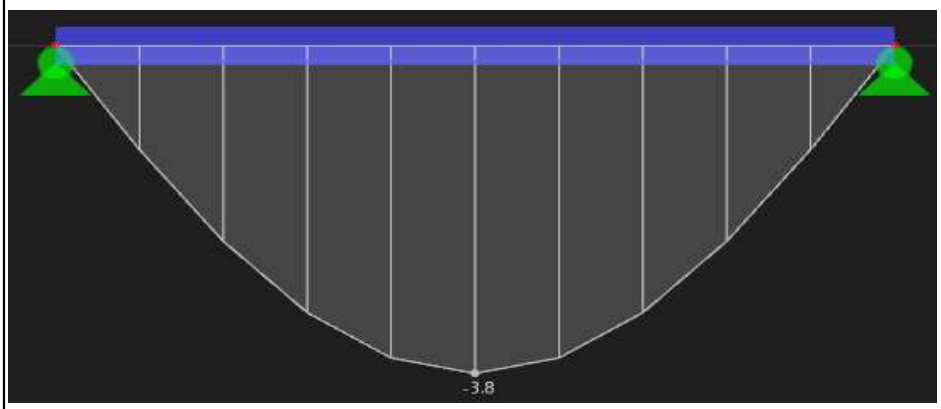

L-Università ta' Malta	Dissertation - Appendix B		
	Subject: Beam subjected to self-weight and masonry wall loads		
CALCULATION SHEET	**Made by:** Stewart Aquilina	**Date:**	25/6/2025

Unless stated otherwise, all references are to EN 1993-1-1:2005

This hand calculation determines the beam's bending moment, shear forces, and deflections under load while verifying its capacity for each. Additionally, it is crucial to assess the beam's capacity under the masonry wall load to ensure that any deformations or strains in the wall are not caused by excessive beam deflection, as this would undermine the purpose of the exercise.

Data related to the Beam :	HEB 300	
Yield Strength (f_y) =	355	N/mm^2
Area of Section (A) =	149	cm^2
Second moment of area (I_{yy})=	25170	cm^4
Height (h) =	300	mm
Breadth (b) =	300	mm
Web Thickness (t_w)=	11	mm
Flange Thickness (t_f)=	19	mm
Root fillet radius (r) =	27	mm
Plastic Section Modulus ($W_{pl,y}$) =	1870	cm^3
Weight of beam (G) =	117	kg/m
Span of beam =	6	m

Data related to the wall

Density of wall =	1212	kg/m^3	(From RFEM 6)
Thickness of wall =	0.22	m	
Height of wall =	3	m	
Length of wall =	6	m	

Loads:

Self-weight of wall =	7.9992	kN/m
Self-weight of beam =	1.17	kN/m
Total Unfactored Load =	9.1692	kN/m

	Section Classification:	
CL 5.5 *Table 5.2*	For the internal compression part: $c = h - 2(t_f) - 2(r)$ $c =$ 208 $c/t_w =$ 18.91 ≤ 72ε where 72ε = 58.32 $(c/t_w) / 72\varepsilon =$ 0.32423 <1 Hence, web is **class 1.**	∴ OK
CL 5.5 *Table 5.2*	For the outstand flange: $c = (b - 2(r) - t_w)/2$ $c =$ 117.5 $c/t_f =$ 6.18 ≤ 9ε where 9ε = 7.29 $(c/t_f) / 9\varepsilon =$ 0.848314 <1 Hence, flange is **class 1.**	
	Therefore, overall section is **class 1.**	
	Bending capacity of beam cross-section:	
	For a simply-supported beam: $M_{Ed} =$ $WL^2/8$ $M_{Ed} =$ 41.26 kNm	(Bending Moments as demonstrated by the model in Section 6.2)
CL 6.2.5	$M_{c,Rd} = M_{pl,Rd} = \frac{W_{pl} f_y}{\gamma_{M0}}$ for class 1 or 2 cross sections $M_{pl,Rd} = M_{c,Rd} =$ 663.85 kNm	
CL 6.2.5	$\frac{M_{Ed}}{M_{c,Rd}} \le 1{,}0$ $M_{Ed}/M_{c,Rd} =$ 0.06 ≤ 1	∴ OK
	Therefore, the bending resistance of the section is adequate.	

Shear capacity of beam cross-section:

For a simply-supported beam:

V_{Ed} = WL/2

V_{Ed} = 27.51 kN

(Shear Forces as demonstrated by the model in Section 6.2)

To find $V_{pl,Rd}$

CL 6.2.6

$$A - 2bt_f + (t_w + 2r)\,t_f$$

A_v = 4735 mm^2

CL 6.2.6

$$V_{pl,Rd} = \frac{A_v\left(f_y/\sqrt{3}\right)}{\gamma_{M0}}$$

$V_{pl,Rd}$ = 970.48 kN

CL 6.2.6

$$\frac{V_{Ed}}{V_{c,Rd}} \le 1{,}0$$

$V_{Ed}/V_{c,Rd}$ = 0.03 ≤ 1

∴ OK

Therefore, the shear resistance of the section is adequate.

Shear buckling of beam cross-section:

CL 6.2.6

$$\frac{h_w}{t_w} > 72\frac{\varepsilon}{\eta}$$

h_w = 262 mm

ε = 0.92

η = 1.2

h_w/t_w = 23.82

$72\varepsilon/\eta$ = 55.2

$(h_w/t_w) / (72\varepsilon/\eta)$ = 0.431489 <1

h_w/t_w is not greather than $72\varepsilon/\eta$ and therefore, shear buckling check need not be considered.

∴ OK

CL 6.2.10

Bending and shear interaction:

(2) Provided that the design value of the shear force V_{Ed} does not exceed 50% of the design plastic shear resistance $V_{pl,Rd}$ no reduction of the resistances defined for bending and axial force in 6.2.9 need be made, except where shear buckling reduces the section resistance, see EN 1993-1-5.

V_{Ed} =	27.51	kN
$V_{pl,Rd}/2$ =	485.24	kN

$V_{Ed} / (V_{pl,Rd}/2)$ =	0.06	<1

∴ OK

V_{Ed} is not greather than $V_{pl,Rd}/2$ and therefore, the bending and shear interaction need not be considered.

Vertical deflection of beam at mid-span:

$$\delta_{max} = \frac{5wL^4}{384EI}$$

w =	9.1692	kN/m
L =	6000	mm
E =	210000	N/mm^2

δ_{max} =	2.93	mm
Δ_{limit} =	16.67	mm

(Deflection as demonstrated by the model in Section 6.2)

$\delta_{max} / \Delta_{limit}$ =	0.17564	<1

∴ OK

Therefore, the vertical deflection of the section at mid-span is satisfactory.

Annex C

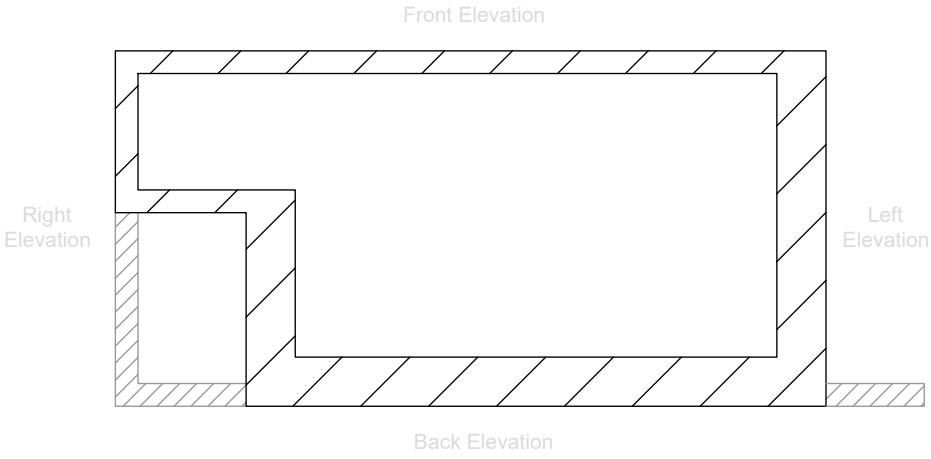

Plan

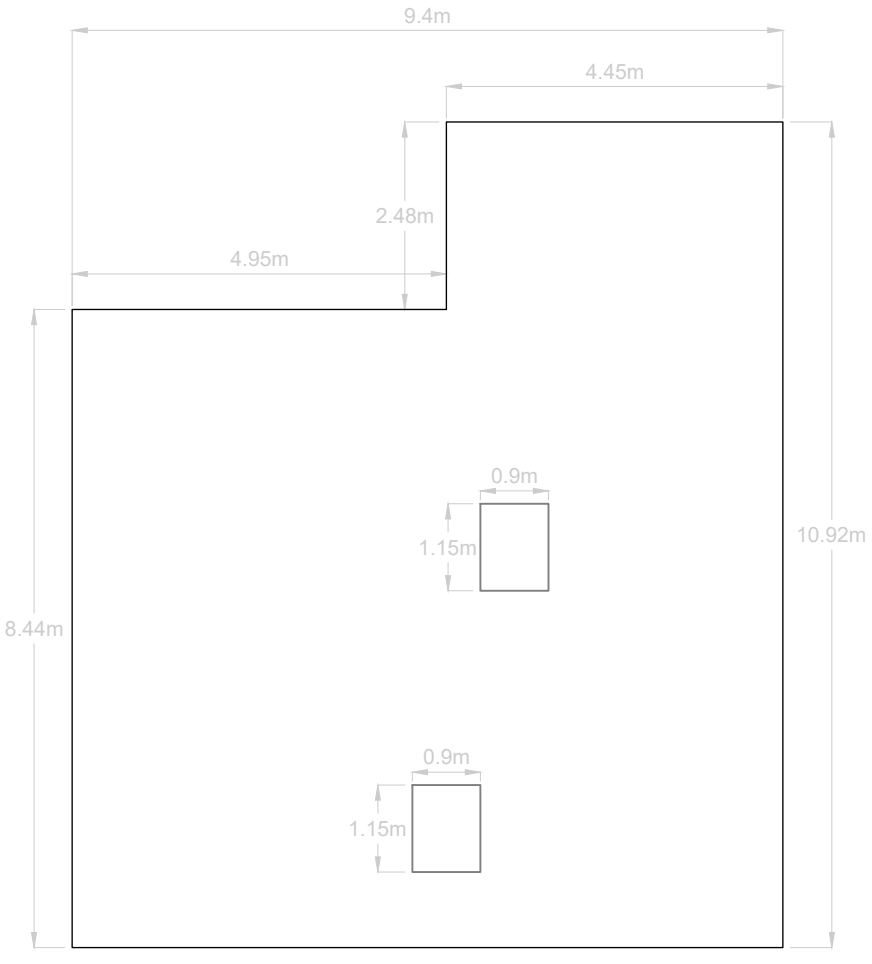

Front Elevation

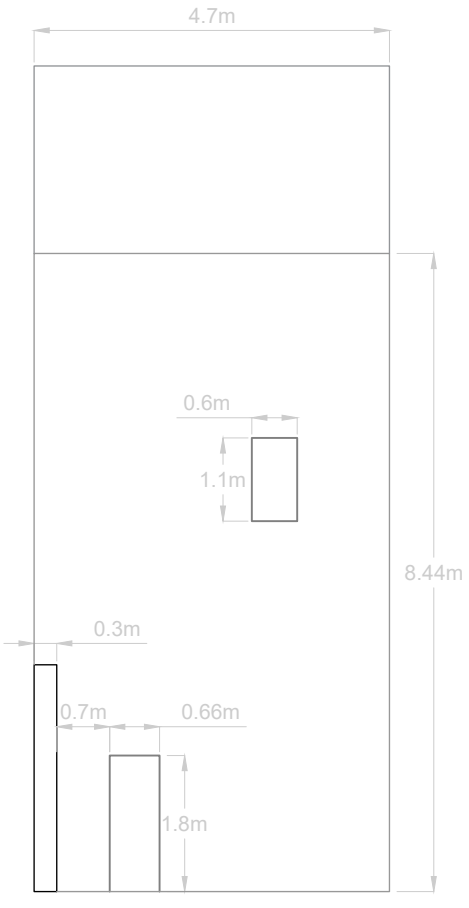

Left Elevation

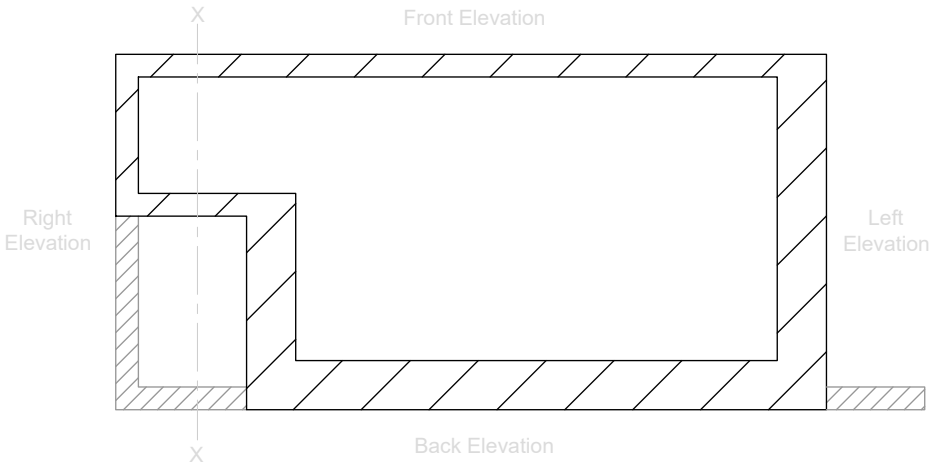

Plan

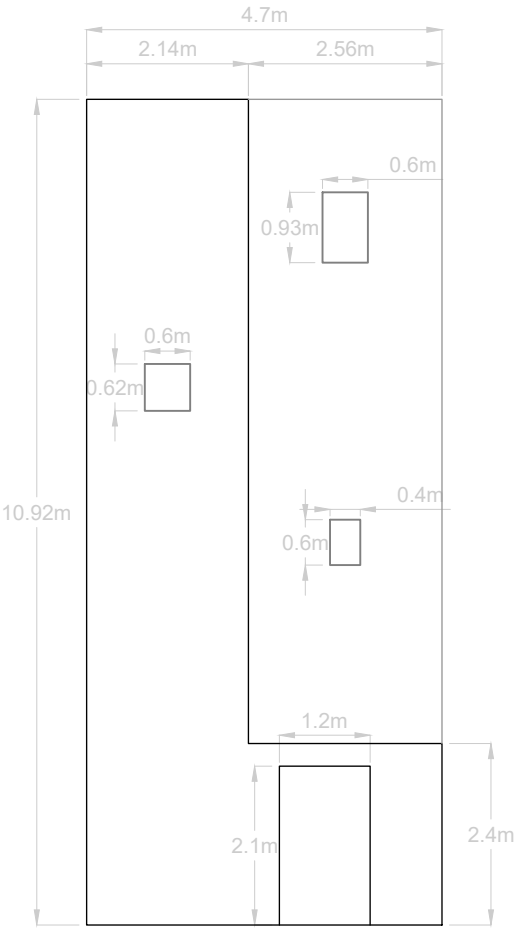

Right Elevation

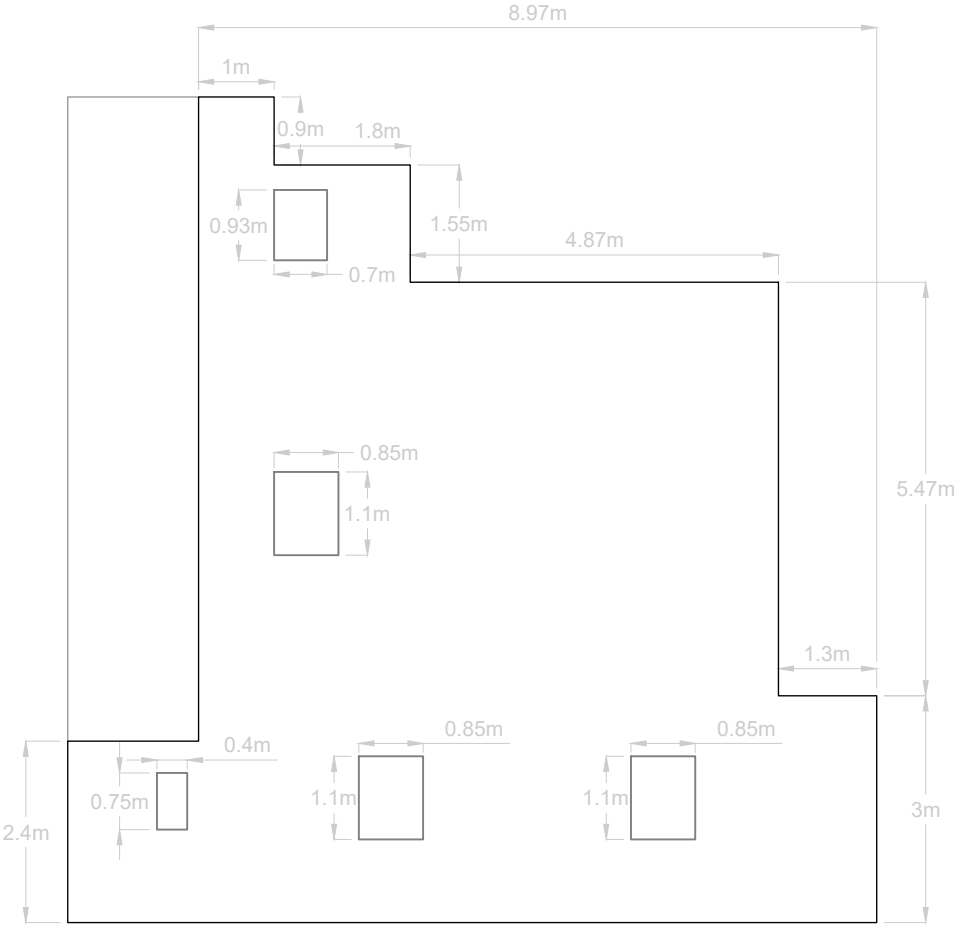

Back Elevation

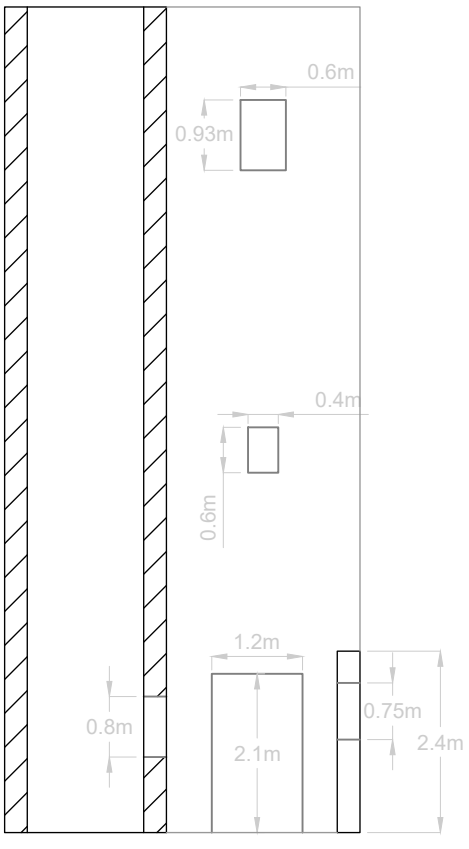

Section XX

Annex D

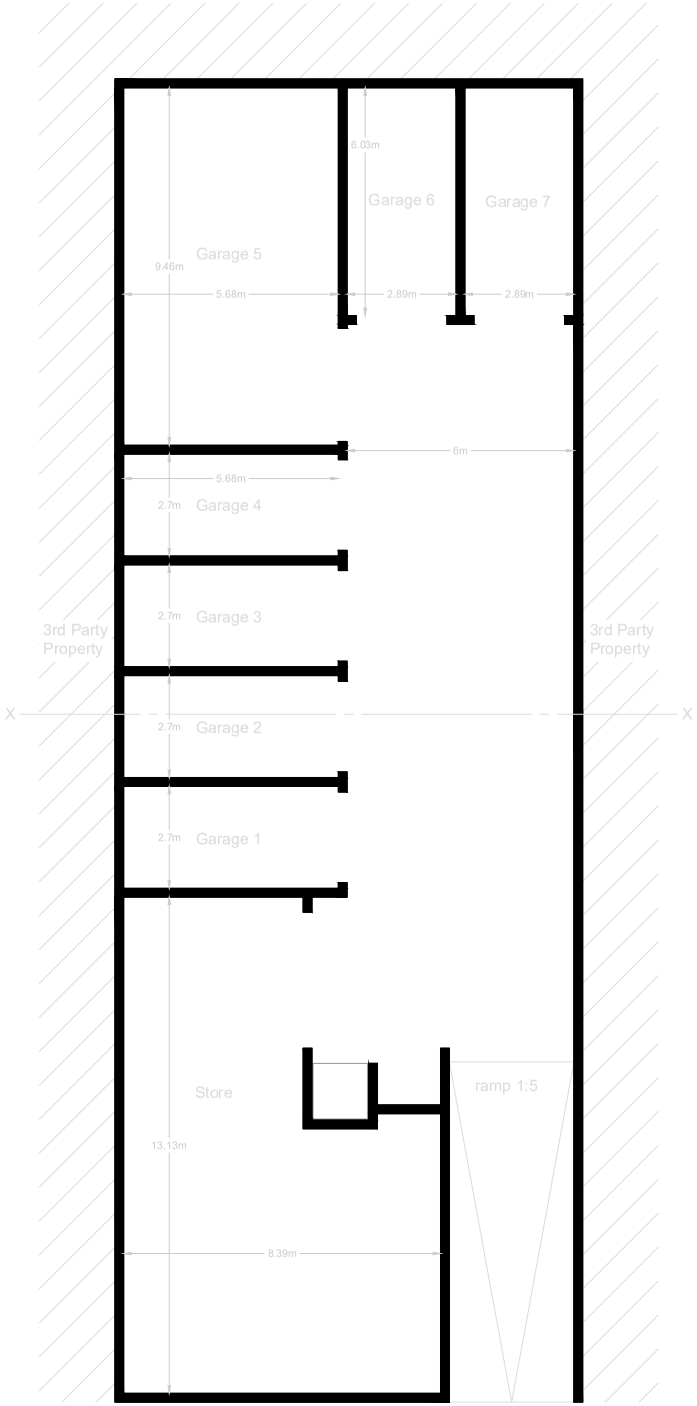

Semi-Basement

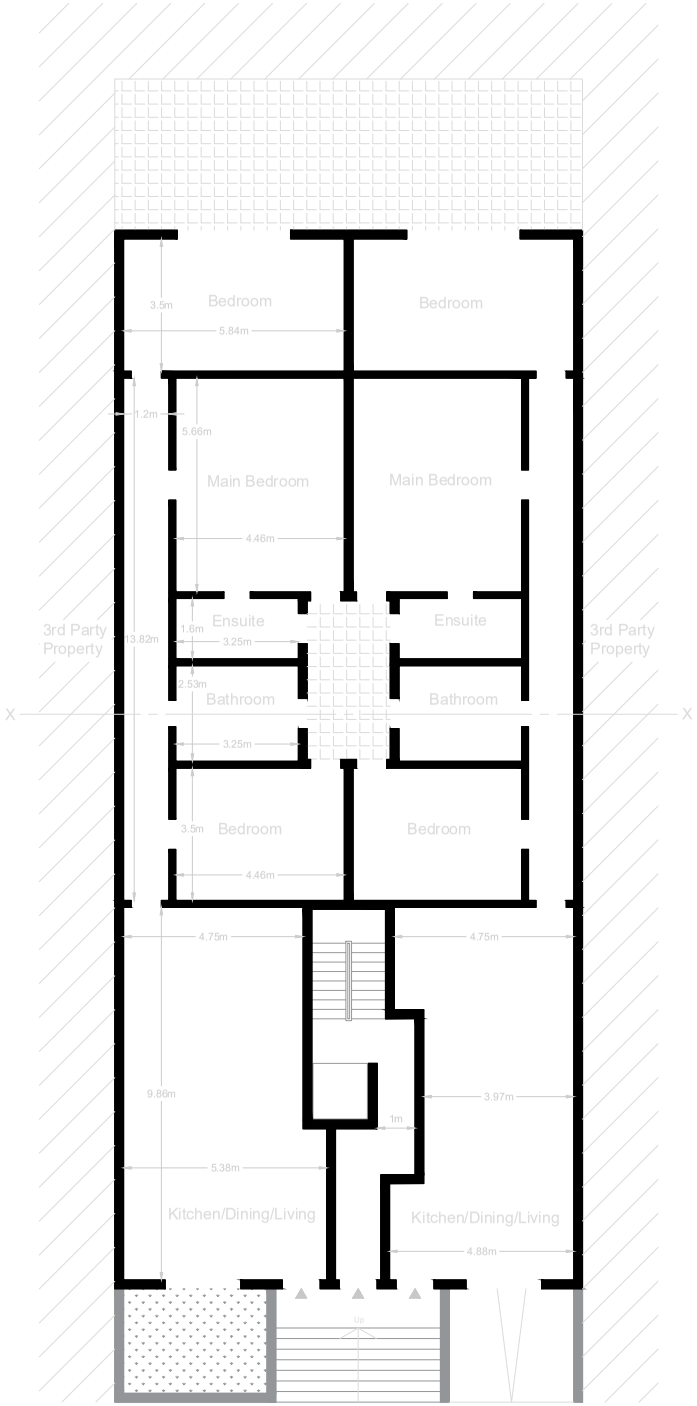

Ground floor - Maisonettes

0m 1m 5m 10m

Scale 1:200

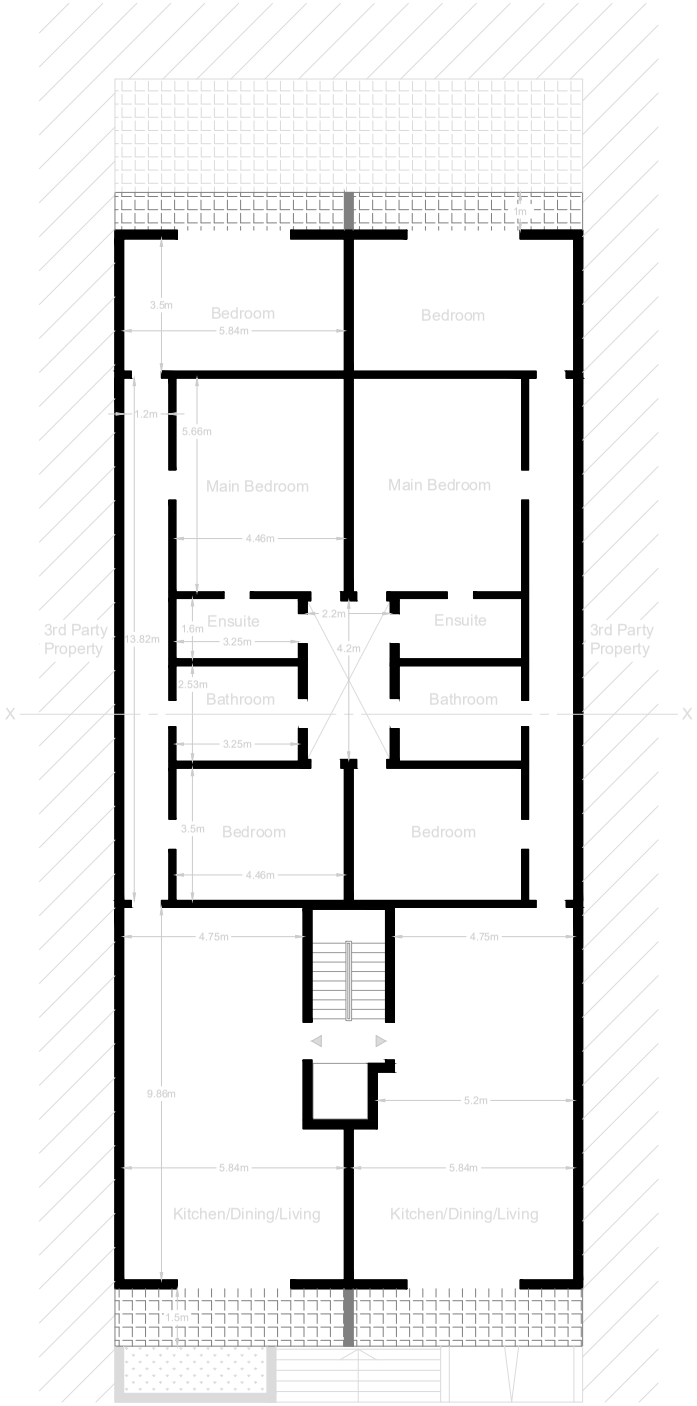

Typical Apartment floor

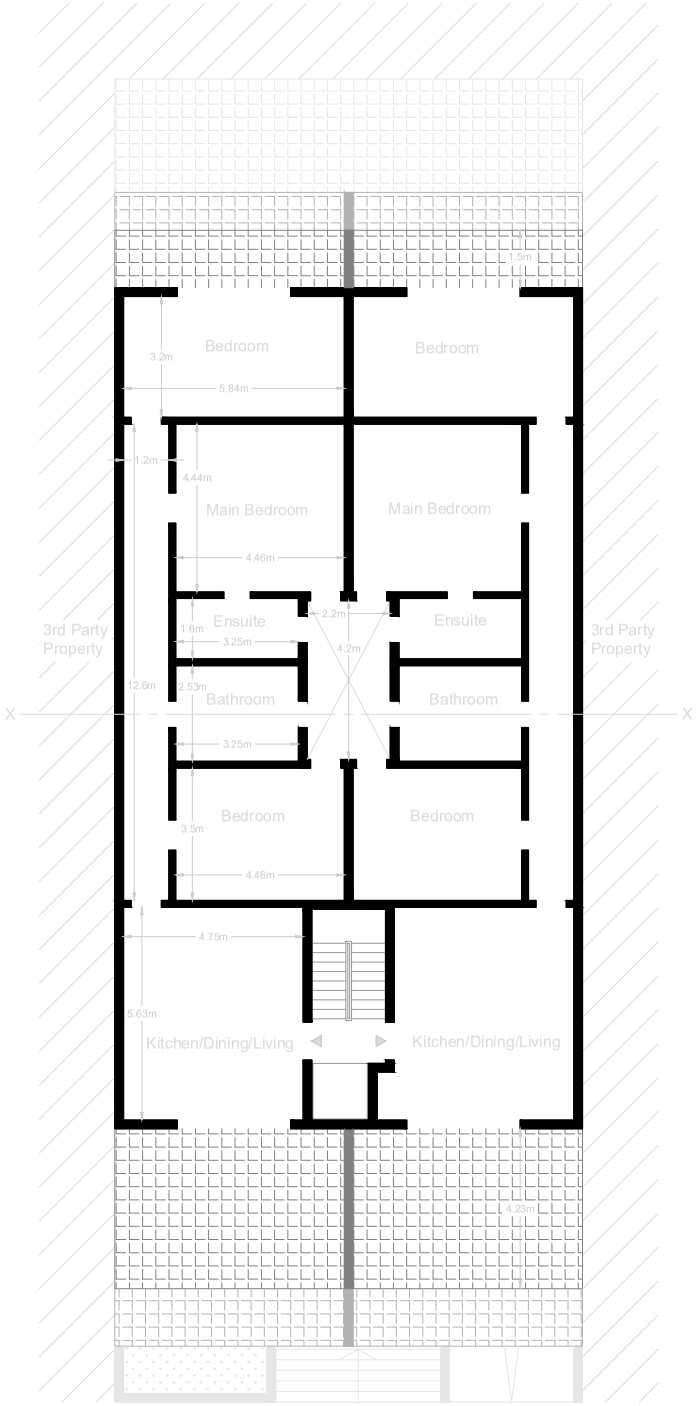

Penthouse Floor

0m 1m 5m 10m

Scale 1:200

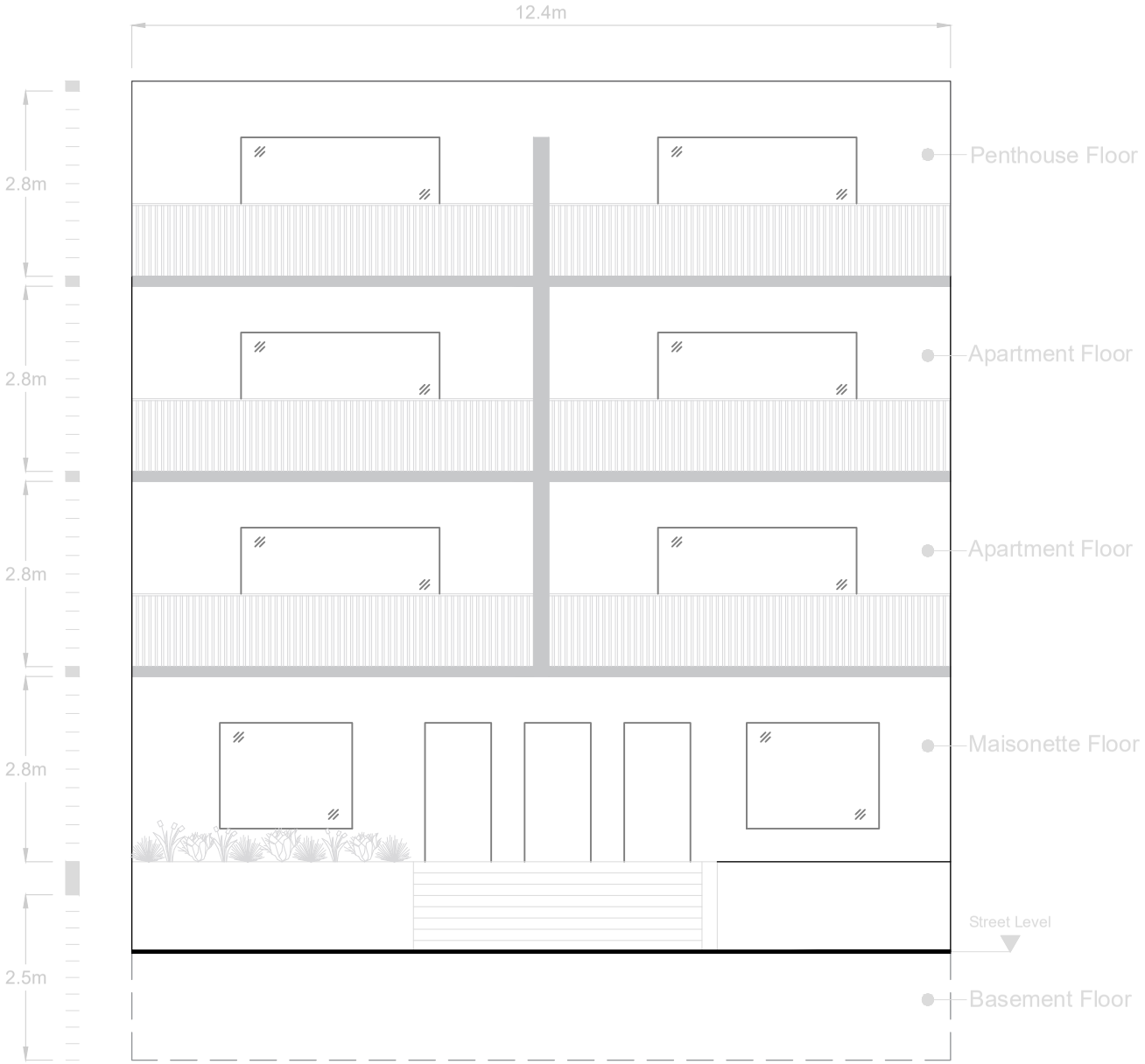

Typical Elevation

0m 1m 5m 10m

Scale 1:100

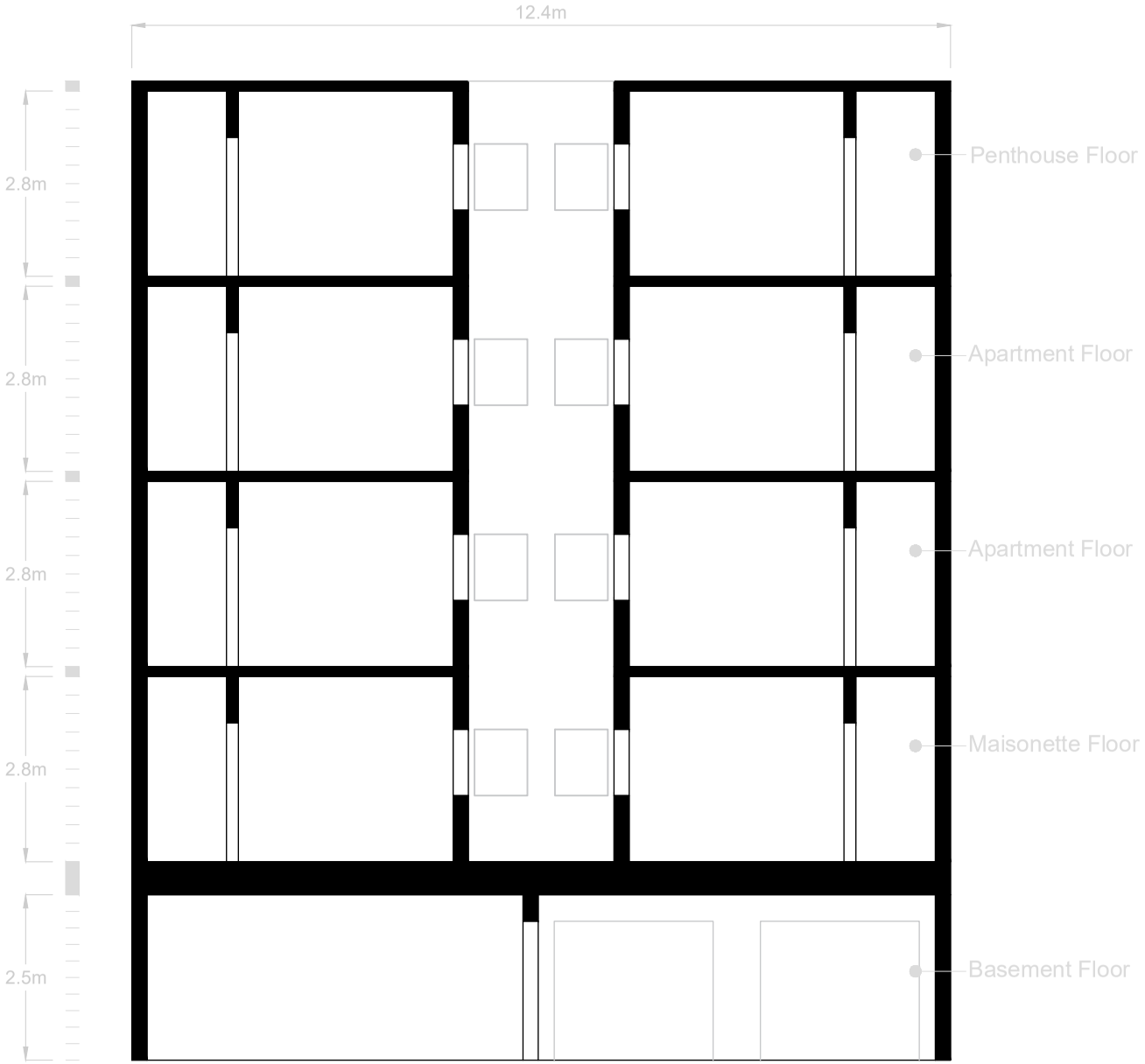

Typical Section XX

0m 1m 5m 10m

Scale 1:100

ATTARD BROS
CONSTRUCTION MATERIALS

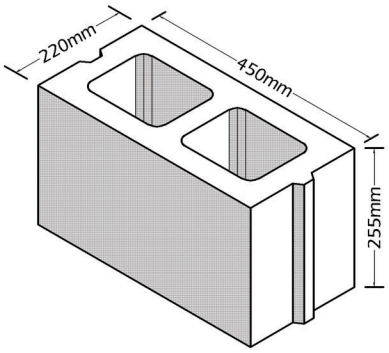

PRODUCT DATASHEET

9" Hollow Concrete Block

Single Density

Top quality product conforming to EN 771-3:2003. This block was designed to bear heavy loads. The 9" single density block is typically used for foundations, external walls, retaining walls and in other high load bearing situations.

FM 35227

PRODUCT SPECIFIATIONS

AVAILABLE SIZES (mm)

Length	Height	Width
450	255	220

PRODUCED FOLLOWING EN 771-3:2003

BENEFITS

- Top quality product conforming to EN 771-3:2003
- Designed to bear heavy loads
- Typically used for foundations, external walls, retaining walls and in other high load bearing situations when infilled with concrete and reinforced.
- Adopts a tongue and groove system for improved bond strength

METHOD OF BEDDING

- Hollow Blocks should be laid on a shell bed of mortar.
- Any excess mortar should be removed immediately and reused.
- It is common practice to displace blocks by ½ a block length alternat ing between one course and another to improve bond.

DELIVERY AND STORAGE

- After unloading, units should be stacked neatly and carefully on a stable, clean and level ground to reduce chipping, breakages and other damages.
- Blocks can be delivered to any location in Malta

SPECIFICATIONS

Compressive Strength:	6N/mm^2

Dimensions (mm):	450	220	255
Approx. Core Dimensions (mm):	158	158	255
Dimensional Tolerances:	+3,-5	+3,-5	+3,-5

Approx. Gross Density:	1212kg/m^3
Approx . Net Density of Concrete:	2072kg/m^3
Percentage of holes:	~41.5%
Approx. Dry Weight:	30.6kg
Shear Bond Strength:	0.15N/mm^2

Reaction to Fire:	Euroclass A1

Attard Bros Group
Mikesand, Industrial Zone,
Ta' Qali - ATD 4000

www.attardbros.com

More Information
+356 21 415 332
sales@attardbros.com

ATTARD BROS
CONSTRUCTION MATERIALS

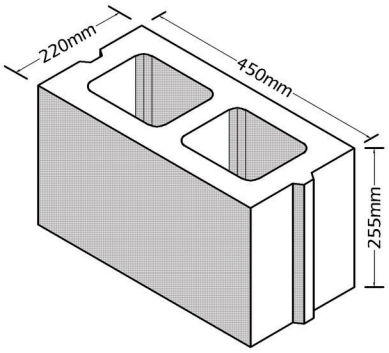

PRODUCT DATASHEET

9" Hollow Concrete Blocks

Single Density

FM 35227

Top quality product conforming to EN 771-3:2003. This block was designed to bear heavy loads. The 9" single density block is typically used for foundations, external walls, retaining walls and in other high load bearing situations.

HEALTH AND SAFETY

- Careful planning of working areas beforehand reduces the risks of incidents.
- Use Mechanical Aids whenever possible
- Use personal protective equipment of good quality.
- Units should be loaded above knee height.
- Eye protection should be used when cutting or trimming units.
- Adopt safe working access platforms when working at heights

*For more details on Health and Safety observe also current Health and Safety legislation

FAQ's

Q: How is the 9" Hollow Single Density Block distinguished from the 9"Hollow Double Density Block?

A: They are of the same size externally, however the 9" Hollow Single Density Block is recognisable through its thinner shell.

Q: What benefits are achievable by using the 9" Hollow Single Density Block as against the 9" Hollow Double Density Block?

A: When using the 9" Hollow Single Density Block infilled with concrete and reinforced, one can achieve higher load-bearing capacities than those achieved by the 9" Hollow Double Density Block; however, in filling the block with concrete reduces its thermal resistance.

Q: Can the 9" Hollow Single Density Block be used externally?

A: It may be used externally; however, it may not achieve the thermal resistance required for external walls unless it is used in double-leaf wall whereby an enhancement of the thermal properties is achieved through the combined effect of the two leaves.

Q: Is there any protection against fire provided by using this product?

A: The fact that the product is entirely made of non-combustible material creates a sufficient barrier and retardation against fire.

Attard Bros Group
Mikesand, Industrial Zone,
Ta' Qali - ATD 4000

www.attardbros.com

More Information
+356 21 415 332
sales@attardbros.com